REFERENCE ONLY

UNIVERSITY OF LONDON THESIS

Degree PhD Year 2006 Name of Author CHENNOTONGCHAI, P

COPYRIGHT

This is a thesis accepted for a Higher Degree of the University of London. It is an unpublished typescript and the copyright is held by the author. All persons consulting the thesis must read and abide by the Copyright Declaration below.

COPYRIGHT DECLARATION

I recognise that the copyright of the above-described thesis rests with the author and that no quotation from it or information derived from it may be published without the prior written consent of the author.

LOANS

Theses may not be lent to individuals, but the Senate House Library may lend a copy to approved libraries within the United Kingdom, for consultation solely on the premises of those libraries. Application should be made to: Inter-Library Loans, Senate House Library, Senate House, Malet Street, London WC1E 7HU.

REPRODUCTION

University of London theses may not be reproduced without explicit written permission from the Senate House Library. Enquiries should be addressed to the Theses Section of the Library. Regulations concerning reproduction vary according to the date of acceptance of the thesis and are listed below as guidelines.

A. Before 1962. Permission granted only upon the prior written consent of the author. (The Senate House Library will provide addresses where possible).

B. 1962 - 1974. In many cases the author has agreed to permit copying upon completion of a Copyright Declaration.

C. 1975 - 1988. Most theses may be copied upon completion of a Copyright Declaration.

D. 1989 onwards. Most theses may be copied.

This thesis comes within category D.

☑ This copy has been deposited in the Library of UCL

☐ This copy has been deposited in the Senate House Library, Senate House, Malet Street, London WC1E 7HU.

On the Fluidization Characteristics of Fine Powders

Parimanan Cherntongchai

Department of Chemical Engineering

University College London

London WC1E 7JE

Thesis submitted to the University of London for the degree of Doctor of Philosophy

November 2005

ProQuest LLC
789 East Eisenhower Parkway
P.O. Box 1346
Ann Arbor, MI 48106-1346

To my family.

ACKNOWLEGMENT

First of all, I would like to acknowledge the Royal Thai Government and the Thai energy policy office for a great opportunity of a higher education and their generous scholarship. Secondly, I would like to acknowledge Professor Stefano Brandani for his genuine supervision and financial support for the research project. For over 4 years of Ph.D research, Professor Brandani has always given me brilliant advices and valuable scientific opinions on my research. Finally, I would like to acknowledge also to Chiang Mai University, Thailand, for all supports and allowance of time to complete the study.

Next, I would like to acknowledge to all members of staffs of the department of chemical engineering, University College London. I would like firstly to thank to Mr David Cheesman for his experiences and helps on designing and setting up the fluidization rig. To all technical staffs in the mechanical workshop, I would like to sincerely acknowledge for their great help, suggestion and the wonderfully finishing experimental rig. In addition, I would like to give a special thank to Sarah for her great work and helps on all electronic devices. I would like to thank also to Martyn, Mark and Dave for their technical support. Finally, I would like to thank to the departmental office staffs for their generous helps.

Furthermore, I would like to thank to the department of biochemical engineering for their allowance to use the laser light scattering machine. Moreover, I would like give a special thank to Mr Phillip for his training on using the machine.

Many thanks to all friends; Jason, Sarah, Andrea, Silvia, Karolina, Hu Bin, Kittipong, Krystina, Wael, Talal, Nan, Sharon, Suet, Monica, Massimillano, Gianluca, Alfeno, Giovanna, Marta, Tom, Panos, Peerada, Phunrawie, Kanok-orn, and Kedsarin for their accompanying, listening, and sharing. For those whom I may not be able to mention all names, I would like to greatly acknowledge all of you.

I would like to genuinely thank to Mr Carlos Amador for generous supports he has given. Thank you for being with me in every situation.

Finally, I would like to reveal my great acknowledgment to my father, my mother and my two sisters. They might not realize that they have given me all energy and brave to accomplish the mission. I also would never forget to thank also to all relatives and friends in Thailand for looking after my parents in place of me when I am away from home.

To my resting father, even he could not make it until the end of my Ph.D, but I know that he is now smiling somewhere and feel proud of his daughter.

ABSTRACT

Powders belonging to group A of the Geldart classification have been studied in detail using the bed collapse technique. To obtain the correct properties of the powders a model is developed, which takes into account the system configuration for both one- and two-valve experiments. An experimental apparatus has been assembled and used to validate the model using glass ballotini in the size range 22-106 μm. The system allows simultaneous measurements of total bed height, using a digital camera, and pressure transients at various positions along the vertical axis. The powders have been sieved to obtain 6 size ranges and the fluidization properties have been measured. Mixtures of particles have been prepared and the effect of the size differences has been investigated.

The experimental results allow the construction of plots of the void fraction vs inlet gas superficial velocity, which show a continuous transition around the minimum bubbling point, with no sudden contraction of the dense phase voidage immediately above the minimum bubbling point for all powders. The plot of ε_d vs U_d yields a characteristic curve, which within the experimental uncertainty has overlapping values for systems below and above the minimum bubbling point. The minimum bubbling point was affected by the structure of the distributor plate, with a coarser sinter leading to premature bubbling.

The experimental data were used to test drag force correlations reported in the literature. It was found that none of the correlations commonly used in CFD simulations describes accurately the experimental ε_d and U_d measurements. Modifying the literature equations it was possible to correlate the experimental ε_d and U_d curve and use this information to

predict the minimum bubbling point using a CFD model recently developed at UCL. The experimental results measured in this study show a strong dependence with voidage, which has allowed the formulation of constitutive equations for the characteristic dimension of the CFD model. The resulting simple correlation of the model parameter was used to obtain a new minimum bubbling criterion and predictions are compared to an extensive database of literature values.

TABLE OF CONTENTS

LIST OF FIGURES

LIST OF TABLES

NOMENCLATURE

A	Bed cross-section area (m^2)
A_d	Projected area of particle (m^2)
Ar	Archimedes number – $g\rho_P d_P^3(\rho_P - \rho_F)/\mu^2$
$A_{bottmdist}$	Bottom distributor pressure drop coefficient (kPa.min/L)
$A_{Topdist}$	Top distributor pressure drop coefficient (kPa.min/L)
A_{bed}	Fixed bed pressure drop coefficient ($kPa.s/m^2$)
b	Height of pressure port from distributor (m)
b_{lower}	Height of the lower pressure port from distributor (m)
C_D	Drag coefficient
De	Density ratio (ρ_p/ρ_f)
d_P	Mean particle size based on the surface to volume ratio (m)
E	Modulus of elasticity (Pa)
F	Fine fraction – fraction of particles with diameter less than 40 μm
F_{Ave}	Average body force per unit volume (kg/m^2s^2)
F_D	Drag force per unit volume (kg/m^2s^2)
$\bar{F}_D$	Average drag force per unit volume (kg/m^2s^2)
F_{FP}	Fluid-particle interaction force per unit volume (kg/m^2s^2)
F_{PP}	Particle-particle interaction force per unit volume (kg/m^2s^2)
f_b	Bubble fraction
f_D	Drag force per unit volume on an individual particle (kg/m^2s^2)
$f(\varepsilon)$	Voidage function
g	Acceleration of gravity (m/s^2)
L	Distance (m)

L_o	Height of bubble escape bed, zone 0 (m)
L_1	Height of sedimentation bed, zone 1 (m)
L_2	Height of fixed bed, zone 2 (m)
L_c	Height of column (m)
L_D	Height of dense phase (m)
L_i	Initial bed height (m)
M_w	Molecular weight (g)
N	Coefficient for voidage function
n	Richardson and Zaki index
p	Absolute pressure (Pa)
p_{atm}	Atmospheric pressure (Pa)
p_w	Absolute pressure in the windbox (Pa)
Q	Gas flow rate (m^3/s)
Q_{atm}	Gas flow rate at atmospheric pressure (m^3/s)
Q_d	Gas flow rate passing distributor (m^3/s)
Q_v	Gas flow rate passing the second valve (m^3/s)
Q_g	Gas flow rate (m^3/s)
Q_p	Particle flow rate (m^3/s)
$Q_{windbox}$	Gas flow rate at windbox pressure (m^3/s)
R	Ideal gas constant (J/mole K)
Re_M	Mixture Reynolds number – $\rho_F \lvert u_{FP} \rvert d_P / \mu_M$
Re_P	Particle Reynolds number – $\rho_F U d_P / \mu_F$
T	Temperature (K)
t	Time (s)
t_{bub}	Bubble escape time (s)

t_c	Collapse time (s) (end of sedimentation stage)
t_{end}	Time end of the consolidation stage (m)
U	Superficial velocity (m/s)
U_1	Superficial velocity of gas in zone 1 (m/s)
U_0	Initial superficial gas velocity (m/s)
U_b	Bubble velocity (m/s)
U_d	Dense phase superficial velocity (m/s)
U_{Dist}	Gas superficial velocity passing distributor (m/s)
$U_{Dist(bottm)}$	Gas superficial velocity passing bottom distributor (m/s)
$U_{Dist(top)}$	Gas superficial velocity passing top distributor (m/s)
$U_{d(max)}$	Maximum dense phase superficial velocity (m/s)
U_D	Dynamic wave velocity (m/s)
U_ε	Continuity wave velocity (m/s)
U_{mb}	Minimum bubbling superficial velocity (m/s)
U_{mf}	Minimum fluidization superficial gas velocity (m/s)
U_t'	Superficial velocity required to give $\varepsilon = 1$ (m/s)
U_t	Terminal falling velocity (m/s)
u_P	Particle velocity (m/s)
u_F	Fluid velocity (m/s)
u_{FP}	Relative fluid-particle velocity (m/s)
W_P	Weight of powder (kg)
V_B	Particle volume in the bed (m^3)
V_W	Windbox volume (m^3)
x	Distance between particles (m)
z	Distance from distributor (m)

Greek Letters

δ	Characteristic length (m)
Δp	Pressure drop (Pa)
$\Delta p_{windbox}$	Windbox pressure drop (Pa)
ΔP	Piezometric (non- recovery) pressure drop (Pa)
ΔP_o	Pressure drop in zone 0 (Pa)
ΔP_1	Pressure drop in zone 1 (Pa)
ΔP_2	Pressure drop in zone 2 (Pa)
ΔP_{Bed}	Bed pressure drop (Pa)
ΔP_{Dist}	Distributor pressure drop (Pa)
$\Delta P_{Dist(bottm)}$	Bottom distributor pressure drop (Pa)
$\Delta P_{Dist(top)}$	Top distributor pressure drop (Pa)
$\Delta P_{freeboard}$	Freeboard pressure drop (Pa)
$\Delta P_{fixedbed}$	Fixed bed pressure drop (Pa)
ΔP_{rota}	Rotameter pressure drop (Pa)
$\Delta P_{windbox}$	Piezometric windbox pressure drop (Pa)
ε	Voidage
$\bar{\varepsilon}$	Average voidage
ε_o	Voidage in zone 0 or initial bed voidage
ε_1	Voidage in zone I
ε_2	Voidage in Zone II
ε_d	Dense phase voidage
$\varepsilon_{d(inf)}$	Limiting dense phase voidage
$\varepsilon_{d(max)}$	Maximum dense phase voidage

ε_{dm}	Fixed bed voidage
ε_{mb}	Minimum bubbling voidage
ε_{mf}	Minimum fluidization voidage
μ_F	Gas viscosity (kg/m s)
μ_M	Mixture viscosity (kg/m.s)
ρ	Density (kg/m^3)
ρ_F	Gas density (kg/m^3)
ρ_P	Particle density (kg/m^3)
τ	Tortuosity factor

Chapter 1: Introduction to Fluidization

1.1 Fluidization

Fluidization (Kunii and Levenspiel, 1969) is a process in which solid and fluid are in contact and the fluid-particle bed has fluid-like properties:

- Light objects float on top of the bed,
- The surface stays horizontal even in tilted beds,
- The solids can flow through an opening in the vessel just like a liquid,
- The bed has a static pressure head due to gravity.

At low fluid flow, when the fluid is passed upwards through a packed bed, the pressure drop increases with fluid velocity, until the force from the fluid on an individual particle equals to the force exerted by gravity and the bed of particles is fully supported by the fluid. In this state, the liquid-like behaviour is achieved and the bed is said to be 'fluidized'. The fluid superficial velocity at this point is called 'minimum fluidizing velocity'. Increasing further the fluid superficial velocity beyond the minimum fluidization velocity results in a constant pressure drop across the bed that equals the weight of the bed per unit area and the fluidized bed can behave in various regimes, depending on the fluid and particle properties.

1.2 Regimes of fluidization

The contact between fluid and particle can generate several fluidization regimes, when the fluid superficial velocity is beyond the minimum fluidization velocity. An increase in velocity above the minimum fluidization velocity results in a smooth progressive expansion of the bed. A bed such as this is called 'homogeneous fluidized bed' (Figure 1.1(b)) (Kunii and Levenspiel, 1969). With further increase in fluid superficial velocity, bubbles are formed in the fluidized bed, especially for gas-solid systems. At this point, the bed is called 'bubbling fluidized bed' (Figure 1.1(c)) (Kunii and Levenspiel, 1969). The bed loses its homogeneity and it is now a heterogeneous fluidized bed. As the velocity is increased further, the bubbles in the bubbling bed will coalesce and grow as they rise. If the ratio of the height to the diameter of the bed is high enough, the size of bubbles may become almost the same as the diameter of the bed, in this regime a fluidized bed is called 'slugging fluidized bed' (Figure 1.1(d)) (Kunii and Levenspiel, 1969). If the particles are fluidized at a high enough fluid flow rate, the velocity exceeds the terminal velocity of the particles. The heterogeneous, two-phase character of the bed firstly peaks, and then gradually gives way to a condition of increasing uniformity. The upper surface of the bed disappears and bubbles tend to lose their distinct shape and the gas can become the continuous phase with streamers of solids in gas. There is a continuous density gradient from the bottom of the vessel to the top. Beds under these conditions are called 'turbulent fluidized bed' (Figure 1.1(e)) (Smolders and Baeyens, 2001). The turbulent bed is bridging two extreme conditions: a regime in which the dense phase is a continuous phase and a regime where the gas is a continuous phase and particle clusters make up the dispersed phase. This later regime is called 'fast fluidized bed' (Figure 1.1(f)) (Smolders and Baeyens, 2001). With further increases of gas

velocity, eventually the fluidized bed becomes an entrained bed, where 'dispersed, dilute or lean phase fluidized bed' (Figure 1.1(g)) (Kunii and Levenspiel, 1969) is observed and the solids are transported pneumatically.

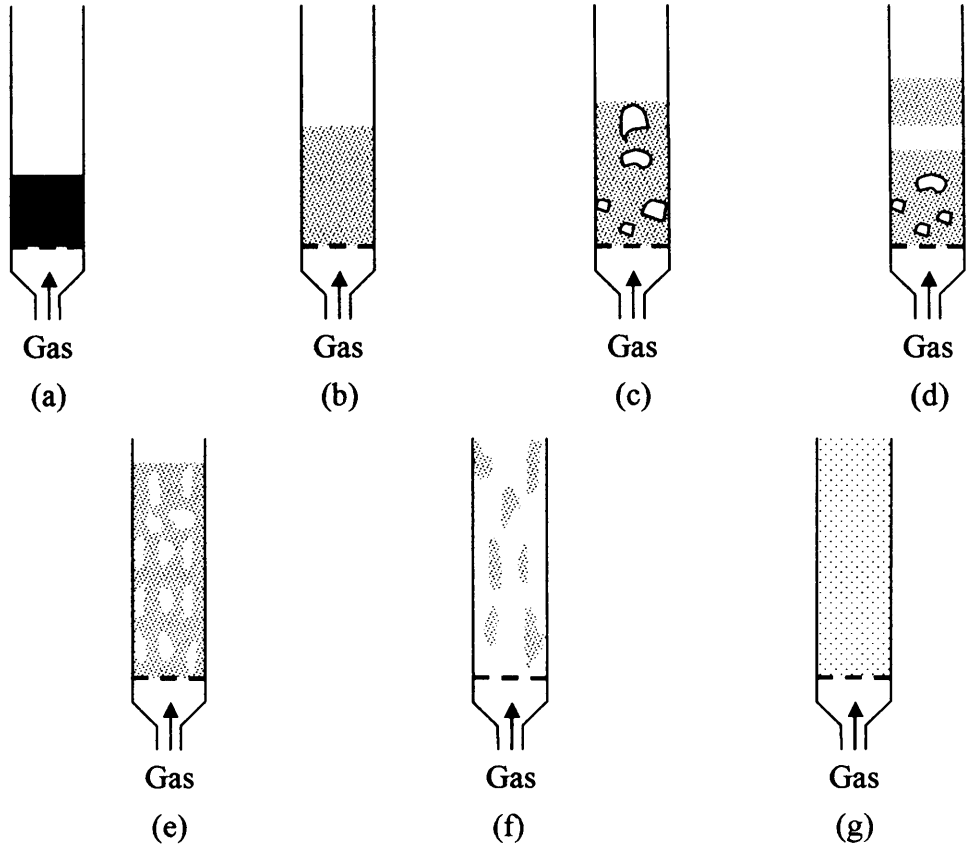

Figure1. 1 Schematic representation of fluidized beds in different flow regimes (a) fixed bed, (b) homogeneous expanded bed, (c) bubbling bed, (d) slugging bed, (e) turbulent bed and (f) Fast fluidized bed, and, (g) dilute bed (Lim et al., 1995)

The regimes mentioned above occur for the non-cohesive particles or small and/or less dense particles. However, for fluidised bed of cohesive powders, channelling bed occurs and gas passes though interconnected vertical and inclined cracks extending from the distributor to the bed surface and the total fluidized bed pressure drop is lower than the weight of the bed per cross section area. On the other hand, for large and /or dense

particles, a spouting behaviour is observed. This phenomenon (Bridgwater, 1985) happens when the gas from the distributor forms an open cylindrical cavity that penetrates to the bed surface, called 'spout'. The solid particles are entrained into the spout from the spout wall at all heights. At the bed surface, the particles then fall back in the downward-moving annular bed of solid.

1.3 Geldart's classification of powders

For each regime of fluidization, the fluidization charcteristic can be different depending on the fluid and particle properties. Geldart (Geldart, 1973 and 1986) identified four regions in which the fluidization character can be distinctly defined, see Figure1.2.

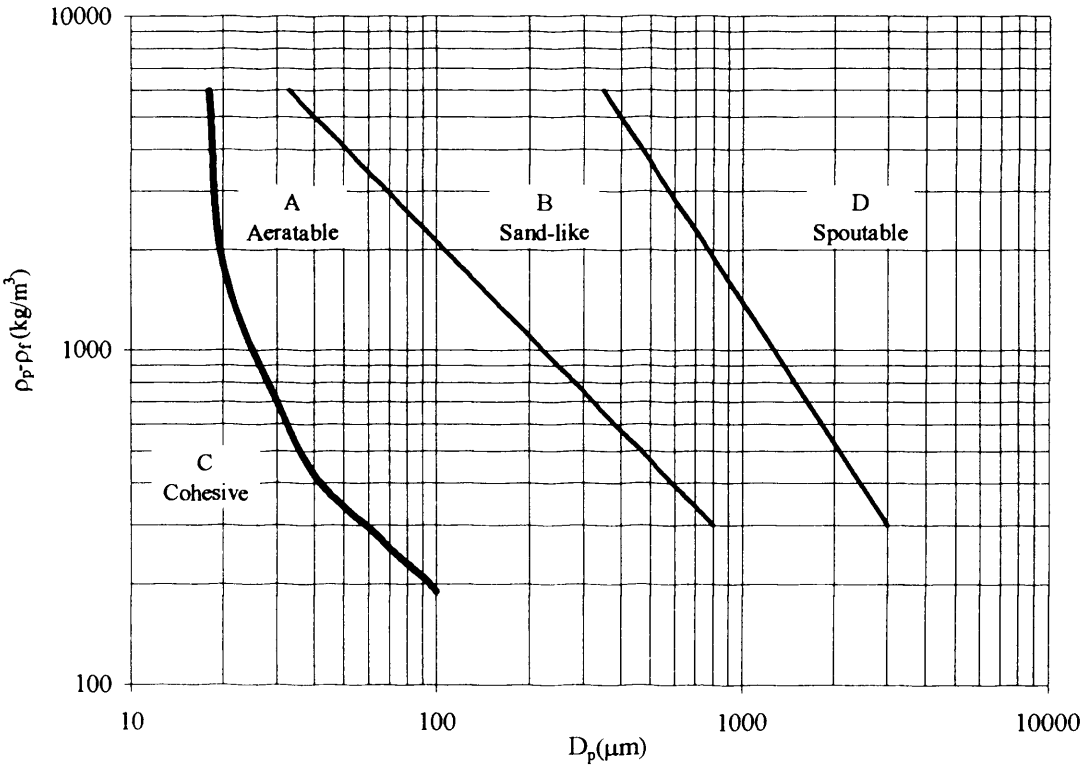

Figure1.2 Geldart's classification of particles. (Geldart, 1973)

Group C powders are cohesive and are characterized by

- Normal fluidization is extremely difficult; the powder lifts as a plug in small diameter tubes, or channels badly.
- Pressure drop across the bed is lower than the bed weight per cross-section area.
- Particle mixing is poor

Group A powders are designated as 'aeratable' particles and are characterized by

- Bed expands considerably at velocities between U_{mf} and U_{mb}.
- When the gas velocity is increased above U_{mb}, the bed height becomes smaller because the dense phase voidage is reduced more quickly with increasing gas velocity than the bubble hold-up increases.
- The dense phase finally assumes a stable voidage between ε_{mf} and ε_{mb}.
- Gas bubbles rise more rapidly than the rest of the gas.
- Bubbles split and coalesce frequently through the bed, resulting in a restricted bubble size.
- Gross circulation of solids occurs even when a few bubbles are present.
- Considerable back-mixing of gas in the dense phase occurs.
- Gas exchange between bubbles and the dense phase is high.

Group B powders are characterized by

- Inter-particle forces are negligible.
- Bubbles start to form at or only slightly above minimum fluidization velocity.
- Bed expansion is small.
- Particle circulation in the absence of bubbles is little
- Most bubbles rise more quickly than the interstitial gas velocity

- Bubble size increases with both bed height and excess gas velocity.
- Coalescence is the predominant phenomenon, and there is no evidence of a maximum bubble size.
- Bubble sizes are independent of both mean particle size and size distribution.
- Backmixing of dense phase gas is relatively low, as well as the gas exchange between bubbles and dense phase.

Group D, large and/or dense particles belong to this group. The particles are characterized by

- Bubbles, except very large bubbles, rise more slowly than the interstitial fluidizing gas.
- As a result, gas flows into the base of the bubble and out of the top, providing a mode of gas exchange and by-passing.
- Gas velocity in the dense phase is high.
- Solid mixing is relatively poor.
- Backmixing of the dense phase gas is small.
- Segregation by size is likely when the size distribution is broad, even at high gas velocities.
- Flow regimes around particles may be turbulent, causing some particle attrition with rapid elutriation of the fines produced.
- Bubble sizes are similar to those in group B powders.
- The bed can be made to spout even when the bed depth is appreciable.

1.4 Quality of fluidization

The fluidization quality is the outcome of the fluidization characteristics for each regime of fluidization. Generally, satisfactory fluidization quality is referred to the conditions in which the fluid-particle contact and the fluid-particle circulation are enhanced.

In practice, the most employed fluidization regime is the bubbling bed. The fluidization quality implies small fluctuations, small bubbles, large bed expansion and slow collapse rate. This kind of behaviour is associated with particles belonging to Geldart's Group A powder classification.

1.5 Scope of this work

In this work, the fluidization characteristics of powders belonging to group A of the Geldart classification were studied and glass ballotini in the size range of 22-100 micron were used. Particular attention was given to the expansion characteristics of powders in the homogeneous and the bubbling bed. The purpose of these studies is to gain an understanding of the effect of particle size distribution on the fluidization characteristics of powders by comparing results from powders of the relevant narrow size cut and those obtained from the original size distribution. The fluidization characteristics of powders of bimodal mixtures were also studied by preparing mixtures composed of powders of two different sizes according to the sieve analysis.

The standard bed collapse technique (Rietema, 1967) is used to investigate Geldart type A powders. Both 1-valve and 2-valve bed collapse experiments are applied and different values for the dense phase voidage and collapse times were observed. To obtain the correct properties of the powders a model is developed, which takes into account the system configuration for both one-valve and two-valve experiments. An experimental apparatus has been assembled to allow simultaneous measurements of total bed height, using a digital camera, and pressure transients at various positions along the vertical axis.

Four different powders with wide "natural" particle size were studied experimentally. In order to understand the effect of each individual size cut on the behaviour of the original powder, the original powders were sieved into 6 different size cuts; according to $2^{1/4}$ sieve size aperture series and fluidization characteristics of each size cut were studied. The narrow size cut powders were then mixed to prepare the bimodal mixture. The mixtures are composed of two narrow cut powders of difference in size at varied percentage. This is to understand the behaviour of the bimodal powder in comparison with the natural size powders and the narrow size cut powders. In addition, preliminary experiments were carried out to exclude effects resulting from column diameter, initial bed height and distributor porosity on the measured fluidization characteristics, in particular the dense phase voidage, ε_d, and the corresponding superficial gas velocity, U_d.

The drag force is the key parameter to describe, for example, the dense phase characteristic and the minimum bubbling point. Therefore, the ε_d and U_d experimental data from the narrow size cut and the natural size powder were used to validate the drag

force correlations reported in the literature. It was found that none of the correlations commonly used in CFD simulations could describe accurately the experimental ε_d and U_d measurements. Modifying the literature equations, it was possible to correlate the experimental ε_d and U_d curve.

The modified drag force correlation was then applied to a CFD model recently developed at UCL to predict the minimum bubbling point. The experimental results show a strong dependence with voidage of the characteristic parameter of the model and a simple correlation was obtained. The predictions from the new minimum bubbling criterion were compared to an extensive database of literature values.

Chapter 2: Literature Reviews

2.1 Expansion characteristics of fine powders

The expansion characteristics of fine powders are the onset of minimum fluidization, the onset of minimum bubbling, the voidage of the dense phase, the bed voidage, bubble fraction and bubble properties. The minimum fluidization stage gives the transition point from the fixed to the fluidised bed and it is a lower limit of the bed expansion. After the minimum fluidization stage, the bed expands homogeneously. The upper limit of the homogeneous expansion is the minimum bubbling point, when the first bubble appears. The difference between these two points, in terms of U_{mb}/U_{mf} or $\varepsilon_{mb}/\varepsilon_{mf}$, gives the indication of the degree of the homogeneous expansion of the bed (Geldart and Abrahamsen, 1978).

At a velocity between the minimum fluidization and the minimum bubbling velocity, the bed of powders shows particulate expansion, where there is no bubble in the bed and the dense phase voidage and the bed voidage are the same. The bed voidage increases with the increasing velocity, until the bubbling starts. At this point, the bed is said be at the minimum bubble point. From this point on the bed expansion increases less rapidly, remains constant or might even decrease. Simone and Harriott (1980) report that at velocities much higher than U_{mb} the bed voidage reaches a minimum and then expands

again. This is because the dense phase voidage can be reduced more rapidly than the bubble holdup increases (Geldart and Wong, 1984). The region of decreasing voidage is called unstable bubbling region (Jacob and Weimer, 1987). As reported for instance by Foscolo et al. (1987), the dense phase voidage lies between the minimum fluidization and the minimum bubbling voidage. At velocities approximately 4-6 times U_{mb} the dense phase voidage reaches a minimum and stays constant (Foscolo et al., 1987).

Gibilaro (2001) considers the behaviour of a fluidized bed just above the minimum bubbling velocity and points to an abrupt and sharp transition in the dense phase voidage. Brandani and Foscolo (1994) described this phenomenon theoretically by applying the jump conditions to the analysis of the equations of change for the particle bed model (Foscolo and Gibilaro, 1987) and showed that the model would predict qualitatively the observed behaviour.

By studying the expansion characteristics of a homogeneous bed it is possible to obtain a relationship between ε_d and U_d. This is generally used to describe the dense phase behaviour of the powder for both homogeneous expanded beds and bubbling beds. A number of researchers (Abrahamsen and Geldart, 1980a; Barreto et al., 1983; De Jong and Nomden, 1974; Geldart and Wong, 1984; Simone and Harriott, 1980) reported that the ε_d and U_d relationship of fine powders at ambient conditions for the bubbling bed deviates from the two-phase theory of Toomey and Johnstone (1952), which assumes that ε_d of the bubbling bed is at ε_{mf} and U_d is U_{mf}.

2.2 Effect of size and size distribution on bed expansion characteristic

It is generally stated that powders with wide particle size distributions and powders with the additions of fines, generally have an improved fluidization quality. This results in a smoother fluidization and a larger expansion ratio than a narrow cut powder. From the point of view of chemical conversion, since chemical reactions occur at the bubble/dense phase interface and within the dense phase, a more expanded dense phase and smaller bubble sizes are preferable and improve the performance of the reactor.

The bed expansion characteristics are varied with particle size and size distribution. Knowing the effect of the particle size and size distribution on the fluidization behaviour will be useful on the selection of size and size distribution for the desired expansion characteristic.

Abrahamsen and Geldart (1980a) developed an empirical correlation of U_{mb}/U_{mf} to describe the homogeneous expansion of natural size distribution fine powder, taking into account the effect of fines. The empirical correlation is based on the data of 23 different powders varying in mean size between 20 μm and 72 μm and with a particle density range from 1100 kg/m^3 to 4600 kg/m^3. The powders were alumina, ballotini and cracking catalyst and the fluidizing gases were air, helium, argon, carbon dioxide and Freon-12.

Using SI units for the physical properties

$$\frac{U_{mb}}{U_{mf}} = \frac{2300\rho_F^{0.126}\mu_F^{0.523}\exp(0.716F)}{d_P^{0.8}g^{0.934}(\rho_P-\rho_F)^{0.934}} \qquad (2.1)$$

The Richardson and Zaki (1954) equation is also often used to determine the expansion coefficient from experimental data.

$$\frac{U_o}{U_t'} = \varepsilon^n \qquad (2.2)$$

A log-log plot of superficial velocity vs void fraction data will yield n as the slope and the terminal falling velocity of an individual particle U_t' as the intercept.

The expansion parameter n correlates with the terminal particle Reynolds number. n acquires constant values in both the creeping flow and inertial flow regimes, which are 4.8 and 2.4 respectively. The parameter n changes with terminal velocity Reynolds number in the intermediate regime between these two limits (Gibilaro, 2001). The relationship developed by Khan and Richardson (1989), eq. 2.4, enables n to be calculated from the Archimedes number defined in eq. 2.3.

$$Ar = d_P^3 \rho_F \frac{\rho_P - \rho_F}{\mu_F^2} \qquad (2.3)$$

$$n = \frac{4.8 + 0.1032\,Ar^{0.57}}{1 + 0.043\,Ar^{0.57}} \qquad (2.4)$$

The Richardson and Zaki correlation was originally developed for solid-liquid systems. Applying this correlation to gas-solid systems leads to values of n that vary widely from system to system.

In general, many researchers reported a higher value of n from that calculated from eq. 2.4. Massimilla et al. (1972) reported this behaviour for an FCC catalyst with a wide size distribution and narrow size cuts at ambient conditions. Kai et al. (1987) made similar observations for fine powders with wide size distribution at ambient experimental conditions. Foscolo et al. (1987) studied the behaviour of an FCC catalyst

with a wide size distribution at ambient conditions and found that both n and U_t were higher than the predicted values.

Geldart and Wong (1984) studied cohesive particles and reported that the n index is higher than the predicted value and that it increases as the particle size decreases and as the powder becomes more cohesive.

The effect of temperature has been studied recently by Lettieri et al. (2002), who reported a higher value of n for the fluidised bed at the elevated temperature for FCC catalysts with a wide size distribution and additions of fines.

The effect of pressure has been investigated by various researchers. Crowther and Whitehead (1978) carried the experiment at a supercritical condition and reported that n increased with average particle diameter. Poletto et al. (1993) also reported the higher value of n for fine powders under near supercritical conditions. Jacob and Weimer (1987) studied the effect of pressure using carbon with a wide size distribution. They reported that n decreases with pressure and yields values higher than those predicted.

A summary of the values reported in the literature for the expansion coefficient n is presented in Table 2.1

Table 2.1 Summary of n index from literature

Author	Powders	PSD	%Fines	Operating Condition	n
Kai et al. (1987)	Alumina	Wide	18	Ambient	5.3
Massimilla et al. (1972)	FCC	Wide Narrow		Ambient	5.4-7
Foscolo et al. (1987)	Catalyst	Wide	5-15	Ambient	4-5.34
Geldart and Wong (1984)	- Alumina - Catalyst - Fly-ash - Metal oxide - Plastic - Glass	Wide		Ambient (For Group A and AC powder)	4.4-60
Lettieri et al. (2002)	FCC	Wide	5-25	High temperature	7-9.6
Jacob and Weimer (1987)	Activated carbon	Wide	30	High pressure	4-7
Crowther and Whitehead (1978)	- Catalyst - Coal	Narrow Wide		Supercritical	5-9 7-19

The terminal velocity U_t can be calculated using the drag force per unit volume on single particle in equilibrium with gravity and the Archimedes buoyant force, eq. 2.5:

$$f_D = (\rho_P - \rho_F)g \qquad (2.5)$$

The drag force is expressed as a function of the drag coefficient, C_D:

$$f_D = \frac{3}{4} C_D \frac{\rho_F U_t^2}{d_P} \qquad (2.6)$$

Table 2.2 summarises drag coefficient correlations generally used in fluidization studies.

Table 2.2 Drag coefficient correlations

Author	C_D correlation
Dallavalle (1948) drag coefficient	$C_D = \left(0.63 + \frac{4.8}{\sqrt{Re_P}}\right)^2$ (For all flow regimes)
Rowe (1961)	$C_D = \frac{24}{Re_p}\left[1 + 0.15(\varepsilon Re_p)^{0.687}\right]$, if $\varepsilon Re_p < 1000$ $C_D = 0.44$, if $\varepsilon Re_p \geq 1000$
Stokes law	$C_D = \frac{24}{Re_P}$, $Re_p < 0.1$

Re_p is particle Reynolds number, where $Re_P = \frac{d_P U \rho_F}{\mu_F}$

The values of U_t' obtained from the experimental expansion data usually exceed the terminal falling velocity calculated from these correlations (Jacob and Weimer, 1987). Similar results were also obtained by Crowther and Whitehead (1978), Foscolo et al. (1987) and Lettieri et al. (2002).

Therefore, as discussed by Barreto et al. (1983), the Richardson and Zaki correlation can be used to describe the velocity-voidage relationship, provided that both the expansion coefficient n and the terminal velocity U'_t are obtained from the experimental expansion data.

2.3 Correlation for bed expansion from the two fluid equations for fluidized beds

One can obtain an implicit relationship between ε_d and U_d from any drag force correlation applicable to fluid particle systems. Consider the equations of change for a fluid- particle suspension (Ishii, 1975; Anderson and Jackson, 1967; Foscolo and Gibilaro, 1987). The typical approach is to consider the system composed of two fluids, schematically shown in Figure 2.1, and derive the mass and momentum balance equations in one-dimension

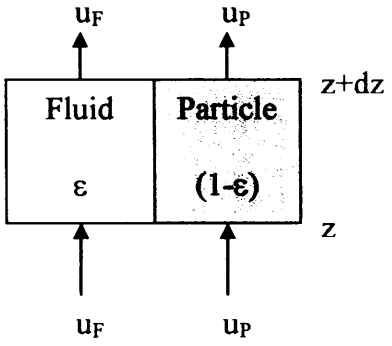

Figure 2.1 Control volume of unit cross-sectional area for a fluidized suspension

Both the particles and the fluid are regarded as being incompressible fluids in contact with each other.

Conservation of mass

Fluid-phase

$$\frac{\partial \varepsilon}{\partial t} + \frac{\partial \varepsilon u_F}{\partial z} = 0 \qquad (2.7)$$

Particle-phase

$$\frac{\partial(1-\varepsilon)}{\partial t}+\frac{\partial(1-\varepsilon)u_P}{\partial z}=0 \qquad (2.8)$$

Combining eqs 2.7 and 2.8, the fluid and particle velocities are linked to the superficial fluid velocity, U_0, by:

$$U_0=(1-\varepsilon)u_p+\varepsilon u_F \qquad (2.9)$$

Therefore the relative velocity between fluid and particle can be expressed as

$$u_{FP}=u_F-u_p=\frac{U_0-u_p}{\varepsilon} \qquad (2.10)$$

Conservation of momentum

Fluid-phase

$$\varepsilon\rho_F\left[\frac{\partial u_F}{\partial t}+u_F\frac{\partial u_F}{\partial z}\right]=-F_D-\varepsilon\rho_F g-\varepsilon\frac{\partial p}{\partial z} \qquad (2.11)$$

Particle-phase

$$(1-\varepsilon)\rho_P\left[\frac{\partial u_P}{\partial t}+u_P\frac{\partial u_P}{\partial z}\right]=F_D-(1-\varepsilon)\rho_P g-(1-\varepsilon)\frac{\partial p}{\partial z} \qquad (2.12)$$

Where F_D is the drag force per unit volume between the fluid and the particle suspension. For a homogenously expanded bed, eqs 2.11 and 2.12 can be simplified to obtain the pressure gradient

$$\frac{\partial p}{\partial z}=[\varepsilon\rho_F+(1-\varepsilon)\rho_P]g \qquad (2.13)$$

and

$$F_D=\varepsilon(1-\varepsilon)(\rho_P-\rho_F)g \qquad (2.14)$$

The drag force for a suspension of particles, F_D, is a function of the fluid velocity and the void fraction. Therefore, eq. 2.14 represents an implicit relationship between ε_d and U_d that can be solved iteratively.

The same approach can be applied to pressure drop correlations available for particle suspensions. Typically these correlations are for the non-recoverable pressure loss, ΔP, which is related to the dynamic pressure by (Gibilaro, 2001):

$$\frac{\partial p}{\partial z} = \frac{\partial P}{\partial z} - \rho_F g \qquad (2.15)$$

At equilibrium we obtain from eq. 2.13:

$$\frac{\partial P}{\partial z} = (1-\varepsilon)(\rho_P - \rho_F)g \qquad (2.16)$$

With the knowledge of a drag force correlation for the particle suspension, or a pressure drop correlation, eqs 2.14 and 2.16 can be used to describe the relationship between ε_d and U_d and the minimum fluidization point.

2.3.1 Pressure drop and drag force correlations for fluidized beds.

Pressure drop correlations are developed typically to describe the pressure loss in a fixed bed which is a result of frictional interaction between the fluid and the particles. Gibilaro (2001) shows that, by analogy with laminar flow of Newtonian fluids in pipes (Hagen-Poiseuille equation), the Blake-Kozeny equation (Carman, 1937) can be obtained.

$$\frac{\Delta P}{L} = 150\frac{\mu_F U(1-\varepsilon)^2}{d_P^2 \varepsilon^3} \qquad (2.17)$$

For higher Reynolds numbers, similar arguments lead to Burke and Plummer (1928) equation:

$$\frac{\Delta P}{L} = 1.75 \frac{(1-\varepsilon)}{\varepsilon^2} \frac{\rho_F U^2}{d_P} \qquad (2.18)$$

Ergun (1952) described the total energy loss for the fixed bed as the sum of the viscous and kinetic energy losses. Ergun's equation is the combination of the Blake-Kozeny and Burke-Plummer equations for the pressure drop in the fixed bed over the full range of flow regimes.

$$\frac{\Delta P}{L} = 150 \frac{\mu_F U (1-\varepsilon)^2}{d_P^2 \varepsilon^3} + 1.75 \frac{(1-\varepsilon)}{\varepsilon^2} \frac{\rho_F U^2}{d_P} \qquad (2.19)$$

Eq.2.19 has been obtained from fixed bed data and should not be applied to higher void fractions. To overcome this limitation, Foscolo et al. (1983) have generalised this equation to any void fraction. Their approach is again based on the pipe flow analogy. However, three features are introduced;

1. A tortuosity factor, taking into accounts the effective length of the fluid path, which from statistical arguments is related to the void fraction: $\tau = 1/\varepsilon$.
2. An expansion/contraction loss in the inertial flow regime proportional to the particle concentration, (1- ε).
3. The correct limit for the single-particle

Their proposed equation for the pressure drop in the fixed and expanded fluidized beds, for the entire flow regime is the 'Revised Ergun equation' and is given by:

$$\frac{\Delta P}{L} = \frac{\rho_F U^2 (1-\varepsilon)}{d_p} \left(\frac{17.3}{Re_P} + 0.336 \right) \varepsilon^{-4.8} \qquad (2.20)$$

Other pressure drop equations are available in the literature. For example, Anderson (1961) presented a pressure drop correlation for the particulate fluidized bed consisting of spheres of uniform size. The equation differed from the Ergun equation since it included a tortuosity factor and a cross-section factor, both of which are void fraction

dependent and the inertial drag coefficient was dependent only on the particle Reynolds number.

$$\frac{\Delta P}{L} = 36 Z \tau^2 \frac{(1-\varepsilon)^2}{\varepsilon^3} \frac{\mu_F U}{d_p^2} + 6 c_i \tau^3 \frac{1-\varepsilon}{\varepsilon^3} \frac{\rho_F U^2}{d_p}$$

$$\tau = 1.71 \left(\frac{1-\varepsilon}{\varepsilon} \right)^{0.15} \quad \text{for } 0.45 \le \varepsilon \le 0.94 \qquad (2.21)$$

$$\tau = \varepsilon^{-2} \quad \text{for } 0.92 \le \varepsilon \le 1$$

$$c_i = \frac{1}{8} \left(C_D - \frac{24}{Re_P} \right)$$

The development of drag force correlations is typically based on finding a relationship between the drag force in a particle suspension, F_D, and the drag force of the isolated particle, f_D. Wen and Yu (1966) introduced the "voidage function" $f(\varepsilon)$. The origin of the voidage function arises from the study reported by Richardson and Zaki (1954) for sedimentation. Wen and Yu (1966) proposed that the voidage function is a function of bed voidage and

$$\frac{F_D}{f_D} = f(\varepsilon) = \varepsilon^N \qquad (2.22)$$

$$F_D = f(\varepsilon) \left(\frac{6 \rho_F U^2}{d_P} \right) \left(\frac{3}{Re_P} + \frac{0.45}{Re_P^{0.313}} \right) \qquad (2.23)$$

$$f(\varepsilon) = \varepsilon^{-4.7} \text{ for } 0.001 < Re_p < 1000$$

The value of the coefficient N is a subject of continuous discussion. In many studies, this exponent was assumed to be constant or a function of physical properties (Wen and Yu, 1966). While Di Felice (1994) showed that the exponent is not constant and should be varied with the bed concentration. Mostoufi and Chaouki (1999) proposed that the exponent is a function of particle Reynolds number at terminal velocity and the Archimedes number. Makkawi and Wright (2003) showed that the exponent depends on

the relative particle Reynolds number. However, in the majority of the studies reported in the literature a constant value was adopted.

Ishii and Zuber (1979) developed drag coefficient and relative motion correlations for dispersed two-phase flows of bubbles, drops and particles from simple similarity criteria and a mixture viscosity model. The correlations proposed cover all concentration ranges and Reynolds number ranges, from the Stokes regime up to Newton's regimes.

$$F_D = C_D \frac{\rho_F u_{FP}^2}{2}(1-\varepsilon)\frac{A_D}{V_P} \qquad (2.24)$$

where

$$C_D = \frac{24}{Re_M}\left(1+0.1Re_M^{0.75}\right) \qquad (2.25)$$

$$Re_M = \frac{d_P \rho_F |u_{FP}|}{\mu_M} \qquad (2.26)$$

and the mixture viscosity for a fluid particle suspension is given by

$$\frac{\mu_M}{\mu_F} = \left(1-\frac{1-\varepsilon}{\varepsilon_{dm}}\right)^{-2.5\varepsilon_{dm}} \qquad (2.27)$$

Gibilaro et al. (1985) used the pressure drop correlation from Foscolo et al. (1983) to produce a drag coefficient correlation for the individual particle, which yield a general and fully predictive expression for the drag force on a particle in a fluidized suspension.

$$F_D = f_D\left(\frac{U}{U_t}\right)^{\frac{4.8}{n}}\varepsilon^{-3.8} \qquad (2.28)$$

where n is the Richardson and Zaki (1954) expansion coefficient.

Syamlal and O'Brien (1987) proposed a new drag function which was used by Gelderbloom et al. (2003) for CFD simulations of bubbling/collapsing fluidized beds.

$$F_D = \frac{3(1-\varepsilon)\varepsilon\rho_F}{4U_{RM}^2 d_P}\left(0.63 + 4.8\sqrt{\frac{U_{RM}}{Re}}\right)^2 u_{FP}^2 \qquad (2.29)$$

The particle Reynolds number is defined by

$$Re = \frac{d_P \rho_F |u_{FP}|}{\mu_F} \qquad (2.30)$$

The drag coefficient for the isolated particle used is that of Dallavalle (1948) and U_{RM} is terminal velocity correlation, developed from the correlation of Garside and Al-Dibouni (1977).

$$U_{RM} = 0.5\left(A - 0.06Re_P + \sqrt{0.0036Re_P^2 + 0.12Re_P(2B - A) + A^2}\right) \qquad (2.31)$$

$$A = \varepsilon^{-4.14} \qquad (2.32)$$

$$B = \begin{cases} Q\varepsilon^{1.28}, & \varepsilon \le 0.85 \\ \varepsilon^R, & \varepsilon > 0.85 \end{cases} \qquad (2.33)$$

Where Q and R are user-defined quantities with defaults of

Q = 0.8, and can be adjusted to match U_{mf}

R = 2.653, and can be adjusted to have function continuity at $\varepsilon = 0.85$.

The drag force correlations mentioned above are generally used in CFD simulations of fluidized beds, as reported by Van Wachem et al. (2001) who applied also a different drag model. They reported that the choice of the drag force correlation used was the main factor that influenced the characteristics of the fluid-particle suspensions.

In general the correlations presented above need appropriate modification in order to describe quantitatively the fluidized suspensions. For instance Kai et al. (1987) used the Ergun equation to describe the relationship between velocity and voidage of fine powders with different percentage of fines, at ambient condition. They found that the constant term in Ergun equation has to be changed from 150 to 226. Simone and Harriott (1980) used the Carman-Kozeny equation in describing the particulate expansion of narrow sized and natural size distribution of fine powders at ambient condition, but they observed a deviation from the predicted behaviour. Jacob and Weimer (1987) used the correlation of Foscolo et al. (1983) for the estimation of the particulate expansion of fine powder fluidised under pressure. They reported that the equation underestimated particulate expansion for the powder containing fines. However, they found that the empirical correlation from Abrahamsen and Geldart (1980a) could adequately describe their results for all pressures.

In this work, the Richardson and Zaki equation as well as the drag force correlations which are generally included in CFD simulations are used to describe the ε_d and U_d characteristic curve of the powders. A summary of the correlations used is presented in Table 2.3 and Figure 2.2 shows the predictions obtained from the different correlations for a representative system. It can be seen that the correlations give a wide range of results. Therefore, one of the aims of this work is to examine how the drag force correlations can be modified to describe correctly the expansion behaviour of the powders studied. The drag force correlation that can predict well the system will be used in the stability criteria for the prediction of the minimum bubbling point.

Table 2.3 Summary of the drag force correlations applied in this work

Author	Correlations
Ergun equation	$\frac{\Delta P}{L} = 150\frac{\mu_F U(1-\varepsilon)^2}{d_P^2 \varepsilon^3} + 1.75\frac{(1-\varepsilon)}{\varepsilon^2}\frac{\rho_F u_F^2}{d_P}$
Revised Ergun equation	$\frac{\Delta P}{L} = \frac{\rho_F U^2 (1-\varepsilon)}{d_p}\left(\frac{17.3}{Re_P} + 0.336\right)\varepsilon^{-4.8}$ (Foscolo et al., 1983)
Richardson and Zaki	$\frac{U_o}{U_t} = \varepsilon^n$ $Ar = d_P^3 \rho_F \frac{\rho_P - \rho_F}{\mu_F^2}$ $U_t = \left(-3.809 + \sqrt{3.809^2 + 1.832\sqrt{Ar}}\right)^2 \frac{\mu_F}{\rho_F d_p}$ (Dallavalle, 1948) $n = \frac{4.8 + 0.1032\,Ar^{0.57}}{1 + 0.043\,Ar^{0.57}}$ (Khan and Richardson, 1989)
Ishii and Zuber (1979)	$F_D = C_D \frac{\rho_F u_{FP}^2}{2}(1-\varepsilon)\frac{A_D}{V_P}$ $C_D = \frac{24}{Re_M}\left(1 + 0.1 Re_M^{0.75}\right)$ $Re_M = \frac{d_P \rho_F \lvert u_{FP} \rvert}{\mu_M}$ $\frac{\mu_M}{\mu_F} = \left(1 - \frac{1-\varepsilon}{\varepsilon_{dm}}\right)^{-2.5\varepsilon_{dm}}$ $\varepsilon_{dm} = 0.62$

Table 2.3 (Continued)

Author	Correlations
Syamlal and O'Brien (1987)	$F_D = \frac{3(1-\varepsilon)\varepsilon\rho_F}{4U_{RM}^2 d_P}\left(0.63 + 4.8\sqrt{\frac{U_{RM}}{Re}}\right)^2 u_{FP}^2$ $Re = \frac{d_P \rho_F \lvert u_{FP} \rvert}{\mu_F}$ U_{RM} correlation developed by Garside and Al-Dibouni (1977) $U_{RM} = 0.5\left(A - 0.06Re_P + \sqrt{0.0036Re_P^2 + 0.12Re_P(2B - A) + A^2}\right)$ $A = \varepsilon^{4.14}$ $B = \begin{cases} Q\varepsilon^{1.28}, \varepsilon \le 0.85 \\ \varepsilon^R, \varepsilon > 0.85 \end{cases}$ $R = 2.653$ and $Q = 0.8$

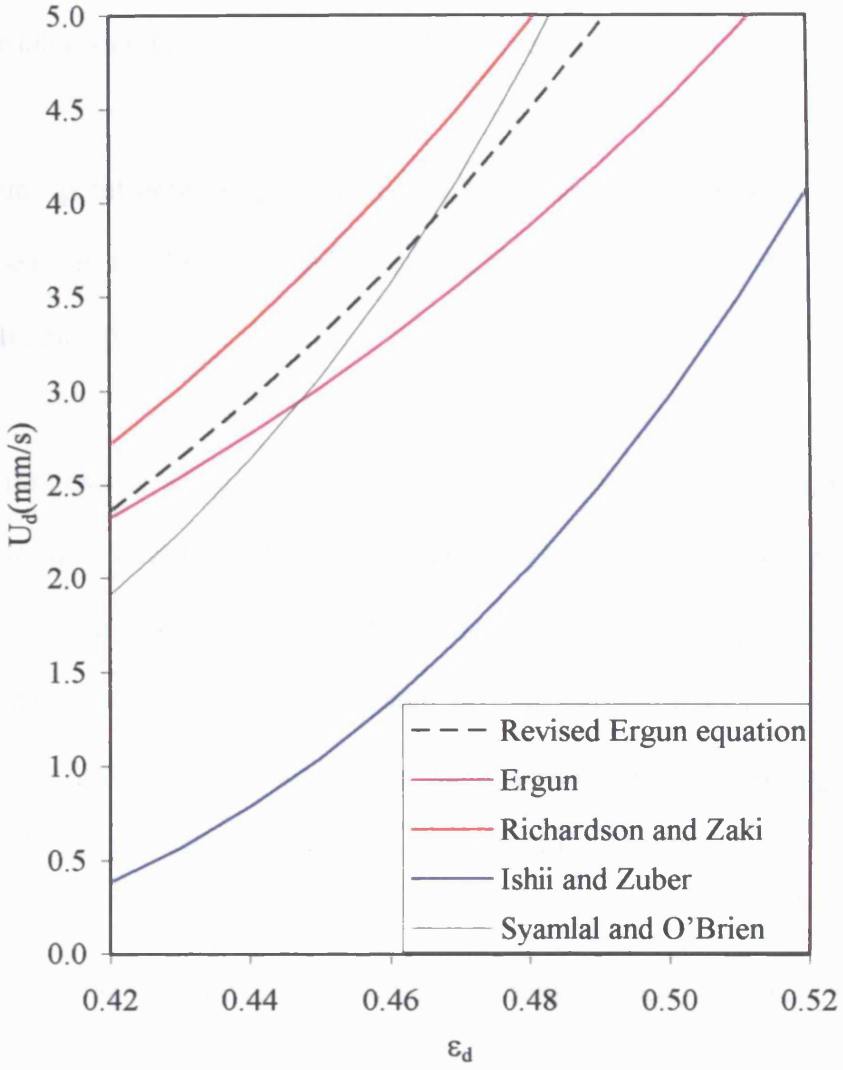

Figure 2.2 Prediction of ε_d and U_d characteristic curve using original pressure drop correlations for 45-53 μm narrow size cut powder

2.4 Prediction of the minimum bubbling point.

Geldart's group A powder at fluid velocities higher than the minimum fluidization velocity initially expand uniformly. The expanded fluidized bed is said to be stable and

is called a 'non bubbling bed'. At higher superficial velocities, the fluidized bed can become unstable and bubbles appear in the fluidized bed.

The transition point between particulate and bubbling bed is the point where the first bubble appears in the fluidized bed. At this point, the voidage of the particulate bed reaches a maximum.

This transition can be seen as a stability problem and two different approaches have appeared in the literature, differing in the physical contributions that lead to the presence of a homogeneous expanded bed. The two approaches suggest either a purely hydrodynamic contribution or the resultant of inter-particle forces. The interparticle forces are based on the assumption of the existence of sufficiently strong electrostatic, van der Waals, or capillary forces that lead to the stability of the bed.

The stability criteria, based on the hydrodynamic consideration, were first mentioned by Harrison et al. (1961), who considered the stability of the spherical cap bubble in a fluidized bed and concluded that the bed was always unstable, and that bubbles always exist in a fluidized bed. According to this approach, only when the maximum bubble size is the same order of magnitude as the particle diameter the fluidized bed appears to be homogeneous. Pigford was the first to show that any two fluid model will lead to an intrinsically unstable bed (Gibilaro, 2001) and this was reported by Jackson (1963), Murray (1965), and Pigford and Baron (1965). These authors all considered the stability of the uniform fluidization linearising the fluid dynamic equations of change for a fluidized suspension. From their analysis, a small perturbation always propagates with time and gas fluidized beds should always be bubbling beds.

Wallis (1969) developed the one dimensional wave theory for both single-phase and two-phase flows. He defined the term 'wave' as a propagation due to continuous changes in some variables and defined the term shock as a propagation due to a step change or a finite discontinuity. The most important waves, involved in the stability, are continuity and dynamic waves.

Continuity waves occur whenever there is a relationship between flow rate and concentration. The continuity waves propagate between two regions of different voidage and the equilibrium of forces is maintained on both sides of the wave and there is no inertia effect. The continuity wave velocity was proposed first by Slis et al. (1959).

$$U_{\varepsilon} = (1-\varepsilon)\frac{dU}{d\varepsilon} \qquad (2.34)$$

Slis et al. (1959) applied the Richardson and Zaki (1954) equation and obtained:

$$U_{\varepsilon} = U_t n(1-\varepsilon)\varepsilon^{n-1} \qquad (2.35)$$

Dynamic waves, on the other hand, depend on the existence of an elastic force, which will accelerate material through the wave as a result of concentration gradients.

The application of the wave theory yields the important conclusion that the fluidised bed is not always unstable if a suitable expression can be found for the elastic force terms. The stability of the flow is governed entirely by the relative magnitude of the dynamic and continuity wave velocities. If the continuity waves overtake dynamic waves, the flow is unstable.

Verloop and Heertjes (1970) were the first to apply the concept of Wallis (1969) for the stability of fluidized beds. The equation of the continuity wave velocity from Slis et al.

(1959) was applied. The equation of dynamic wave velocity was developed by considering that the particle phase has an elasticity E and the dynamic wave is then:

$$U_D = \sqrt{\frac{E}{\rho_F}} \qquad (2.36)$$

Assume that the fluidized system consists of vertical rows of particles, each individually supported by the fluid stream. A pulse given to one of the particles will be transmitted to the other particles, because of the increasing drag with decreasing distance between the particles. The transmission velocity is the longitudinal pulse velocity. By neglecting interparticle forces, the modulus of elasticity (E) can be defined by the drag coefficient-interparticle distance relation, eq. 2.37.

$$E = \frac{\Delta F_D}{\Delta x}\frac{x + d_P}{A} \qquad (2.37)$$

x = distance between particles

Under laminar flow condition, the drag force correlation of Rowe (1961) was applied.

$$U_D = \sqrt{128 d_P g \left(\frac{U_{mf}}{U}\right)^a} \qquad (2.38)$$

$a = 1$ for $Re_p < 2$

$a = 1.4$ for $2 < Re_p < 500$

Foscolo and Gibilaro (1984) considered no effect of interparticle forces, adopting the approach of Verloop and Heertjes (1970). The drag force correlation developed by Foscolo et al. (1983) was employed for the calculation of the dynamic wave velocity and the correlation from Slis et al. (1959) was applied for the continuity wave velocity. The fully predictive stability criteria for whole range of flow from laminar, intermediate and turbulent, yields:

$$\frac{\sqrt{d_p g}}{U_t}\sqrt{\frac{\rho_p - \rho_F}{\rho_p}} = 0.56 n\sqrt{1-\varepsilon}\,\varepsilon^{n-1} \qquad (2.39)$$

Foscolo and Gibilaro (1987) derived a model for the description of fluidized bed. They considered the fluidized bed as an 'inter-penetrating continuum' and presented an interpretation of the terms in the equations of change that can account for the compressibility of the particle phase where the force can be transmitted between particles for particulate behaviours without the need to include particle-particle interactions. Their two-fluid model modifies the particle momentum balance;

Momentum balance - Particle phase

$$(1-\varepsilon)\rho_P\left[\frac{\partial u_P}{\partial t} + u_P\frac{\partial u_P}{\partial z}\right] = F_D - (1-\varepsilon)\rho_P g - (1-\varepsilon)\frac{\partial p}{\partial z} - F_{FP} \qquad (2.40)$$

F_{FP} = Fluid-particle interaction force (Transmission force)

This transmission force is a function of the voidage. By considering the control volume to be large compared with the size of particles, the transmission force was added in the particle momentum balance equation. Applying the drag force correlation of Foscolo and Gibilaro (1984) and Gibilaro et al. (1985) the following expression for F_{FP} was obtained;

$$F_{FP} = -U_D^2\,\rho_P\frac{\partial \varepsilon}{\partial z} \qquad (2.41)$$

where

$$U_D = \sqrt{3.2 g d_p (1-\varepsilon)\frac{\rho_P - \rho_F}{\rho_P}} \qquad (2.42)$$

Epstein (1984) and Jean and Fan (1992) modified the buoyancy force to be based on the density of the fluid alone. Jean and Fan (1992) modified the stability criteria of Gibilaro and Foscolo (1984) as follows:

$$\frac{\sqrt{d_p g}}{U_t}\sqrt{\frac{\rho_p - \rho_F}{\rho_p}} = 0.56 n\sqrt{1-\varepsilon}\,\varepsilon^{n-0.5} \qquad (2.43)$$

Lettieri et al. (2001) generalised the particle bed model of Foscolo and Gibilaro (1987), allowing for the use of the experimentally determined values of n, the Richardson and Zaki expansion coefficient.

All these approaches include a correction term only in the particle momentum balance and this leads to a fundamental inconsistency in all these approaches. If the nature of the additional force term is a fluid-particle interaction, Newton's third law is not fulfilled.

An alternative approach is to include a stress tensor in the dense phase, resulting from interparticle cohesion forces. Rietema et al. (1967) suggested that the origin of the elasticity is to be found in the existence of interparticle forces. This work discussed the interparticle forces in terms of van der Waals forces between the two neighbouring particles. Rietema (1973) showed that interparticle forces like cohesion and friction give a fluidized bed a sufficiently stable structure. It is questionable whether this is the case for highly expanded or liquid fluidized beds. Rietema (1973) also introduces an elastic term, now as a consequence of the interparticle forces. The stability criterion is based on Wallis' analysis. The same approach was applied by Kai and Takahashi (1989).

Foscolo et al. (1985) introduced the effect of the interparticle forces into their analysis. They showed that the continuity wave velocity is unaffected, whereas the dynamic wave

velocity increases with increasing interparticle attraction. However, they pointed out that the interparticle forces can play an important role only when there are very strong interparticle forces due to deformable particles, electrostatic or strong magnetic forces.

Brandani and Astarita (1996) included magnetic forces acting on the particles in the particle bed model of Foscolo and Gibilaro. The dynamic velocity with the inclusion of the magnetic effects becomes:

$$U_D^2 = 3.2 g d_p (1-\varepsilon)\frac{\rho_P - \rho_F}{\rho_P} + \frac{18(1-\varepsilon)\chi_P^2}{[3+\chi_P+2(1-\varepsilon)\chi_P]^3}\frac{B_0^2}{\mu_0 \rho_P} \qquad (2.44)$$

where

χ_P = Particle magnetic susceptibility

μ_0 = Permeability of free space

B_0 = Mean induction

Mutsers and Rietema (1977a) introduced the interparticle forces and wall friction into the momentum balance of the dispersed phase and applied the perturbation theory to the linearized momentum equations. This leads to a stability criterion based on a dynamic equilibrium.

Kono et al. (1986a) also considered the dense phase as an elastic body and developed a model to describe the stability of the bed, based on Wallis' analysis, with the inclusion of interparticle adhesion forces. The tensile strength, which represents the particle cohesive force developed by the authors, was applied to formulate the dynamic wave velocity and the viscous term in Ergun equation was used for the continuity wave velocity.

Brandani and Zhang (2004) derived a new model for the description of fluidized bed, which resolves the fundamental inconsistency of the Foscolo and Gilibaro particle bed model (Foscolo and Gibilaro, 1987). The equations of change are those of a two fluid model, but both the fluid and particle momentum balances are modified as shown below.

Fluid phase

$$\varepsilon\rho_F\left[\frac{\partial u_F}{\partial t}+u_F\frac{\partial u_F}{\partial z}\right]=-F_D-\varepsilon\rho_F g-\varepsilon\frac{\partial p}{\partial z}+F_{FP}+F_{FAve} \qquad (2.45)$$

Particle phase

$$(1-\varepsilon)\rho_P\left[\frac{\partial u_P}{\partial t}+u_P\frac{\partial u_P}{\partial z}\right]=F_D-(1-\varepsilon)\rho_P g-(1-\varepsilon)\frac{\partial p}{\partial z}-F_{PP}-F_{FP}-F_{PAve} \qquad (2.46)$$

The model is derived from the two-fluid formulation and the inclusion of the effect of the finite size of the particles. F_{PP} are additional particle-particle interactions; F_{FP} are additional fluid-particle interactions; F_{Ave} are additional terms that result from averaging body forces over the finite dimension of the particles.

Brandani and Zhang (2004) argue that the term F_{PP} becomes dominant when the bed voidage is close to that of the fixed bed or when the velocity of the fluid is less than the minimum fluidization velocity. Once the bed is fluidized, F_{PP} becomes negligible and is not considered in the determination of the minimum bubbling criterion.

The averaging procedure over a characteristic length 2δ, where δ should be of the order of the particle diameter, leads to the following terms

$$\bar{F}_D=F_D+\delta\frac{\partial F_D}{\partial z} \qquad (2.47)$$

$$\bar{\varepsilon} = \varepsilon + \delta \frac{\partial \varepsilon}{\partial z}$$

To simplify their model, Brandani and Zhang (2004) introduce the quasi-equilibrium approximation which was applied in order to obtain the derivative of the drag force. Based on the quasi-equilbrium approximation, all quantities are a function of the void fraction and the derivative can be calculated at equilibrium.

$$\frac{\partial F_D}{\partial z} \approx \left(\frac{\partial F_D}{\partial \varepsilon} \right)_{Equil} \frac{\partial \varepsilon}{\partial z} \qquad (2.48)$$

At equilibrium eq. 2.14 holds and

$$\frac{\partial F_D}{\partial z} \approx (1-2\varepsilon)(\rho_p - \rho_F) g \frac{\partial \varepsilon}{\partial z} \qquad (2.49)$$

and the particle momentum balance becomes

$$\begin{aligned} (1-\varepsilon)\rho_P \left(\frac{\partial u_P}{\partial t} + u_P \frac{\partial u_P}{\partial z} \right) &= F_D - (1-\varepsilon)\rho_P g - (1-\varepsilon)\frac{\partial p}{\partial z} \\ &+ \delta[2(1-\varepsilon)\rho_P + (2\varepsilon - 1)\rho_F] g \frac{\partial \varepsilon}{\partial z} \end{aligned} \qquad (2.50)$$

while the fluid momentum balance becomes

$$\begin{aligned} \varepsilon \rho_F \left(\frac{\partial u_F}{\partial t} + u_F \frac{\partial u_F}{\partial z} \right) &= -F_D - \varepsilon \rho_F g - \varepsilon \frac{\partial p}{\partial z} \\ &- \delta[(1-2\varepsilon)\rho_P + 2\varepsilon \rho_F] g \frac{\partial \varepsilon}{\partial z} \end{aligned} \qquad (2.51)$$

To obtain the minimum bubbling criterion the equations of change are linearized and the drag force correlation of Gibilaro (2001) was used.

$$F_D = \frac{3}{4} \frac{\rho_F}{d_P} C_D U^2 (1-\varepsilon) \varepsilon^{-3.8} \qquad (2.52)$$

Where C_D is calculated from the Dallavalle (1948) equation.

Following Wallis (1969) the criterion of minimum bubbling is expressed in terms of the continuity and dynamic wave velocities:

$$U_{\varepsilon} = U_{D} \qquad (2.53)$$

where

$$U_{\varepsilon} = (1-\varepsilon)\left(\frac{\partial U}{\partial \varepsilon}\right)_{Equil} = \frac{1-\varepsilon}{\varepsilon}\frac{4.8U}{2+\frac{dC_D}{dRe_p}\frac{Re_p}{C_D}} \qquad (2.54)$$

and the dynamic wave is given by

$$U_{D} = \sqrt{V^2 - G} + V \qquad (2.55)$$

$$V = \frac{1-\varepsilon}{\varepsilon}\frac{\rho_F U}{\varepsilon\rho_P + (1-\varepsilon)\rho_F}$$
$$G = \frac{\frac{1-\varepsilon}{\varepsilon^2}\rho_F U^2 - \delta[(1-\varepsilon)\rho_P + \varepsilon\rho_F]g}{\varepsilon\rho_P + (1-\varepsilon)\rho_F} \qquad (2.56)$$

A further aim of this study is to validate the minimum bubbling criterion of Brandani and Zhang (2004) with the powders used in this work, that are non cohesive. Therefore, the influence of the inter-particle force on the bed expansion behaviour and the minimum bubbling point should be negligible.

Although other correlations for the minimum bubbling point exist in the literature, such as that of Abrahamsen and Geldart (1980a), these will not be used in the present study, because the emphasis will be on correlations that can be used in CFD simulations of fluidized beds. Therefore, the stability criterion developed by Brandani and Zhang (2004) is used to describe the minimum bubbling point of the powders studied, since the experimental results on the narrow size-cut powders and the appropriate drag force

correlation can be used to examine the voidage dependency of the characteristic length, δ, of this model.

Chapter 3: Materials and Methods

3.1 Introduction

In this study, the fluidization characteristics of different sizes of powders belonging to group A of the Geldart classification were investigated using the fluidization and de-fluidization experiments and the 1-valve and 2-valve bed collapse experiments. The fluidization and de-fluidization experiments allow us to observe fluidization properties obtained from the measurement of pressure-drop, while the 1-valve and 2-valve bed collapse experiments are carried out to observe the bed expansion behaviour and to determine the properties of the dense phase in a bubbling bed.

In this Chapter the properties of the materials and the full description of the experimental apparatus will be presented. While the interpretation of the fluidization and de-fluidization experiments is straightforward, the correct analysis of the 1-valve and 2-valve bed collapse experiments will require the formulation of an appropriate model, which will be presented in Chapter 4.

3.2 Experimental set-up

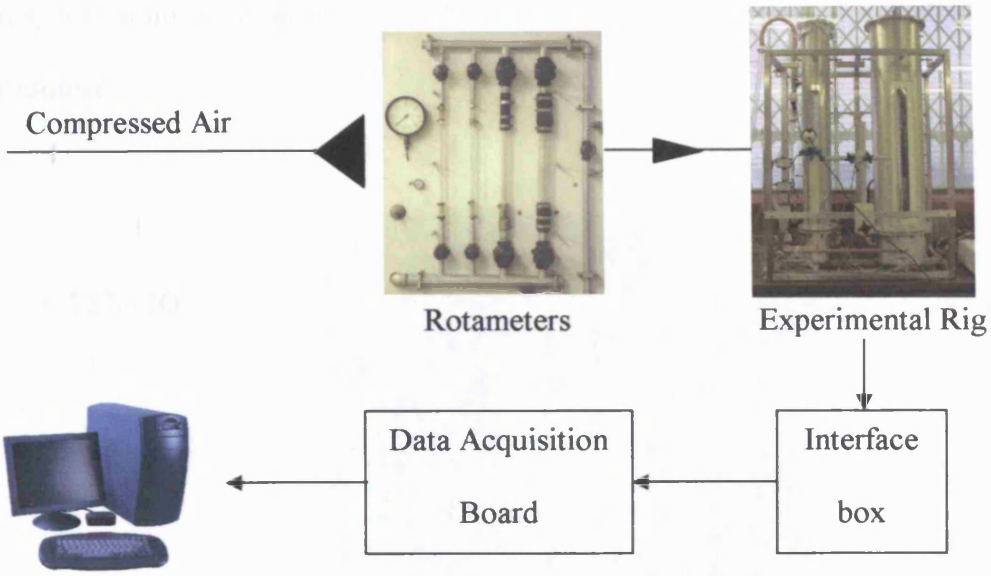

Figure 3.1Experimental set-up

Figure 3.1 shows a schematic diagram of the connections of the experimental set-up. The compressed air is fed to the rotameter, which is used to control the air flow rate. The fluidized beds are instrumented with pressure ports and a lateral window for direct visual observation of the fluidization dynamics is present. The pressure readings are recorded via an interface box connected to the data acquisition board of the computer, which is also used to obtain digital films of the bed dynamics.

3.2.1 Fluidization beds

Figure 3.2 shows the two columns used for the fluidization experiments reported in Chapter 5. The column diameters are 0.127m ID and 0.243 m ID and were used to ensure that the experimental results are independent of the column size. After an initial

validation of this assumption, most of the experiments were carried out in the smaller 0.127 m ID column, since, especially for the experiments with the narrow particle size cuts, less solid material is required and for the same superficial velocity less gas is consumed.

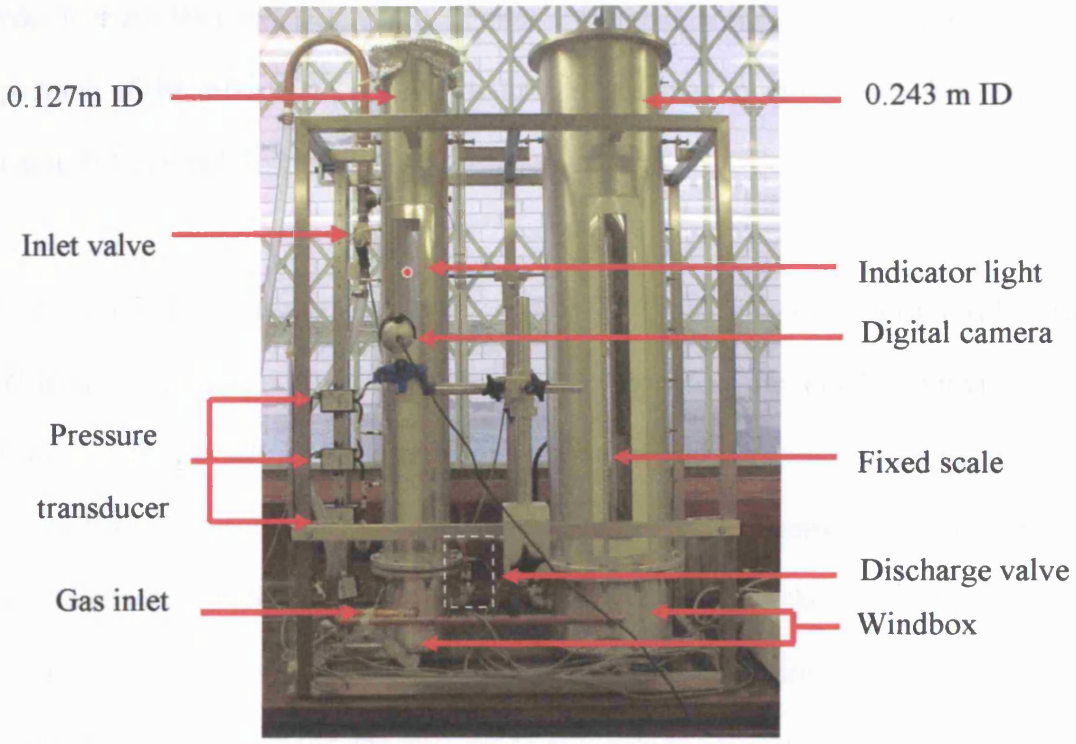

Figure 3.2 Experimental apparatus

From Figure 3.2, it is possible to see that the system is equipped with a three-way valve (solenoid type), the inlet being connected to the rotameter and one outlet is connected to vent and the other to the windbox of the fluidized bed. A discharge valve (solenoid type) is also connected to the windbox in order to allow the operation of the bed collapse experiment in which the air residue is vented, i.e. the 2-valve experiment. To eliminate any powder loss from the fluidized bed, a second distributor plate is placed at the top of the column.

The inlet valve, the discharge valve and an indicator light are controlled by the interface box. The inlet valve is switched between feeding the windbox and venting to air, while a synchronous control opens the discharge valve and turns on the indicator. When carrying out visual observations, the indicator is placed in the view of the digital camera in order to mark the exact start of the experiment. The data logging system records also the position of the valve and the pressure data are obtained in spreadsheet form through the Labtech Notebook software.

A linear scale is fixed next to the window and has been calibrated with a rigid ruler. The signal from the web cam of the computer is recorded using the windbox movie maker software, which also allows the control of the camera and the frame by frame analysis. To measure the bed pressure drop, pressure transducers are connected to the windbox and the freeboard, which is typically at 0.70 m or 0.80 m above the distributor and well above the top surface of the bed of the particles. In addition, pressure transducers are also mounted vertically along the column to measure the vertical differential pressure drop profile from 0.05 m to 0.60 m above the distributor; with a probe spacing of 0.10 m. The exact dimensions of the pressure ports, as well as those of the columns will be summarised in section 3.2.2.

3.2.2 Dimension of the fluidization column

- Column diameter

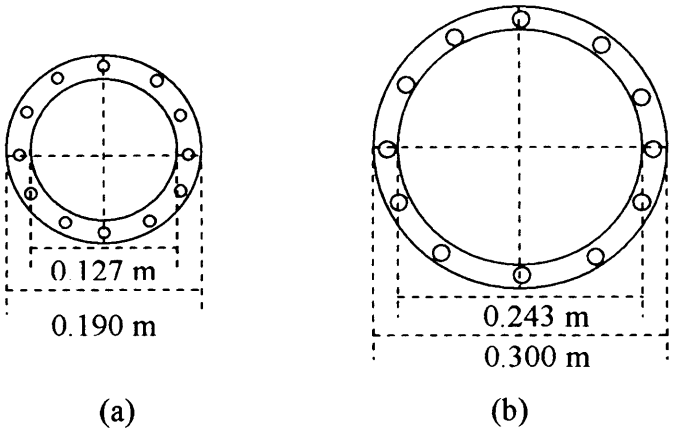

Figure 3.3 Inside diameter of columns (a) 0.127 m ID and (b) 0.243 m ID

- Winbox dimensions

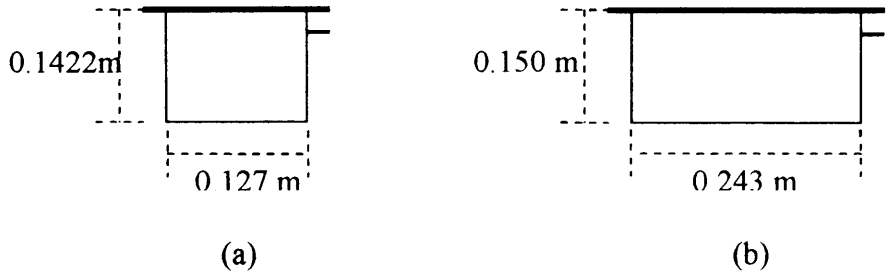

Figure 3.4 Winbox dimension for (a) 0.127 m ID and (b) 0.243 m ID

- Probe locations – relative distances.

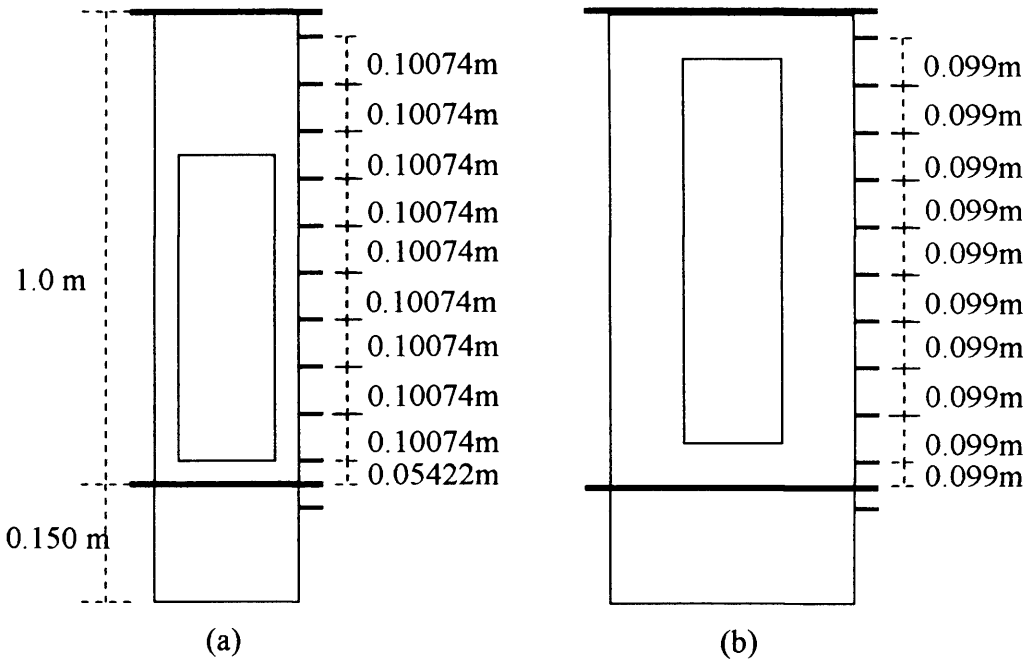

Figure 3.5 Probe locations for (a) 0.127 m ID and (b) 0.243 m ID

- Offset of the window from the inner wall of the column

The viewing windows are made of Plexiglas and their thickness is slightly less than that of the column walls. For the 0.127 m ID column, the front window plate leaves a gap of approximately 0.003 m and the back window plate is lined up with the column wall. For the 0.243 m ID column, the front and the back plates are off approximately by 0.002 m. These exact dimensions become important when comparing the pressure drops in the two columns.

The dimension of the window (inner wall side) is shown in Figure 3.6.

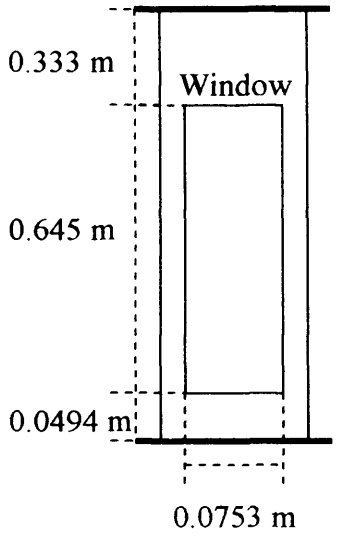

Figure 3.6 Dimension of the window from the inner wall of the column

- Fixed scale calibration

On applying the tape scale on the side of the column it is difficult to stretch the scale exactly and for accurate measurements a rigid ruler was used as a calibration. Correction factors of 0.998 and 0.99 have to be applied to the readings for the 0.127 m ID and the 0.243 m ID column respectively.

3.2.3 Rotameters

With reference to Figure 3.7, only the 3 rotameters named A, B, and C were used in this study. At room temperature and atmospheric pressure, the range of the air flow rates of rotameters A, B, and, C are 0-8 L/min, 0-40 L/min and 0-230 L/min respectively.

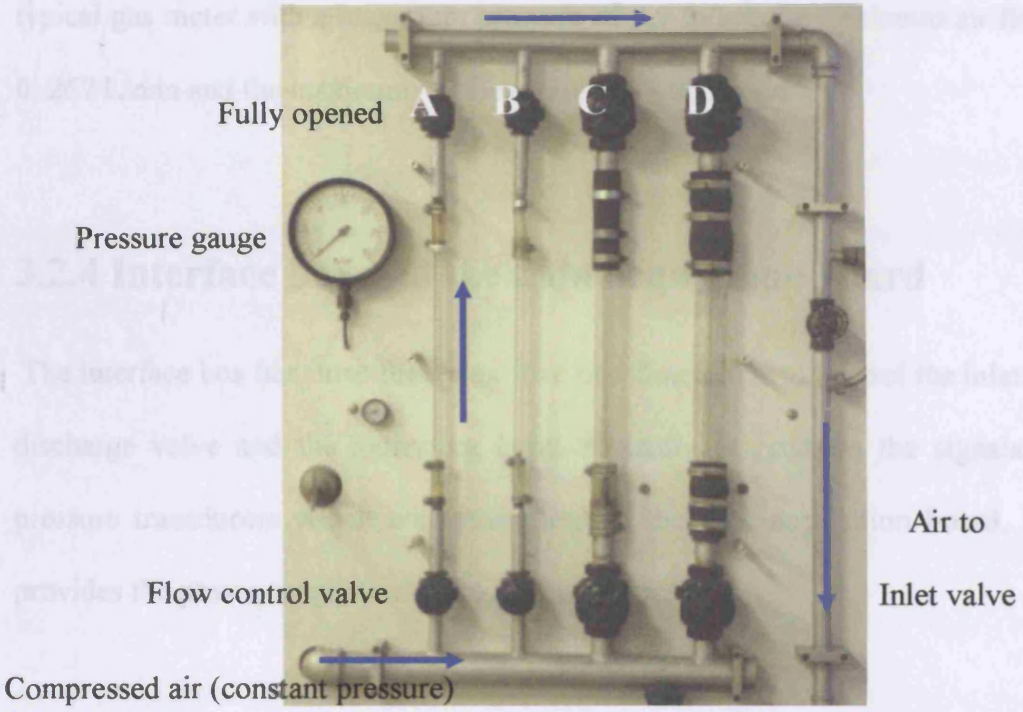

Figure 3.7 Rotameters utilised in this work

At zero flow rate, all the flow control valves (bottom valve) and the top valves are closed, except the one of the rotameter in use, which is fully opened. The compressed air available from the main supply is at 100 lb/in^2, with a relative humidity at room temperature of approximately 60% as measured by a wet bulb thermometer. During the experiments the pressure at the inlet of the rotameter was reduced to 20 lb/in^2.

At different air flow rates, the control valve is regulated until the float is stable and the rotameter scale is read at the top rim of the float. In addition, at each air flow rate, the pressure drop from the pressure gauge, representing the pressure loss from the inside the rotameter to the windbox, is also recorded.

The rotameter flows were calibrated using a volumetric air flow meter. The meter is a typical gas meter with a maximum pressure of 2.9 lb/in^2, the minimum air flow rate of 0. 267 L/min and the maximum air flow rate of 41.66 L/min.

3.2.4 Interface box and the data acquisition board

The interface box has three functions. The first function is to control the inlet valve, the discharge valve and the indicating light. Secondly, it receives the signals from the pressure transducers which are transmitted to the data acquisition board. Finally, it provides the power supply to the pressure transducers.

3.3 Materials

3.3.1 Powders

The glass ballotini were purchased from Guyson International Limited. The glass ballotini was used in this study because of the standard properties of this material, which are non-porous, spherical and non-cohesive. Therefore, the uncertainty due to porosity, shape irregularity and particle cohesion will have no influence on the fluidization characteristics, studied. This also yields more reliable results needed to validate the theoretical models.

The size range of the ballotini is between 22 to 106 μm. As mentioned in Chapter 1, this covers the whole range of Geldart's Group A powders at this density.

From the "natural" size distribution obtained from the manufacturer, powders of narrow size cuts and bimodal mixtures were prepared and studied. The detailed discussion of the particle size analysis, as well as the particle density measurements is given in Appendix A. The sieve analysis as well as the laser light scattering method is used for the size analysis, while the density bottle using distilled water as a medium is used for the density measurement.

Four different average sizes of the natural size distribution powders were studied. They are 37 μm, 46 μm, 72 μm and 89 μm. For 37 μm, two batches were used, namely 37 μm (Batch 1) and 37 μm (Batch 2). The particle size distributions of these powders are shown in Figure A1 to A5 in appendix A. The Summary of the powder properties is shown in Table 3.1. For this natural size distribution, the powder contains particles of the adjacent sieve size cut. In other words, the powder contains the particles of adjacent size and the mixture is continuously dispersed.

Table 3.1 Properties of ballotini powder with natural size distribution

d_p (μm)	Density (kg/m^3)	Shape	% fines	Dispersion
37 (batch 1)	2480	Sphere	64	Poly dispersion
37 (batch 2)	2480	Sphere	62	Poly dispersion
46.61	2480	Sphere	44	Poly dispersion
72	2480	Sphere	0	Poly dispersion
89	2480	Sphere	0	Poly dispersion

To study the effect of each individual size cut on the powders with a natural size distribution, the powders were classified using sieving, according to the standard $2^{1/4}$ consecutive sieve aperture series. Based on the sieve analysis of the natural size powders, these original powders were classified into six narrow size cuts, which are 0-45 μm, 45–53μm, 53-63μm, 63-75μm, 75-90μm and 90-106μm. The particle size distributions of these powders are shown in Figure A6 to A11 in appendix A. The summary of the powder properties is shown in Table 3.2.

Table 3.2 Properties of ballotini powder with narrow size cut

d_p (μm)	Size range (μm)	Density (kg/m^3)	shape	% fine	dispersion
33.50	0-45	2480	Sphere	100.0	Poly dispersion
45.10	45-53	2480	Sphere	7.5	Mono dispersion
55.08	53-63	2480	Sphere	0	Mono dispersion
68.41	63-75	2480	Sphere	0	Mono dispersion
81.81	75-90	2480	Sphere	0	Mono dispersion
97.82	90-106	2480	Sphere	0	Mono dispersion

Finally, bimodal mixtures of different narrow size cut were prepared in such a way that two narrow size powders of different size by three consecutive sieve sizes were mixed in a varied percentage. As a consequence, mixtures of 106-90 μm and 53-45 μm were prepared, as well as mixtures of 90-75 μm and 45-0 μm (Fines). This is to study behaviour of the bimodal mixture, in comparison with the narrow size cut and the natural size powder. For the later bimodal mixture, the effect of fines will be studied in comparison with the narrow size cut powders and the natural size powder. The

summary of the powder properties is shown in Table 3.3. At the start of experiments using the mixed powders, a high gas flowrate is used to ensure proper mixing.

Table 3.3 Properties of ballotini powder with mixed size cut

d_p (μm)	Size range (μm)	Density (kg/m^3)	shape	% fine	dispersion
60.21	25%(0-45)+75%(75-90)	2480	Sphere	25	Bimodal
47.57	50%(0-45)+50%(75-90)	2480	Sphere	50	Bimodal
39.31	75%(0-45)+25%(75-90)	2480	Sphere	75	Bimodal
75.70	25%(45-53)+75%(90-106)	2480	Sphere	0	Bimodal
61.74	50%(45-53)+50%(90-106)	2480	Sphere	0	Bimodal
52.13	75%(45-53)+25%(90-106)	2480	Sphere	0	Bimodal

3.3.2 Distributor characteristics

The distributor has the important function of ensuring a uniform gas flow at the inlet of the fluidized bed. This can greatly influence the bubbling properties and the structure of the bed.

There are two types of distributors: porous plates and perforated devices. Porous plates are typical in small scale applications and ensure a very uniform gas inlet condition. Perforated devices are widely employed in industrial equipment, due to the ease of scale-up and the reduced pressure drop. The drawbacks of the perforated devices are the presence of stagnant zones and the solids attrition caused by gas jet formation.

On selecting a distributor, the most important consideration is that it should distribute the gas uniformly, and should not induce excessive resistance to the gas flow. In addition, the distributor chosen should prevent solids loss by leakage, minimize solid erosion and avoid choking.

A bronze sintered distributor, with 0.050 m thickness was used in the experimental set-up. In order to investigate the distributor porosity effect on fluidization properties, two average pore sizes were used: a 7 μm average pore size with a permeability constant of $2.5*10^{-8}$ cm^2 and a 35 μm average pore size with permeability constant of $30*10^{-8}$ cm^2. The theoretical distributor pressure drop can be calculated from:

$$\Delta P_{Dist} = \frac{Q \mu_F \lambda_d}{\Phi A} \qquad (3.1)$$

ΔP_{Dist} is the distributor pressure drop; Q is the air flow rate, A is the distributor cross section area; Φ is the permeability constant and λ_d is the thickness of the distributor.

It should be noted here that the permeability constant is the ability of a porous material to pass gas or liquid on application of a differential pressure, under the condition of viscous flow.

3.3.3 Pressure transducer

The pressure transducers used in this study are series 851 and 860 pressure transducers from AutoTran Incorporated. The electronic signal from the pressure transducer is 0-5 volts and this voltage signal is converted into kPa pressure units using a calibration. The locations, the pressure range, the data logging frequency, and, the input/output channel are shown in Table 3.4.

Table 3.4 Pressure transducer information

Pressure transducer	Mode (absolute or differential)	Location from distributor (m)	Pressure range (kPa)	I/O channel	Data logging freq(Hz)
A	Absolute	-0.05 m (Windbox)	0-13.79	8	90/15
H	Differential	0.05-0.15	+/-3.45	2	90/15
E	Differential	0.15-0.25	+/-1.49	3	90/15
F	Differential	0.25-0.35	+/-1.49	4	90/15
G	Differential	0.35-0.45	+/-1.49	5	90/15
B	Differential	0.45-0.50	0-1	6	90/15
C	Absolute	0.65	+/-0.50	7	90/15
D	Absolute	0.75	0-1	1	90/15

3.3.4 Web cam digital camera and the movie maker software

The web cam, Logitech QuickCam Pro4000 with a resolution of 640 by 680 video pixels was used in this study. The digital camera was controlled using the Windows Movie Maker software. The acquisition speed is set at 30 frames/s, but while the

program allows grabbing pictures at the speed of 30 frames /sec, the frame analysis can be carried out only every 3 frames. This system allows the determination of 10 points/s, which is perfectly adequate for bed collapse experiments but accuracy and frequency of this measurement does not allow the statistical analysis of bed surface fluctuations.

3.3.5 Data acquisition program

The Labtech Notebook data acquisition software used converts the analogue signal from the pressure transducers according to:

$$\Delta P(kPa) = Scale * (volts) + offset \qquad (3.2)$$

The pressure transducers are calibrated with a water U-tube manometer. By using a T-connection, both the pressure transducer and the manometer are connected to the pressure port located at the windbox. At different air flow rates, the distributor pressure drops, read from the pressure transducer and the manometer are recorded. The calibration curves are shown in the Appendix B.

The conversion factors used for each pressure transducer and inserted in the data acquisition software are reported in Table 3.5.

Table 3.5 Conversion factor

Name	Input/output channel	Pressure range (kPa)	Conversion factor	
			Scale	Offset
A	8	0-13.79	3.447	-3.447
H	2	+/-3.45	1.724	-5.171
E	3	+/-1.49	0.7464	-2.2392
F	4	+/-1.49	0.7464	-2.2392
G	5	+/-1.49	0.7464	-2.2392
B	6	0-1	0.2488	-0.2488
C	7	+/-0.50	0.2488	-0.7464
D	1	0-1	0.2488	-0.2488
Indicating light	0	-	1	0

3.4 Experimental methods

3.4.1 Rotameter calibration

1. Calibration of rotameter A, using the airflow meter.

- Connect air inlet tube to the air flow meter
- At each rotameter scale, measure volume of air passing through the meter in a given period of time and read the rotameter pressure gauge.
- Assuming that the pressure drop inside the meter is negligible, volumetric flow rate of air is at atmospheric condition (Q_{atm}) and the pressure reading from rotameter pressure gauge is the pressure drop inside the rotameter (ΔP_{rota})
- Rotameter scale versus Q_{atm} is the rotameter A characteristic (Figure 3.8)

2. Calibration fine distributor in 0.243 m ID column

- Empty the column
- Connect the air inlet tube to the windbox
- Make sure that inlet valve is opened and discharge valve is closed
- At different rotameter scales for A, B and C, record the distributor pressure drop (ΔP_{Dist}), using the pressure transducer at the windbox.
- Plot ΔP_{Dist} versus Q_{atm} from rotameter A and the mathematical correlation can be obtained (Figure 3.9)

3. Calibration of rotameter B and C

- Disconnect the inlet tube from the windbox
- At different rotameter scale, record the pressure from the rotameter pressure gauge. This is the pressure drop inside the rotameter (ΔP_{rota}) B and C.
- From Figure 3.9 and the ΔP_{Dist} of rotameter B and C, Q_{atm} versus rotameter scale of B and C can be obtained.

The rotameter characteristic curve is the graph of rotameter scale versus Q_{atm} and of rotameter scale versus ΔP_{rota}. These can be seen in Appendix C.

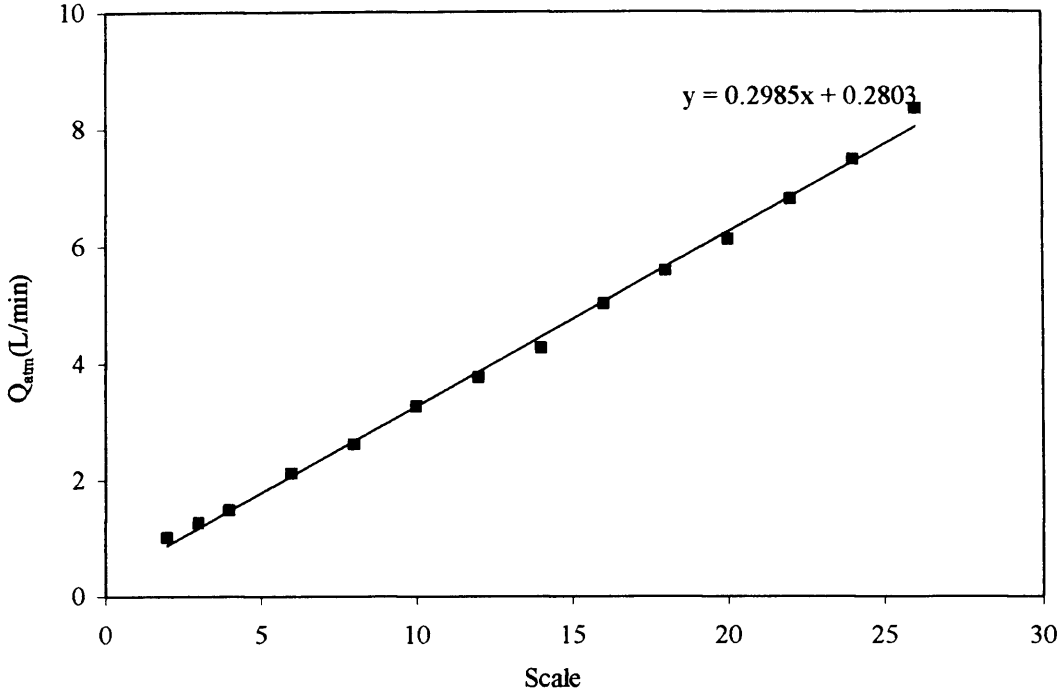

Figure 3.8 Rotameter A characteristic curve

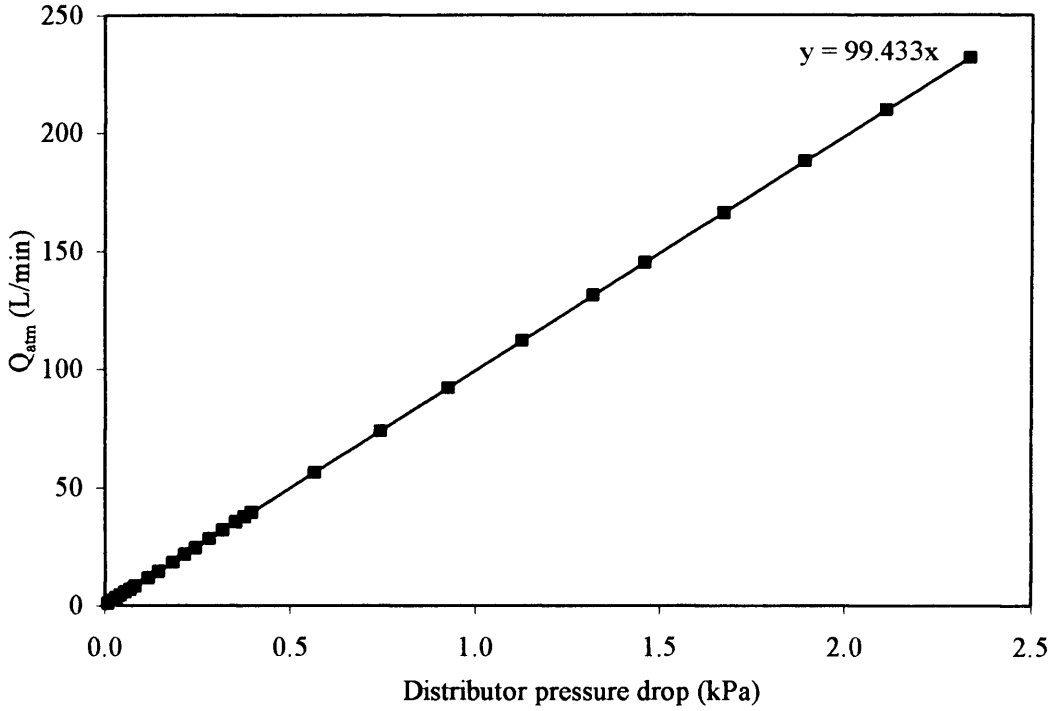

Figure 3.9 Fine distributor pressure drop in 0.243 m ID versus the atmospheric air flow rate from rotameter A

3.4.2 Distributor calibration

- Empty the column
- Connect the air inlet tube to the windbox
- Make sure that inlet valve is opened and discharge valve is closed
- At different rotameter scale A, B and C, record the distributor pressure drop (ΔP_{dist}), using the pressure transducer at the windbox.
- Record the pressure reading at the rotameter pressure gauge, which is now pressure drop inside rotameter and windbox ($\Delta P_{rota+windbox}$).
- Convert Q_{atm} to windbox air flowrate ($Q_{windbox}$)

$$Q_{windbox} = Q_{atm} \frac{14.7}{(14.7 + \Delta P_{windbox+rota} - \Delta P_{rota})} \qquad (3.3)$$

- Plot ΔP_{dist} versus $Q_{windbox}$

Distributor characteristic curves can be seen in Appendix C.

3.4.3 Discharge valve calibration

- Empty the column.
- Connect the air inlet tube to the windbox.
- Make sure that inlet valve is opened and discharge valve is opened
- At different rotameter scale A, B and C, record the distributor pressure drop (ΔP_{dist}), using the pressure transducer at the windbox.
- Record the pressure reading at the rotameter pressure gauge, which is now pressure drop inside rotameter and windbox ($\Delta P_{rota+windbox}$).
- Convert Q_{atm} to windbox air flowrate ($Q_{windbox}$)

$$Q_{windbox} = Q_{atm} \frac{14.7}{(14.7 + \Delta P_{windbox+rota} - \Delta P_{rota})} \quad (3.4)$$

- Use the distributor characteristic curves to calculated air flow rate passing distributor (Q_d)
- Calculate the air flow rate passing discharge valve (Q_v)

$$Q_v = Q_{windbox} - Q_d \quad (3.5)$$

- Plot ΔP_{dist} versus Q_v

Discharge valve characteristic curves can be seen in Appendix C.

3.4.5 Fluidization experiments

A fluidization experiment is carried out by varying the inlet gas superficial velocity from zero velocity up to approximately 4-8 times the minimum bubbling velocity. At each velocity, the total bed heights, the pressure drops in the windbox and in the freeboard, and the vertical differential pressure drop profiles were recorded.

With regard to the total bed height, the calibrated scale fixed next to the column's window was used to indicate the height. The pressure drops in the windbox and the freeboard and the vertical differential pressure drop profiles were recorded over 90 sec with the data logging frequency of 15 Hz or 90 Hz.

3.4.6 De-fluidization experiments

A de-fluidization experiment is then carried out by reducing the inlet superficial gas velocity from approximately 4-8 times the minimum fluidization velocity to zero.

Likewise, the total bed heights, the pressure drops in the windbox and the freeboard, and the vertical differential pressure drop profiles were recorded.

3.4.7 Bed collapse experiments

Two modes of the bed collapse experiments were carried out, termed '1-valve experiment' and '2-valve experiment' respectively.

For the 1-valve experiment, the bed of particles is fully fluidized at a certain inlet superficial gas velocity. Then, the inlet valve is suddenly shut, which is synchronized with the switching on of the indicator light bulb. After this, the bed surface will collapse until all particles are at rest and the bed collapse process finishes. In this case the windbox is not vented and any residual gas escapes through the collapsing bed.

For the 2-valve experiment, the bed of particles is fluidized as before. However, once the inlet valve is shut down, the discharge valve, together with the indicator light bulb, is synchronized to be turned on. Similarly, the bed surface collapses until the settlement of all particles is reached. In this case the gas can escape the bed both from the top and from the windbox.

During the experiment, the variation with time of the bed height, the pressure drop in the windbox and freeboard, and the vertical differential pressure drop profile was continuously recorded using the web cam digital camera and the differential pressure transducers. In practice, the recording of the bed height is started 5 seconds before energizing the valves, while the pressure measurement is started 15-20 seconds before.

After energizing the valves, the recording of the bed height is carried out until the end of the bed collapse process, while the pressure signals are recorded for 70-75 seconds, which ensures that the flow of gas has reached completion within the recording time.

The bed collapse experiment is generally used to study to dense phase properties. Figure3.10 shows the bed collapse curve from 1-valve and 2-valve experiment for 46 μm natural size powders, $U_0 < U_{mb}$. The collapse curves from 1-valve and 2-valve behave differently. However, these should yield one set of the dense phase properties. In Chapter 4, a new model for the interpretation of both these experiments is developed, which can be used to interpret the bed collapse curve and return the intrinsic properties of the dense phase, which are independent of the system configuration

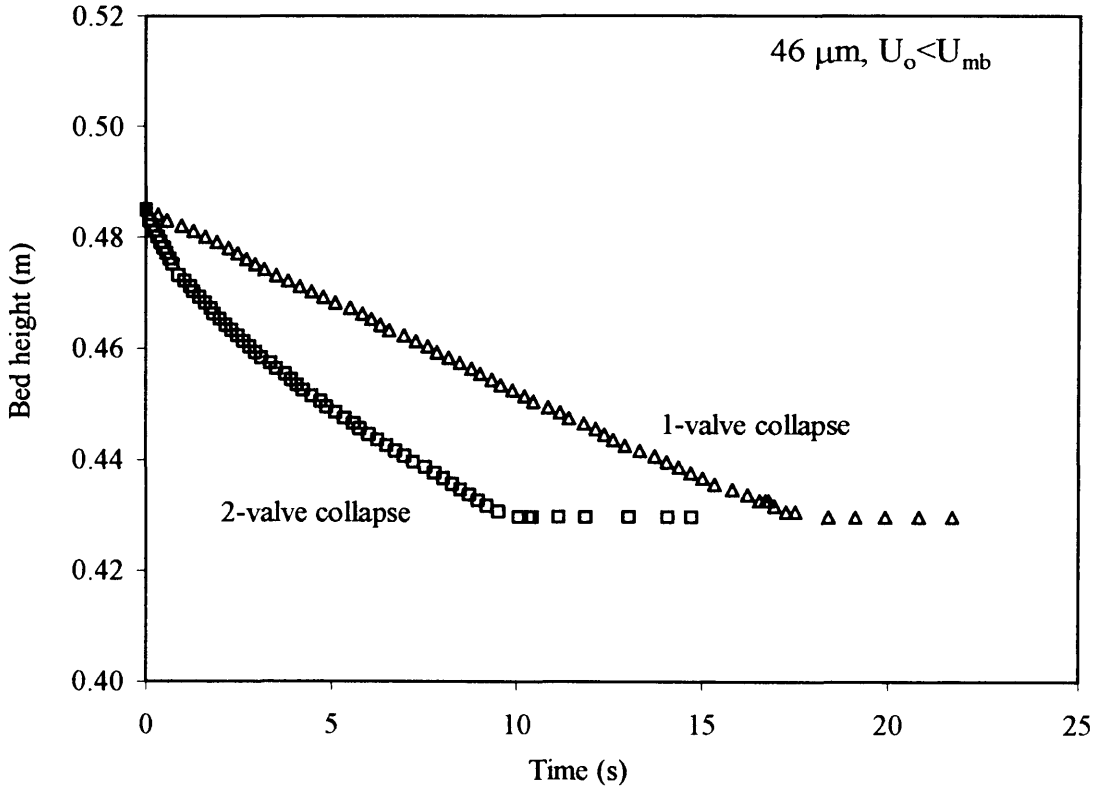

Figure3.10 Bed collapse curves from 1-valve and 2-valve experiment, 46 μm natural size powder, $U_o<U_{mb}$

3.5 Parameter calculations

Prior to obtaining the finalised fluidization properties, some parameters, which are the column cross section area, the windbox volumetric flow rate, the windbox inlet superficial velocity, corrected bed height, bed voidage, and total bed height, need to be calculated from the raw experimental results. The parameter calculations are as follow;

For 0.127 m ID

- Column cross sectional area

$$\text{Area} = \pi\frac{0.127^2}{4} + (0.0753 * 0.003) \qquad (3.6)$$

- Windbox volumetric flow rate

$$Q_{windbox} = Q_{atm}\frac{14.7}{(14.7 + \Delta P_{windbox+rota} - \Delta P_{rota})} \qquad (3.7)$$

- Windbox inlet superficial velocity

$$U_o = \frac{Q_{windbox}}{\text{Area}} \qquad (3.8)$$

- Corrected bed height

$$\text{Corrected\_bed\_height(L)} = L_{reading} * \text{correction\_factor} \qquad (3.9)$$

- Bed voidage (from corrected bed height)

$$\varepsilon = 1 - \frac{W_p}{\rho_p[(\pi\frac{(0.127)^2}{4}L) + ((L - 0.04941) * 0.0753 * 0.003)]} \qquad (3.10)$$

- Total bed pressure drop

The total bed pressure drop can be backed out from the windbox pressure drop using the following expression.

$$\Delta P = \Delta P_{windbox} - \Delta P_{freeboard} - A_{bottmdist} \cdot Q_{windbox} \quad (3.11)$$

ΔP = Total bed pressure drop (kPa)

$\Delta P_{windbox}$ = Piezometric windbox pressure drop (kPa)

$\Delta P_{freeboard}$ = Freeboard pressure drop (kPa)

$A_{bottmdist}$ = Bottom distributor pressure drop coefficient (kPa.min/L)

For 0.243 m ID

- Column cross section area

$$\text{Area} = \pi \frac{0.243^2}{4} + (0.07 * 0.004) \quad (3.12)$$

- Windbox volumetric flow rate

$$Q_{windbox} = Q_{atm} \frac{14.7}{(14.7 + \Delta P_{windbox+rota} - \Delta P_{rota})} \quad (3.13)$$

- Windbox inlet superficial velocity

$$U_o = \frac{Q_{windbox}}{\text{Area}} \quad (3.14)$$

- Corrected bed height

$$\text{Corrected\_bed\_height}(L) = L_{reading} * \text{correction\_factor} \quad (3.15)$$

- Bed voidage (from corrected bed height)

$$\varepsilon = 1 - \frac{W_p}{\rho_p[(\pi \frac{(0.243)^2}{4} L) + ((L - 0.04941) * 0.07 * 0.004)]} \quad (3.16)$$

- Total bed pressure drop

$$\Delta P = \Delta P_{windbox} - \Delta P_{freeboard} - A_{bottmdist} \cdot Q_{windbox} \quad (3.17)$$

The last terms in the RHS of eqs 3.6 and 3.12 take into account the small area associated with the windows that are not perfectly aligned with the walls.

3.6 Summary of the experiment conditions

In conclusion, experimental studies on the fluidization characteristic of powders, belonging to Geldart's Group A powder, were carried out on the natural size powders, the narrow size cut powders, and the bimodal mixture powders, In addition to these experiments, the effects of the column diameter, the distributor porosity and the initial bed height on the fluidization characteristic of the same powder were also investigated. The summaries of the experimental conditions are reported in Table 3.6 to Table 3.10.

Table 3.6 Experimental conditions for the study of the effect of the initial bed height and the column diameter on the fluidization properties

d_p (μm)	Dispersion	ID (m)	L_i (m)	W_p (kg)	Distributor type		U_o (mm/s)
					Top	Bottom	
37(B1)	Poly dispersion	0.127	0.40	7.7971	Fine	Fine	0-8Umb
			0.30	5.4022	Fine	Fine	0-8Umb
		0.243	0.40	28.4350	Coarse	Fine	0-8Umb
			0.30	19.3876	Coarse	Fine	0-8Umb
72	Poly dispersion	0.127	0.40	7.7971	Fine	Fine	0-8Umb
			0.30	5.4022	Fine	Fine	0-8Umb
		0.243	0.30	19.3876	Coarse	Fine	0-8Umb
37(B2)	Poly dispersion	0.127	0.40	7.7971	Fine	Fine	0-8Umb
			0.30	5.4022	Fine	Fine	0-8Umb

Table 3.7 Experimental conditions for the study of the effect of the distributor porosity on the fluidization properties

d_p (μm)	Dispersion	ID (m)	L_i (m)	W_p (kg)	Distributor type		U_o
					Top	Bottom	
72	Poly dispersion	0.127	0.30	5.4022	Fine	Fine	0-8Umb
			0.30	5.4022	Coarse	Coarse	0-8Umb
		0.243	0.30	19.3876	Coarse	Fine	0-8Umb
			0.30	19.3876	Fine	Coarse	0-8Umb

Table 3.8 Experimental conditions for the study of the fluidization properties of natural size distribution powder at the different average particle diameter

d_p (μm)	Dispersion	ID (m)	L_i(m)	W_p (kg)	Distributor type		U_o
					Top	Bottom	
37(B1)	Poly dispersion	0.127	0.40	7.7971	Fine	Fine	0-8Umb
37(B2)	Poly dispersion	0.127	0.40	7.7971	Fine	Fine	0-8Umb
46.61	Poly dispersion	0.127	0.40	7.7971	Fine	Fine	0-8Umb
72	Poly dispersion	0.127	0.40	7.7971	Fine	Fine	0-8Umb
89	Poly dispersion	0.127	0.40	7.7971	Fine	Fine	0-8Umb

Table 3.9 Experimental conditions for the study of the fluidization properties of the narrow size cut powder at the different average particle diameter

d_p (μm)	Size range (μm)	Dispersion	ID (m)	L_i (m)	W_p (kg)	Distributor type		U_o
						Top	Bottom	
33.50	0-45	Mono dispersion	0.127	0.40	7.7971	Fine	Fine	0-8Umb
45.1	45-53	Mono dispersion	0.127	0.40	7.7971	Fine	Fine	0-8Umb
55.08	53-63	Mono dispersion	0.127	0.40	7.7971	Fine	Fine	0-8Umb
68.41	63-75	Mono dispersion	0.127	0.40	7.7971	Fine	Fine	0-8Umb
81.81	75-90	Mono dispersion	0.127	0.40	7.7971	Fine	Fine	0-8Umb
97.82	90-106	Mono dispersion	0.127	0.40	7.7971	Fine	Fine	0-8Umb

Table 3.10 Experimental conditions for the study of the fluidization properties of mixed size cut powder at the different average particle diameter

d_p (μm)	Size range (μm)	Disper-sion	ID (m)	L_i (m)	W_p (kg)	Distributor type		U_o
						Top	Bottom	
60	25%(0-45)+ 75%(75-90)	Bimodal	0.127	0.40	7.7971	Fine	Fine	0-8Umb
47	50%(0-45)+ 50%(75-90)	Bimodal	0.127	0.40	7.7971	Fine	Fine	0-8Umb
39	75%(0-45)+ 25%(75-90)	Bimodal	0.127	0.40	7.7971	Fine	Fine	0-8Umb
75.70	25%(45-53)+ 75%(90-106)	Bimodal	0.127	0.40	7.7971	Fine	Fine	0-8Umb
52.12	50%(45-53)+ 50%(90-106)	Bimodal	0.127	0.40	7.7971	Fine	Fine	0-8Umb
61.73	75%(45-53)+ 25%(90-106)	Bimodal	0.127	0.40	7.7971	Fine	Fine	0-8Umb

Chapter 4: Bed Collapse Model

4.1 Introduction

The bed collapse technique, introduced in 1967 by Rietema is one of the standard techniques widely used to study hydrodynamic properties of a fluidized bed. The experiment is carried out allowing the fluidized bed to reach a steady state condition with a subsequent abrupt shut off of the gas supply. As a result, the fluidizing bed starts to collapse and the time dependence of the bed surface is recorded. It is also possible to measure simultaneously the gas pressure along the bed height. The experiment is schematically represented in Figure 4.1

Three distinct regions can be distinguished (Figure 4.1): the bubble escape (I), where the surface fluctuates due to gas bubbles reaching the top of the bed; the sedimentation stage (II), where the top section of the bed is still fluidized, while the bottom has settled to a fixed bed and interface between these two regions is moving upward while the bed surface is collapsing; the consolidation stage (III), where the fixed bed settles to a final compacted bed. The sedimentation stage yields a linear region, which is used to

extrapolate the dense phase height back to time 0 to obtain the dense phase voidage. The bed collapse curve also yields the collapse time, t_c.

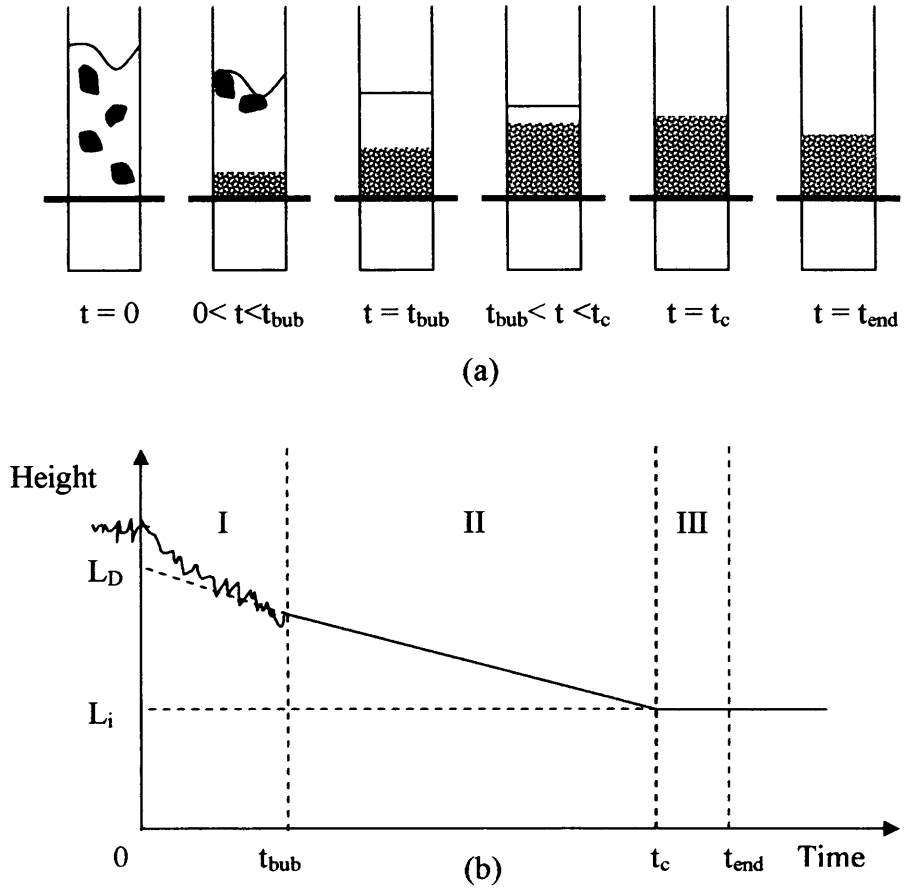

Figure 4.1 Illustration of (a) the collapsing fluidized bed and (b) its corresponding collapse curve

The primary information is from the sedimentation collapse curve, which is the y-intercept value from the extrapolation of sedimentation curve, the slope of the sedimentation curve, called the collapse rate, and the fluidization characteristic from the overall shape of the collapse curve. For instance, a powder will belong to Geldart's Group A powder if the collapse curve has all three stages. For Group B powders, the typical collapse curve will have only the bubble escape stage and the solid consolidation

stage. Furthermore, for group A powder homogeneous fluidized bed, there will be no bubble escape stage. Finally, for group C powders where the fluidizing bed tends to show channelling effects, the bed collapses faster at the beginning and it slows with time. This is due to the gradual disappearing of the channels.

Slis et al. (1959) were the first to analyse the behaviour of a homogeneously expanded bed subject to a variation in inlet flows. They developed a kinematic approach, i.e. assuming that the momentum balance instantaneously equilibrates, and the fluid is incompressible. The theory is based on the continuity equation and applies the Richardson and Zaki (1954) equation. Their results were confirmed by Gibilaro et al. (1984). These approaches were developed for liquid beds, where the inlet velocity can be changed abruptly. In gas systems, the gas flow is distributed using a porous disc and a windbox, therefore even when the gas inlet is shut off there is a residual gas flow into the bed.

Abrahamsen and Geldart (1980b) were the first to realise that the gas in the windbox will have an effect on the collapse rate and Tung and Kwauk (1982) included this effect in their analysis by considering the total gas flowing from the windbox and assuming an average of this over the entire collapse process. Barreto et al. (1988) extended the same approach to include the bubble escape with a bubble wake region. With the application of the constant average gas deaeration rate (Tung and Kwauk, 1982), Nei and Liu (1998) studied the collapsing process based on the analysis of pressure variations with time during the collapse process.

The parameters of the bed collapse experiment reported in the literature are therefore the dense phase voidage and the standard deaeration time defined by Geldart and Wong (1984):

$$\frac{t_c}{L_i} = \frac{\left(L_D/L_i - 1\right)}{dL_1/dt + \overline{U}_{dis}} \tag{4.1}$$

where $\overline{U}_{dis}$ = Average gas velocity in the distributor

L_i = Initial fixed bed height

L_D = Height of the dense phase

L_1 = Height of the sedimentation bed

t_c = Collapsing time

To minimize the effect of the windbox gas residue there are various design options: low pressure drop distributor; small windbox volume; the installation of a venting valve (second valve) in the windbox, which is synchronized, with the gas inlet valve. While the first options will reduce the efficiency of the gas distribution at the base of the fluidized bed, the use of a second valve is considered the best option and recent measurements are typically carried out using this system (Lettieri et al., 2000).

Park et al. (1991), who were among the first to use the bed collapse experiment with a venting valve in the windbox, carried out a careful experimental study of the effect of the second valve and suggested that the aperture of this valve should be adjusted in order to optimise the discharge of gas from the windbox. More recently Lettieri et al. (2000) observed a significant difference in the collapse rate, depending on the use of one or two valves.

Since what is measured is a property of the powder, it should be independent of the system's configuration. It should be possible to predict the response of a 2-valve system from that of a 1-valve system and vice versa, and this would allow an experimental confirmation of the validity of the measured particle properties. Therefore, in this work, the bed collapse model was developed with the inclusion of the effect of the design configurations, which are the windbox volume, the distributor pressure drop and the system with 1- or 2-valve configuration. The model can predict the bed collapse curve, the upward movement of the fixed bed interface, the transient pressure drop profile, the bubble escape time and the de-aeration times. By taking these system configurations into account, the model can give the intrinsic value of the dense phase voidage, dense phase superficial velocity and the bed voidage.

4.2 Bed collapse model

To derive the model equations, it is useful to start with the description of the dynamic response of a homogeneously expanded bed (Figure 4.2b). We will see that the bubble escape region can be described very easily from a simple overall mass balance, and can be superimposed on the solution at a later stage. We will not consider the consolidation stage, which is typically modelled as a first order kinetic process (Tung and Kwauk, 1982) even though the first part of this process is most likely due to the upward propagation of voidage waves (Brandani, 2005).

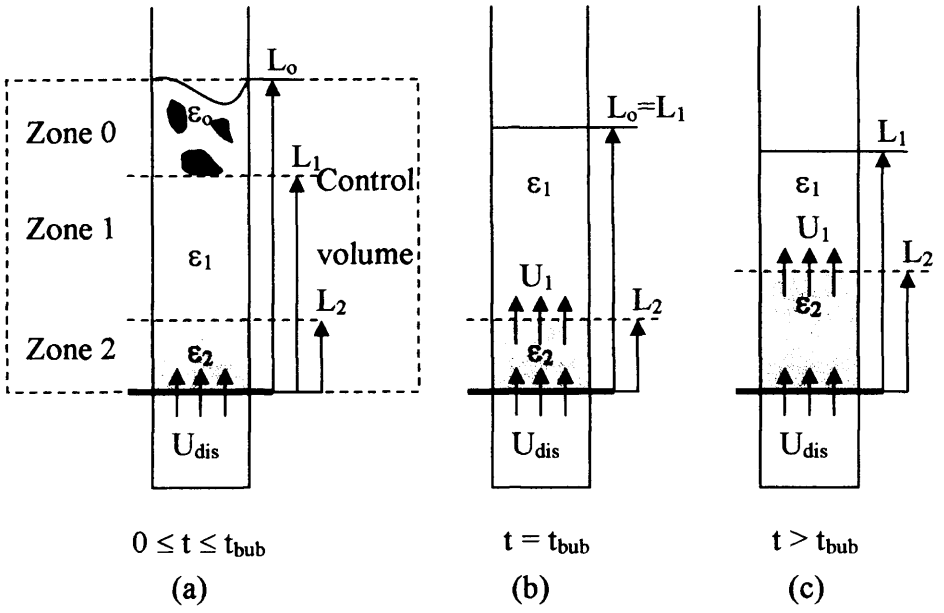

Figure 4.2 Schematic of (a) bubble escape stage, (b) and (c) sedimentation stage for 1-valve configuration system

The 1-valve configuration is easier to interpret since as soon as the gas inlet is switched off, the homogeneously expanded bed will start to collapse and a settled bed section will form at the bottom and rise upwards. Between these two regions of differing void fractions is a moving boundary where gas is displaced since the bottom section will have a smaller void fraction, i.e. $\varepsilon_1 > \varepsilon_2$. In the 1-valve configuration, the maximum pressure will always be in the windbox and the gas generated at the interface (L_2) will always flow upwards. The situation is slightly more complicated when the second valve is introduced, since the windbox pressure will drop below the pressure at the interface (L_2) and the gas generated at the interface (L_2) will partition itself and flow both upwards and downwards. This must be taken into account when deriving the mass balances.

The main assumptions made in deriving the model equations are:

- One-dimensional system
- In the bed sections the fluid is incompressible.
- Negligible inertial effects.
- The top fluidized section remains at a constant void fraction ε_1 corresponding to a gas velocity U_d
- The gas in the windbox is compressible and is considered ideal.

4.2.1 Sedimentation stage

1-valve configuration

The solid mass balance yields (Figure 4.2 (b))

$$V_B = (1-\varepsilon_2)L_2 + (1-\varepsilon_1)(L_1 - L_2) = (1-\varepsilon_1)L_1 + (\varepsilon_1 - \varepsilon_2)L_2 \qquad (4.2)$$

where V_B = Volume of the bed occupied by the particles

L_1 = Height of the sedimentation bed (zone 1)

L_2 = Height of the fixed bed zone (zone 2)

ε_1 = Bed voidage in zone1

ε_2 = Bed voidage in zone 2

From eq. 4.2

$$\frac{dL_2}{dt} = \frac{1-\varepsilon_1}{\varepsilon_2 - \varepsilon_1}\frac{dL_1}{dt} \qquad (4.3)$$

The gas phase mass balance across the bottom section yields

$$U_1 = U_{dis} - (\varepsilon_2 - \varepsilon_1)\frac{dL_2}{dt} = U_{dis} - (1-\varepsilon_1)\frac{dL_1}{dt} \qquad (4.4)$$

where U_1 = Superficial velocity of gas passing zone 1

U_{dis} = Superficial velocity of gas passing the distributor

The top section is a homogenously fluidized bed (Slis et al., 1959) and

$$\frac{U_1}{\varepsilon_1} - \frac{dL_1}{dt} = \frac{U_d}{\varepsilon_1} \tag{4.5}$$

Combining eqs 4.4 and 4.5 yields the bed collapse rate

$$\frac{dL_1}{dt} = U_{dis} - U_d \tag{4.6}$$

Where U_d = dense phase superficial velocity

Hence, from eq. 4.4

$$\frac{dL_2}{dt} = \frac{(1-\varepsilon_1)(U_d - U_{dis})}{(\varepsilon_1 - \varepsilon_2)} \tag{4.7}$$

To close the problem an equation for the distributor velocity is needed, and this is obtained from the mass balance in the windbox, applying the ideal gas law

$$-\frac{V_w}{RT}\frac{dp_w}{dt} = \frac{\rho_f}{M_w} U_{dis} A \tag{4.8}$$

or

$$-\frac{dp_w}{dt} = \frac{p_w}{V_w} U_{dis} A \tag{4.9}$$

where A = Fluidized bed cross section area

M_w = Gas molecular weight

p_w = Absolute windbox pressure

R = Ideal gas constant

T = Temperature

V_w = Windbox volume

ρ_f = Gas density

U_{dis} can be calculated from the knowledge of the pressure drop across the distributor. In order to determine the distributor pressure drop, the momentum balance needs to be evaluated.

In zone I, the fluid-particle system is at equilibrium and

$$\Delta P_1 = (\rho_p - \rho_f)(1-\varepsilon_1)(L_1 - L_2)g \qquad (4.10)$$

where ΔP_1 = Pressure drop in zone 1 (homogeneous bed)

ρ_p = Particle density

In zone II, there is a fixed bed and the pressure drop can be measured independently or calculated from a standard pressure drop correlation.

$$\Delta P_2 = f\left(U_{dis}\right) \qquad (4.11)$$

where ΔP_2 = Pressure drop in zone 2 (fixed bed)

Combining these values, the pressure drop through the distributor is given by

$$\Delta P_{Dist} = \left(p_w - p_{atm}\right) - \rho_f g L_1 - \Delta P_1 - \Delta P_2 \qquad (4.12)$$

where ΔP_{Dist} = Distributor pressure drop

p_{atm} = Absolute atmospheric pressure drop

The system of equations is completely formulated through the inclusion of the flow characteristics of the distributor and the bed collapse model can be solved through integration of eqs 4.6, 4.8, and 4.7.

The parameters needed are:

- The void fraction of the settled bed, which can be measured from the final bed height.
- The void fraction of the expanded bed, ε_1.
- The equilibrium superficial velocity of the homogeneously expanded bed, U_d.

2-valve configuration

Following the same procedure as above, and taking into account the possibility of flow reversal through the distributor and fixed bed sections, the mass balance in the windbox becomes:

$$-\frac{dp_w}{dt} = \frac{p_w}{V_w}(\pm U_{dis}A + Q_v) \tag{4.13}$$

where Q_v = gas flow rate through the discharge valve

The bed collapse rate is

$$\frac{dL_1}{dt} = \pm U_{dis} - U_d \tag{4.14}$$

L_2 correlation is

$$\frac{dL_2}{dt} = \frac{(1-\varepsilon_1)(U_d \pm U_{dis})}{(\varepsilon_1 - \varepsilon_2)} \tag{4.15}$$

and the pressure drop across the distributor is

$$\Delta P_{Dist} = (p_w - p_{atm}) - \rho_f g L_1 - \Delta P_1 \pm \Delta P_2 \tag{4.16}$$

The solution of the model equations requires the knowledge of the flow characteristics of the discharge valve and the top sign in eqs 4.13-4.16 applies when the gas is flowing from the windbox to the particle bed.

4.2.2 Bubble escape stage

1-valve configuration

The collapsing bed structure is shown in Figure 4.2a.The total mass balance over the control volume sketched in Figure 4.2a yields

$$U_{dis}A = Q_g + Q_p = \varepsilon_1(1-f_b)U_dA + f_bU_bA + U_pA \tag{4.17}$$

Where f_b = Volume fraction of bubbles

Q_g = Gas flow rate

Q_p = Particle flow rate

U_b = Bubble velocity

U_p = Particle velocity

The properties in the bubbling zone are assumed to be similar to those in the steady state bubbling fluidised bed.

$$U_o A = \varepsilon_1 (1 - f_b) U_d A + f_b U_b A \tag{4.18}$$

Combining eqs 4.17 and 4.18

$$U_p = \frac{dL_o}{dt} = U_{dis} - U_o \tag{4.19}$$

The pressure drop through the distributor is given by

$$\Delta P_{Dist} = (p_w - p_{atm}) - \rho_f g L_c - \Delta P_o - \Delta P_1 - \Delta P_2 \tag{4.20}$$

$$\Delta P_o = (\rho_p - \rho_f)(1 - \varepsilon_o)(L_0 - L_1)g \tag{4.21}$$

Where ΔP_0 = Pressure drop in zone 0 (Bubbling bed)

L_0 = Height of the bubble escape bed

ε_0 = Bed voidage in zone 0

L_2 can be calculated from eq. 4.7 and L_1 is obtained from eq.4.6, where the initial condition for L_2 and L_1 is zero. L_1 increases until the end of the bubble escape stage, where $L_0 = L_1$. After this, the sedimentation stage starts and L_1 falls. L_2 increases for the whole process of the bed collapse until it reaches the top of the bed.

If the distributor velocity is neglected the equation originally derived by Barreto (1984) is obtained. The bubble escape stage has a rate of collapse equal to the difference between the distributor velocity and the gas velocity before the valve shut off. Eq. 4.19

has to be integrated simultaneously with eqs 4.6, 4.9, and 4.7 (1-valve configuration) to yield the full solution to the bed collapse model.

The parameters needed are:

- The void fraction of the settled bed, which can be measured from the final bed height.
- The void fraction of the dense phase, ε_1.
- The equilibrium superficial velocity of the homogeneously expanded bed, U_d.
- The void fraction of the bed voidage, ε_0.

The sedimentation stage will start only when U_{dis} becomes less than U_1 (see eq.4.4), and the bubble escape will end when $L_0 = L_1$.

2-valve configuration

There are two possible bed collapse structures during the bubble escape stage, in the case of the 2-valve configuration. This is due to the possibility of flow reversal of the gas generated at the interface L_2 moving downward through the distributor. The first possible structure is as shown in Figure 4.2a, when zone 1 can exist and stay in between zone 2 and zone 0. Another possible structure is when zone 1 can not exist and zone 2 is in direct contact with zone 0 (Figure 4.3).

To determine the existence of zone 1 during the bubble escape stage, U_1, is calculated based on the assumption that zone 1 exists. From gas mass balance at L_2, U_1 can be calculated from eq. 4.4:

$$U_1 = \varepsilon_1(\pm U_{dis}) + (1-\varepsilon_1)U_d \qquad (4.22)$$

If U_1 is greater than zero, the bed collapse structure is as shown in Figure 4.2(a). The bed collapse rate can be expressed as follows;

$$\frac{dL_0}{dt} = U_0 \pm U_{dis} \qquad (4.23)$$

As for the 1-valve configuration, eq. 4.23 has to be integrated simultaneously with eqs 4.13, 4.14 and 4.15 (2-valve configuration) to yield the full solution to the bed collapse model.

If U_1 is less than zero, the region of homogeneous expanded bed cannot exist. The collapsing bed structure can only have the bubbling bed zone in contact with the fixed bed zone and the bed structure is shown in Figure 4.3.

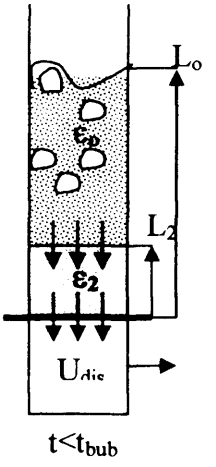

Figure 4.3 Bubble escape stage collapsing structure when $U_1<0$ for 2 valve experiment

In this case, eq. 4.23 is still valid and it has to be integrated with eqs 4.13 and 4.14 as before. L_2 can be calculated as a function of L_0 and from a mass balance:

$$\frac{dL_2}{dt} = \frac{(1-\varepsilon_0)(U_0 - U_{dis})}{(\varepsilon_0 - \varepsilon_2)} \qquad (4.24)$$

This case is true especially at a very high inlet flow rate and for the initial part of the bubble escape stage.

4.2.3 Modification of the model for the column with top cover

In this work, the experimental apparatus used a distributor covering the top part of the column in order to avoid the loss of very fine powders through the freeboard. On using this distributor, the only modification that should be made in the bed collapse model is in the momentum balance for the calculation of the distributor pressure drop.

Collapsing bed momentum balance

$$\Delta p_w - \rho_f g L_c = \Delta P_o + \Delta P_1 \pm \Delta P_2 \pm \Delta P_{Dis(Bottm)} \pm \Delta P_{Dis(top)} \qquad (4.25)$$

Where $\Delta P_{Dis(top)}$ = Top distributor Pressure drop

$\Delta P_{Dis(bottm)}$ = Bottom distributor Pressure drop

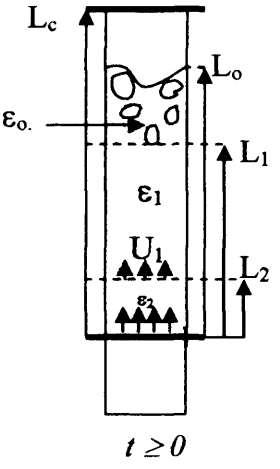

Figure 4.4 Structure of the collapsing bed for 1 valve configuration system t > 0 for the system with top distributor

The gas mass balance from bottom distributor to top distributor (Figure 4.4)

$$U_{dis(bottm)}A + (\varepsilon_1 - \varepsilon_2)\frac{dL_2}{dt} + (\varepsilon_{o.} - \varepsilon_1)\frac{dL_1}{dt} + (1 - \varepsilon_{o.})\frac{dL_o}{dt} = U_{dis(top)}A \quad (4.26)$$

From the particle mass balance (Figure 4.4)

$$\frac{dV_B}{dt} = (1 - \varepsilon_o)\frac{dL_o}{dt} + (\varepsilon_o - \varepsilon_1)\frac{dL_1}{dt} + (\varepsilon_1 - \varepsilon_2)\frac{dL_2}{dt} = 0 \quad (4.27)$$

$$U_{dis(bottm)} = U_{dis(top)} = U_{dis} \quad (4.28)$$

Hence by using the same type of the distributor plate, $\Delta P_{Dis(top)} = \Delta P_{Dis(bottm)}$

4.2.4 Collapsing bed pressure drop profile

On solving the system of differential equations mentioned above, L_0, L_1, and L_2 can be defined, based on the corrected values of ε_0,ε_d and U_d. As a consequence, the transient pressure drop profile during the bed collapse can be obtained from the momentum balance, as described below.

If x is the location of pressure port, when the location is at the freeboard ($x>L_0$), the pressure drop is;

$$\Delta p_{x>L_0} = (A_{Topdis}(U_{dis}A)) + \rho_f(L_C - x)g \quad (4.29)$$

Where A_{topdis} = Top distributor pressure drop coefficient

L_C = Height of the column

When $L_1<x<L_0$

$$\Delta p_{L_1<x>L_o} = (\rho_p - \rho_f)(1-\varepsilon_o)(L_o - x)g + (A_{Topdis}(U_{dis}A)) + \rho_f(L_c - x)g \quad (4.30)$$

When $L_2<x<L_1$

$$\Delta p_{L_2<x>L_1} = (\rho_p - \rho_f)(1-\varepsilon_1)(L_1 - x)g + (\rho_p - \rho_f)(1-\varepsilon_o)(L_o - L_1)g + (A_{Topdis}(U_{dis}A)) + \rho_f(L_c - x)g \quad (4.31)$$

When $x<L_2$

$$\Delta p_{x<L_2} = A_{bed}U_{dis}(L_2 - x) + (\rho_p - \rho_f)(1-\varepsilon_1)(L_1 - L_2) + (\rho_p - \rho_f)(1-\varepsilon_o)(L_o - L_1)g + (A_{Topdis}(U_{dis}A)) + \rho_f(L_c - x)g \quad (4.32)$$

Where A_{bed} = Fixed bed pressure drop coefficient

4.2.5 The model prediction for the sedimentation collapse curve

There are two limiting cases for the sedimentation collapse curves, depending on the ratio of the pressure drop in the distributor to that in the bed ($\Delta P_{Dist}/\Delta P_{Bed}$). If $\Delta P_{Dist}/\Delta P_{Bed}$ is small, then most of the gas will escape through the discharge valve. The sedimentation curves are shown in Figure 4.5(a). However, if $\Delta P_{Dist}/\Delta P_{Bed}$ is large, only the gas in the windbox will escape through the collapsing bed. The collapsing curves are shown in Figure 4.5(b).

Based on the model predictions we can conclude that if $\Delta P_{Dist}/\Delta P_{Bed}$ (Figure 4.5(a)) is large then the 2-valve experiment will yield the correct extrapolation to obtain the dense phase voidage. The residual gas in the windbox will generate a time lag in the 1-valve collapse curve. If $\Delta P_{Dist}/\Delta P_{Bed}$ (Figure 4.5 (b)) is small, the flow reversal will dominate in the 2-valve experiment accelerating the bed collapse, yielding an under-estimated extrapolation of the linear portion. In this case the 1-valve configuration will yield the correct pair of ε_1 and U_d. When $\Delta P_{Dist} \approx \Delta P_{Bed}$ particular care should be used since the 1-valve experiment extrapolation will overpredict ε_1, while the 2-valve experiment

extrapolation will underpredict it. In this case, the numerical solution should be coupled to a non-linear fitting algorithm to obtain ε_1 and the remaining model parameters.

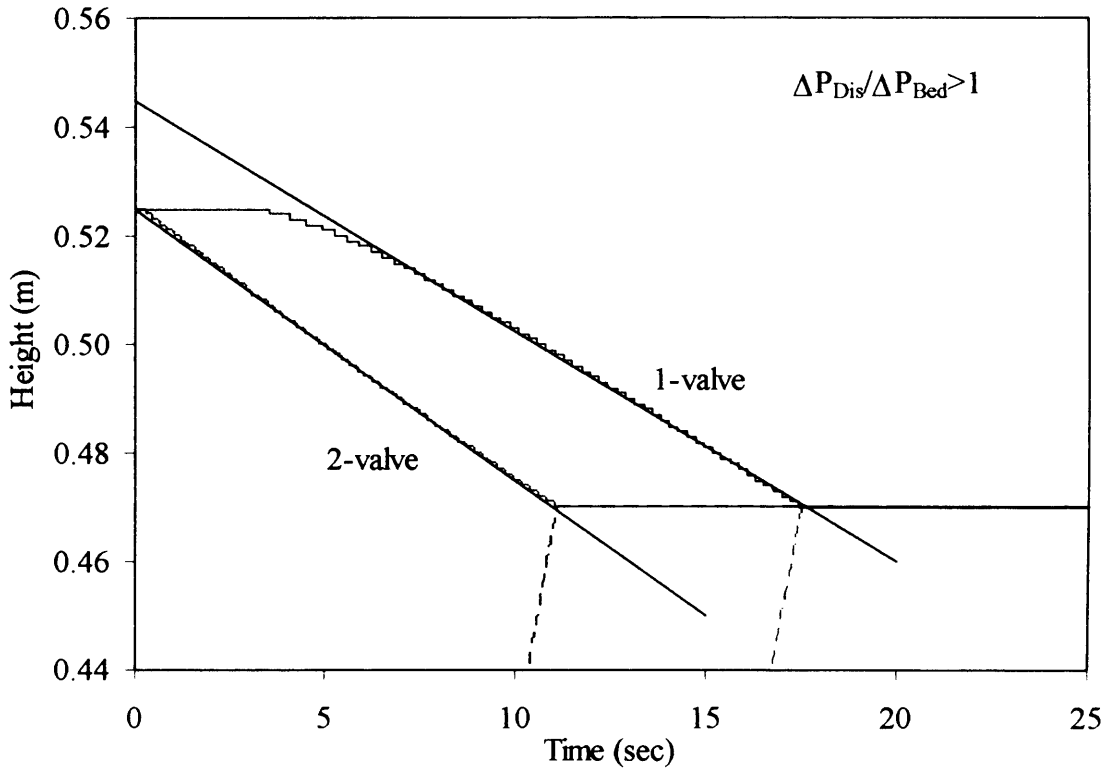

(a)

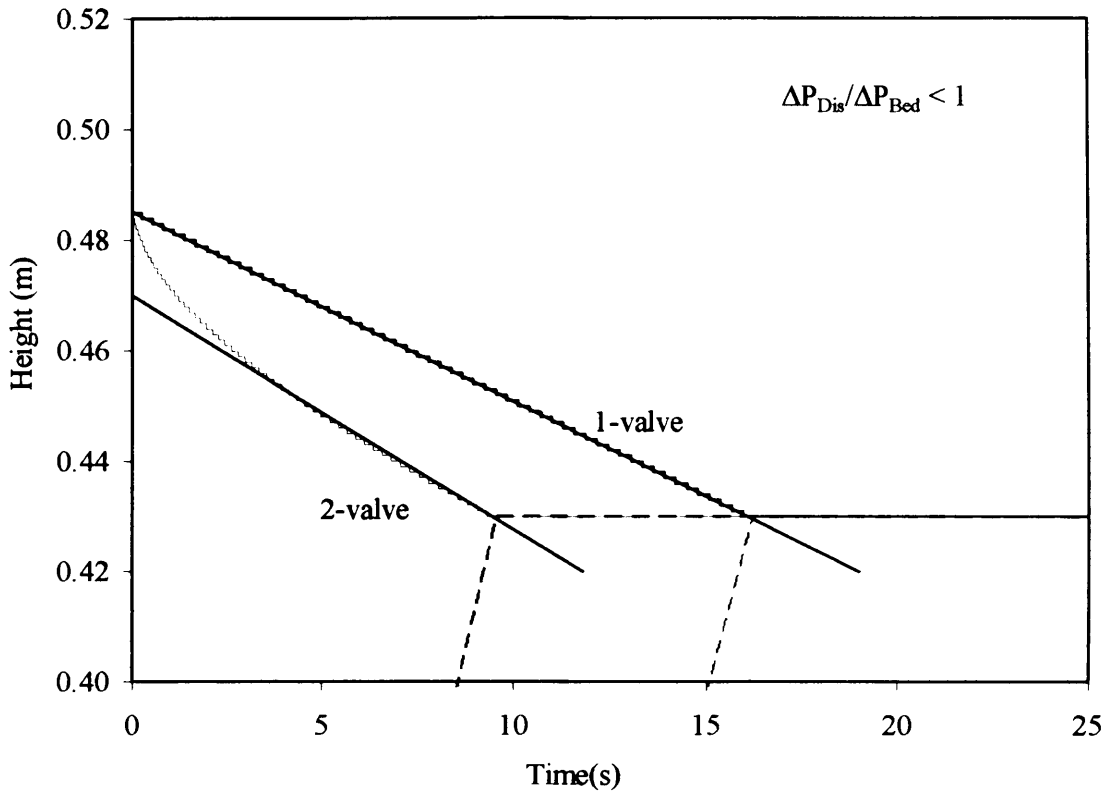

(b)

Figure 4.5 Limiting behaviour of 1-valve and 2-valve experiments (a) $\Delta P_{Dist}/\Delta P_{Bed}>1$ and (b) $\Delta P_{Dist}/\Delta P_{Bed}<1$.

In fluidization studies, the particle size is often varied to optimize the fluidization quality of a powder. From our model predictions based on a fixed distributor, discharge valve and bed weight, we can also observe that carrying out experiments with larger particles, i.e. higher fluidization velocities, may mean that the experiments are in the range $\Delta P_{Dist}/\Delta P_{Bed} > 1$. Reducing the particle sizes also means a reduction in fluidization velocity and a possible switch to $\Delta P_{Dist}/\Delta P_{Bed} < 1$. To avoid ambiguity in the interpretation of the results we would suggest carrying out both 1- and 2-valve experiments where possible and interpreting both sets of results using the model presented above.

4.2.6 The model prediction of pressure drop profile

Once the entire collapse curve has been predicted, based on the correct value of ε_d, U_d and ε_0, the transient pressure drop profile can be calculated. In this work, the differential pressure drop profile was measured and the model predictions are shown in Figure 4.6 (a) and (b) for the homogeneous expanded bed of 1-valve and 2-valve experiments, respectively. Figure 4.7 (a) and (b) show a model prediction of the differential pressure drop profile for bubbling bed of 1-valve and 2-valve experiments, respectively.

The collapsing bed pressure drop profile is a useful measurement since it gives a clear indication of location of L_2 which is not possible to detect visually. The pressure drop profile can also be used for the direct interpretation of the dense phase voidage and the bed voidage. In addition, properties of fixed bed zone (zone 2) of the collapse bed and the windbox gas de-aeration through the fixed bed zone can also be observed quantitatively.

From Figure 4.6 (a) and (b), the transition points as marked by the circles indicate the location of L_2 once it reaches the lower port. The pressure value indicated by (A) can be used for the direct calculation of the dense phase voidage using:

$$\Delta p = (\rho_p - \rho_f)(1-\varepsilon_d)g(0.10\text{m}) + g\rho_f(0.10\text{m}) \qquad (4.33)$$

The pressure reading at point B can be described by eq. 4.34 and represents the pressure drop through the fixed bed zone.

$$\Delta p = A_{bed}U_{dis}(0.10\text{m}) + \rho_f(0.10\text{m})g \qquad (4.34)$$

Figure 4.6(b) clearly shows the flow reversal in the 2-valve experiment, since the pressure drop changes sign.

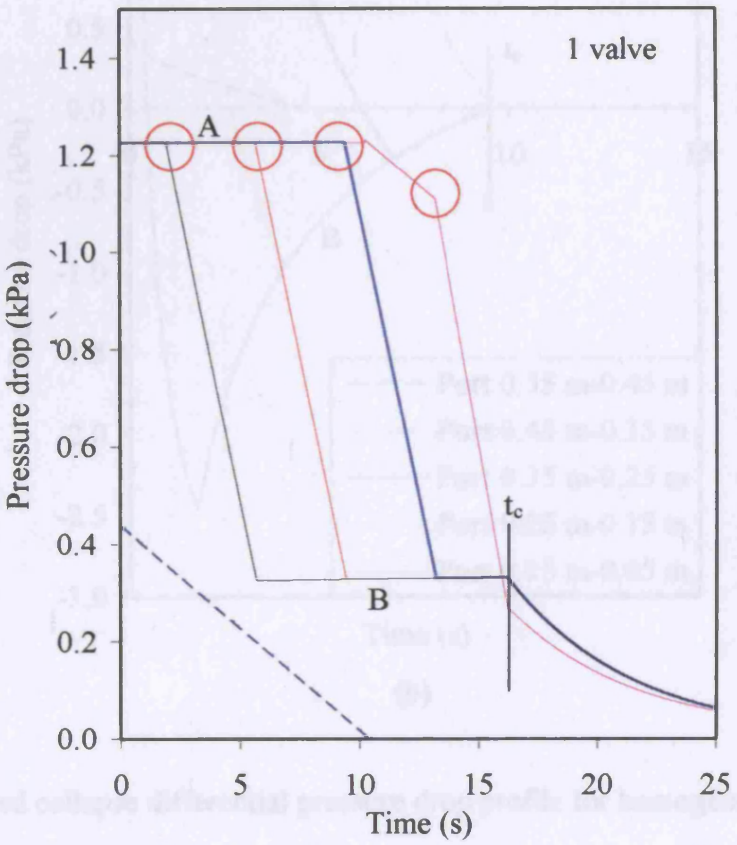

(a)

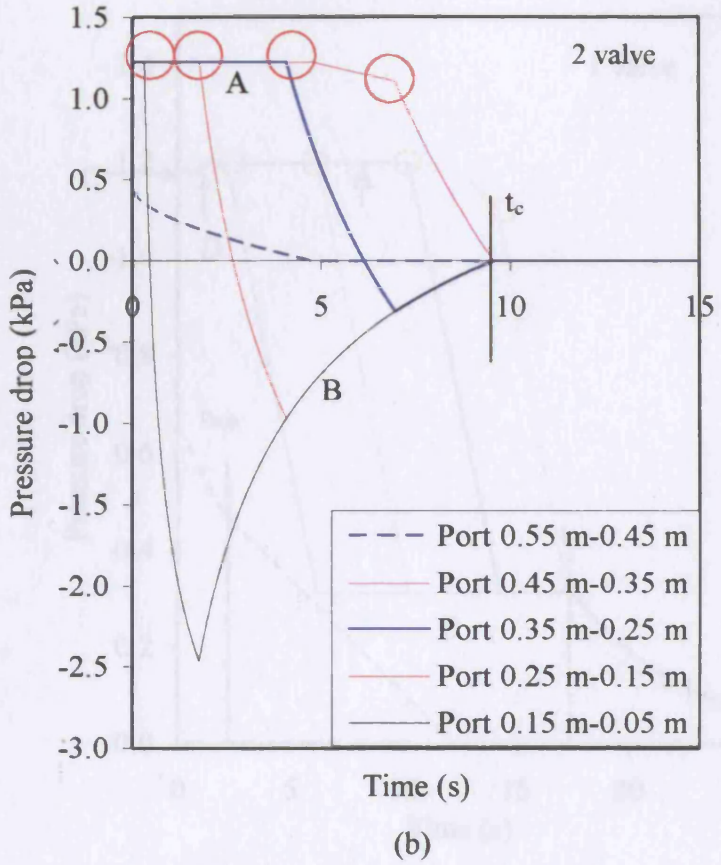

(b)

Figure 4.6 Bed collapse differential pressure drop profile for homogeneous expanded bed of (a) 1-valve and (b) 2-valve experiments (46 μm Ballotini, U_0 = 0.0039 m/s)

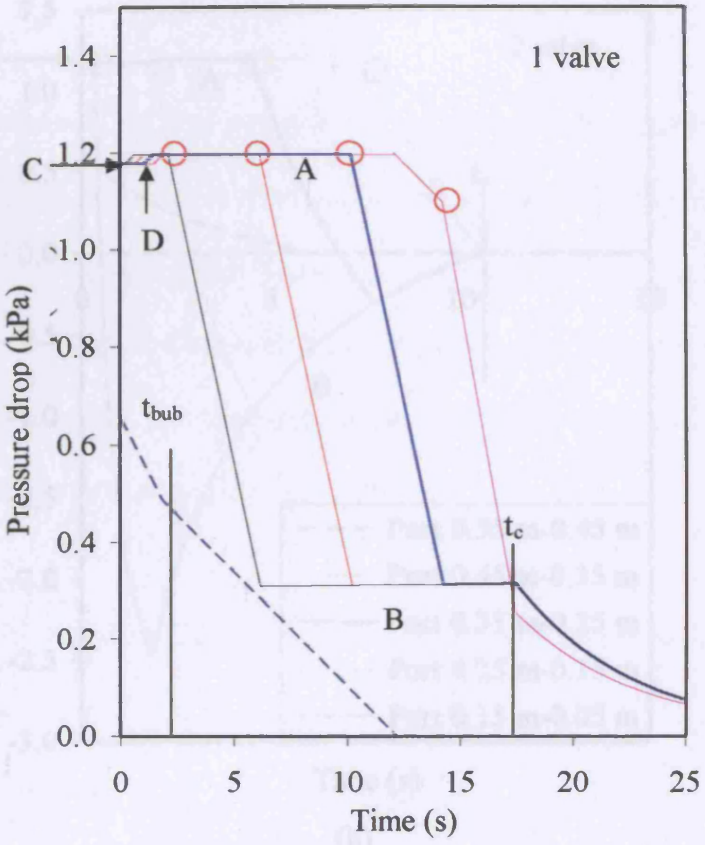
1 valve
1.4
1.2
1.0
0.8
0.6
0.4
0.2
0.0
C
D
A
B
t_{bub}
t_c
Pressure drop (kPa)
0
5
10
15
20
25
Time (s)

(a)

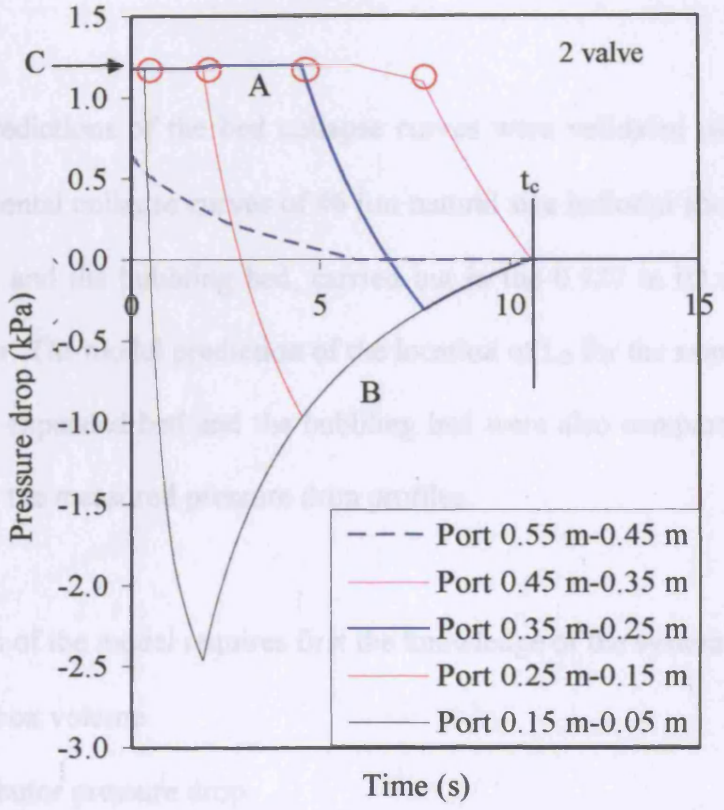

(b)

Figure 4.7 Bed collapse differential pressure drop profile for bubbling bed of (a) 1-valve and (b) 2-valve experiments (46 μm Ballotini, U_0 = 0.0081 m/s)

For a bubbling bed, Figure 4.7, the bed voidage can also be calculated using the pressure drop reading from point (C) and eq. (4.35). For the 1-valve experiment, bubbling bed collapse curves can show clearly enough the location of L_1 (point D), before the end of the bubbling escape stage, when it reaches the lower pressure port.

$$\Delta p = (\rho_p - \rho_f)(1-\varepsilon_o)(0.10m)g + \rho_f g(0.10m) \qquad (4.35)$$

4.3 Experimental validation of the model

The model predictions of the bed collapse curves were validated using the 1- and 2-valve experimental collapse curves of 46 μm natural size ballotini for the homogeneous expanded bed and the bubbling bed, carried out in the 0.127 m ID column, using the fine distributor. The model prediction of the location of L_2 for the same powder for both homogeneous expanded bed and the bubbling bed were also compared with the values obtained from the measured pressure drop profiles.

The prediction of the model requires first the knowledge of the system configuration:

- Windbox volume
- Distributor pressure drop
- Discharge valve (second valve) pressure drop.

To fulfil the model prediction, the correct model parameters, listed below, are also needed.

- Fixed bed pressure drop
- Bed voidage, ε_0
- Dense phase voidage, ε_d
- Fixed bed voidage, ε_2
- Inlet superficial velocity, U_0
- Dense phase superficial velocity, U_d,

While the windbox volume was obtained from a careful measurement of the dimensions, the distributor pressure drop and the discharge valve pressure drop were characterized using the procedure reported in Chapter 3.

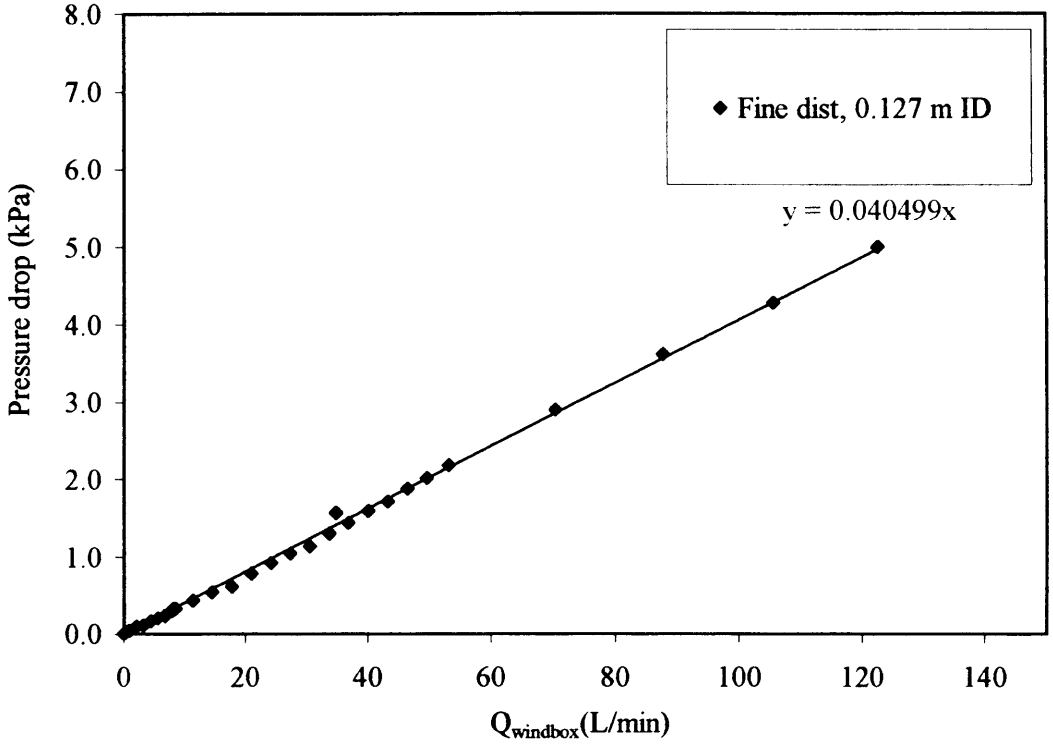

Figure 4.8 Experimental characterization of the distributor.

Figures 4.8 and 4.9 report the experimental pressure drop correlations used for the distributor and the discharge valve, which showed a quadratic dependence on flow rate.

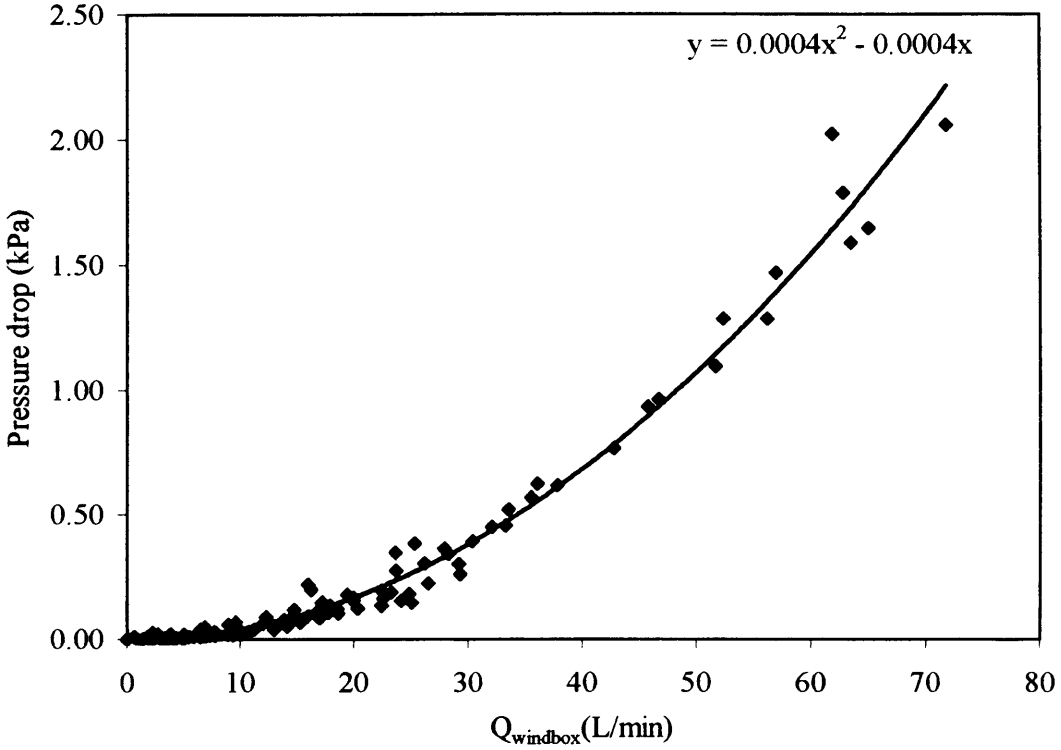

Figure 4.9 Experimental characterization of the discharge valve.

4.3.3 Fixed bed pressure drop

After loading a known quantity of powder in the column, fixed bed pressure drop versus flow rate measurements were carried out. In the range of flow rates which correspond to a fixed bed, the pressure drop varies linearly with superficial gas velocity as shown in Figure 4.10, indicating that the viscous terms dominate.

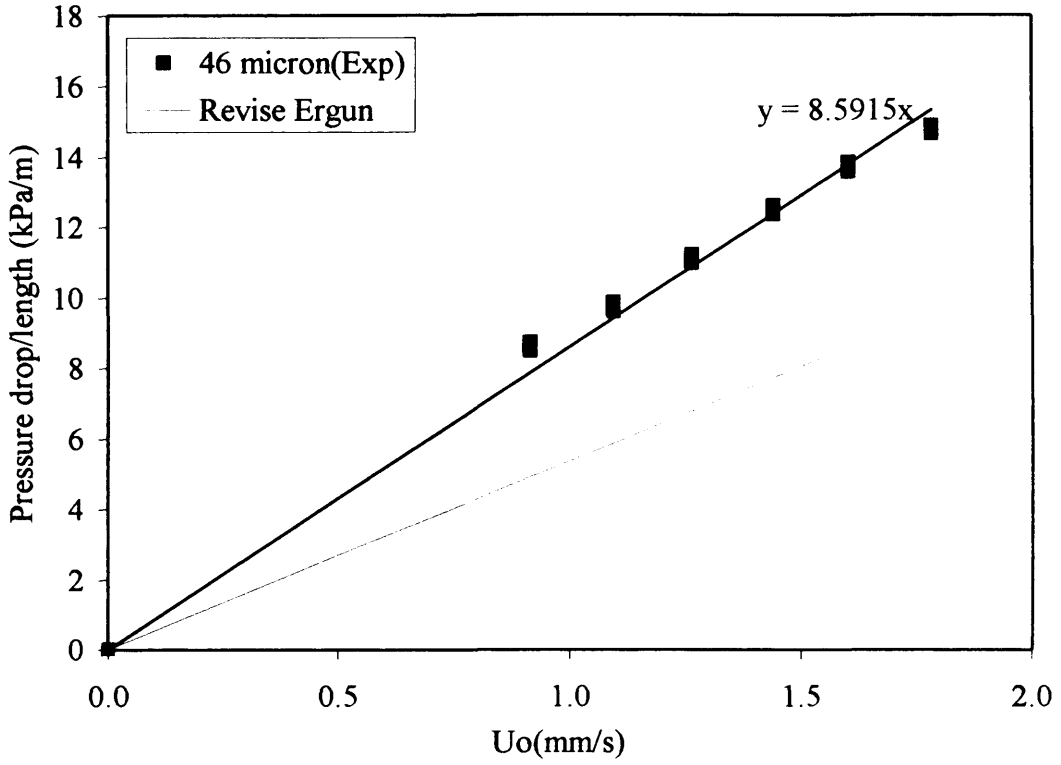

Figure 4.10 Experimental characterization of the fixed bed pressure drop.

What has been outlined above represents the standard procedure that should be followed before performing any bed collapse experiment. Having obtained the system parameters typical for our experimental set-up, we are now in the position of applying the model to obtain quantitative predictions of the effect of the 1-valve vs 2-valve configuration.

4.3.4 Comparison of the model prediction with the experiments

Figure 4.11 shows the experimental bed collapse curves obtained using the 46 μm ballotini powder at a gas flow rate lower than the minimum bubbling point. Figure 4.11 shows that two sets of ε_d and U_d are obtained from the two experiments when the linear

extrapolation is applied. However, with the application of the bed collapse model, both 1-valve and 2-valve collapse curve can be predicted using the correct single set of ε_d and U_d.

In order to complete the model prediction, the model parameters, which are ε_0, U_0, and ε_2, are needed. ε_0 and ε_2 can be calculated from the expanded bed height and fixed bed height, respectively. U_0, which is the gas superficial velocity at the windbox, can be obtained from the careful calibration of the rotameter as discussed in the previous chapter.

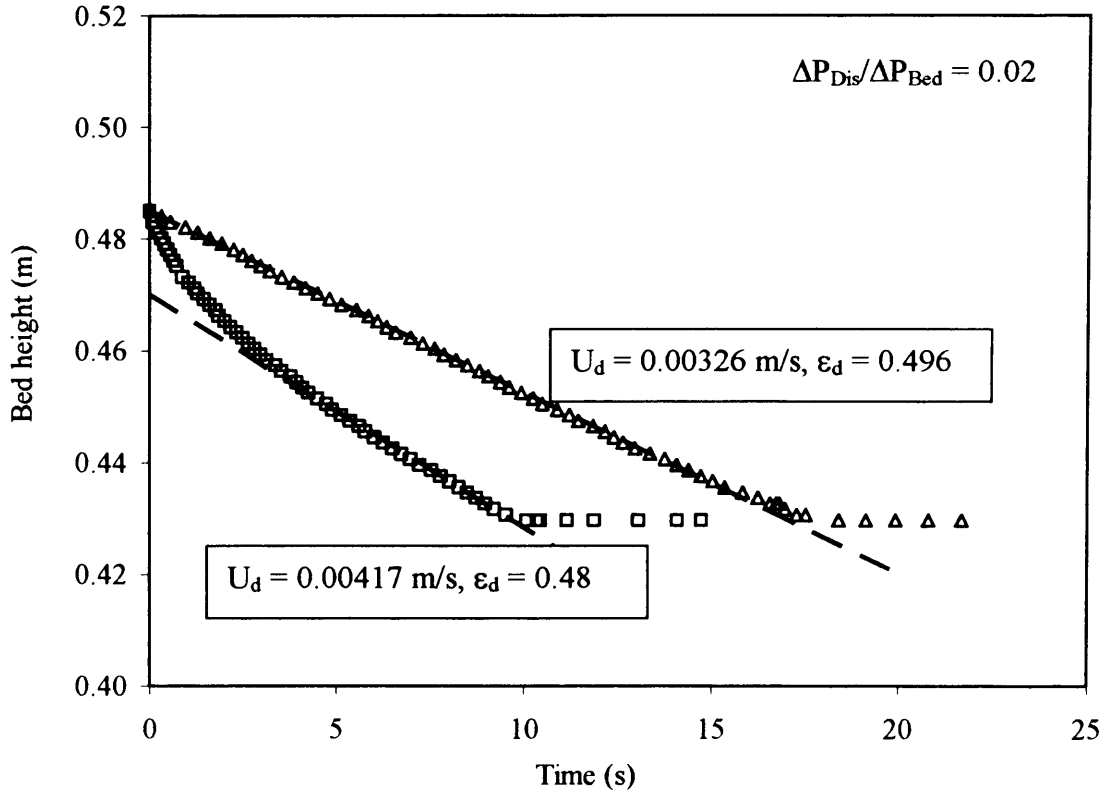

Figure 4.11 Experimental 1-valve and 2-valve bed collapse experiments, U_0 = 0.0039 m/s.

The experimental results show that we are in the $\Delta P_{Dist}/\Delta P_{Bed} < 1$ regime. In this case, the linear intercept of the 1-valve experiment is used to determine the correct value for ε_d. Then, U_d, equivalent to U_0, is used to predict correctly the entire 1-valve collapse curve (Figure 4.12). Using the same set of ε_d and U_d, the 2-valve experiment is fully predicted (Figure 4.12). This provides the means to assure the correctness of the values extracted for ε_d and U_d.

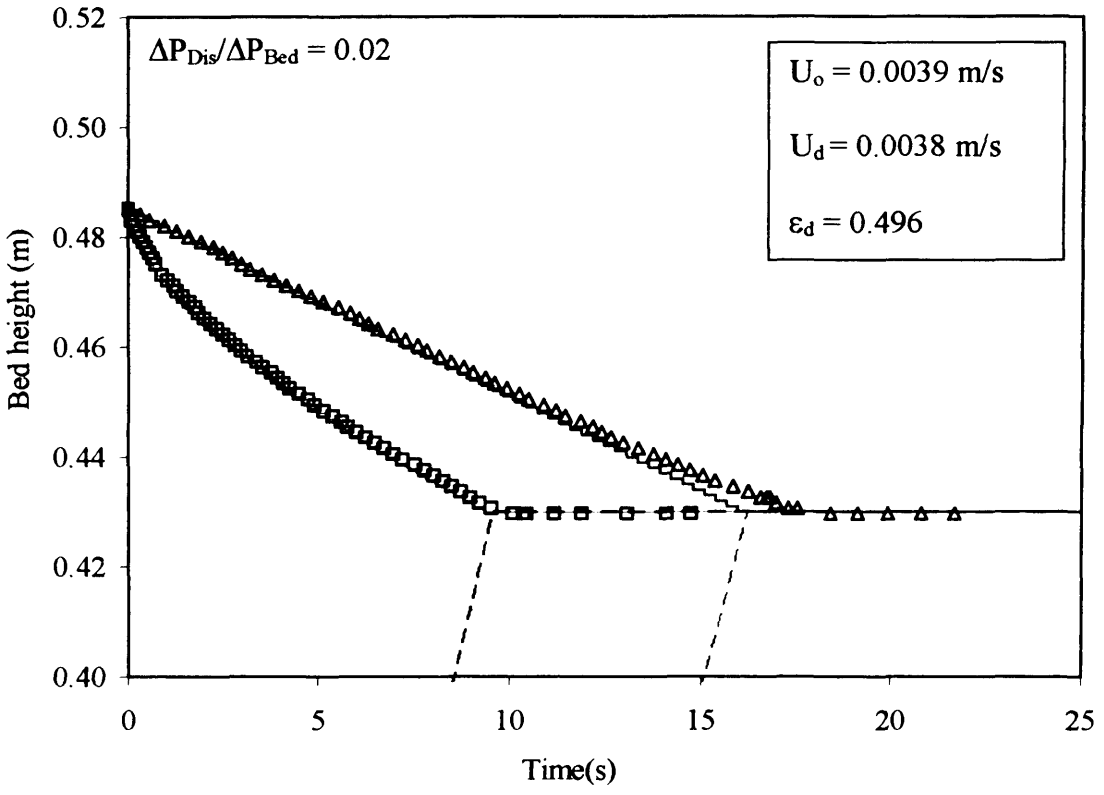

Figure 4.12 Model fit of 1-valve experiment and prediction of 2-valve collapse curve, $U_0 = 0.0039$ m/s

An experimental bubbling bed collapse curve is shown in Figure 4.13. The model parameters, ε_2 and U_0, can be identified as before. However, ε_0 has to be carefully selected as it affects the model prediction during the bubble escape stage. The value of ε_0 was selected to match the bubble escape time. For ε_d, the experimental results show

that the $\Delta P_{Dist}/\Delta P_{Bed} < 1$ regime and ε_1 was from the intercept of the extrapolation of the linear part of the sedimentation stage. U_d was selected so that the predicted 1-valve sedimentation curve would match the experimental results (Figure 4.13). The 2-valve collapse curve (Figure 4.13) was fully predicted using the same set of ε_0, ε_d and U_d.

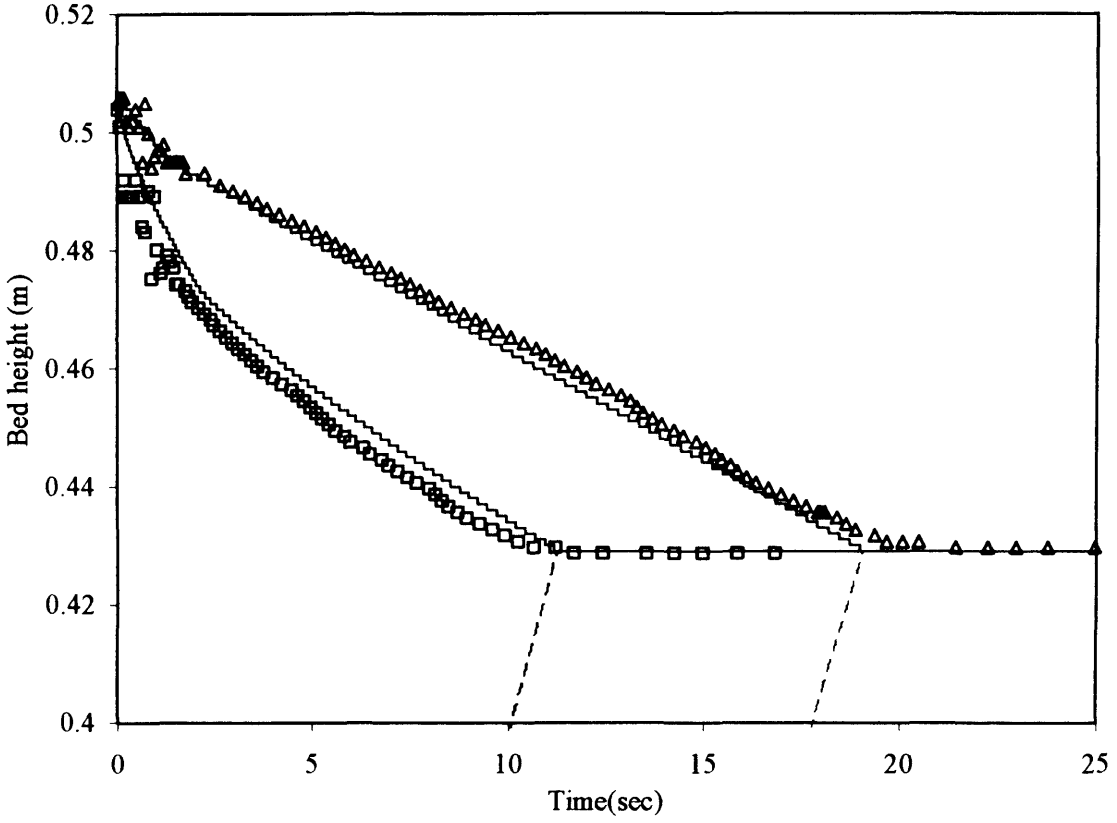

Figure 4.13 Model fit of 1-valve experiment and prediction of 2-valve collapse curve for bubbling bed, $U_o = 0.0081$ m/s

Figure 4.13 shows that the 2-valve experiment can be predicted with remarkable accuracy using the kinematic description of the bed collapse experiment. It should be noted that the 2-valve experiment is very sensitive to the pressure drop in the fixed bed, and performing the pair of 1- and 2-valve experiments could be used for a rapid

determination of the dense phase properties and the pressure drop characteristics of the fixed bed from a simultaneous fit of both experiments using the model presented.

From the experimental differential pressure drop profile measurements the location of L_2 can be obtained as the bed collapses. Figure 4.14 shows the bed collapse pressure drop profile of the 1- and 2-valve experiments, for the homogeneous expanded bed. The locations of the interface L_2 are marked as circles. Figure 4.15 shows the agreement of the model prediction and the experimental values.

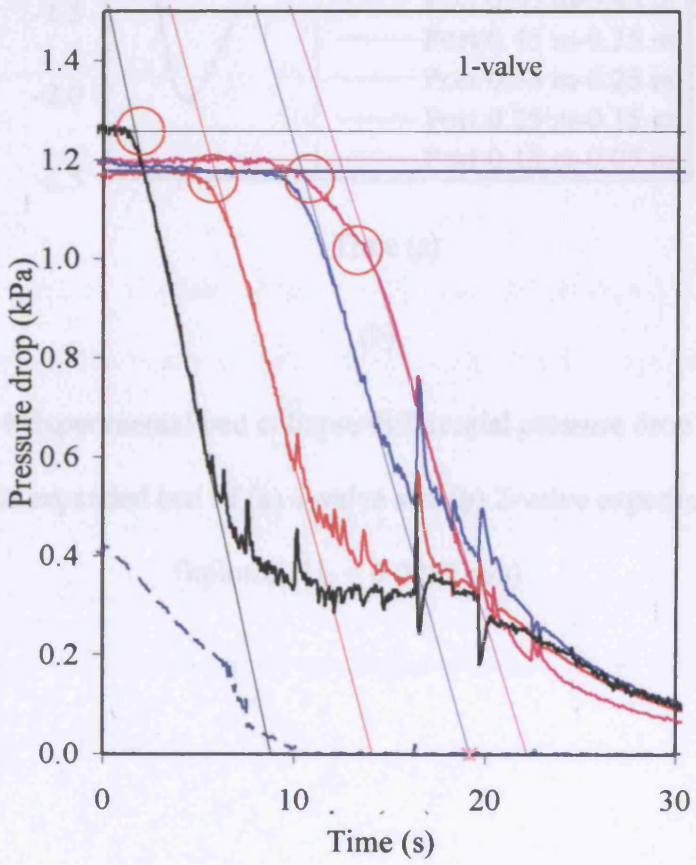

(a)

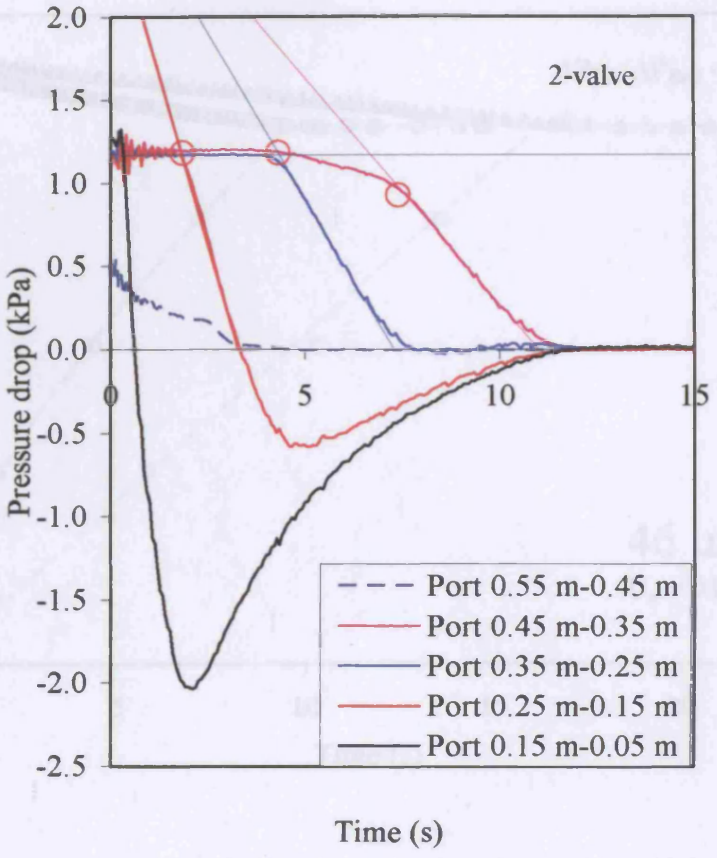

(b)

Figure 4.14 Experimental bed collapse differential pressure drop profile for homogeneous expanded bed of (a) 1-valve and (b) 2-valve experiments (46 μm Ballotini, U_0 = 0.0039 m/s)

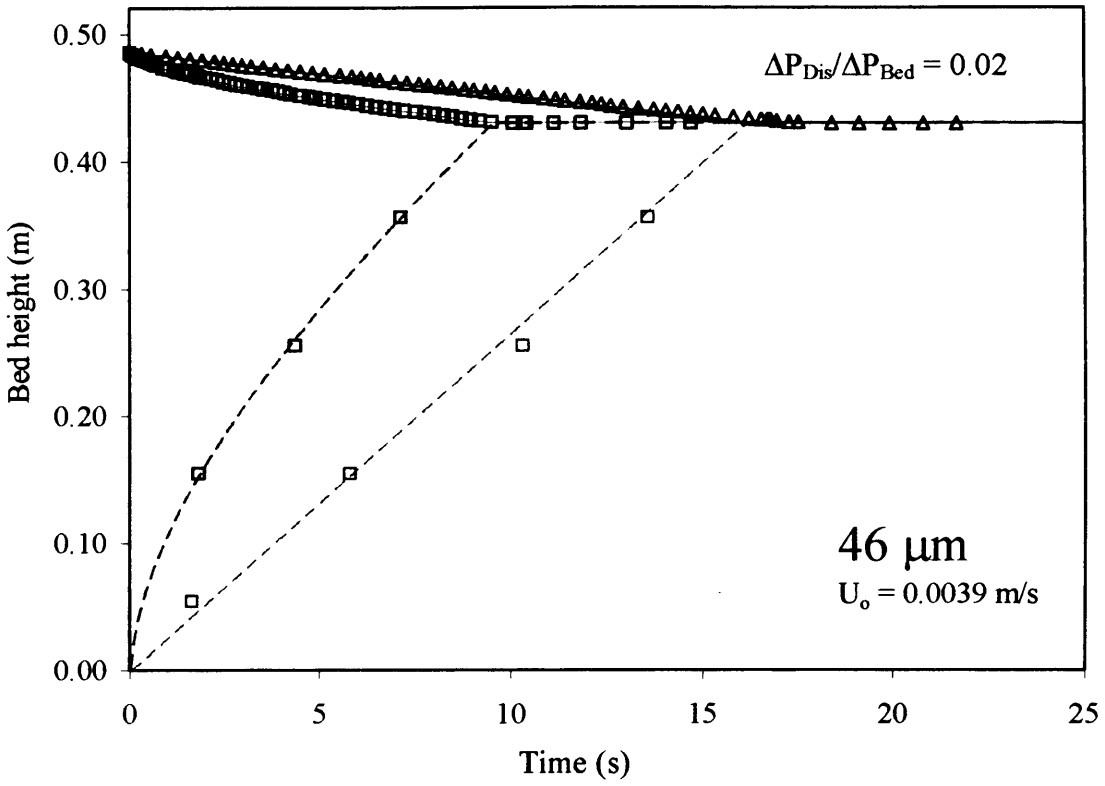

Figure 4.15 Comparison of model prediction of L_2 and experimental L_2 for collapse of homogeneous expanded bed of 1-valve and 2-valve experiments

Figure 4.16 shows the bed collapse pressure drop profile of the 1- and 2-valve experiments, for an initially bubbling bed. The locations of the L_2 interface are marked as circles. Figure 4.17 shows the agreement of the model prediction and the experimental values.

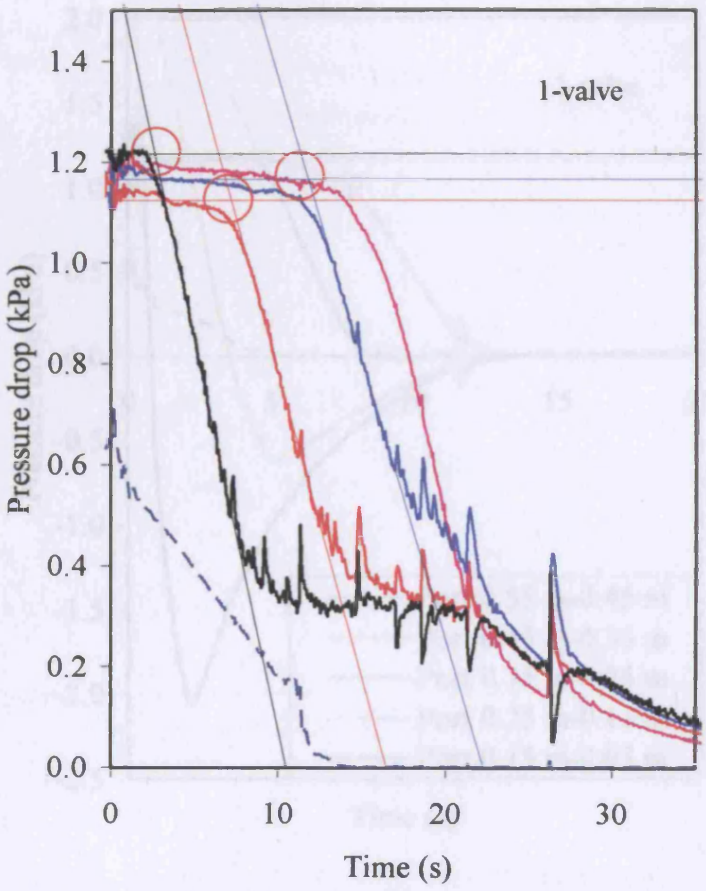

(a)

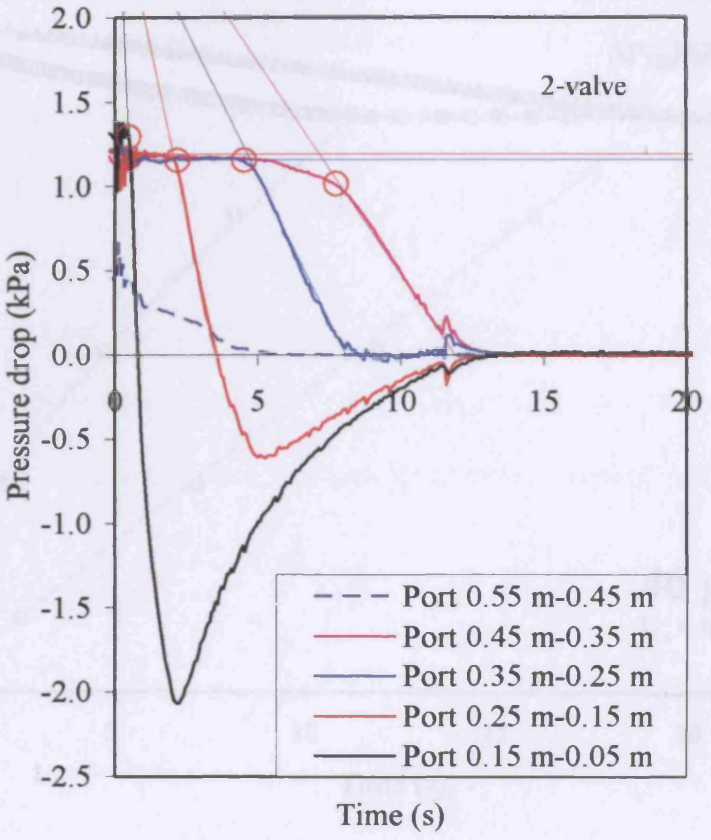

(b)

Figure 4.16 Experimental bed collapse differential pressure drop profile for bubbling bed of (a) 1-valve and (b) 2-valve experiments (46 μm Ballotini, U_o = 0.0088 m/s)

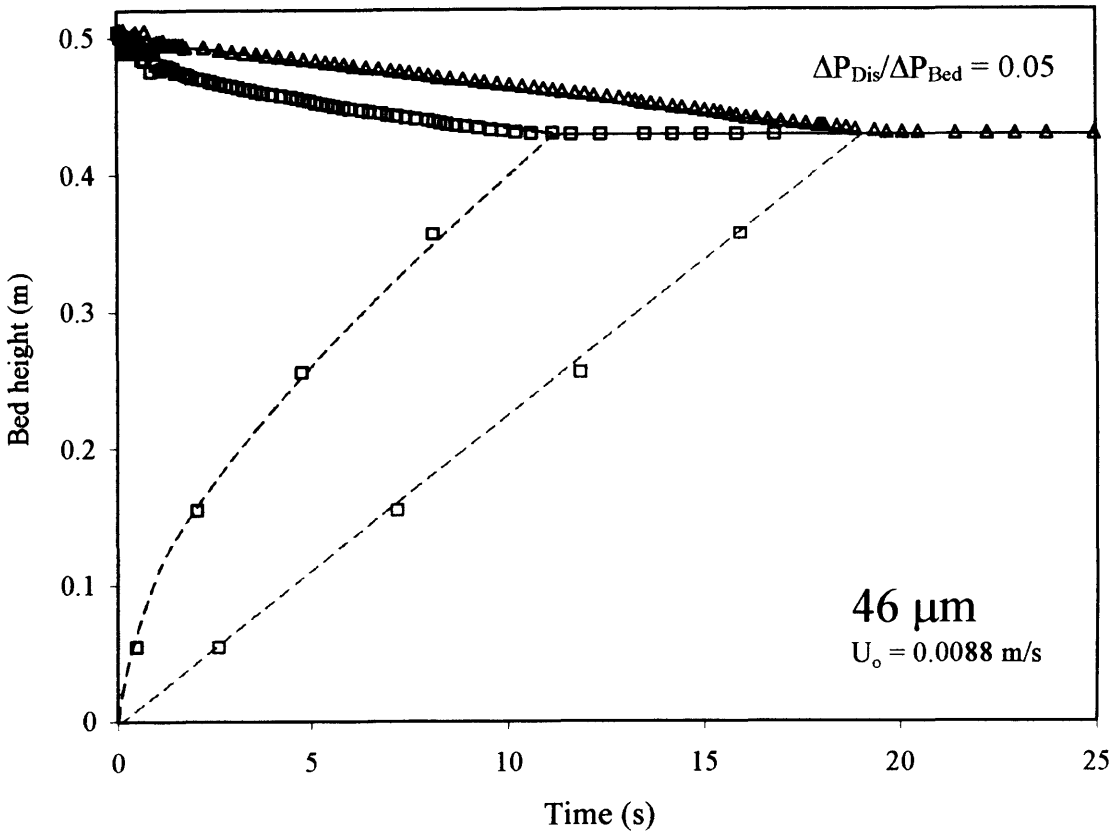

Figure 4.17 Comparison of model prediction and experimental L_2 for collapse of bubbling bed of 1-valve and 2-valve experiments.

4.4 Results of the model validation

The proposed model can be used to predict under which conditions the 1-valve or 2-valve configuration will yield the correct extrapolation to obtain the dense phase voidage from the experimental curve. Taking into account the system configuration, the model developed can be used to represent correctly the bed collapse curve, the bubble escape time, the de-aeration times, the fixed bed interface, and, the transient pressure drop profile. The new model can also illustrate clearly the variation with time of the gas windbox deaeration rate as well as the effect of the second valve on its deaeration rate.

The procedure used to determine the system properties - distributor pressure drop, discharge valve flow characteristics and fixed bed pressure drop - has been outlined and has allowed the interpretation of experimental bed collapse curve for the determination of the dense phase properties alone.

Based on this study we can conclude that both 1-valve and 2-valve experiments have advantages and limitations, and for this reason both should be performed to unambiguously determine the intrinsic properties of Geldart type A powders.

Chapter 5: Pressure Drop Characteristics

5.1 Introduction

Several fluidization properties can be inferred from total bed pressure drop and differential pressure drop profiles. For example fixed bed pressure drop can be measured and the onset of minimum fluidization can be determined easily from a plot of the pressure drop versus superficial velocity. The differences between pressure drops measured as the velocity increases or decreases give a clear indication of the cohesive nature of the particles. Also, if the pressure drop is less than that corresponding to the weight of the particles/area, one has a measure of the extent of the de-fluidization. The fluidization characteristics obtained from the pressure drop measurement for the different types of powders used in this work are discussed in this chapter, as well as the effects of initial bed height, column diameter and the distributor porosity.

5.1.1 Fluidization quality

The fluidization quality obtained from the pressure drop information is the extent of the de-fluidization. If the bed is fully fluidized, the bed pressure drop is equal to that corresponding to the total weight of the bed/area.

5.1.2 Onset of minimum fluidization point

The minimum fluidization velocity can be simply obtained from the relationship between the bed pressure drop and the inlet superficial gas velocity as described in Figure 5.1. The minimum fluidization velocity (U_{mf}) is the point where the extrapolation of the fixed bed pressure drop crosses the extrapolation of the constant fluidized bed pressure drop. While U_{mf} can read from the graph of ΔP versus U_0, the voidage at minimum fludization, ε_{mf}, can be calculated directly from the fixed bed height.

At the onset of the minimum fluidization, the interaction force between fluid and particle is equal to the weight of particles and the particles are supported completely by the fluid. For a higher velocity, the total bed pressure drop is always equal to the weight of the bed/area.

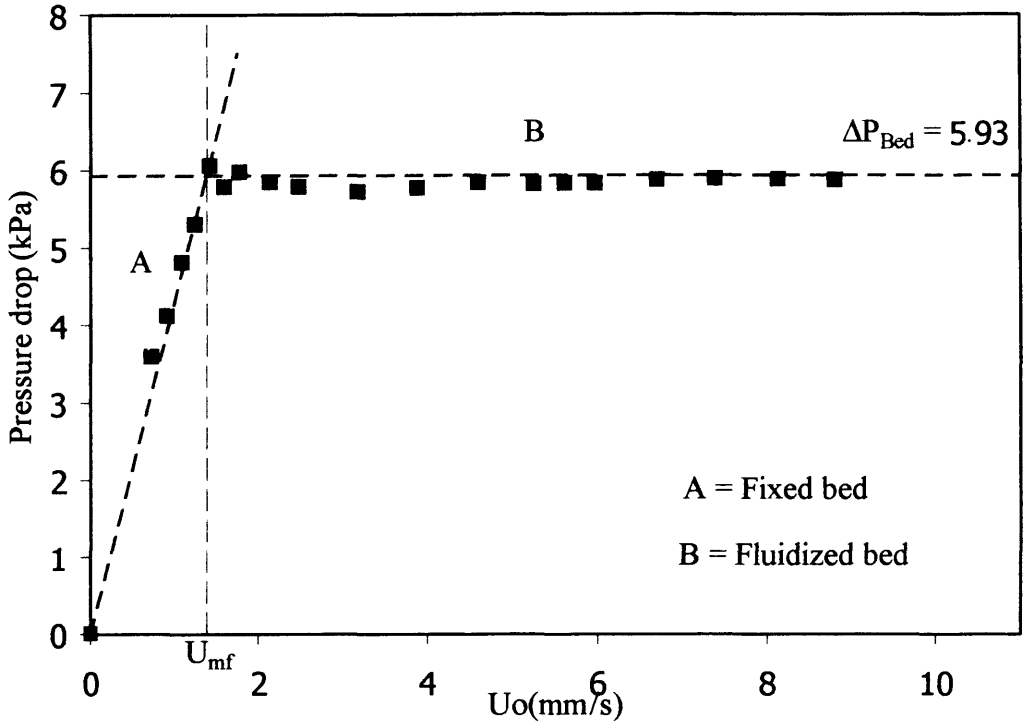

Figure 5.1Total bed pressure drop versus inlet superficial gas velocity (d_P = 37 μm (Original powder, Batch 1), ID = 0.127 m, L_I = 0.43 m)

The average particle size has an effect on the fixed bed pressure loss and U_{mf}. Simone and Harriott (1980) reported that the minimum fluidization velocity increases with the average size and the minimum fluidization voidage decreases with the particle size for the narrow size cut powder. The powder with a wide size distribution and with fines was reported to have a lower minimum fluidization velocity (Geldart and Buczek, 1989; Simone and Harriott, 1980) and a lower minimum bubbling voidage (Simone and Harriott, 1980). DeJong and Nomden (1974) reported that the powder with a wide size distribution follows the same pressure drop relation as the narrow size cuts.

5.1.3 Fixed bed pressure drop

The fluid pressure loss in a fixed bed is due to frictional dissipation, but the fluid-particle interaction force is insufficient to support the weight of particles.

The fixed bed pressure drop/length can be obtained from the direct measurement of the total bed pressure drop at the windbox/corrected bed height and the differential pressure drop profile/probe separation, at various flows before the minimum fluidization velocity. This information can be used to predict the 1- and 2-valve bed collapse experiments as shown in the previous chapter.

5.1.4 Fluidization and de-fluidization experiments

For the case of fixed beds of fine particles, at $U < U_{mf}$, the pressure increase linearly with velocity and the bed height remains constant. When the superficial velocity is increased above U_{mf}, a maximum in the pressure drop is sometimes observed. When the pressure is higher than the weight of the bed a momentum balance indicates that a yield stress in the particle assembly resulting from friction forces between the particles or between the particles and the wall (De Jong and Nomden, 1974; Mutsers and Rietema, 1977a; Srivastava and Sundaresan, 2002; Rietema and Piepers, 1990) is present. If the powder is cohesive the overshoot in the pressure drop becomes more obvious. In this case even above U_{mf} the pressure drop at each velocity can be less than the weight of the particles as some powders are supported by the wall (Jackson, 1998).

When the gas fluidization velocity is reduced, i.e. the de-fluidization experiment, the particles start from a condition in which direct contact is minimal and the yield stress is less or can be neglected and the transition from fluidized to fixed bed is gradual.

5.1.5 Pressure drop profile of fluidized bed

The differential pressure drop profile can be used to study the local properties of the fluidized bed. The pressure drop profile in the fixed bed region can give information about the local fixed bed voidage along the vertical bed height. The pressure drop profile at the transition from the fixed to fluidized bed can give information about the local mechanical stress from the fluidization and de-fluidization experiment. For the fluidized bed, the pressure drop profile can give an indication of the general expansion behaviour and also the local bed voidage.

5.2 Effect of column diameter and bed height

Experiments have been carried out on the two size natural size distribution powders, with average particle diameters of 37 μm and 72 μm. The detail of the experimental conditions are summarised in Table 3.6.

5.2.1 Fluidization quality

As shown in Figure 5.2 and Figure 5.3, the total bed pressure drop of the fluidized bed of powders is equal to the weight of the bed/area. This means that the powders are fully fluidized.

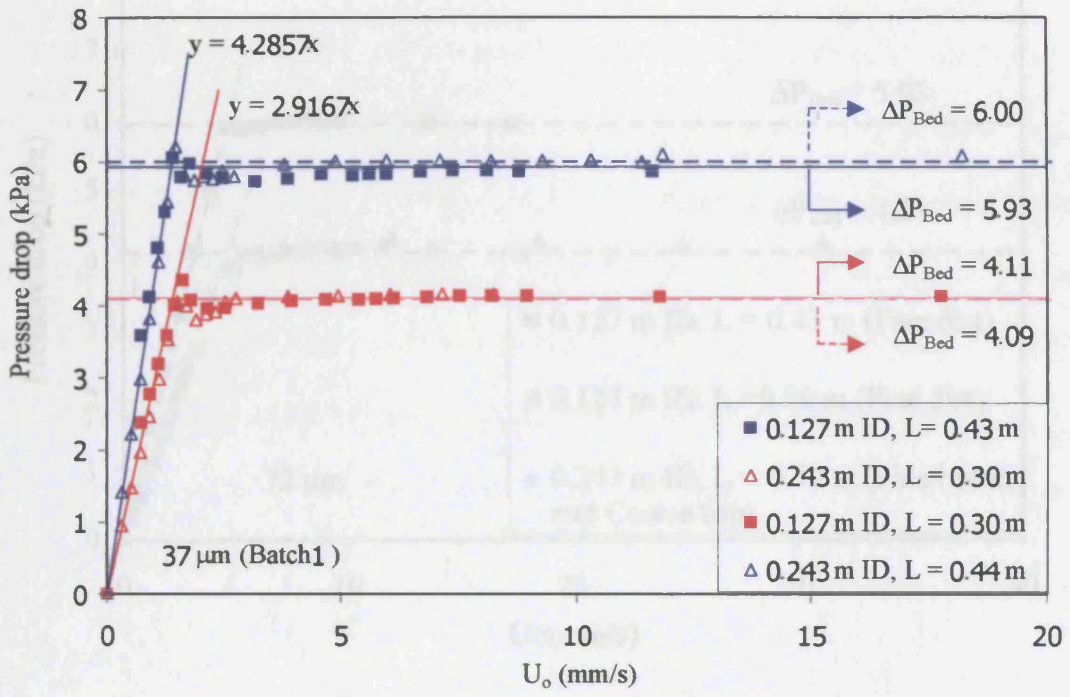

Figure 5.2 Total bed pressure drop versus U_o for 37 μm Ballotini (Batch 1)

However, for the 37 μm powder (Batch 2), Figure 5.4, the total bed pressure drop is slightly lower than the weight of the bed, by approximately 1.34 % and 2.68 % for 0.4 m and 0.3 m initial bed height, respectively. This means the finer powders are slightly cohesive and partially de-fluidized.

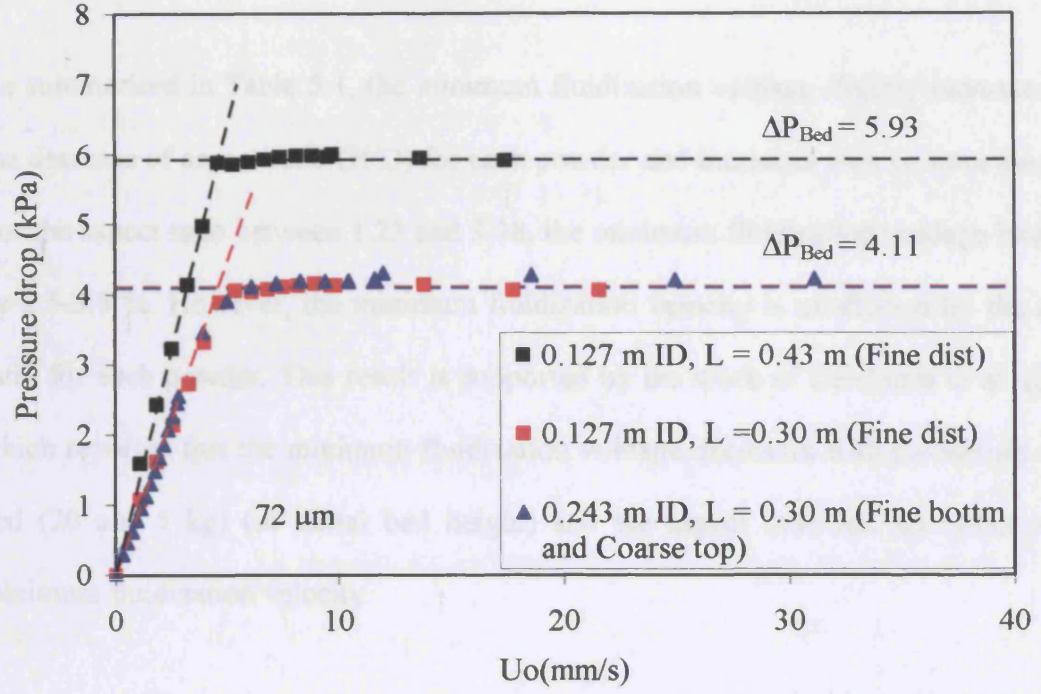

Figure 5.3 Total bed pressure drop versus U_o for 72 µm Ballotini

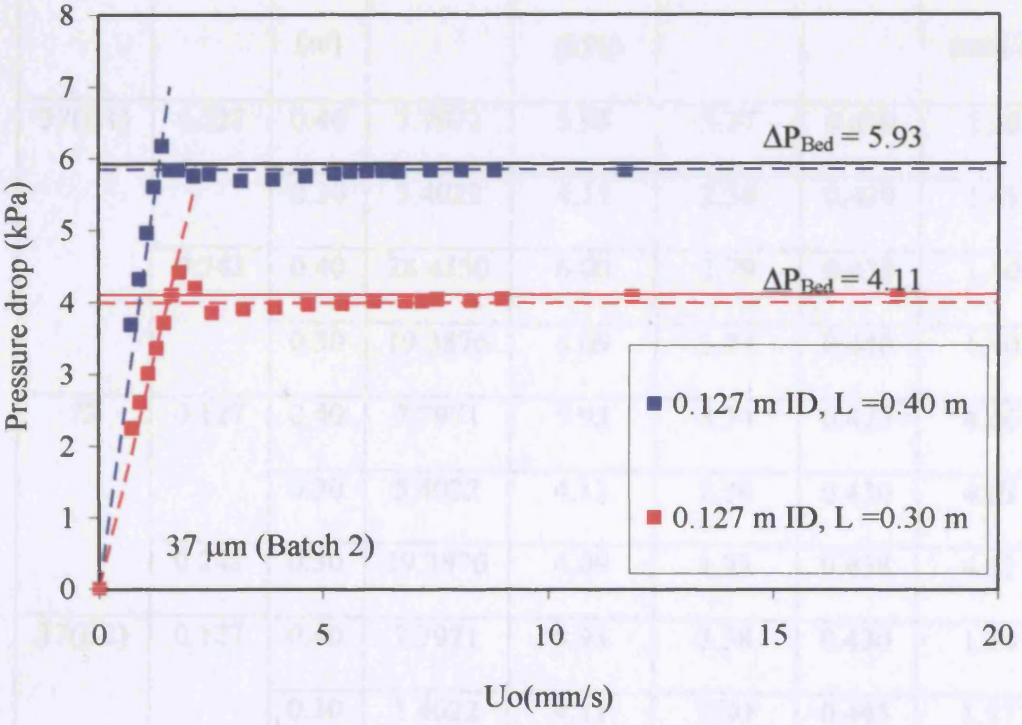

Figure 5.4 Total bed pressure drop versus U_o for 37 µm Ballotini (Batch 2)

5.2.2 Onset of the fluidization stage

As summarised in Table 5.1, the minimum fluidization voidage slightly increases with the decrease of aspect ratio (H/D) for each powder and increases with column diameter. For the aspect ratio between 1.23 and 3.38, the minimum fluidization voidage increased by 2.5-3.5 %. However, the minimum fluidization velocity is unaffected by the aspect ratio for each powder. This result is supported by the work of Delebarre et al. (2004), which reported that the minimum fluidization voidage decreases with the weight of the bed (20 and 5 kg) (or initial bed height) and the aspect ratio has no effect on the minimum fluidization velocity.

Table 5.1 Aspect ratio, bed pressure drop, and, minimum fluidization point of powders

d_P (μm)	ID (m)	L_I (m)	W_P (kg)	ΔP_{Bed} (kPa)	H/D	ε_{mf}	U_{mf} (mm/s)
37(B1)	0.127	0.40	7.7971	5.93	3.37	0.429	1.38
		0.30	5.4022	4.11	2.38	0.439	1.41
	0.243	0.40	28.4350	6.00	1.79	0.433	1.40
		0.30	19.3876	4.09	1.24	0.440	1.40
72	0.127	0.40	7.7971	5.93	3.34	0.423	4.66
		0.30	5.4022	4.11	2.34	0.430	4.63
	0.243	0.30	19.3876	4.09	1.23	0.438	4.61
37(B2)	0.127	0.40	7.7971	5.93	3.38	0.430	1.34
		0.30	5.4022	4.11	2.40	0.445	1.57

For the 37 μm Ballotini (Batch 2), the minimum fluidization velocity is not the same for two different aspect ratios and is also different from Batch 1 which has the same average diameter. The possible explanation for this case is that this powder shows a degree of cohesiveness, and thus it tends to agglomerate and the results are not fully reproducible.

5.2.3 Fixed bed pressure drop

Figure 5.5 to Figure 5.6 show that the fixed bed pressure drop/length gradually changes according to the fixed bed voidage for the same type of powder since, as mentioned earlier, the fixed bed voidage itself changed according to the aspect ratio and the column diameter. For 37 μm Ballotini (batch 2) (Figure 5.7), the fixed bed pressure drop/length changed according to the fixed bed voidage as before. However, the difference of the pressure drop/length for each aspect ratio does not depend only on the voidage but it appears to indicate that some agglomeration of the powder may result in channelling and the extent of this varies for different experiments.

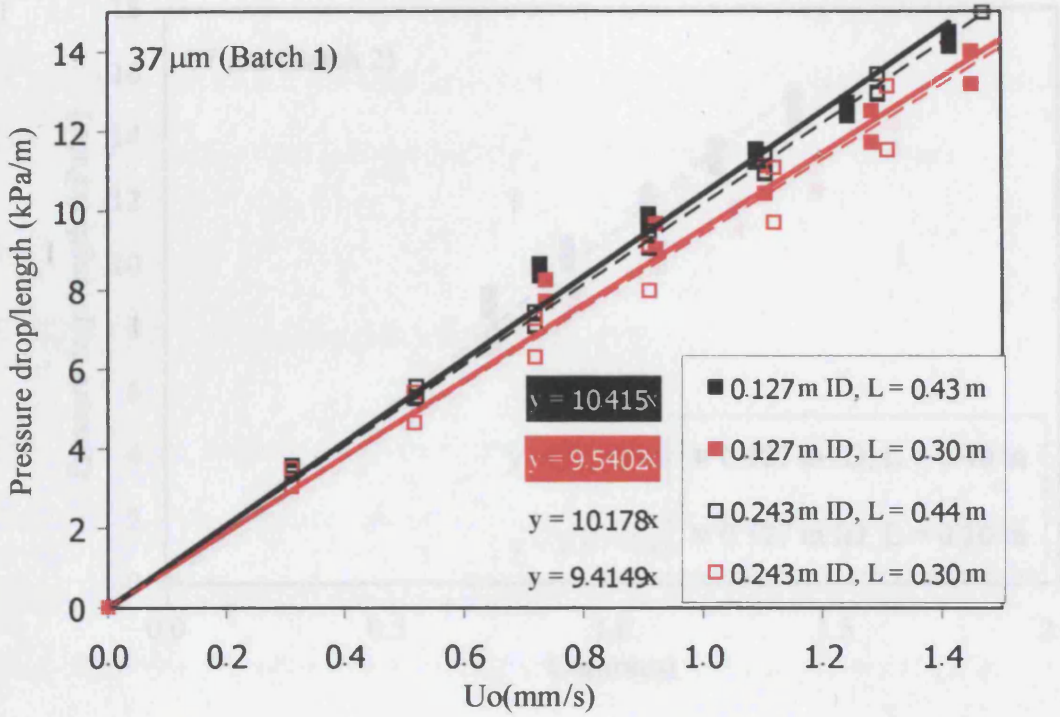

Figure 5.5 Fixed bed pressure drop/length for 37 µm Ballotini (Batch 1)

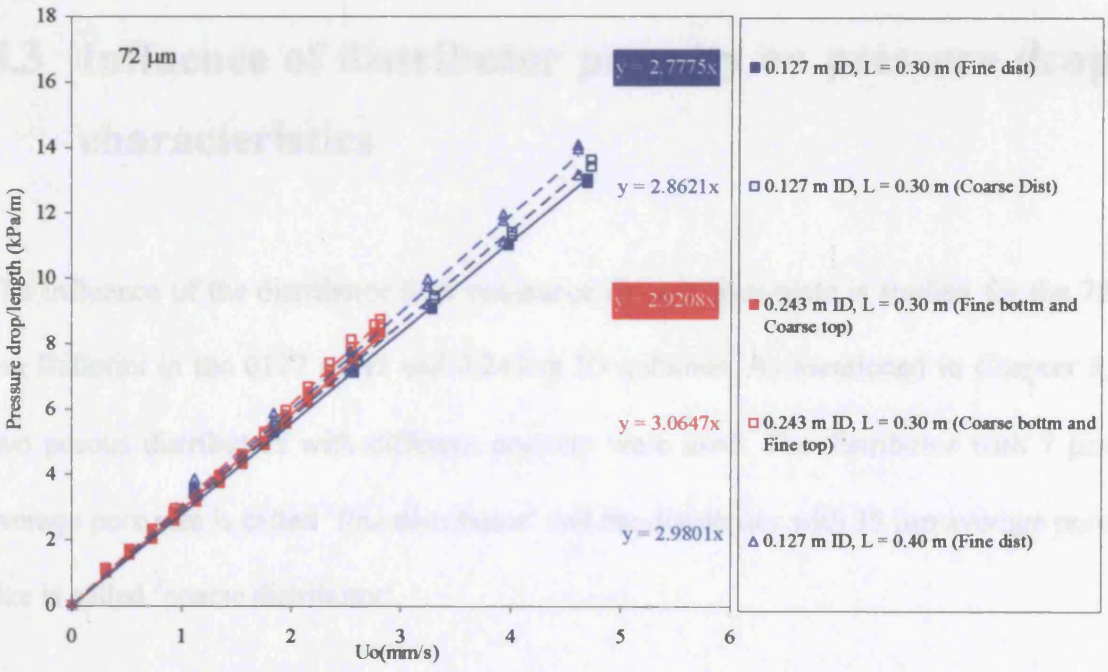

Figure 5.6 Fixed bed pressure drop/length for 72 µm Ballotini

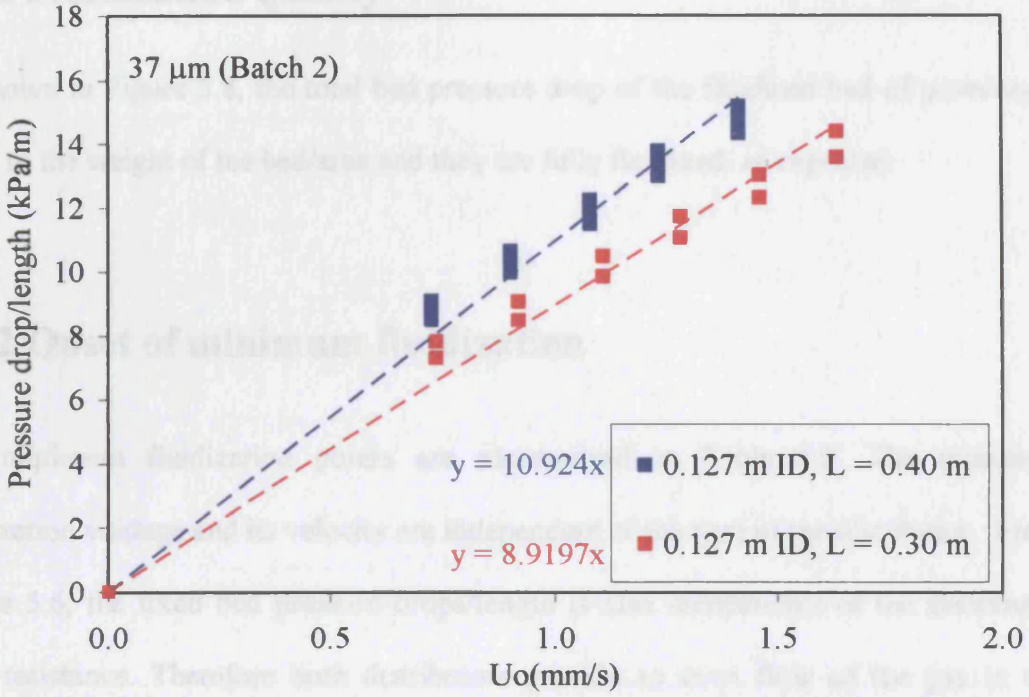

Figure 5.7 Fixed bed pressure drop/length for 37 µm Ballotini (Batch 2)

5.3 Influence of distributor porosity on pressure drop characteristics

The influence of the distributor flow resistance for a porous plate is studied for the 72 µm Ballotini in the 0127 m ID and 0.243 m ID columns. As mentioned in Chapter 3, two porous distributors with different porosity were used. The distributor with 7 µm average pore size is called 'fine distributor' and the distributor with 35 µm average pore size is called 'coarse distributor'.

5.3.1 Fluidization quality

As shown in Figure 5.8, the total bed pressure drop of the fluidized bed of powders is equal to the weight of the bed/area and they are fully fluidized, as expected.

5.3.2 Onset of minimum fluidization

The minimum fluidization points are summarised in Table 5.2. The minimum fluidization voidage and its velocity are independent of the type of the distributor. From Figure 5.6, the fixed bed pressure drops/length is also independent of the distributor flow resistance. Therefore both distributors provide an even flow of the gas in the columns and no voidage in-homogeneities are detected.

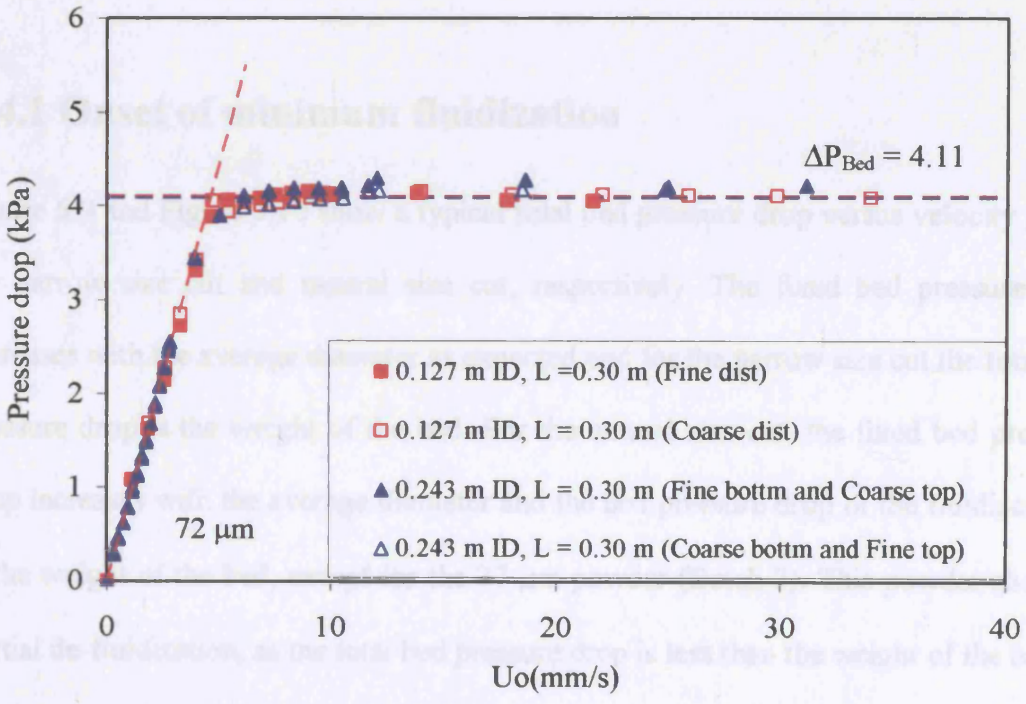

Figure 5.8 Total bed pressure drop versus U_o for 72 µm Ballotini at different column diameter and distributor flow resistance

Table 5.2 Summary of the minimum fluidization point for 72 mm Ballotini at different column diameter and distributor flow resistance

d_P (μm)	ID (m)	ΔP_{Bed} (kPa)	H/D	Distributor type		U_{mf} (mm/s)	ε_{mf}
				Top	Bottom		
72	0.127	4.11	2.34	Fine	Fine	4.63	0.430
		4.11	2.32	Coarse	Coarse	4.63	0.426
	0.243	4.09	1.23	Fine	Coarse	4.61	0.438
		4.09	1.22	Coarse	Fine	4.61	0.432

5.4 Pressure drop characteristics of narrow size cut powders and natural size cut powders

5.4.1 Onset of minimum fluidization

Figure 5.9 and Figure 5.10 show a typical total bed pressure drop versus velocity graph for narrow size cut and natural size cut, respectively. The fixed bed pressure drop increases with the average diameter as expected and for the narrow size cut the total bed pressure drop is the weight of the bed. For the natural size cut, the fixed bed pressure drop increases with the average diameter and the bed pressure drop of the fluidised bed is the weight of the bed, except for the 37 μm powder (Batch 2). This powder shows a partial de-fluidization, as the total bed pressure drop is less than the weight of the bed.

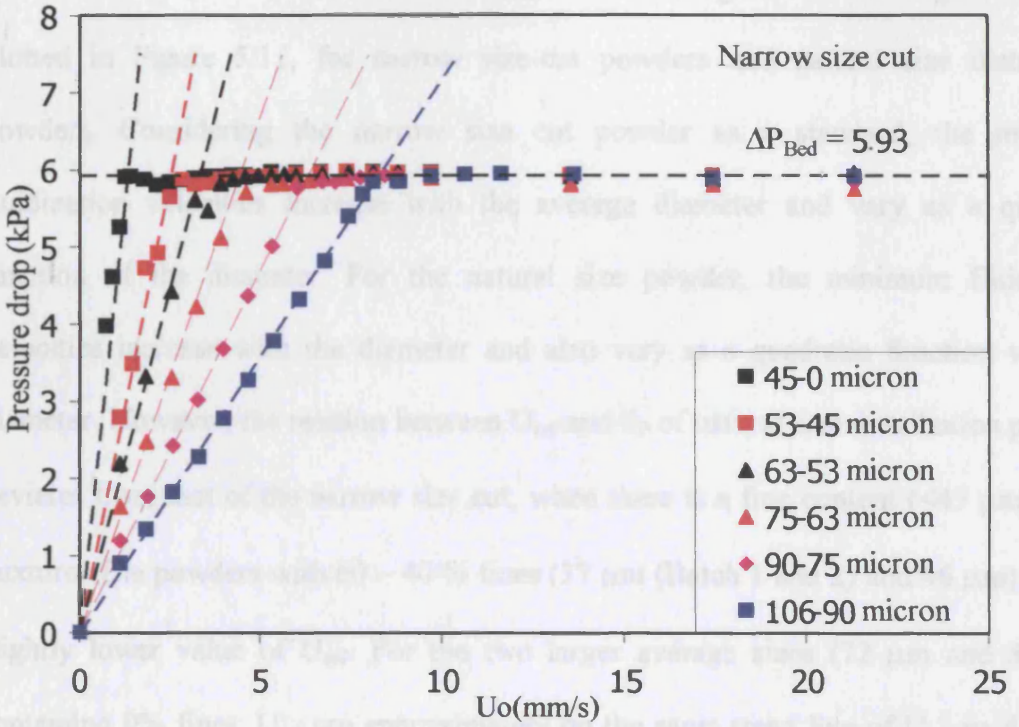

Figure 5.9 Total bed pressure drop versus U_o for narrow size cut powders

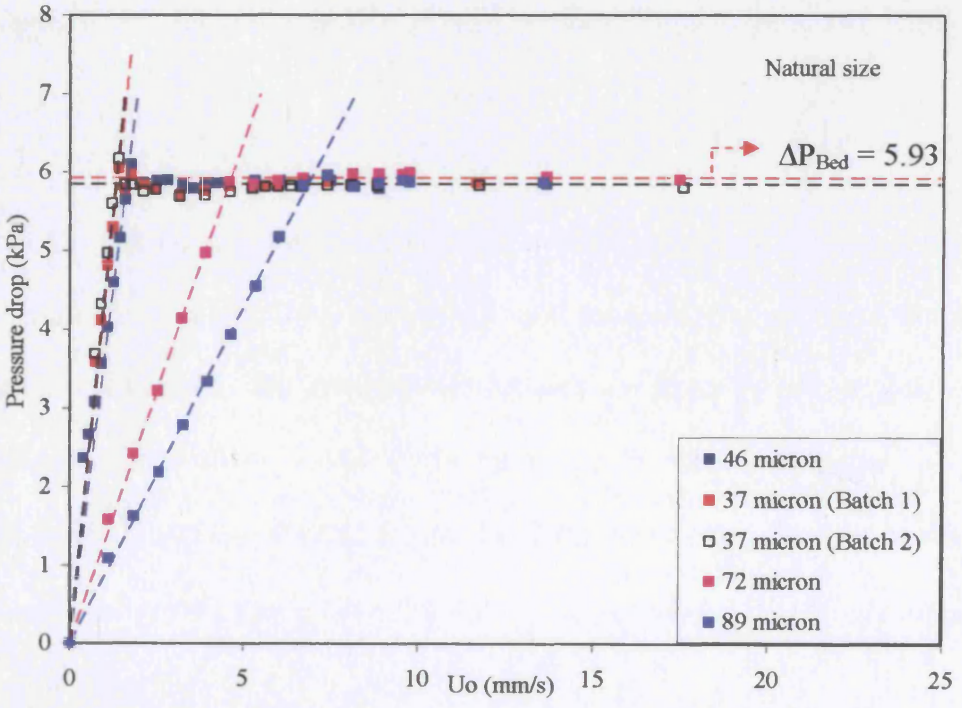

Figure 5.10 Total bed pressure drop versus U_o for natural size powders

The minimum fluidization velocities obtained from Figure 5.9 and Figure 5.10 are plotted in Figure 5.11, for narrow size-cut powders and natural size distribution powders. Considering the narrow size cut powder as a standard, the minimum fluidization velocities increase with the average diameter and vary as a quadratic function of the diameter. For the natural size powder, the minimum fluidization velocities increase with the diameter and also vary as a quadratic function with the diameter. However, the relation between U_{mf} and d_P of natural size distribution powders deviates from that of the narrow size cut, when there is a fine content (<45 μm) in the mixture. The powders with 60 – 40 % fines (37 μm (Batch 1 and 2) and 46 μm) show a slightly lower value of U_{mf}. For the two larger average sizes (72 μm and 89 μm), containing 0% fines, U_{mf} are approximately on the same trend line of U_{mf} vs d_P as for the narrow size cut.

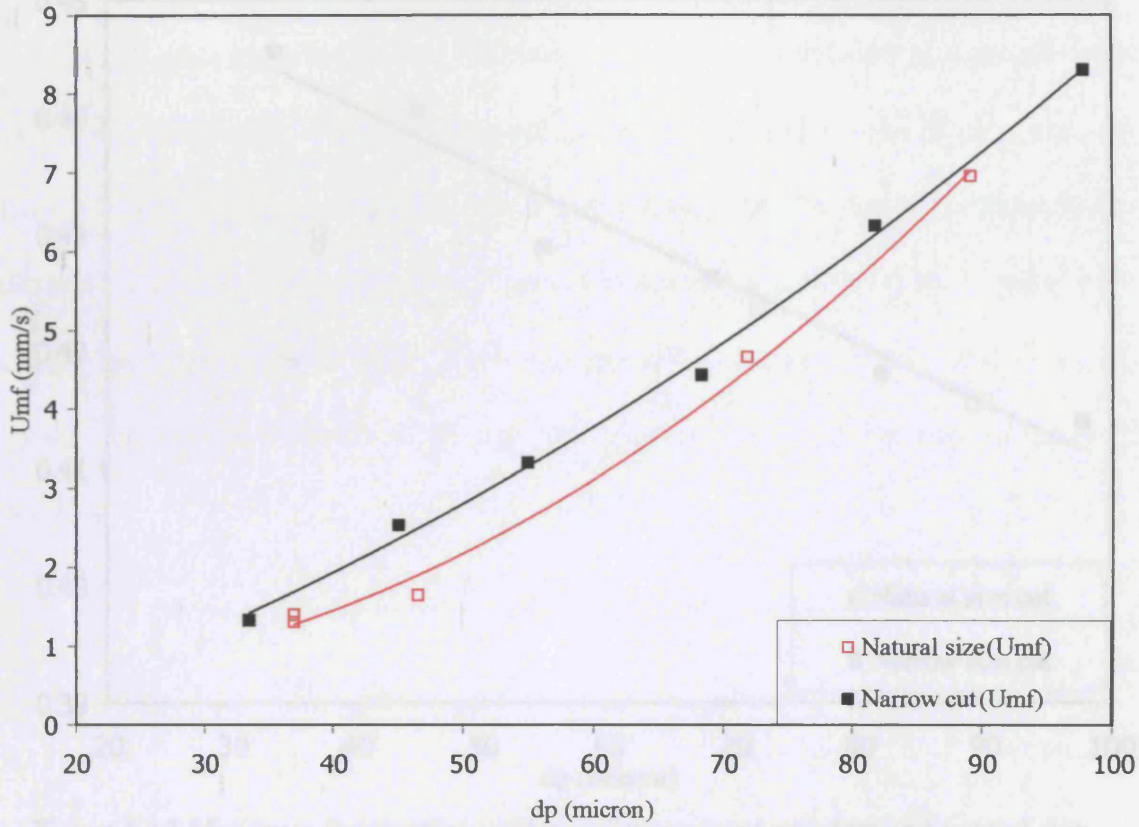

Figure 5.11 Minimum fluidization velocity of narrow size powders and natural size powders

Figure 5.12 shows the minimum fluidization voidage of narrow size cut powders and natural size powders. For the narrow size cut powders, the minimum fluidization voidages decrease with the increases of the average diameter and vary as a linear function with the average diameter. The minimum fluidization voidages for powder without fines, 72 μm and 89 μm, are on the linear trend of ε_{mf} from narrow size cut powders. ε_{mf} of powders with 60-40 % fines, 37 μm (Batch 1 and 2) and 46 μm, are found to be lower.

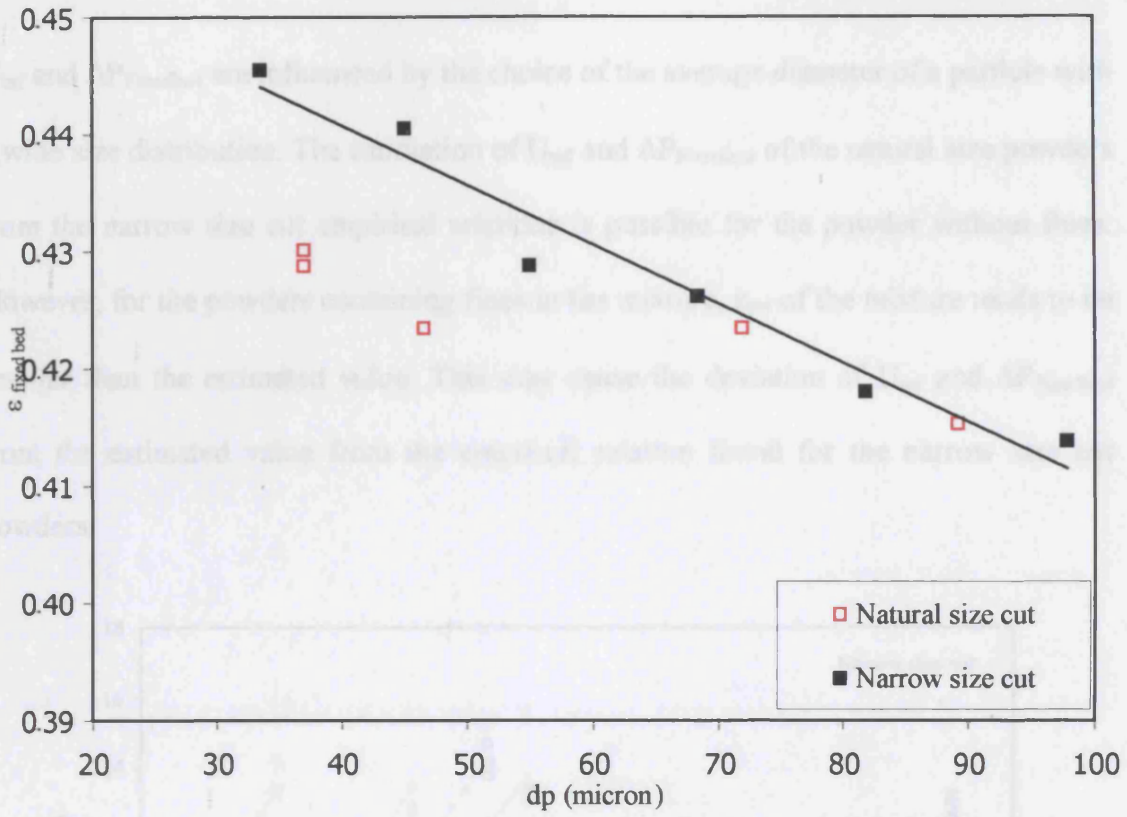

Figure 5.12 Minimum fluidization voidage of narrow cut powders and natural size powders

5.4.2 Fixed bed pressure drop

Fixed bed pressure drop/length for the narrow size cut powders and the natural size powders are shown in Figure 5.13 and Figure 5.14, respectively. The powders with smaller size induce more fixed (Figure 5.12). The coefficients of the gas flow resistance of the fixed bed, 'fixed bed pressure drop/ (length.U_0)', for narrow size cut powders and natural size powders are shown in Figure 5.15. For the narrow size cut powders, the coefficient is higher for smaller average size powders and is related with the average size by a logarithmic function. For the natural size powder, the coefficients of those without fines can be estimated from the relation found for the narrow size cut powders, while the powders with fines have higher coefficients.

U_{mf} and $\Delta P_{Fixedbed}$ are influenced by the choice of the average diameter of a particle with a wide size distribution. The estimation of U_{mf} and $\Delta P_{Fixedbed}$ of the natural size powders from the narrow size cut empirical relations is possible for the powder without fines. However, for the powders containing fines in the mixture, ε_{mf} of the mixture tends to be smaller than the estimated value. This may cause the deviation of U_{mf} and $\Delta P_{Fixedbed}$ from the estimated value from the empirical relation found for the narrow size cut powders.

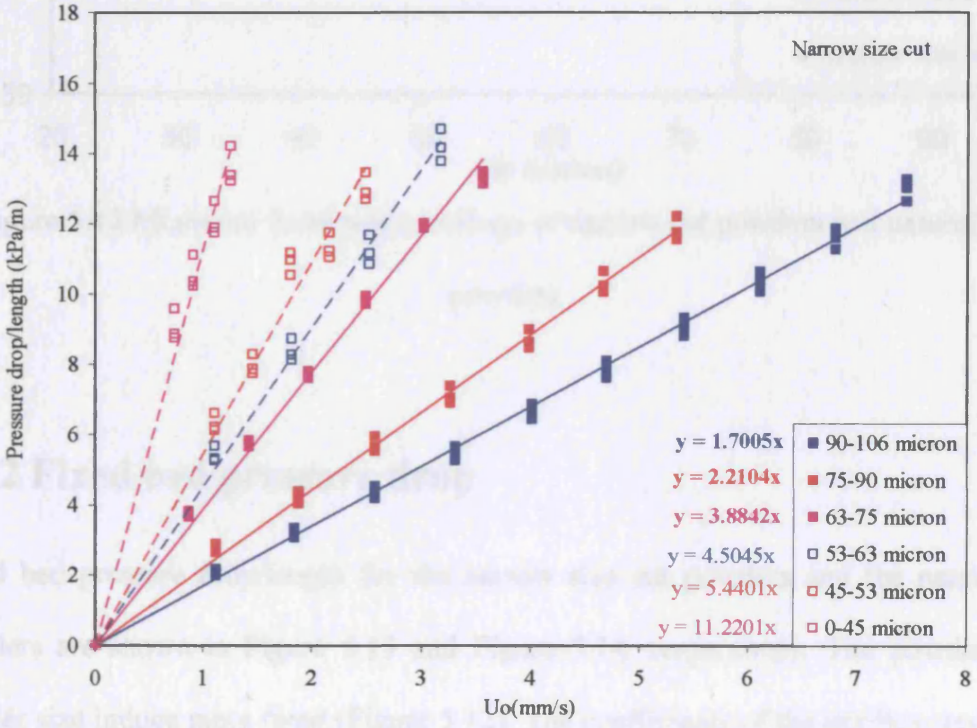

Figure 5.13 Fixed bed pressure drop/length for narrow size cut powder

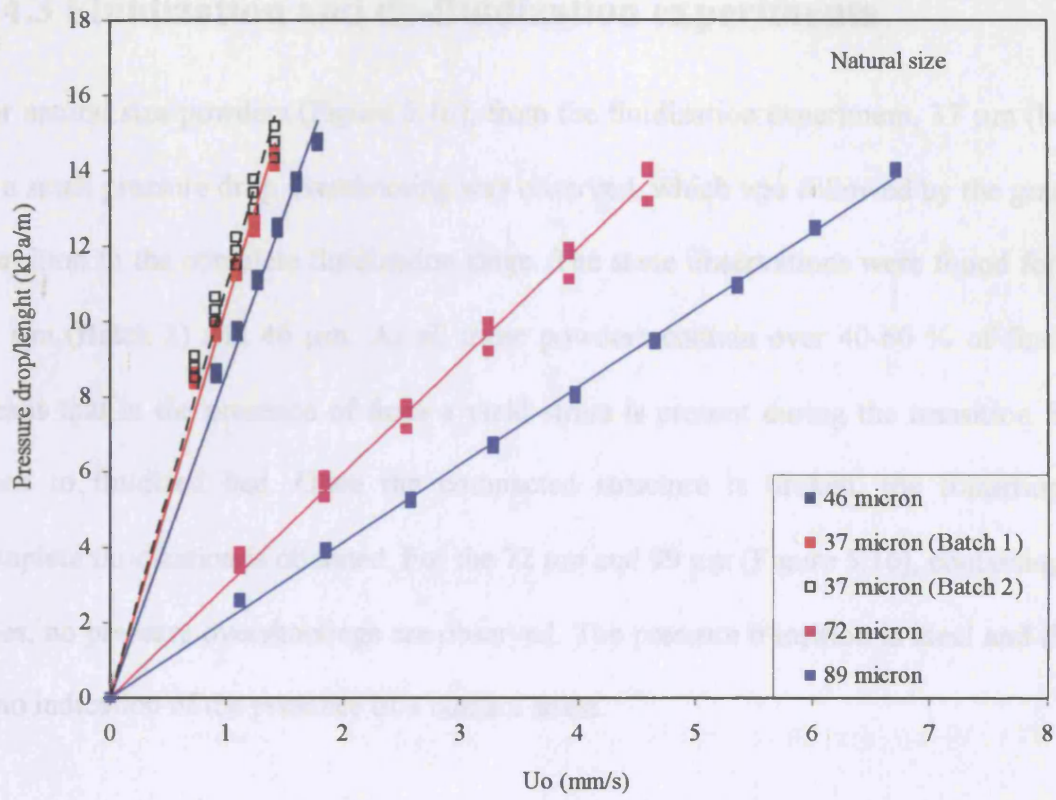

Figure 5.14 Fixed bed pressure drop of natural size powders

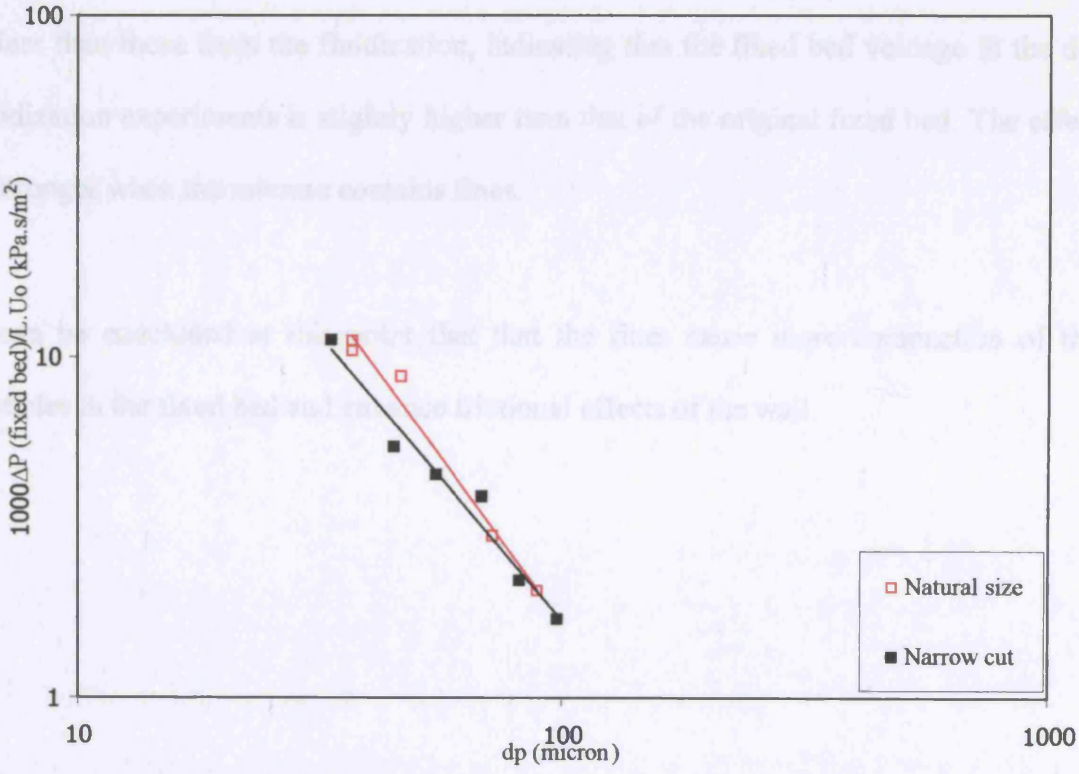

Figure 5.15 Fixed bed pressure drop/ $(L \cdot U_0)$ for narrow size cut and natural size cut

5.4.3 Fluidization and de-fluidization experiments

For natural size powders (Figure 5.16), from the fluidization experiment, 37 μm (batch 1) a small pressure drop overshooting was observed, which was followed by the gradual transition to the complete fluidization stage. The same observations were found for the 37 μm (Batch 2) and 46 μm. As all these powders contain over 40-60 % of fines, it means that in the presence of fines a yield stress is present during the transition from fixed to fluidized bed. Once the compacted structure is broken, the transition to complete fluidization is obtained. For the 72 μm and 89 μm (Figure 5.16), containing no fines, no pressure overshootings are observed. The pressure transition is ideal and there is no indication of the presence of a contact stress.

From the de-fluidization experiments, (Figure 5.16-Figure 5.18), all the powders show a gradual transition. In addition (Figure 5.16- Figure 5.18), the pressure at each velocity is less than those from the fluidization, indicating that the fixed bed voidage in the de-fluidization experiments is slightly higher than that of the original fixed bed. The effect is stronger when the mixture contains fines.

It can be concluded at this point that that the fines cause more compaction of the particles in the fixed bed and enhance frictional effects of the wall.

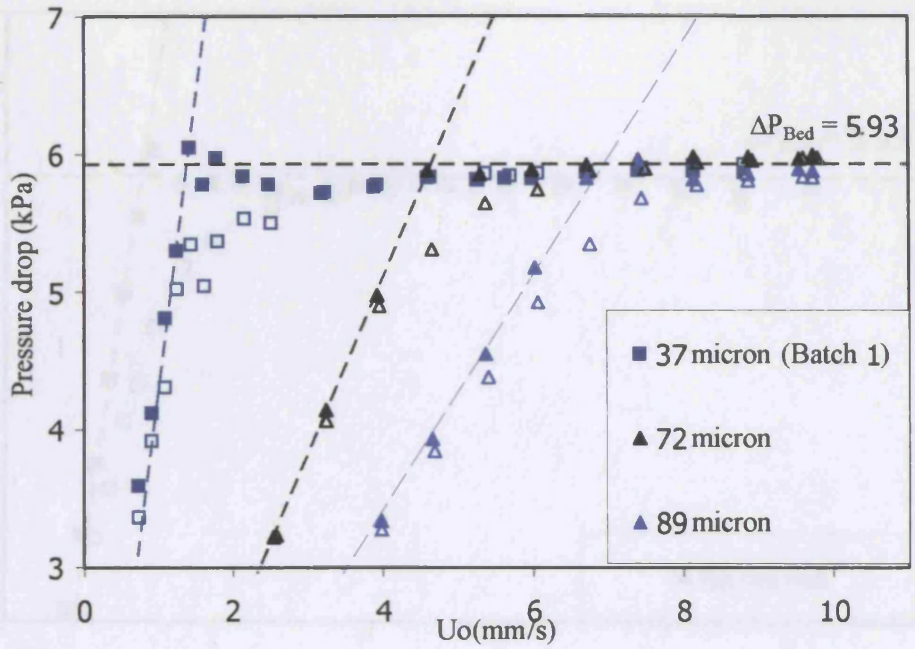

Figure 5.16 Fixed to fluidized bed transition behaviour of natural size powders (37 μm (batch 1), 72 μm and 89 μm) [Full symbols = fluidization and empty symbols = de-fluidization]

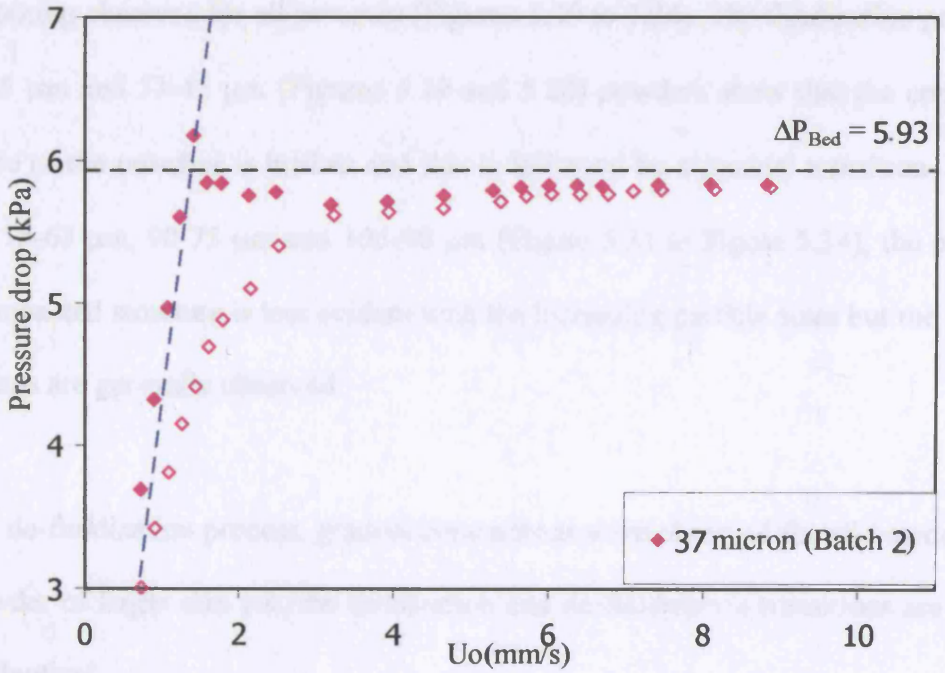

Figure 5.17 Fixed to fluidized bed transition behaviour of natural size powders (37 μm (batch 2)) [Full symbols = fluidization and empty symbols = de-fluidization]

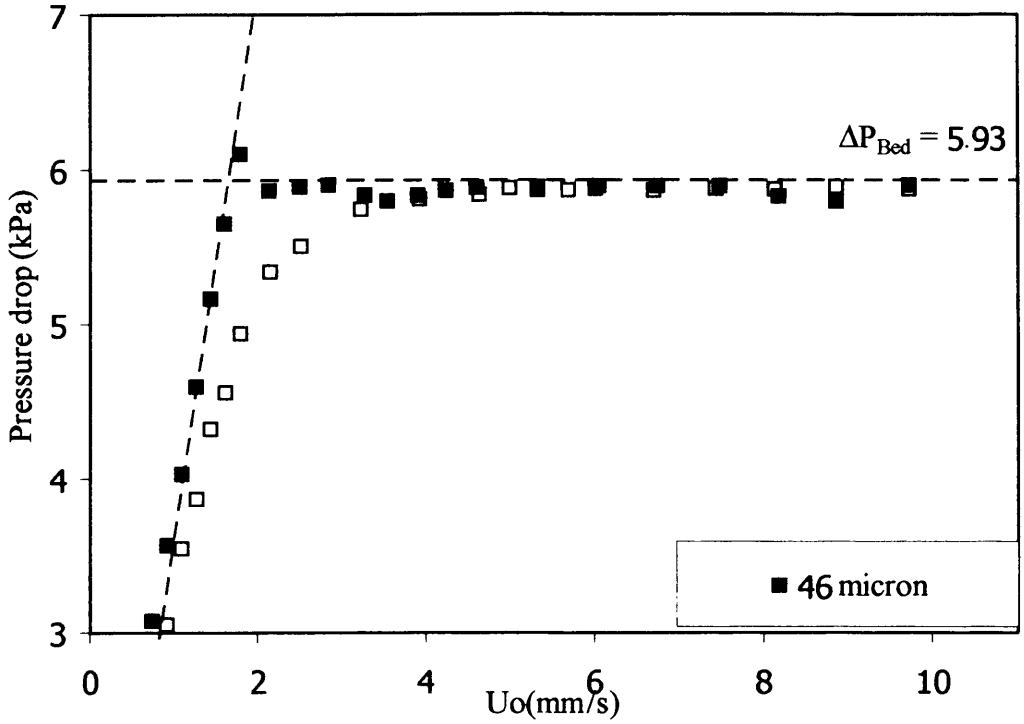

Figure 5.18 Fixed to fluidized bed transition behaviour of natural size powders (46 μm)

[Full symbols = fluidization and empty symbols = de-fluidization]

For the narrow size cut powder, during the fluidization experiment, there is no pressure overshooting observed for all powders (Figures 5.19 to 5.24). The fluidization processes for 0-45 μm and 53-45 μm (Figures 5.19 and 5.20) powders show that the compacted structure of the powders is broken and this is followed by a gradual transition. For 63-53μm, 75-63 μm, 90-75 μm and 106-90 μm (Figure 5.31 to Figure 5.34), the presence of a compacted structure is less evident with the increasing particle sizes but the gradual transitions are generally observed.

For the de-fluidization process, gradual contractions were observed for all powders. For the powder of larger size cut, the fluidization and de-fluidization transitions are almost in the identical.

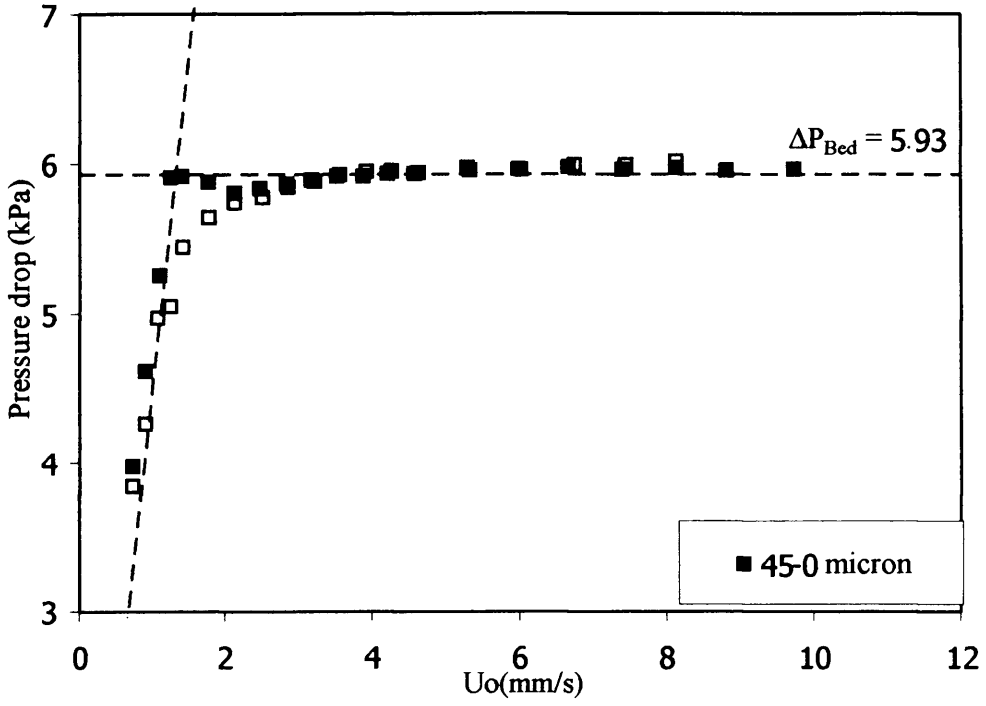

Figure 5.19 Fixed to fluidized bed transition behaviour of narrow size cut powders (45-0 μm) [Full symbols = fluidization and empty symbols = de-fluidization]

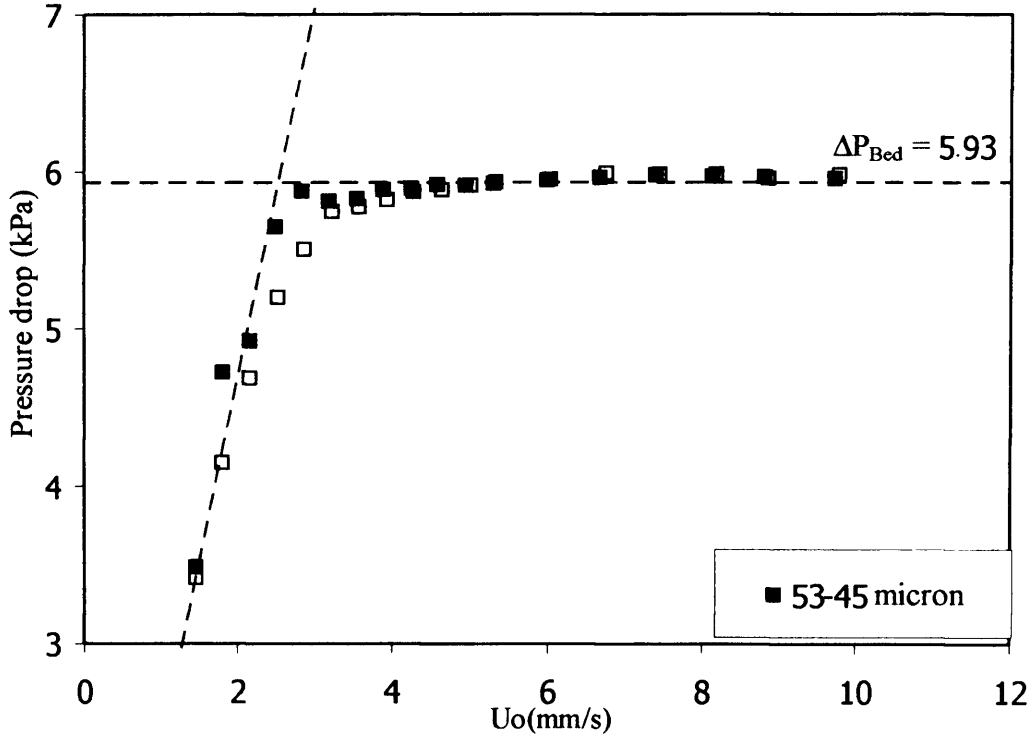

Figure 5.20 Fixed to fluidized bed transition behaviour of narrow size cut powders (53-45 μm) [Full symbols = fluidization and empty symbols = de-fluidization]

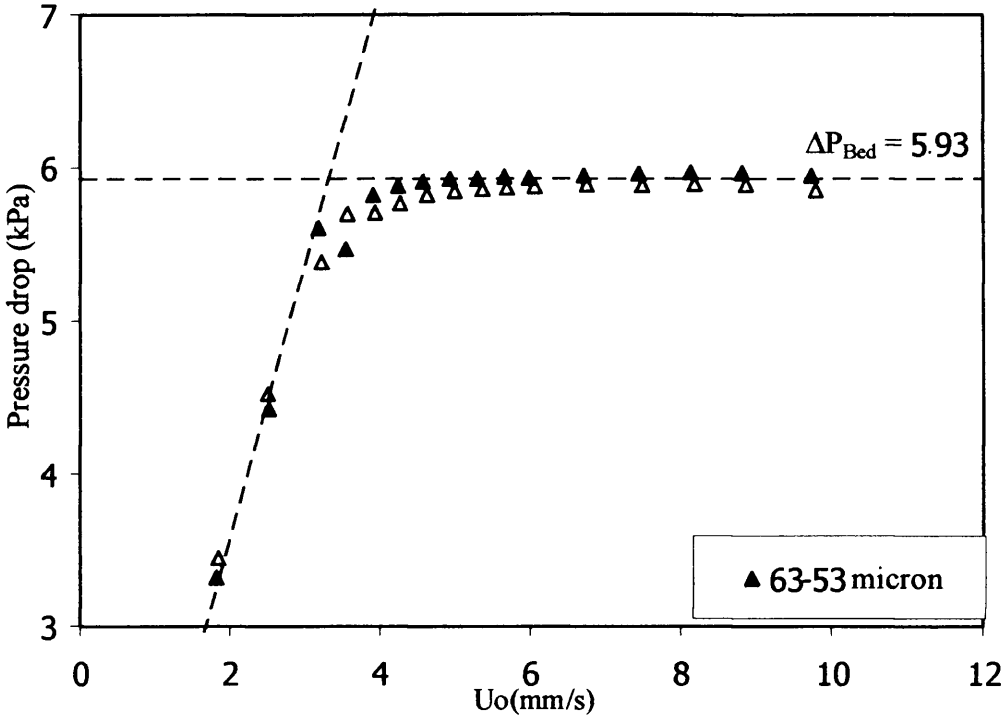

Figure 5.21 Fixed to fluidized bed transition behaviour of narrow size cut powders (63-53 μm) [Full symbols = fluidization and empty symbols = de-fluidization]

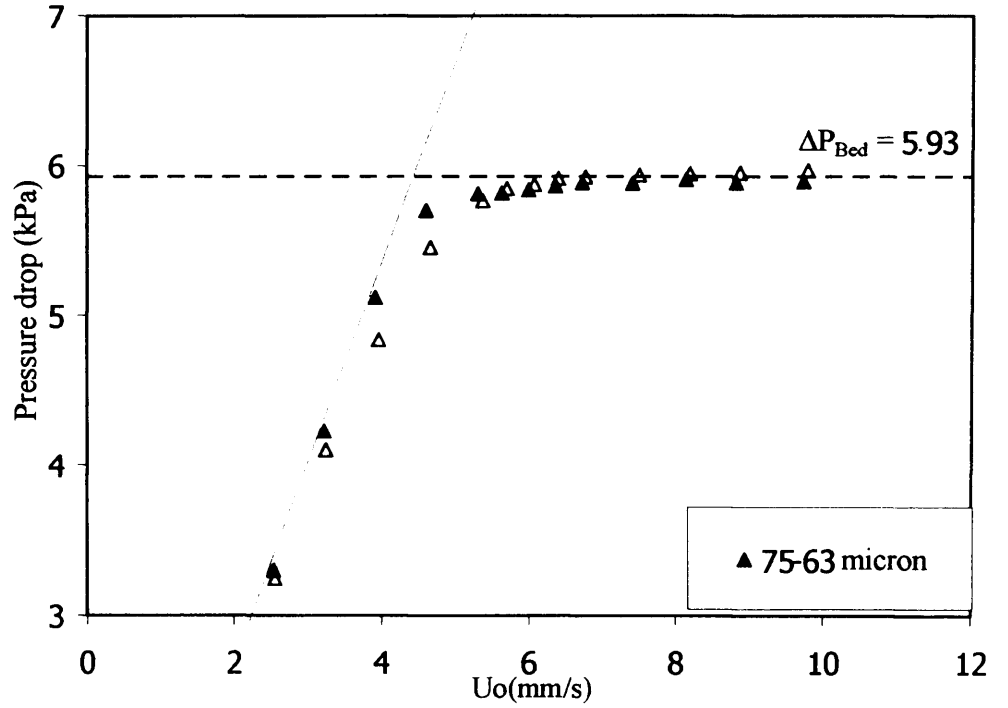

Figure 5.22 Fixed to fluidized bed transition behaviour of narrow size cut powders (75-63 μm) [Full symbols = Fluidization and empty symbols = de-fluidization]

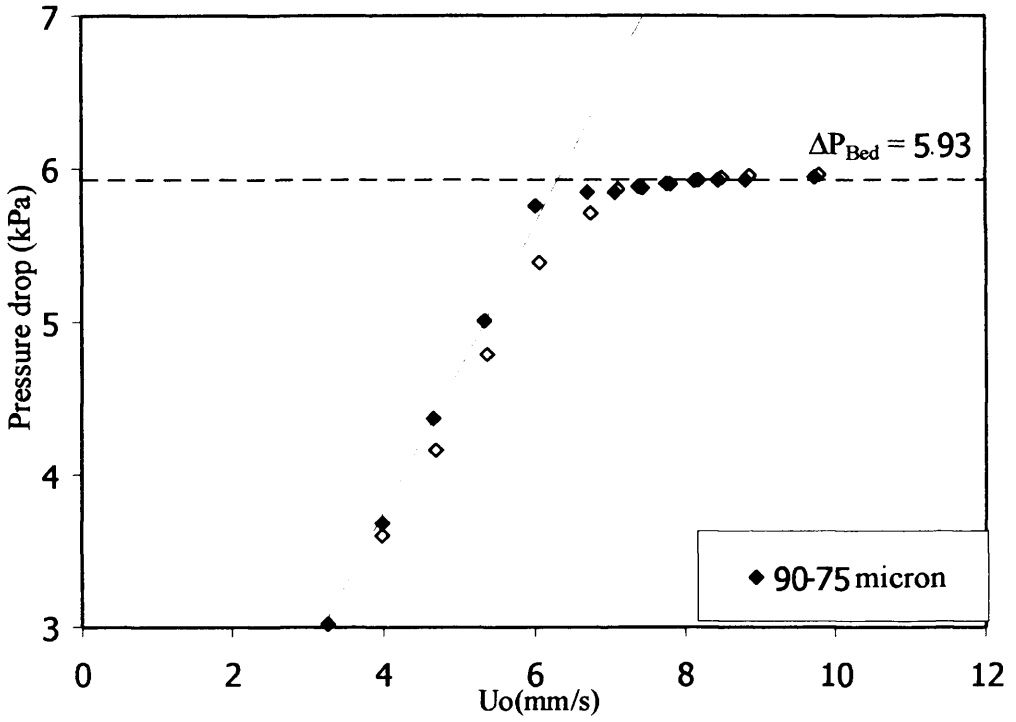

Figure 5.23 Fixed to fluidized bed transition behaviour of narrow size cut powders (90-75 μm) [Full symbols = fluidization and empty symbols = de-fluidization]

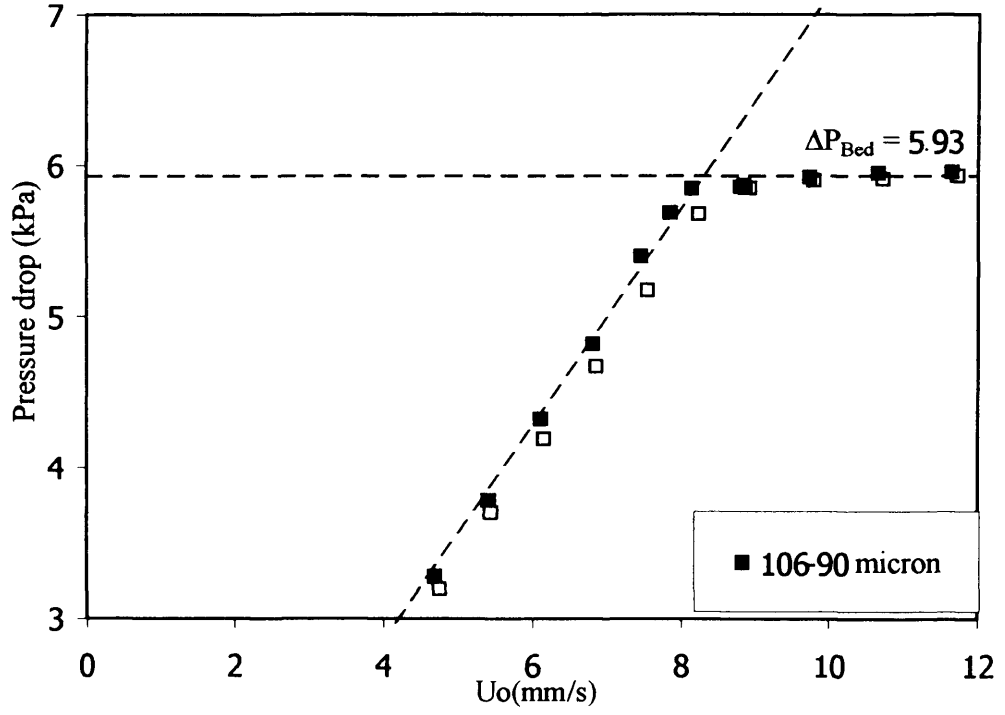

Figure 5.24 Fixed to fluidized bed transition behaviour of narrow size cut powders (106-90 μm) [Full symbols = fluidization and empty symbols = de-fluidization]

General conclusions;

- The natural size powders have more bed compaction and the wall friction plays a more important role than for the narrow size cuts.
- The degree of the compaction and the wall friction increases with the decrease in the size of the powder and increases with fine content.
- The bed compaction and the wall friction are generally dominant during the fluidization process.
- The de-fluidization process is generally gradual.

5.4.4 Pressure drop profile of the fluidized bed

The differential pressure drop profile represents the local bed voidage of the fixed and fluidized bed. From Figure 5.25 to Figure 5.34, region A represents the fixed bed where the pressure increases with the velocity. The pressure differences between the readings from each port location represent the differences in the local bed voidage. For both natural size distributions and narrow size cut powders (Figure 5.25 - Figure 5.34), the pressure readings from each location is almost the same, except the lowest pressure reading. Once the minimum fluidization point is reached, the bed expands homogeneously and this corresponds to region B. The more the bed expands, the lower the pressure drop. In this region, the differences of the pressure drop at different heights become more obvious. The pressure drop at the lower height, near the distributor region is higher compared to those of the higher locations, where the pressure drops are approximately the same. This means there is no difference in bed voidage along the bed except near the distributor. The possible explanation may be that there is a gas flow effect near the distributor area or that there is a small segregation where the larger

particles accumulate at the bottom of the bed. However, this is observed even with the narrow size cut where there is no size dispersion. This indicates a lower void fraction near the distributor, but the fact that the pressure drop increases indicates that the particles are fluidized.

The differential pressures drop decreases continuously, indicating homogeneous expansion, and reaches the minimum at the minimum bubbling point. From (Figure 5.25 - Figure 5.34), at each height the pressure drop reaches the minimum point at different velocities. Generally, the higher pressure ports reach the minimum bubbling point before the lowest port. This tends to confirm the fact that the void fraction near the distributor is slightly lower than that in the sections above. The range of the velocities where the differential pressure drop reaches the minimum point indicates the possible range of the minimum bubbling point. To be able to pinpoint the exact value of the minimum bubbling point, the maximum dense phase voidage should be used and that should be the average value of the entire fluidized bed.

After reaching the minimum value, the differential pressure drops gradually increase, as shown in region C. This means the bed voidage gradually decreases and the dense phase voidage decreases faster than the bubble hold up in the bed. However, from the pressure drop profile, it is hard to tell how rapidly the dense phase voidage decreases. The bed voidage reaches a stable value in region D and tends to level off at 2-3.5 times U_{mb} for the natural size distribution powders and 1.5-3 times U_{mb} for narrow size cut powders. The smaller size of the powders, the higher the U/U_{mb} ratio at which the bed voidage levels off.

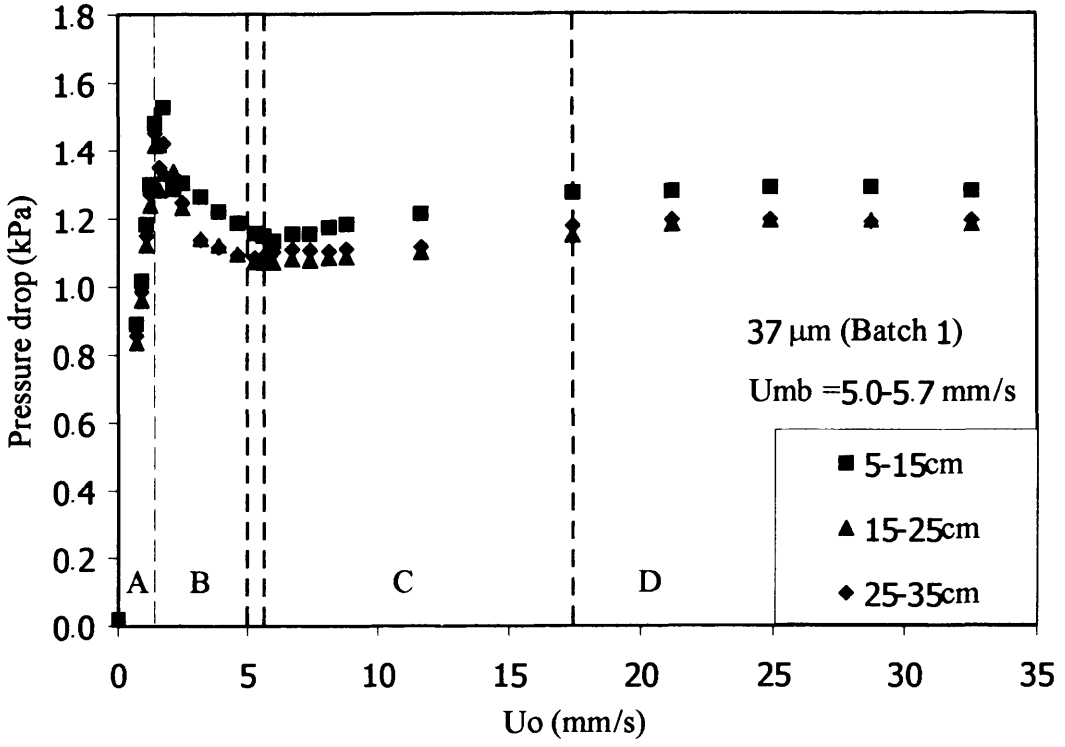

Figure 5.25 Pressure drop profile of 37 μm Batch 1 (natural size)

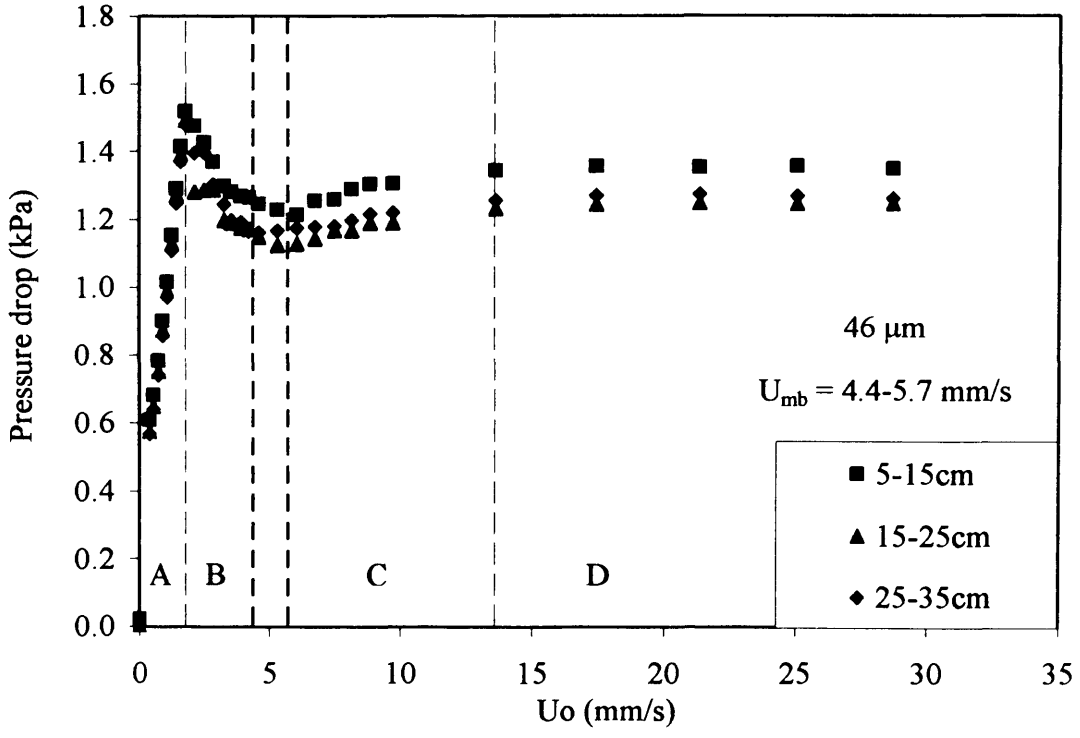

Figure 5.26 Pressure drop profile of 46 μm (natural size)

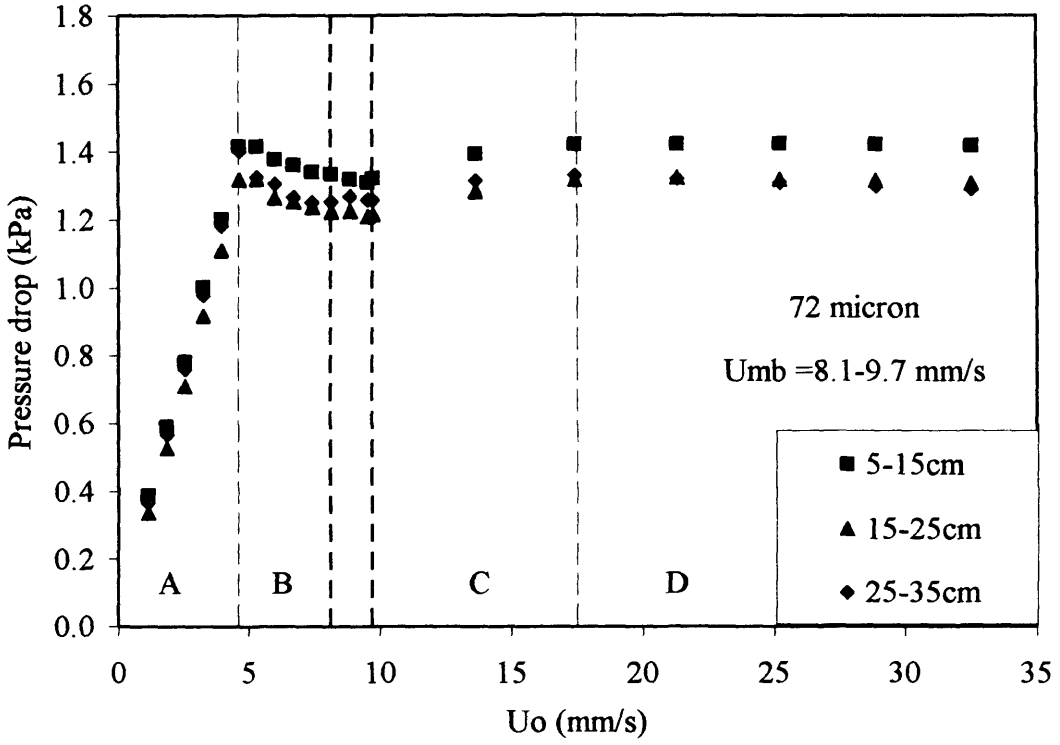

Figure 5. 27 Pressure drop profile of 72 μm (natural size)

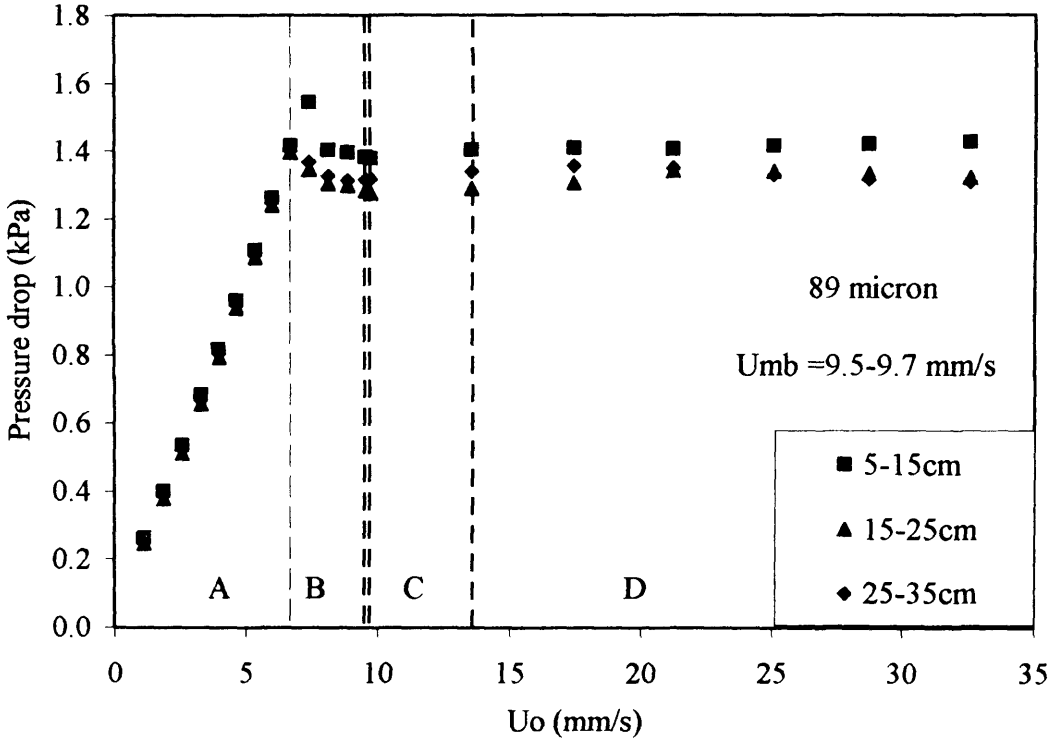

Figure 5.28 Pressure drop profile of 89 μm (natural size)

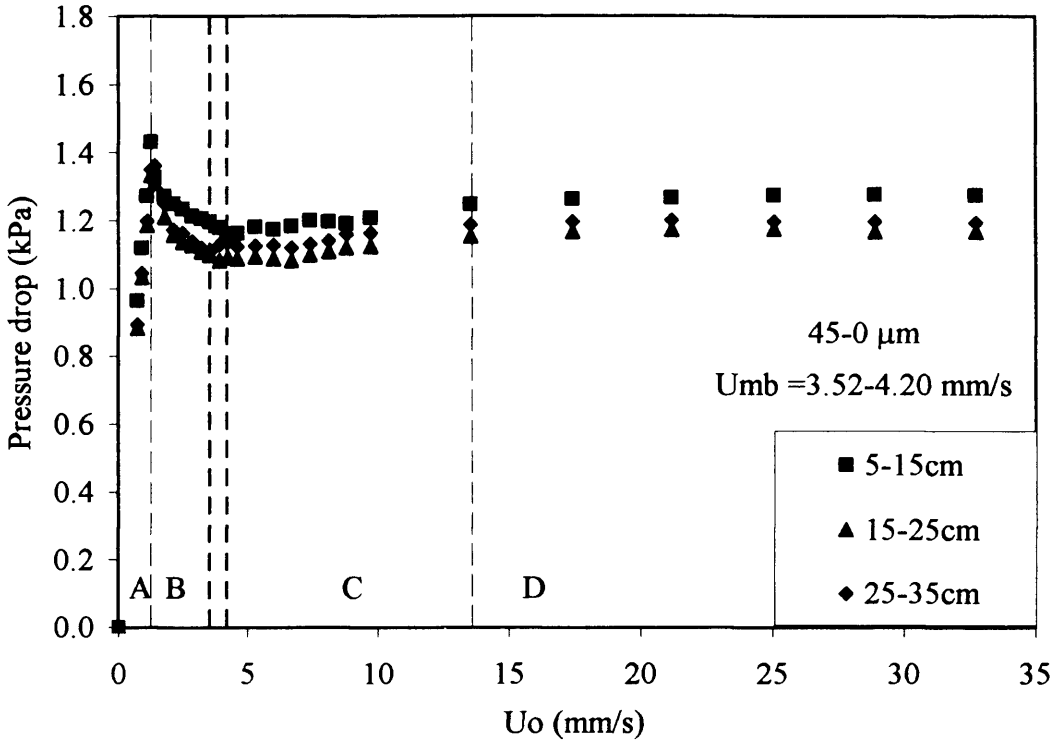

Figure 5.29 Pressure drop profile of 45-0 μm (narrow cut)

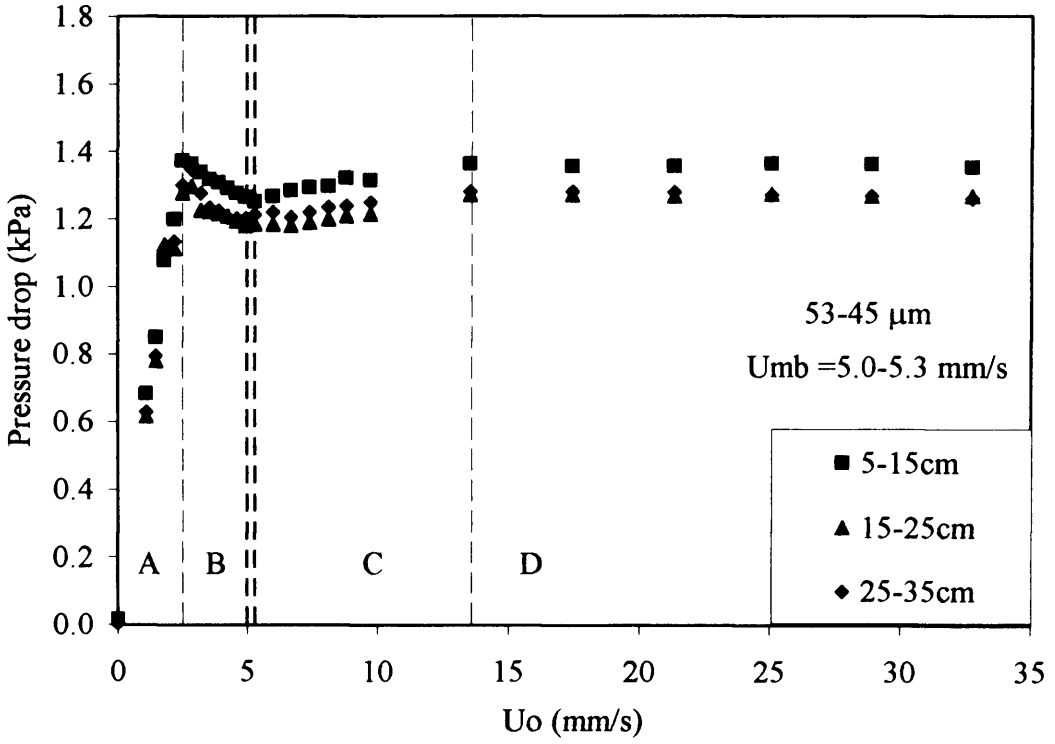

Figure 5.30 Pressure drop profile of 53-45 μm (narrow cut)

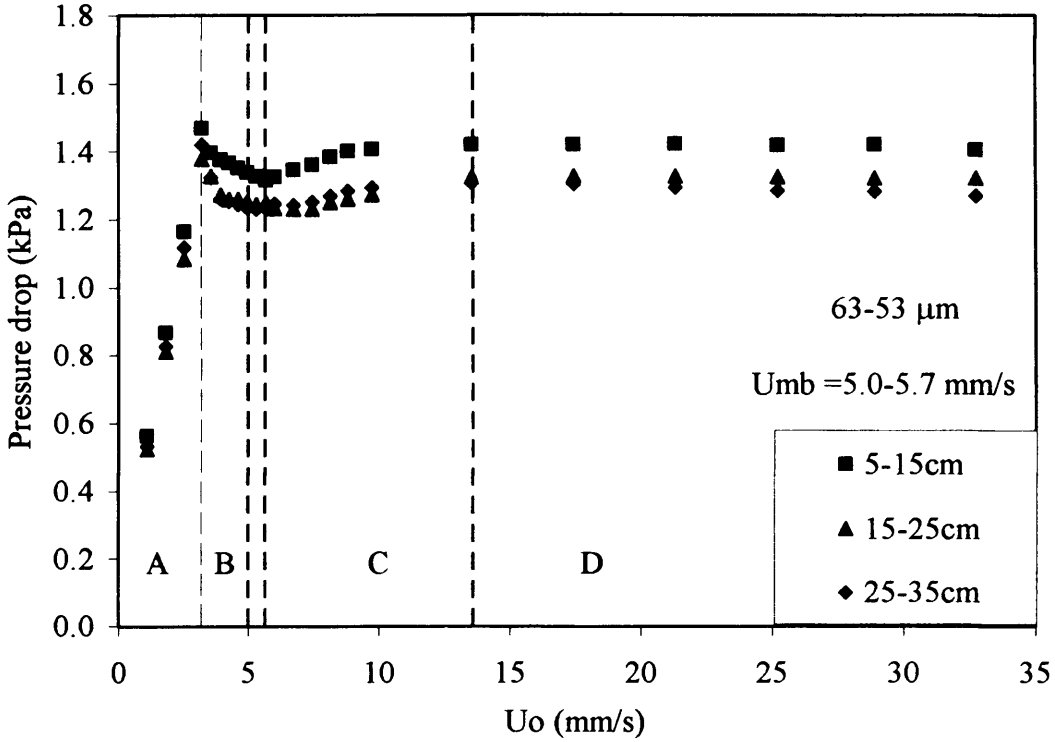

Figure 5.31 Pressure drop profile of 63-53 μm (narrow cut)

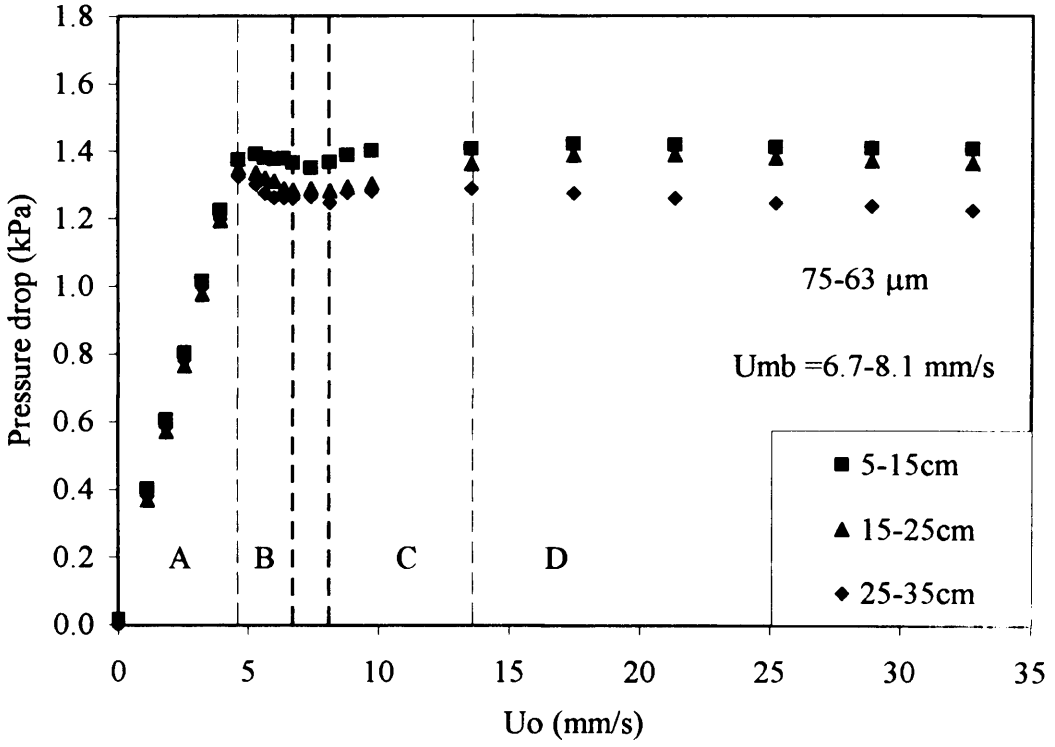

Figure 5.32 Pressure drop profile of 75-63 μm (narrow cut)

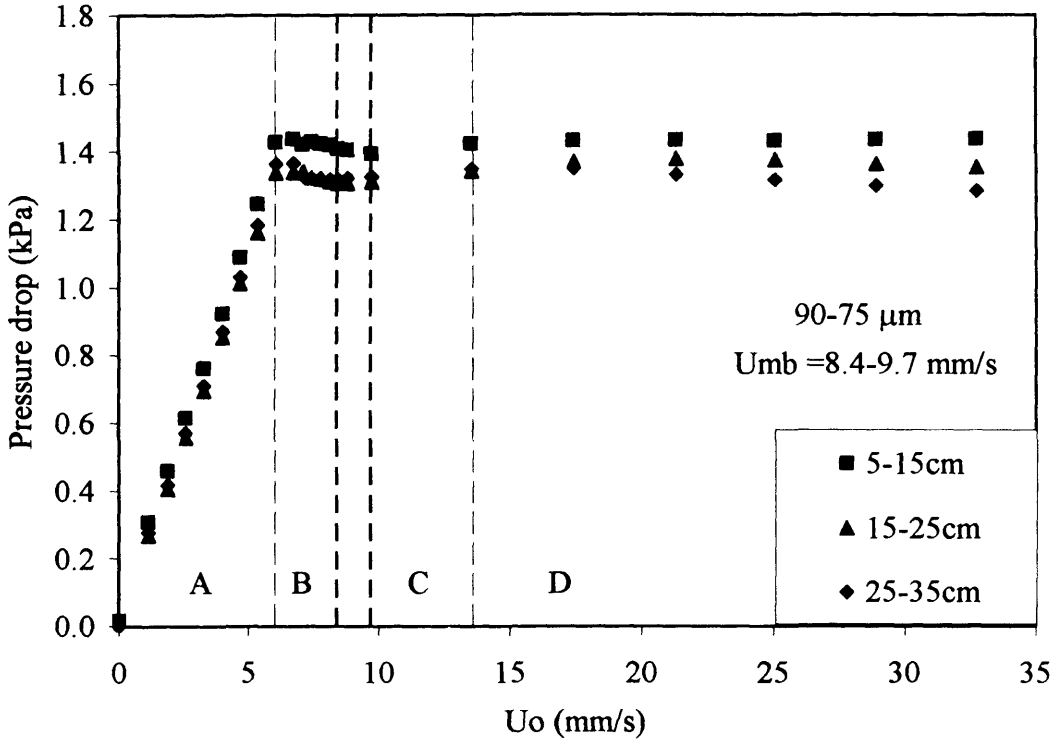

Figure 5.33 Pressure drop profile of 90-75 μm (narrow cut)

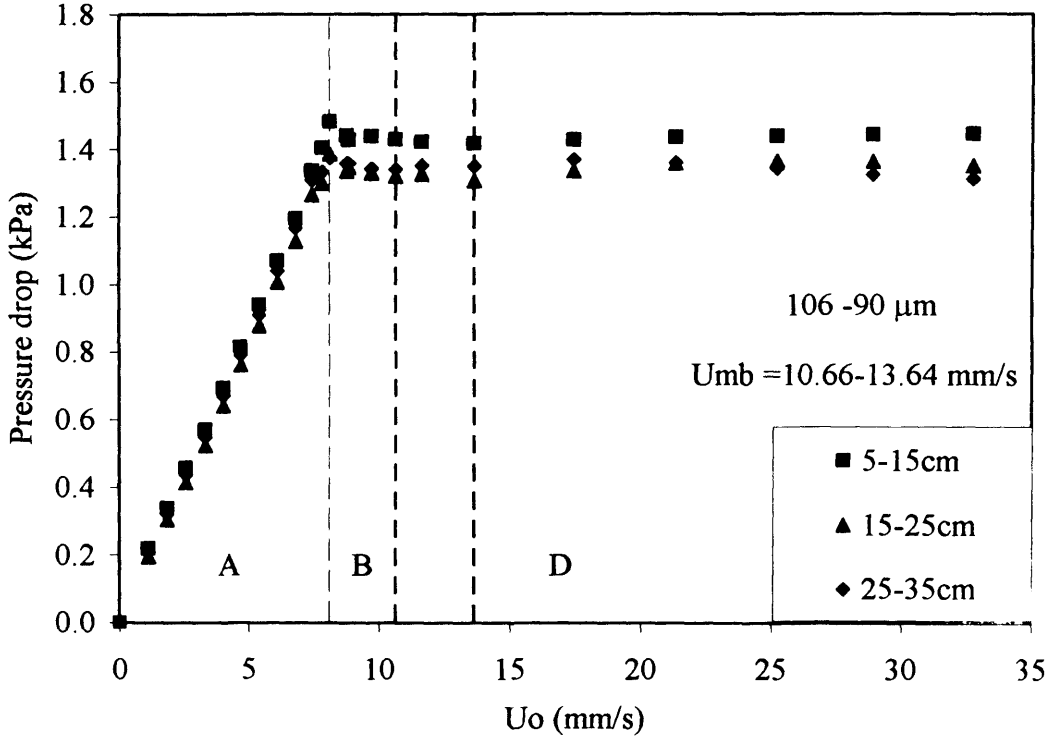

Figure 5.34 Pressure drop profile of 106-90 μm (narrow cut)

5.5 Pressure drop characteristics of bimodal powders

5.5.1 Onset of minimum fluidization

Figure 5.35 and Figure 5.36 show a typical total bed pressure drop versus velocity graph for the bimodal mixtures of 90-75μm/45-0μm and 109-90μm/53-45μm, respectively. The fixed bed pressure drop decreases with the increase of the average diameter as expected and the total bed pressure drop is the weight of the bed/area.

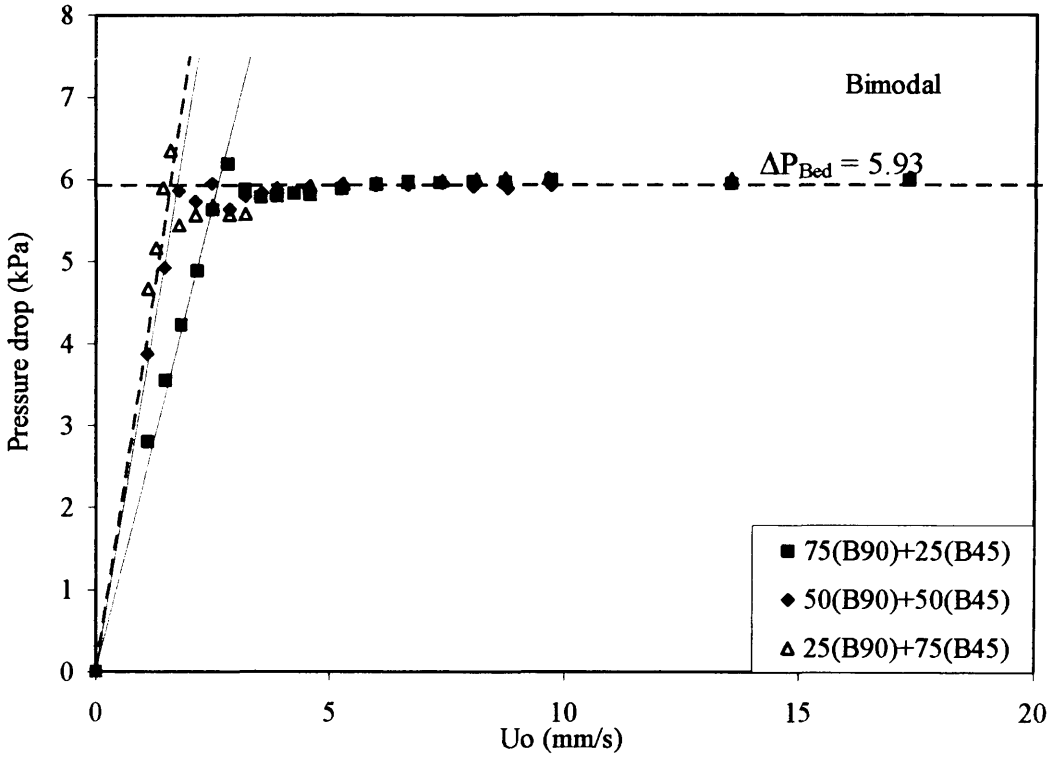

Figure 5.35 Total bed pressure drop vs U_0 for bimodal mixture 90-75 μm/45-0 μm

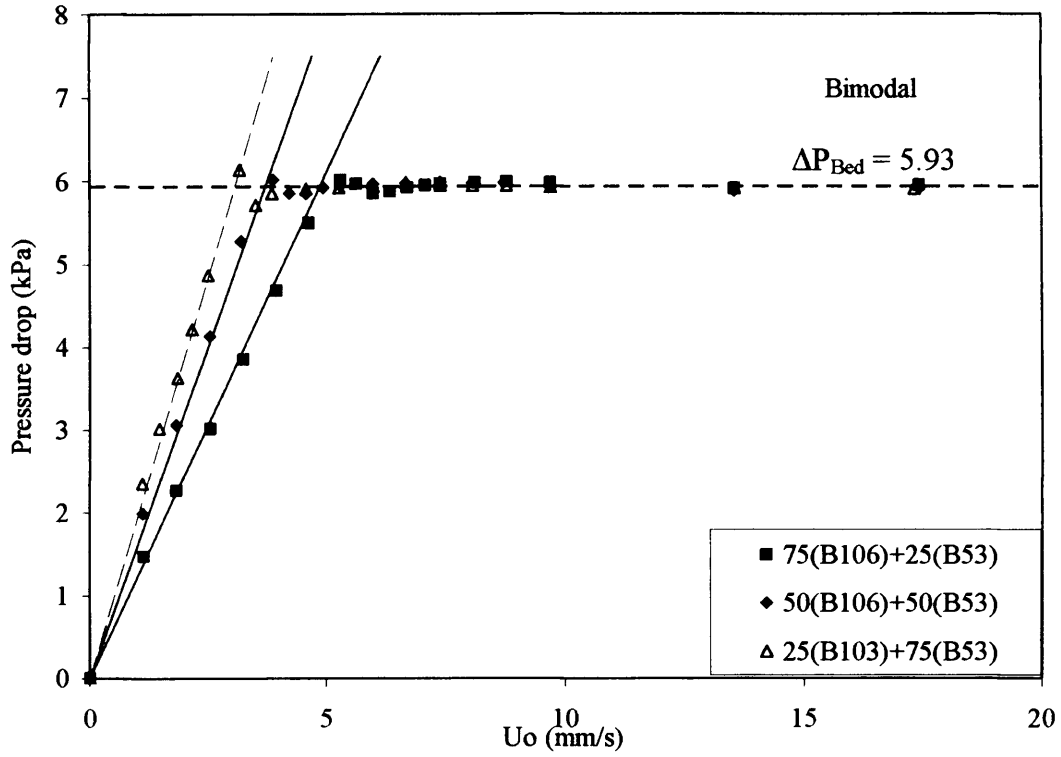

Figure 5.36 Total bed pressure drop vs U_0 for bimodal mixture 106-90 μm/53-45 μm

The minimum fluidization velocities obtained from Figure 5.35 and Figure 5.36 are plotted in Figure 5.37, for bimodal powders, in comparison with the narrow size cut powders and the natural size powders. The minimum fluidization velocities of bimodal mixtures of 106-90μm/53-45 μm show approximately the same trend as that for the narrow size cut powders and the natural size powder without fines. However, the bimodal mixtures with varied percent fines have lower minimum fluidization velocities and follow approximately the trend of the natural size powders with fines.

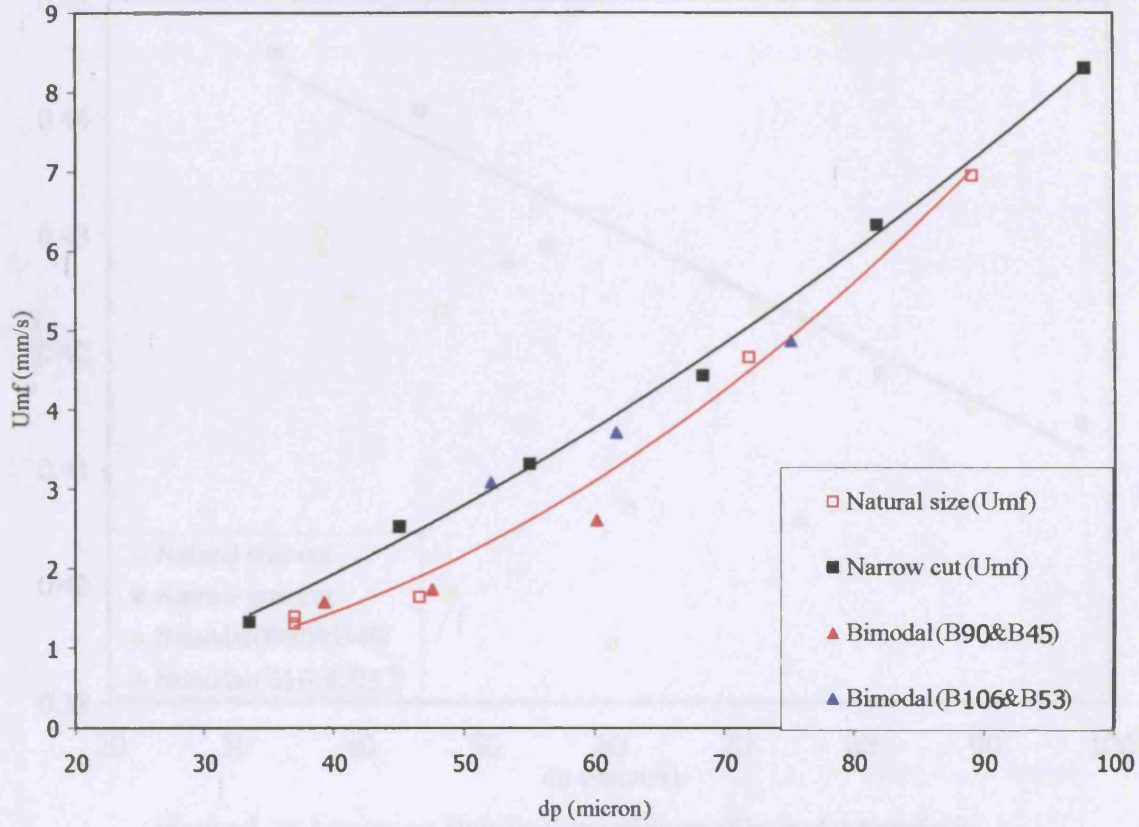

Figure 5.37 Minimum fluidization velocity of bimodal powders

Figure 5.38 shows the minimum fluidization voidage of bimodal powders in comparison with the narrow size cut powders and the natural size powders. The minimum fluidization voidages of bimodal mixtures were found to be lower than the narrow size cut and decrease with increase the average diameter. The mixtures containing fines have even lower minimum fluidization voidage and the mixtures without fines.

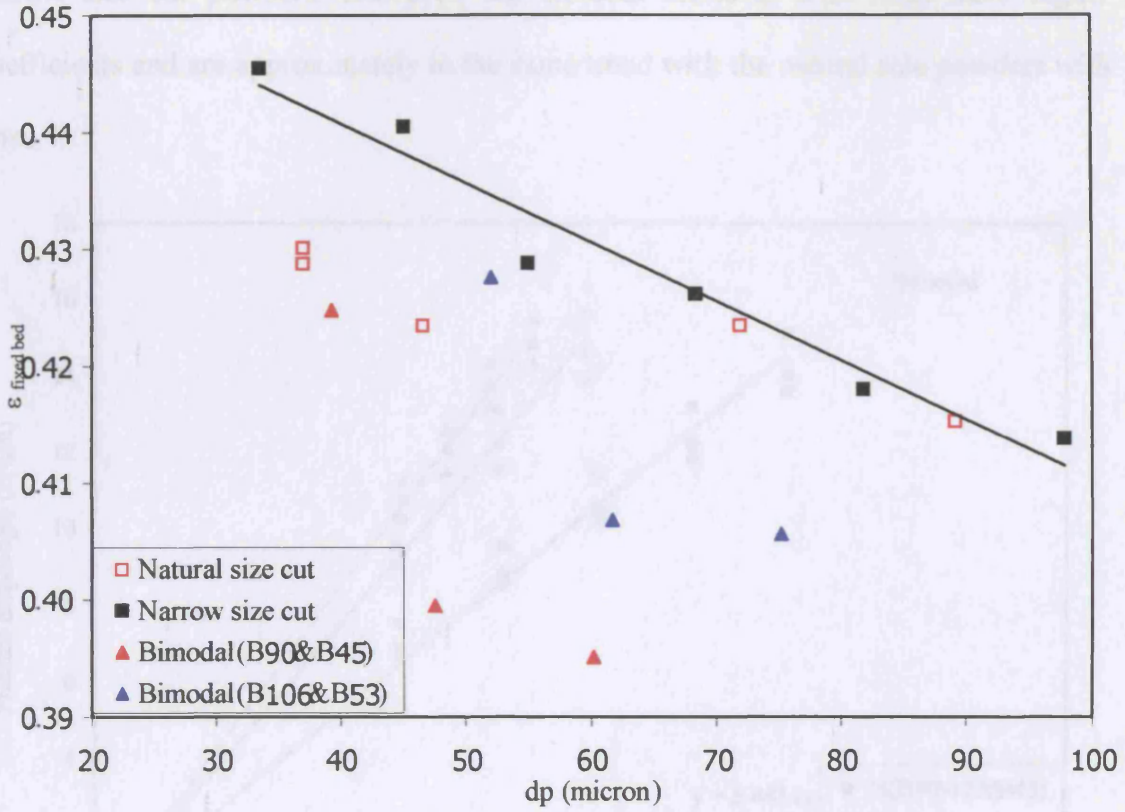

Figure 5.38 Minimum fluidization voidage of bimodal powders

This last result indicates, as one would expect, that particles of differing sizes can rearrange to reduce void space.

5.5.2 Fixed bed pressure drop

Fixed bed pressure drop/length for the bimodal mixture of 90-75μm/45-0μm and 106-90μm/53-45μm are shown in Figure 5.39 and Figure 5.40, respectively. The powders with smaller size induce more fixed bed gas flow resistance (Figure 5.38). The coefficient of the gas flow resistance of the fixed bed, 'fixed bed pressure drop/(length.U_0)', for the bimodal mixtures in comparison with the narrow size cut powders and the natural size powders are shown in Figure 5.41. For bimodal mixtures, the coefficients of those without fines can be estimated from the relation found for the

narrow size cut powders. However, the bimodal mixtures with fines have higher coefficients and are approximately in the same trend with the natural size powders with fines.

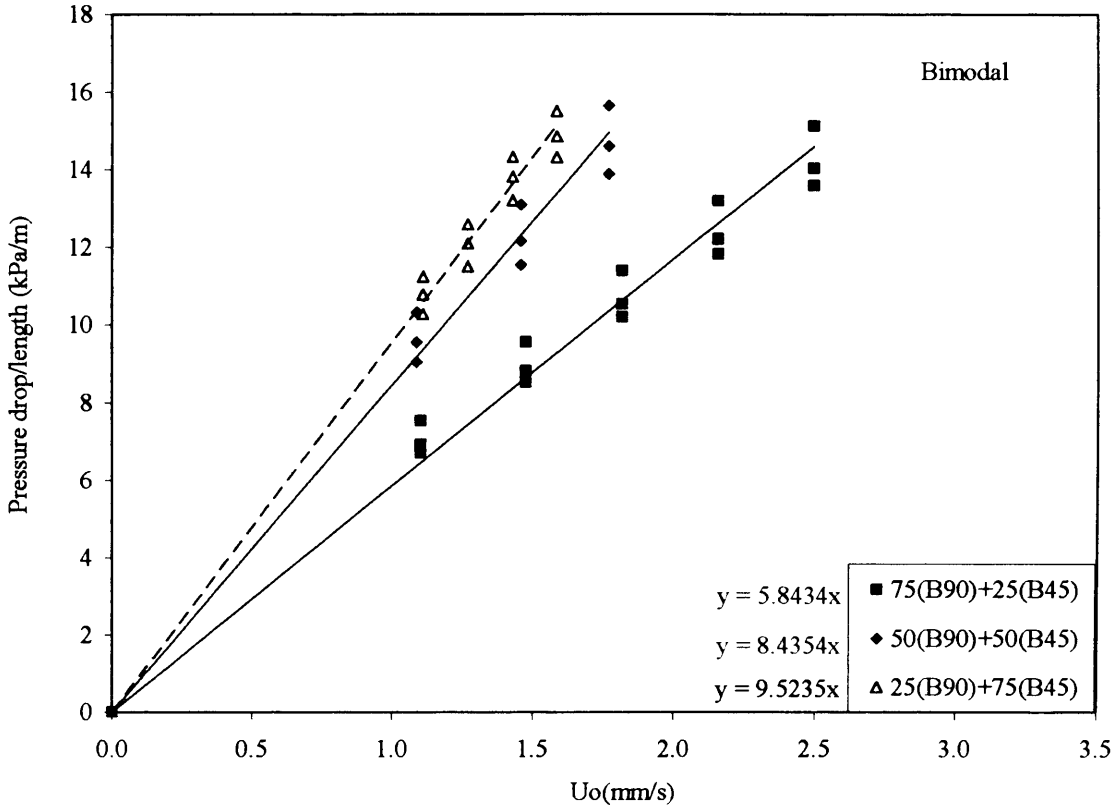

Figure 5.39 Fixed bed pressure drop/length for bimodal mixture 90-75 μm and 45-0 μm

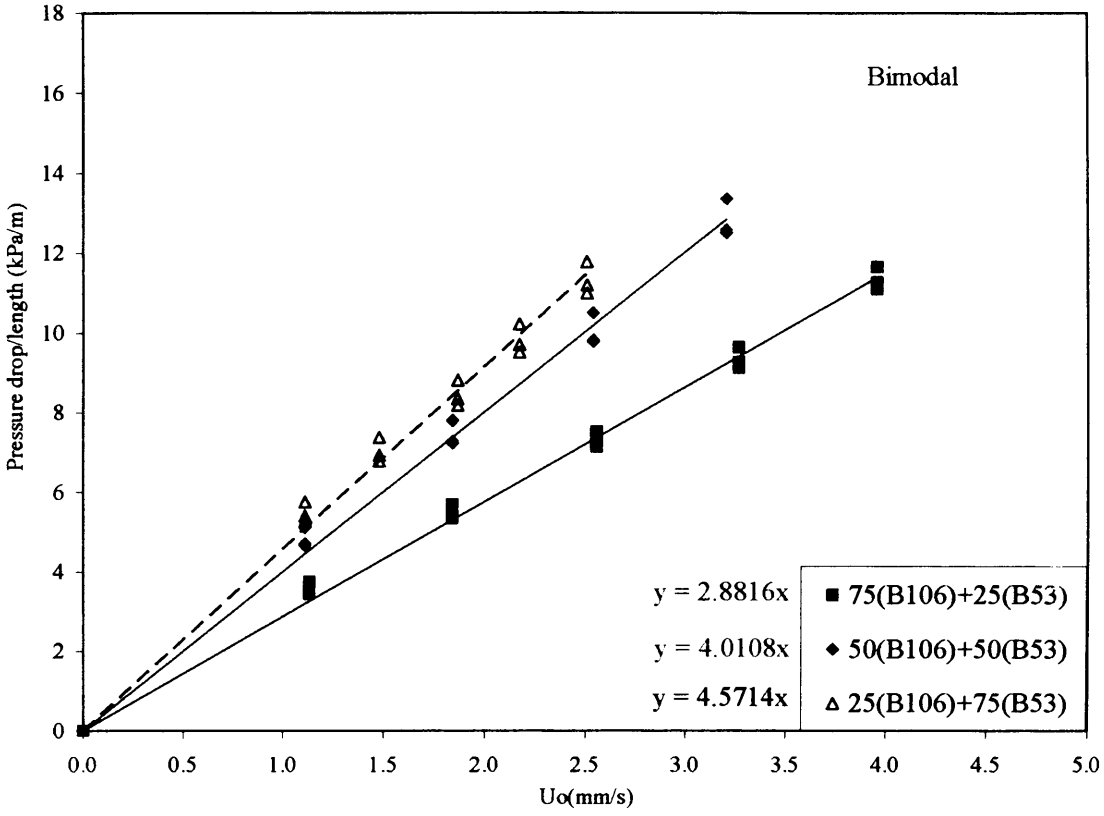

Figure 5.40 Fixed bed pressure drop/length for bimodal mixture 90-75 μm and 45-0 μm

For bimodal mixtures, U_{mf} and $\Delta P_{Fixedbed}$ are influenced by the definition of the average diameter, as found for the natural size distribution powders. The estimation of U_{mf} and $\Delta P_{Fixedbed}$ of the bimodal powders from the narrow size cut empirical relations is feasible, as long as there are no fines in the mixture. With fines in the mixture, U_{mf} and $\Delta P_{Fixedbed}$ deviate from the empirical relation found for the narrow size cut powders. U_{mf} is lower and $\Delta P_{Fixedbed}$ is higher. However, these values are approximately in the same trend as the natural size distribution powders containing fines. From Figure 5.38 , it was found that ε_{mf} has a weak effect on U_{mf} and $\Delta P_{Fixedbed}$ compared to the average diameter and this should not be the cause of the deviation from the narrow size cut prediction for the mixture with fine content.

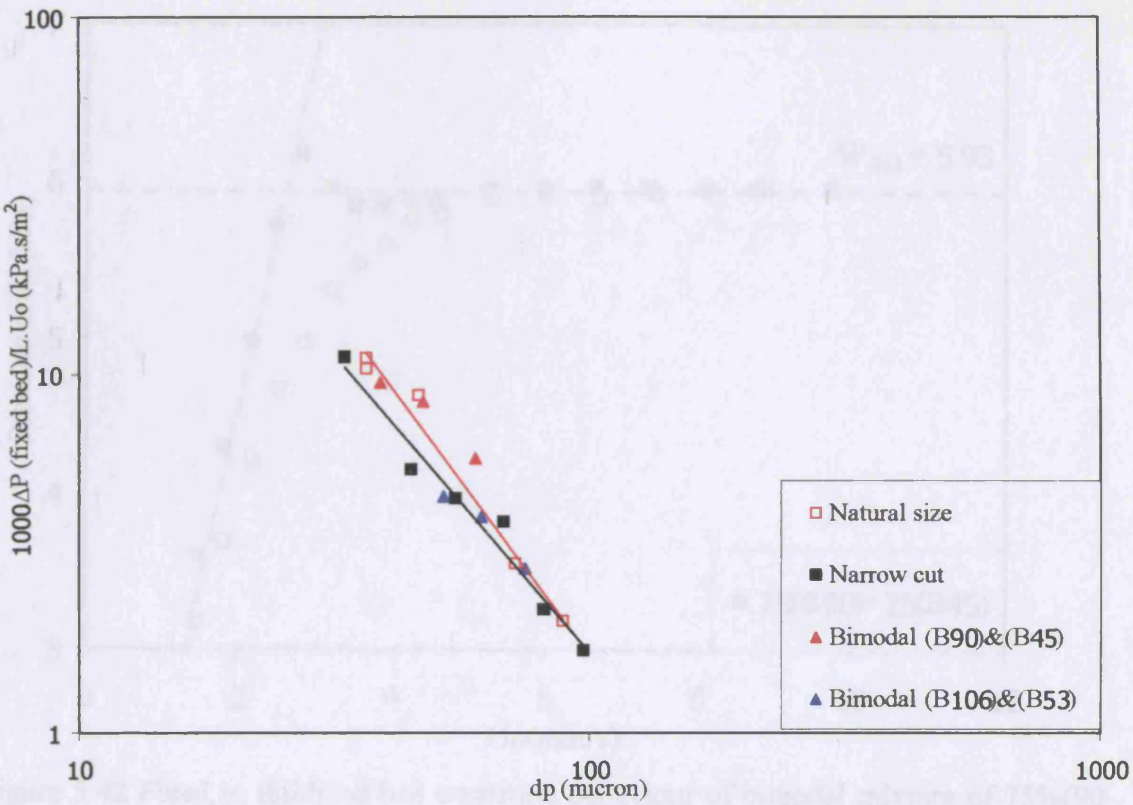

Figure 5.41 Fixed bed pressure drop/ (L.Uo) for bimodal powders

5.5.3 Fluidization and de-fluidization experiments

For all bimodal mixtures (Figure 5.42 to Figure 5.47), the pressure overshooting was observed and was followed by the gradual transition to the complete fluidization stage, for the fluidization experiment. The pressure overshooting is stronger for the mixtures containing fines. From the de-fluidization experiment, (Figure 5.42 to Figure 5.47), all the powders show a gradual transition.

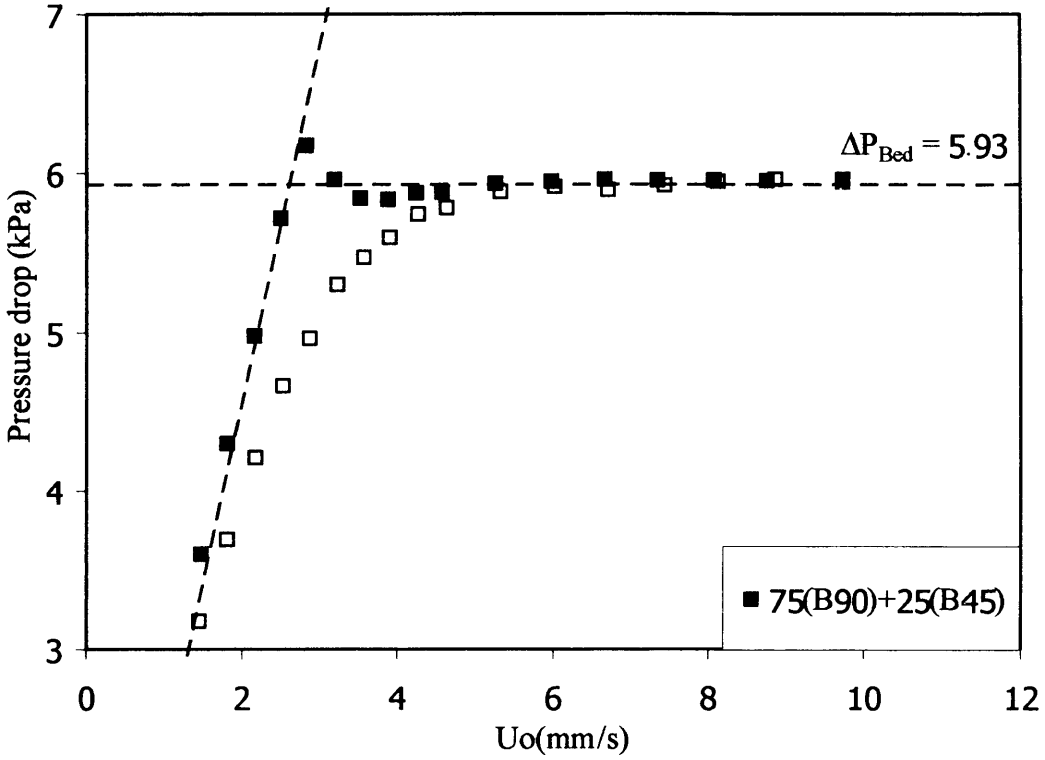

Figure 5.42 Fixed to fluidized bed transition behaviour of bimodal mixture of 75%(90-75μm) and 25%(45-0μm) [Full symbols = Fluidization and Empty symbols = De-fluidization]

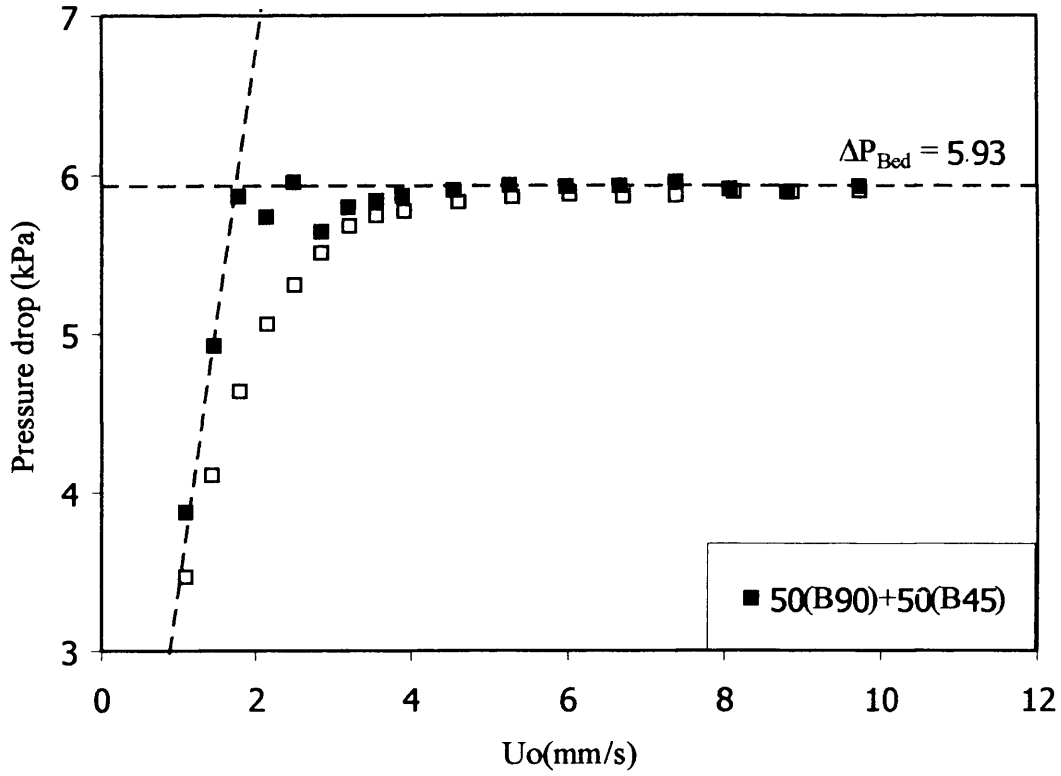

Figure 5.43 Fixed to fluidized bed transition behaviour of bimodal mixture of 50%(90-75μm) and 50%(45-0μm) [Full symbols = Fluidization and Empty symbols = De-fluidization]

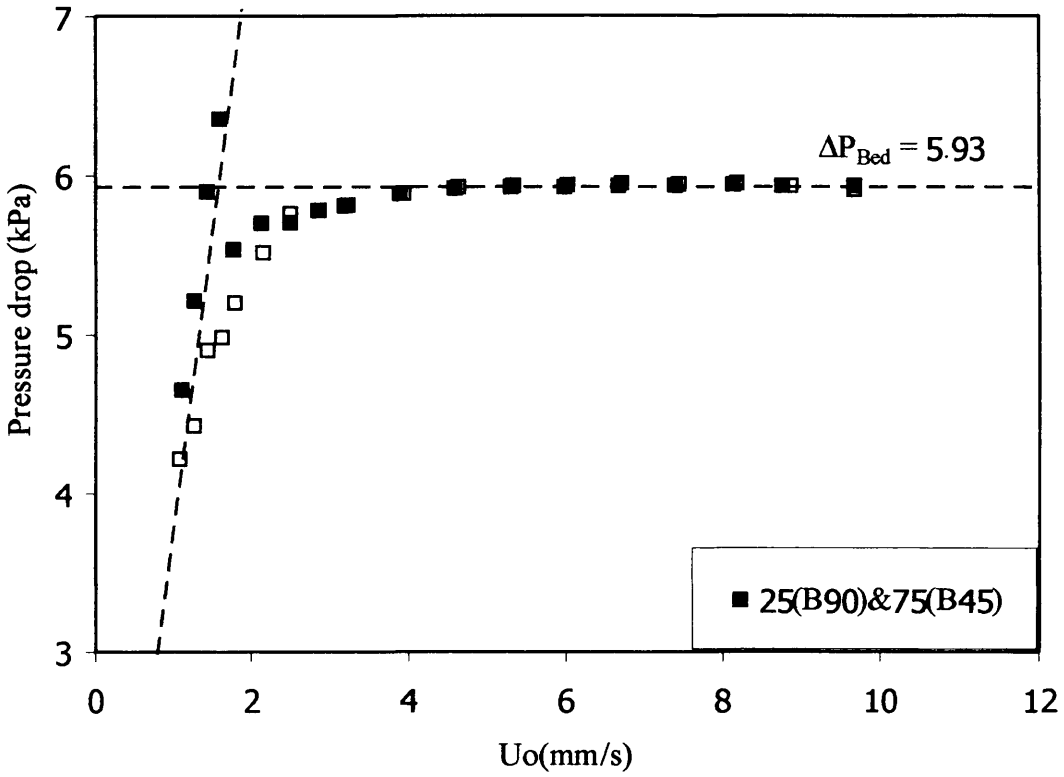

Figure 5.44 Fixed to fluidized bed transition behaviour of bimodal mixture of 25%(90-75μm) and 75%(45-0μm) [Full symbols = Fluidization and Empty symbols = De-fluidization]

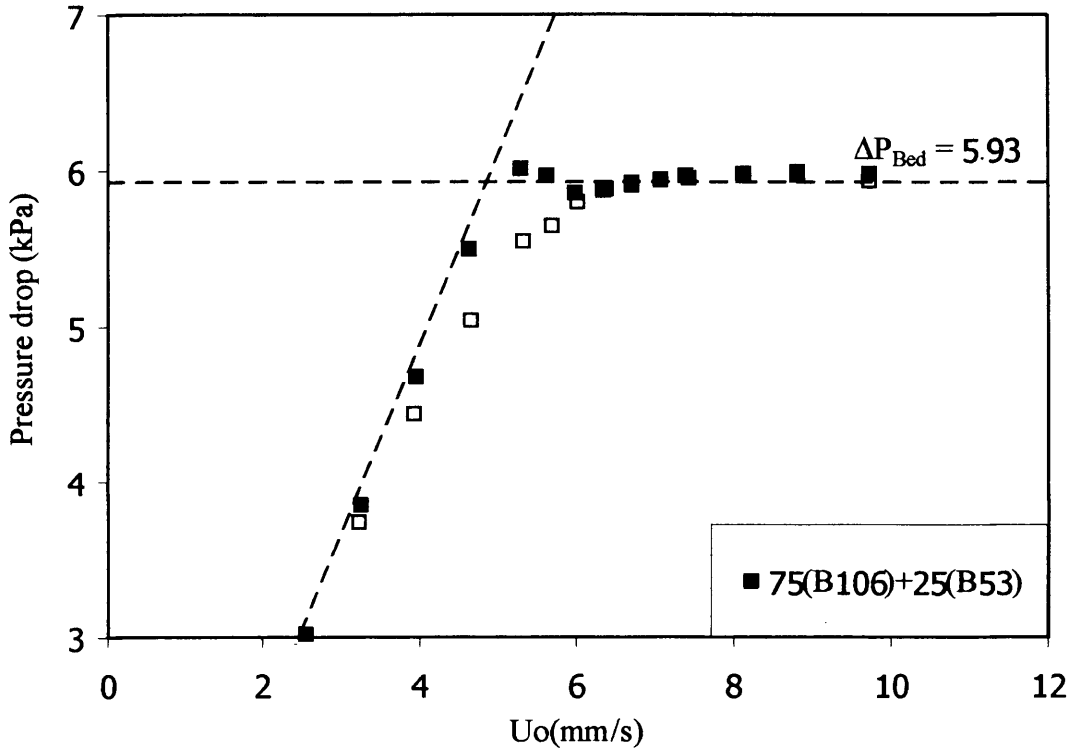

Figure 5.45 Fixed to fluidized bed transition behaviour of bimodal mixture of 75%(106-90μm) and 25%(53-45μm) [Full symbols = Fluidization and Empty symbols = De-fluidization]

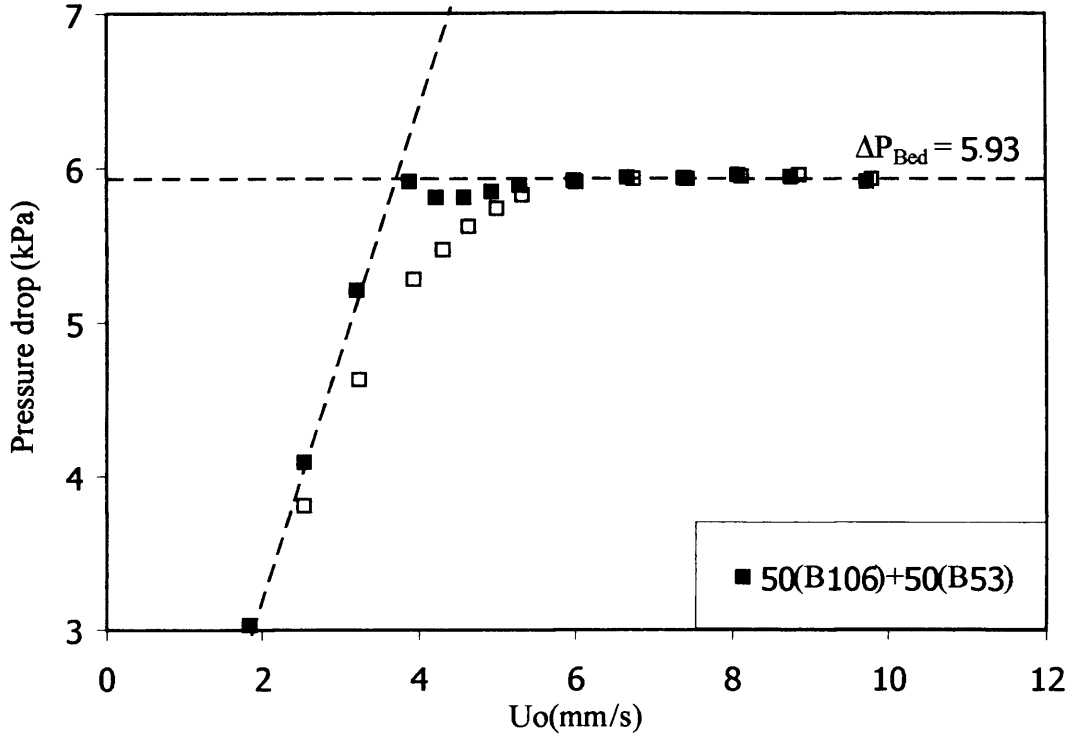

Figure 5.46 Fixed to fluidized bed transition behaviour of bimodal mixture of 50%(106-90μm) and 50%(53-45μm) [Full symbols = fluidization and empty symbols = de-fluidization]

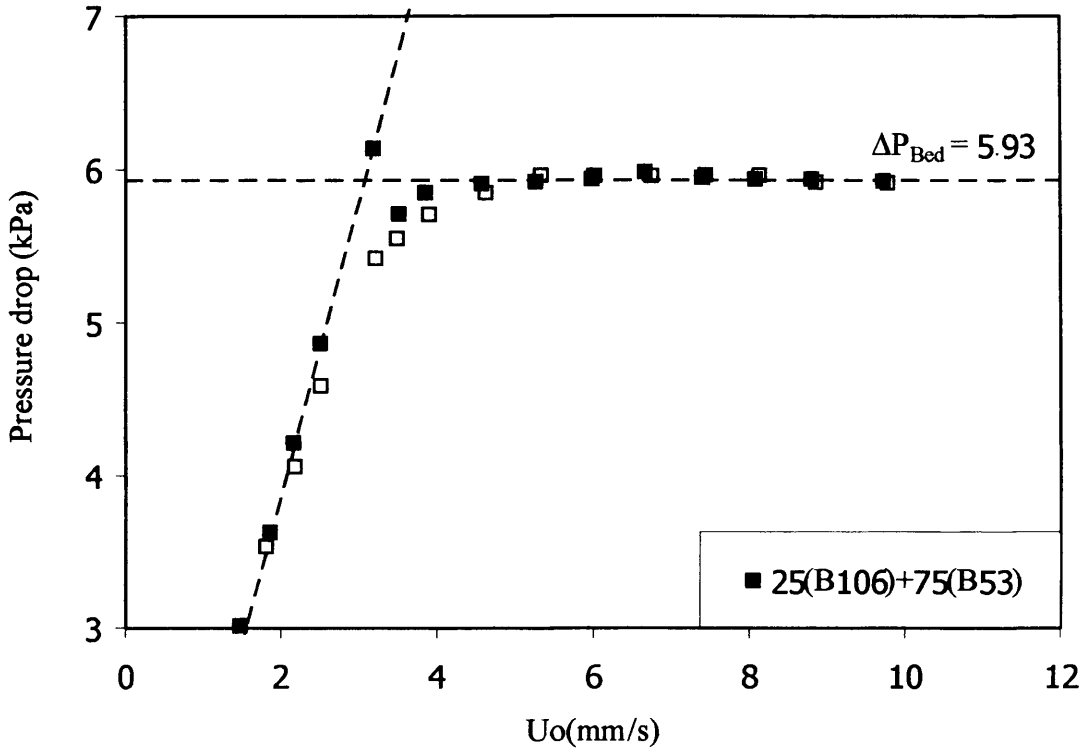

Figure 5.47 Fixed to fluidized bed transition behaviour of bimodal mixture of 25%(106-90μm) and 75%(53-45μm) [Full symbols = Fluidization and Empty symbols = De-fluidization]

5.5.4 Pressure drop profile of the fluidized bed

Figure 5.48 and Figure 5.53, the pressure drop profile above the minimum fluidization velocity showing no particle segregation. This is confirmed by the fact that the pressure drop measured at different heights, except near the distributor, shows approximately the same values for all bimodal mixtures. This is similar to the result observed for the narrow size cut powders.

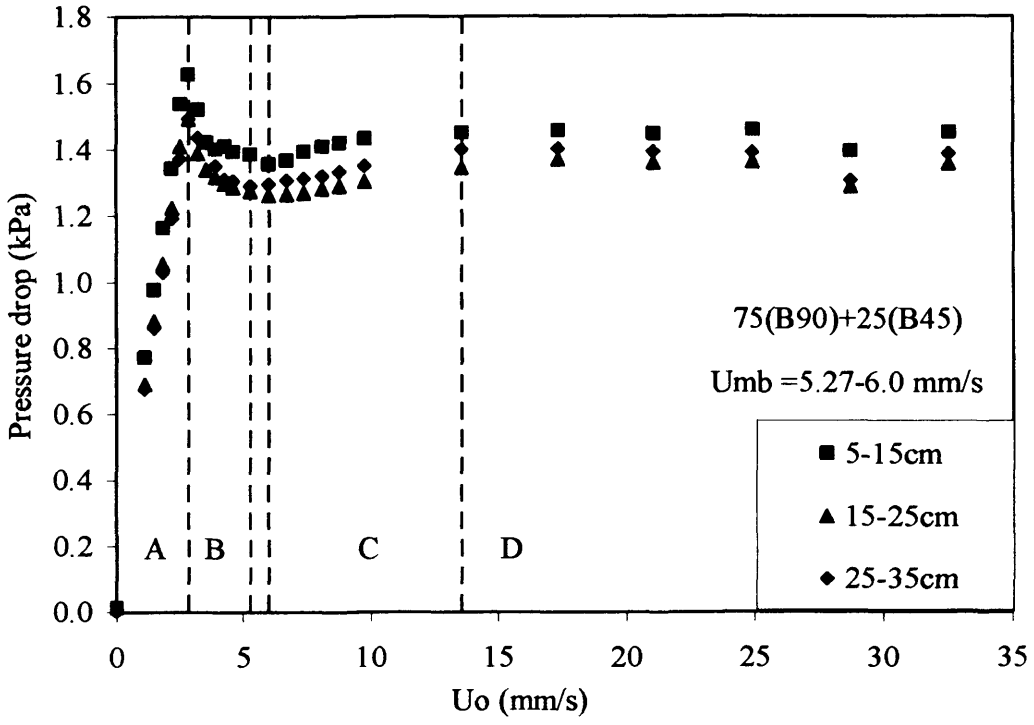

Figure 5.48 Pressure drop profile of bimodal mixture 75%(90-75μm)/25%(45-0μm)

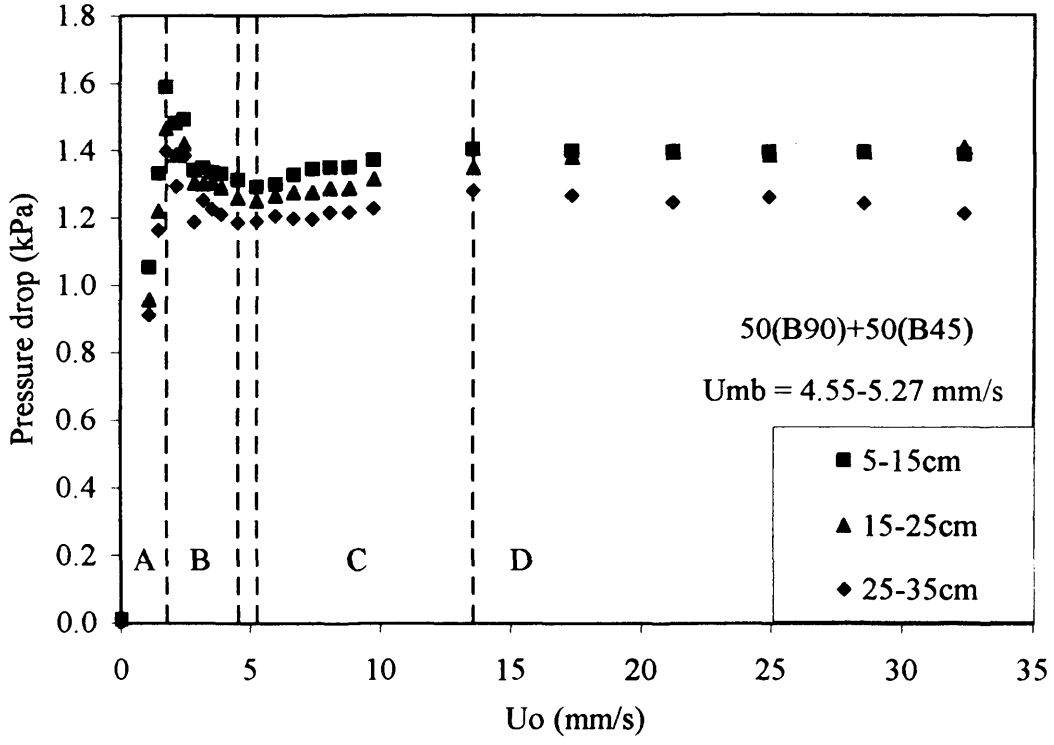

Figure 5.49 Pressure drop profile of bimodal mixture 50%(90-75μm) /50%(45-0μm)

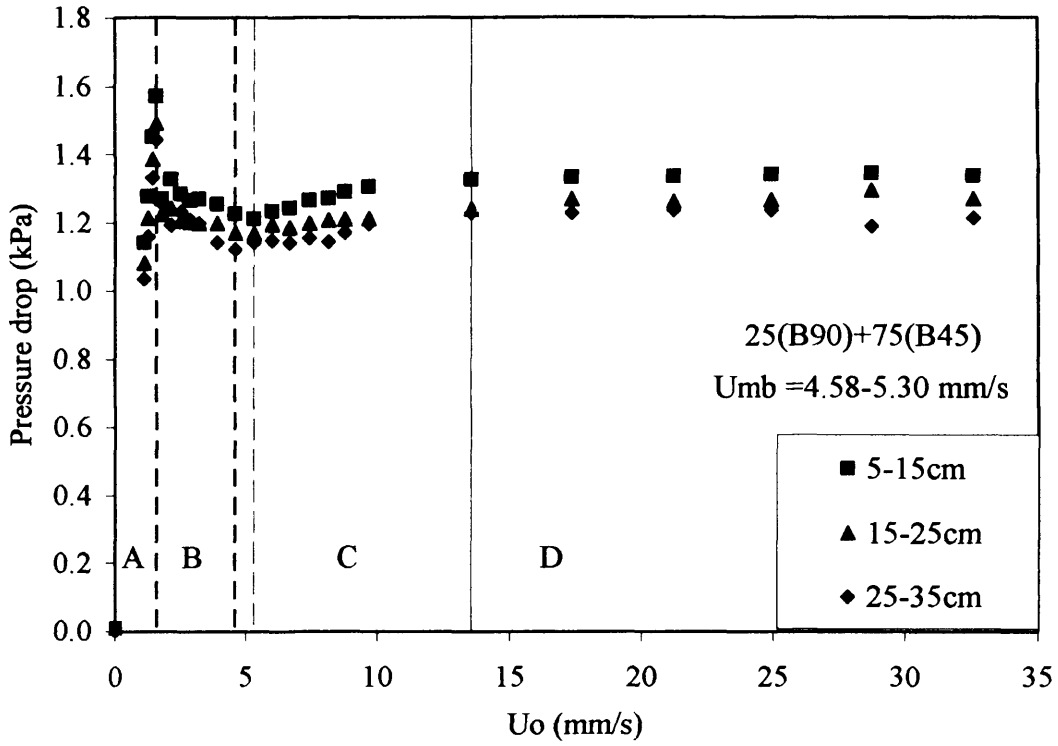

Figure 5.50 Pressure drop profile of bimodal mixture 25%(90-75μm)/75%(45-0μm)

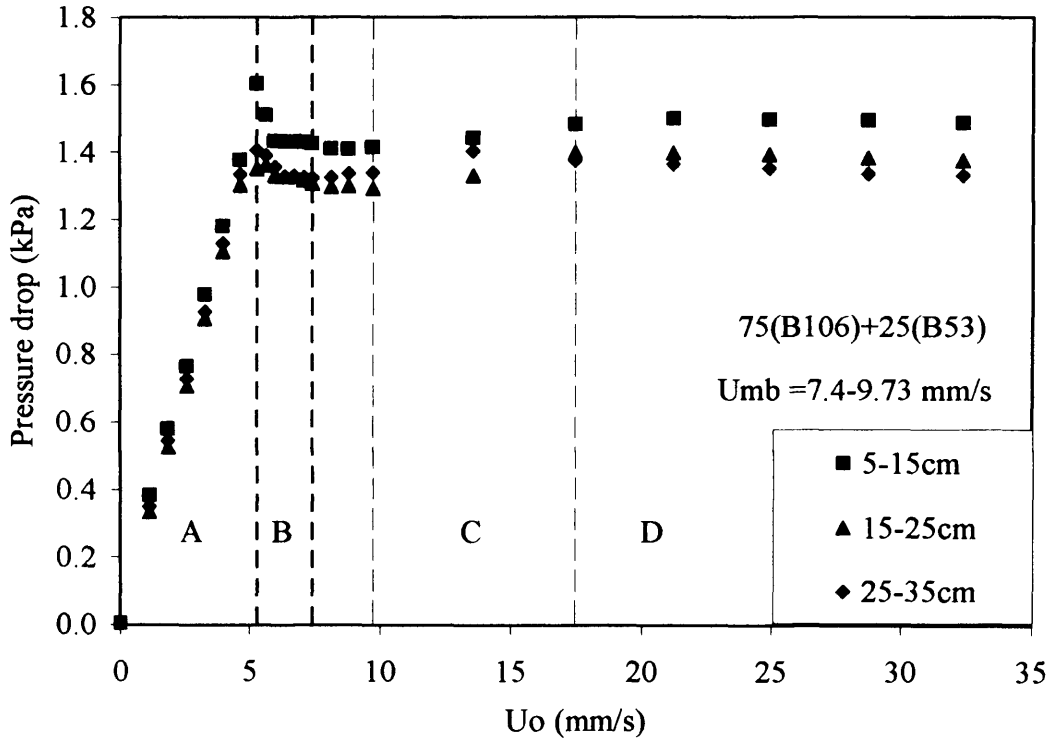

Figure 5.51 Pressure drop profile of bimodal mixture 75%(106-90μm)/25%(53-45μm)

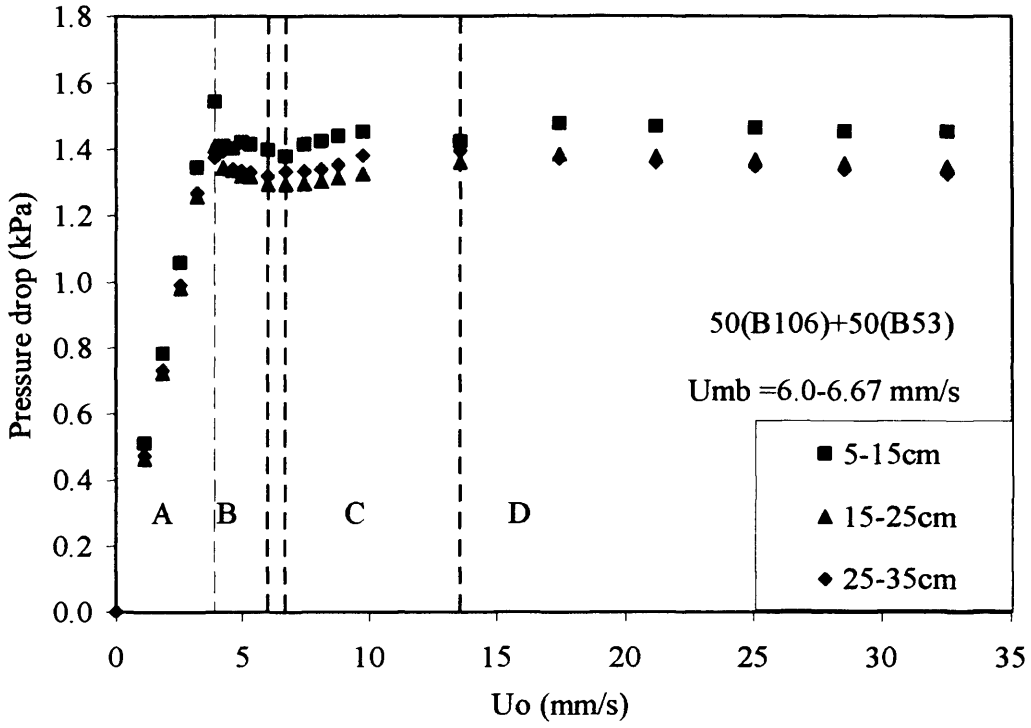

Figure 5.52 Pressure drop profile of bimodal mixture 50%(106-90μm)/50%(53-45μm)

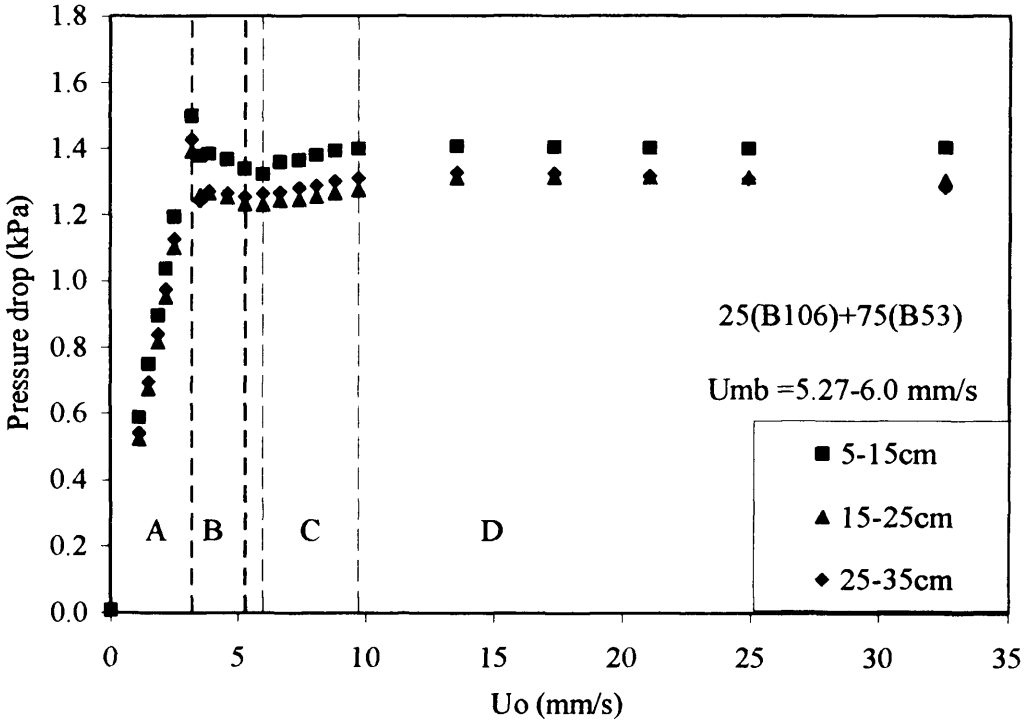

Figure 5.53 Pressure drop profile of bimodal mixture 25%(106-90μm)/ 75%(53-45μm)

5.6 Comparison with correlations

The Revised Ergun equation (Foscolo et.al., 1983) was used to the describe the fixed bed pressure drop of the narrow size cuts, natural size distribution powders and bimodal powders, as shown in Figure 5.54 and Figure 5.57. The prediction from the Revised Ergun equation was found to be lower than the experimental results for all powders. This may be due to the compact mechanical structure of the fixed bed that causes higher-pressure loss or the drag force correlation is not actually appropriate for describing the fluidization characteristic of these powders, even for the particle in suspension where there is now contact stress. Therefore, the Revised Ergun equation will be re-examined again as well as the drag force correlation reported in the literature, using the ε_d and U_d characteristic curves.

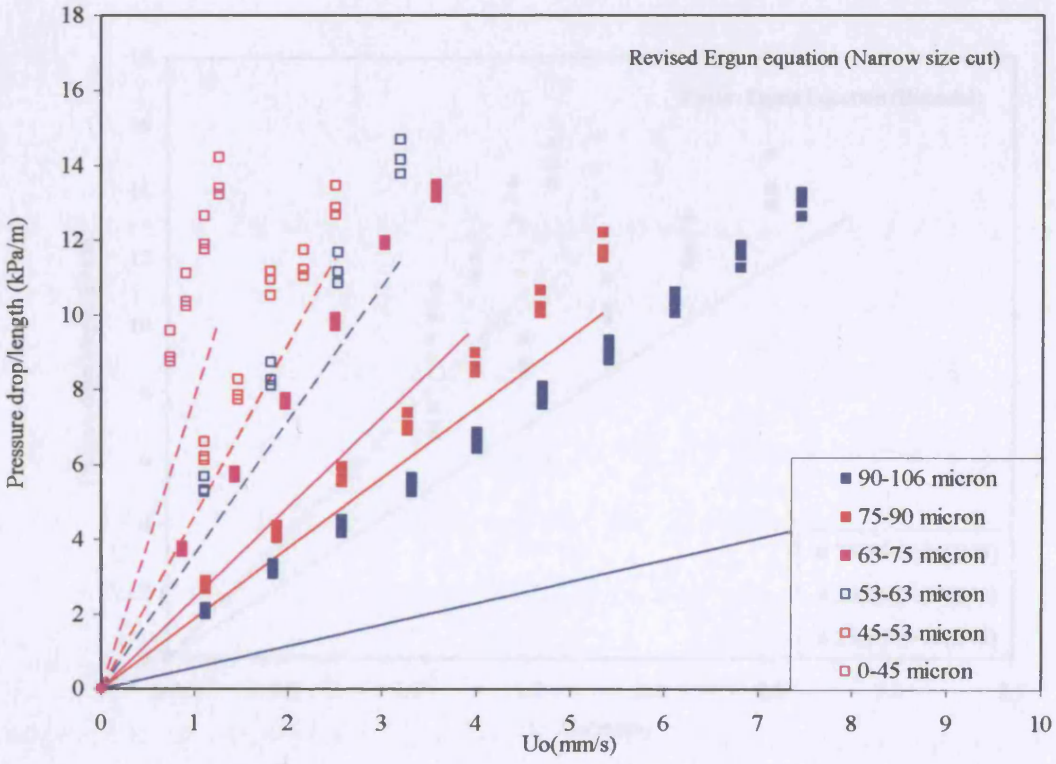

Figure 5.54 Comparison of fixed bed pressure drop/length with prediction using Revised Ergun equation (narrow size cut)

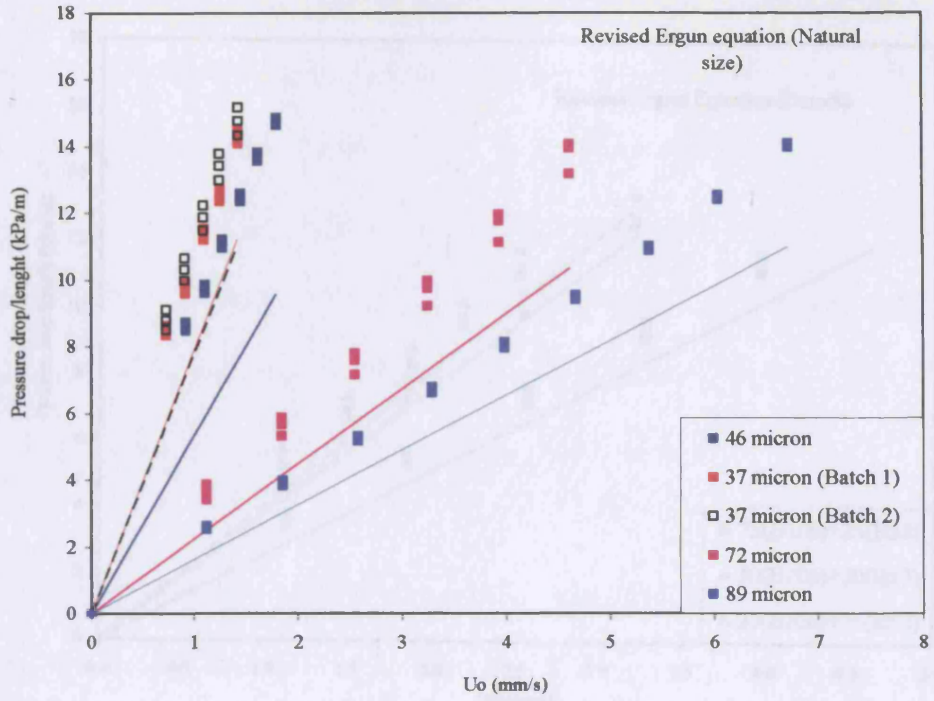

Figure 5.55 Comparison of fixed bed pressure drop/length with prediction using Revised Ergun equation (natural size powders)

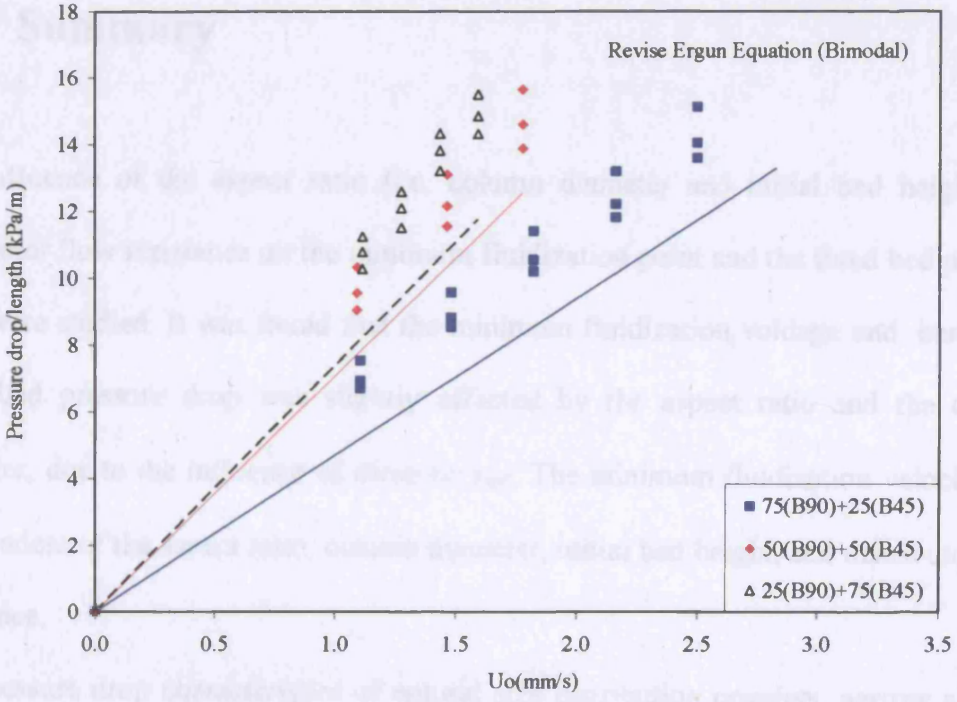

Figure 5.56 Comparison of fixed bed pressure drop/length with prediction using Revised Ergun equation (Bimodal mixture of ballotini 90-75μm and 45-0 μm)

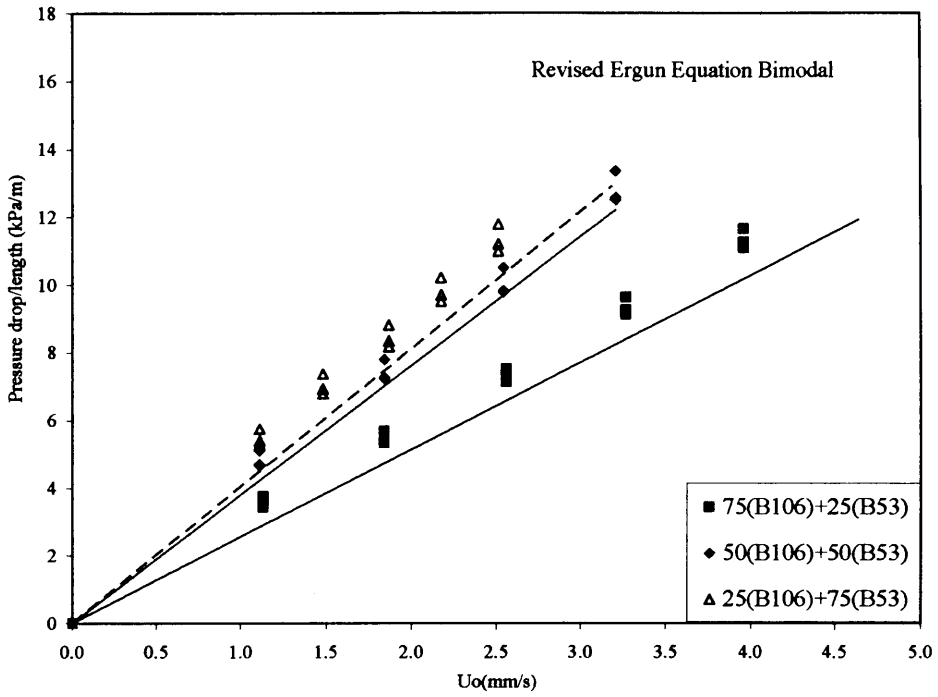

Figure 5.57 Comparison of fixed bed pressure drop/length with prediction using Revised Ergun equation (Bimodal mixture of ballotini 106-90μm and 53-45 μm)

5.7 Summary

The influence of the aspect ratio (i.e. column diameter and initial bed height) and distributor flow resistance on the minimum fluidization point and the fixed bed pressure drop were studied. It was found that the minimum fluidization voidage and, hence, the fixed bed pressure drop was slightly affected by the aspect ratio and the column diameter, due to the influence of these on ε_{mf}. The minimum fluidization velocity was independent of the aspect ratio, column diameter, initial bed height, and distributor flow resistance.

The pressure drop characteristics of natural size distribution powders, narrow size cut powders and bimodal powders were investigated. It can be generally concluded that minimum fluidization velocity is increased as a quadratic function with the increase of

the average diameter. With the increase of the average diameter, the minimum fluidization voidage is decreased, and the fixed bed gas flow resistance is decreased. In addition, the relation of U_{mf} and $\Delta P_{Fixedbed}$ with d_P of the narrow size cut can be used to estimate of U_{mf} and $\Delta P_{Fixedbed}$ natural size distribution powder and bimodal mixtures as long as there is are fines in the powders. When the powders contain fines, U_{mf}, and $\Delta P_{Fixedbed}$ of the natural size distribution cut and bimodal mixtures showed good agreement, but deviate from the values found for the narrow size cuts.

The minimum fluidization voidage of the natural powders with fines and the bimodal mixtures, with and without fines, is smaller than that estimated from the narrow size cut relation.

The overshooting in the pressure drop during fluidization experiments was observed for natural size distribution powders. The degree of compaction and wall friction increased with the decreasing of the size of powder and increasing fine content.

From the pressure drop profile of all powder mixtures, there is no particle segregation observed in the fluidized bed.

Applying the Revised Ergun equation (Foscolo et.al., 1983) to the prediction of the fixed bed pressure drops showed that it underestimated the experimental result for powders. This means the experimental drag forces of these powders are higher than the theoretical prediction. Therefore, this correlation will be re-examined again in the following chapter along with the drag force correlations reported in the literature, using the ε_d and U_d characteristic curves determined from the bed collapse experiments.

Chapter 6: Bed Expansion

6.1 Introduction

In this Chapter the bed voidage, the dense phase voidage and the dense phase superficial velocities will be measured using the 1- and 2-valve bed collapse experiments. The model presented in Chapter 4 will be applied to the experimental results obtained for the natural size distribution, the narrow size cut and the bimodal mixture powders. The measured dense phase voidage and superficial velocities will be compared with correlations taken from literature.

6.2 Influence of column diameter and initial bed height on bed expansion

Initial experiments were carried out using both columns to verify that the results were independent of the column diameter and also to establish which measurement of the dense phase voidage was more accurate. Figure 6.1 and Figure 6.2 show the comparison of the bed voidage and the dense phase voidage for the 0.127 m ID column obtained from the analysis of the visual observations and the voidage calculated from the

differential pressure drop measurements using the ID value of the column. A similar comparison for the 0.243 m ID column is shown in Figure 6.3 and Figure 6.4.

While the results for the initial bed voidage give an indication of the uncertainty of this measurement, the dense phase voidages should be determined with a greater accuracy.

For the 0.127 m ID column, the dense phase voidage from matching the model predictions to the bed collapse dynamics are approximately 5% higher than those obtained from the differential pressure drop readings. The bed voidages at very high velocities tend to give consistent results.

For the 0.243 m ID column, the difference is reduced to approximately 2.5%. This is the same for the results for the 1- and 2-valve experiments and for all powders studied.

This small discrepancy could be attributed to different reasons. The first possible explanation is the fact that a small layer of solid is present near the wall. Given the larger surface to volume ratio of the smaller column, a larger effect should be present in the smaller column as observed experimentally.

Another interpretation could be the error from the pressure measurement itself. The inaccuracy of the use of the pressure measurement for the determination of the bed voidage may be due to the fluctuation of the signal, but this should be mitigated by the fact that an average voidage is calculated from all the pressure readings along the vertical height.

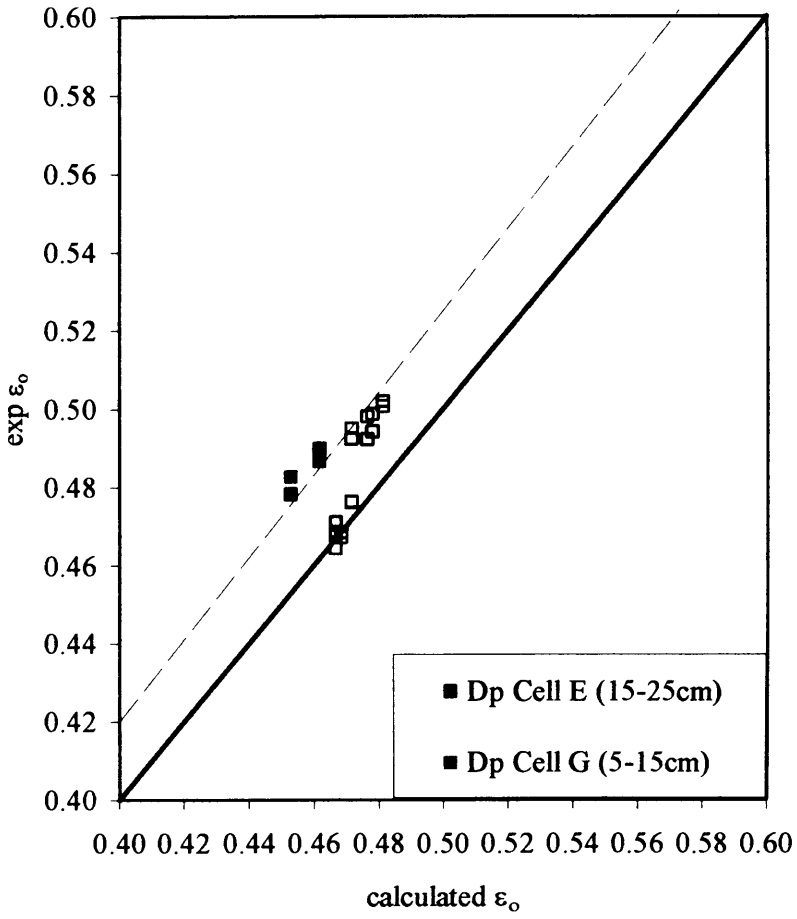

Figure 6.1 Comparison of bed voidage (ε_o) from bed collapse model prediction and pressure reading for 72 μm (0.127 m ID, Li = 0.30 m)

[Full square = $U_0 < U_{mb}$ and empty square = $U_0 > U_{mb}$]

If one considers the uncertainty in the cross-sectional area due to the presence of the windows, it is possible to estimate that the possible error in the calculated voidage from the pressure drops is of the same magnitude as the observed discrepancy. Therefore, within the experimental uncertainty, we must conclude that these differences are not due to the diameter of the columns. Even though the pressure drop profile seems would be the more convenient method to determine the dense phase voidage, in subsequent

calculations the bed voidage and the dense phase voidage will be taken from the bed collapse curves observed visually and analysed using the model presented in Chapter 4.

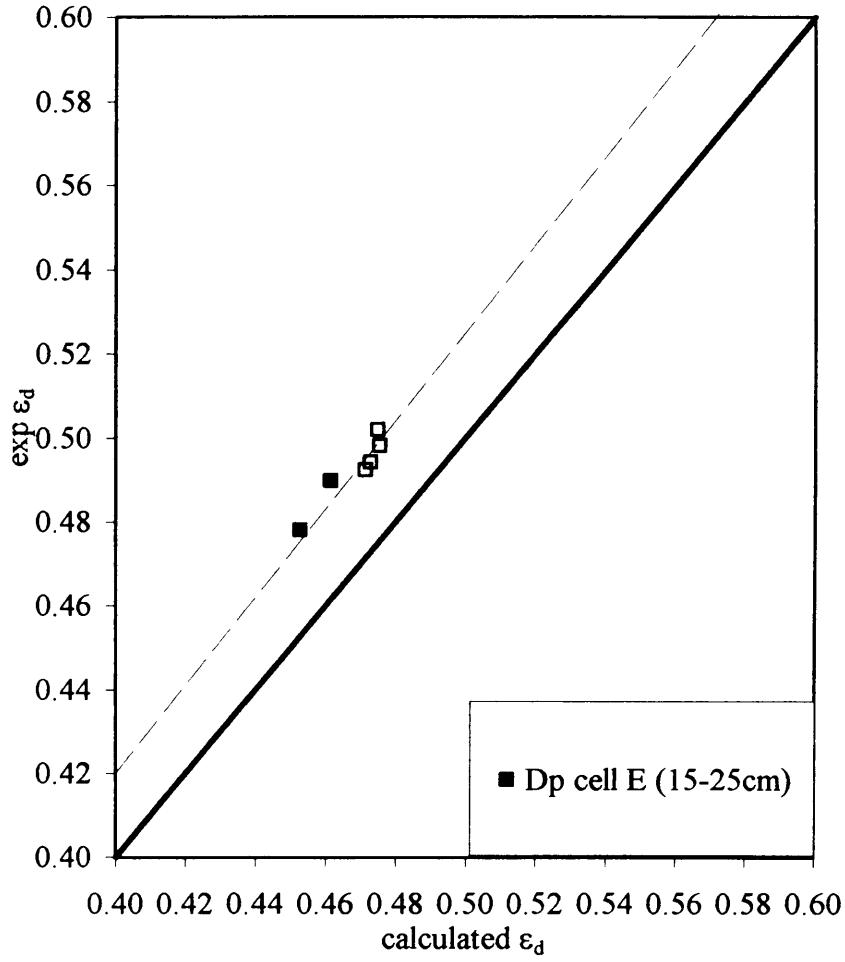

Figure 6.2 Comparison of dense phase voidage (ε_d) from bed collapse model prediction and pressure reading for 72 μm (0.127 m ID, Li = 0.30 m)

[Full square = $U_0 < U_{mb}$ and Empty square = $U_0 > U_{mb}$]

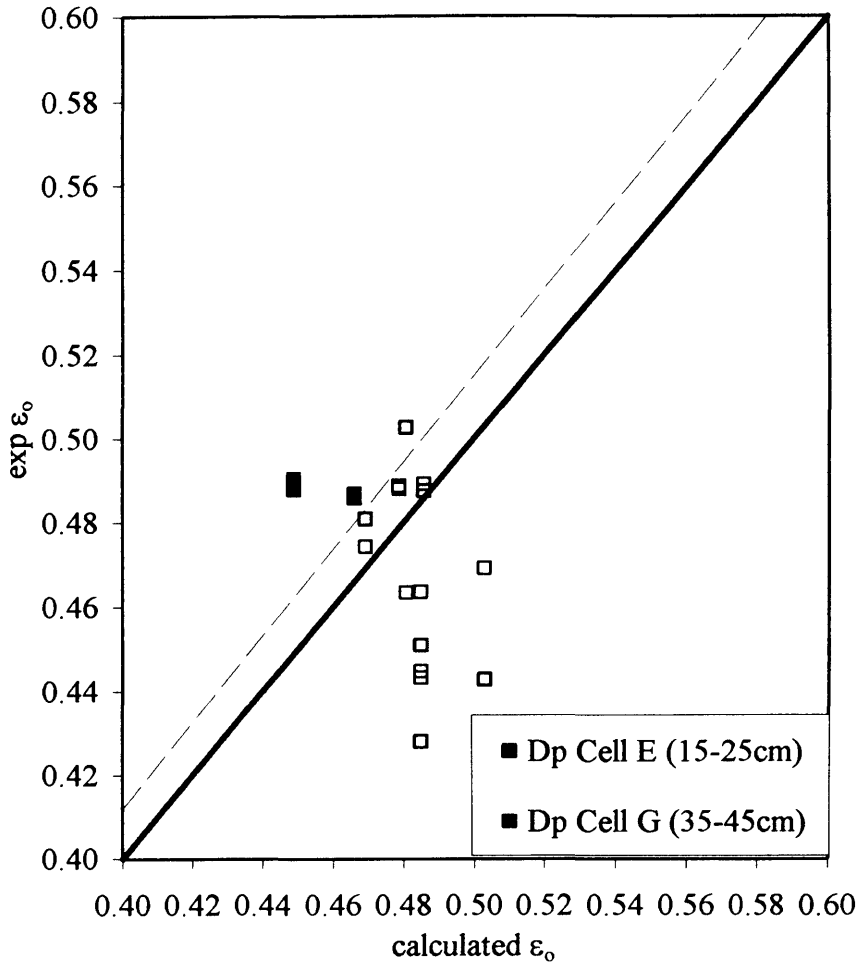

Figure 6.3 Comparison of bed voidage (ε_o) from bed collapse model prediction and pressure reading for 72 μm (0.243 m ID, Li = 0.30 m)

[Full square = $U_0 < U_{mb}$ and Empty square = $U_0 > U_{mb}$]

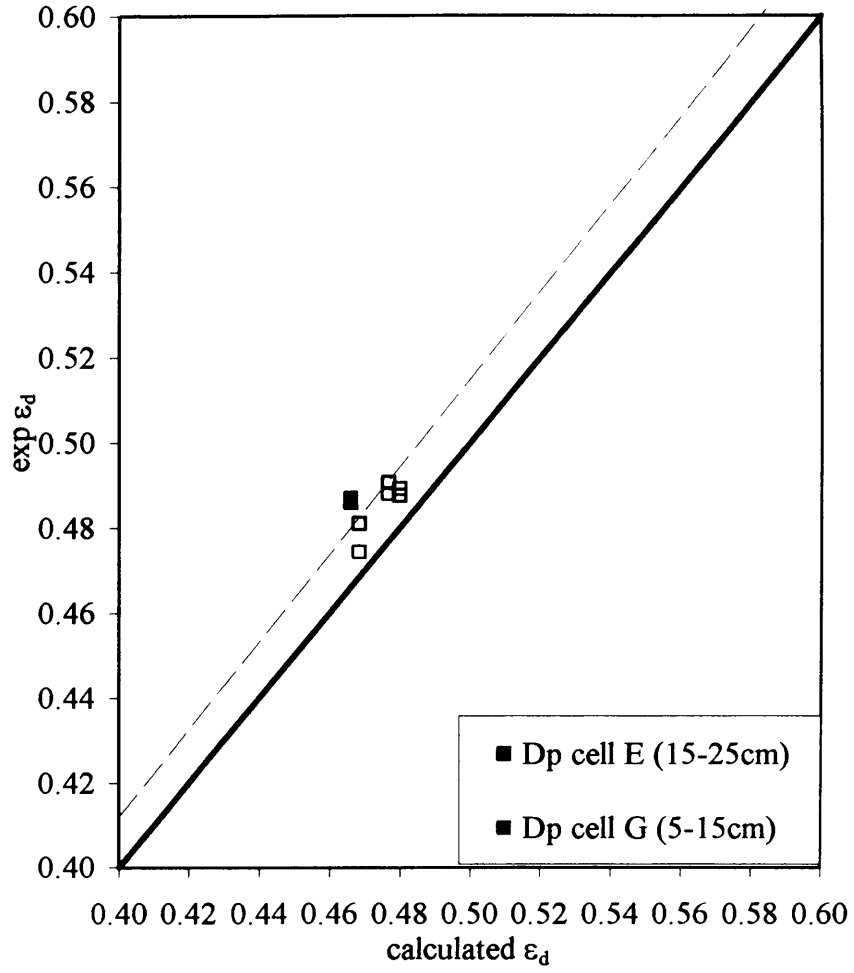

Figure 6.4 Comparison of dense phase voidage (ε_d) from bed collapse model prediction and pressure reading for 72 μm (0.127 m ID, Li = 0.30 m)

[Full square = $U_0 < U_{mb}$ and Empty square = $U_0 > U_{mb}$]

6.2.1 ε_d and U_d characteristic curves

Figure 6.5 to Figure 6.7 are the U_d and ε_d characteristic curves for the 37 μm (Batch 1), 72 μm and 37 μm (Batch 2) powders, respectively. For the non cohesive powder, (Figure 6.5 and Figure 6.6), the U_d and ε_d relationships from two different initial bed heights (0.30 m and 0.40 m) and column diameters (0.127 m and 0.243 m) for each

powder approximately the same trends are observed. Thus, it can be concluded that the column diameter and the initial bed height, where the aspect ratio is within 1.2–3.4, have no effect on the relation of U_d and ε_d. The same results for the homogeneous expanded bed were reported, by Mazumadar and Ganguly (1985). They reported that for aspect ratios (1.10-4.67) no effect was observed on the U_d and ε_d relationship for a liquid phase homogeneous expanded bed. For gas systems, Simone and Harriott, (1980) reported that the column diameter (0.05 and 0.124 m) has no effect on the dense phase voidage for the gas phase homogeneous expanded bed.

For the cohesive powder (Figure 6.7), the U_d and ε_d relationship from different initial bed heights are different. This may be due to the agglomeration of powder and the presence of channelling in the system.

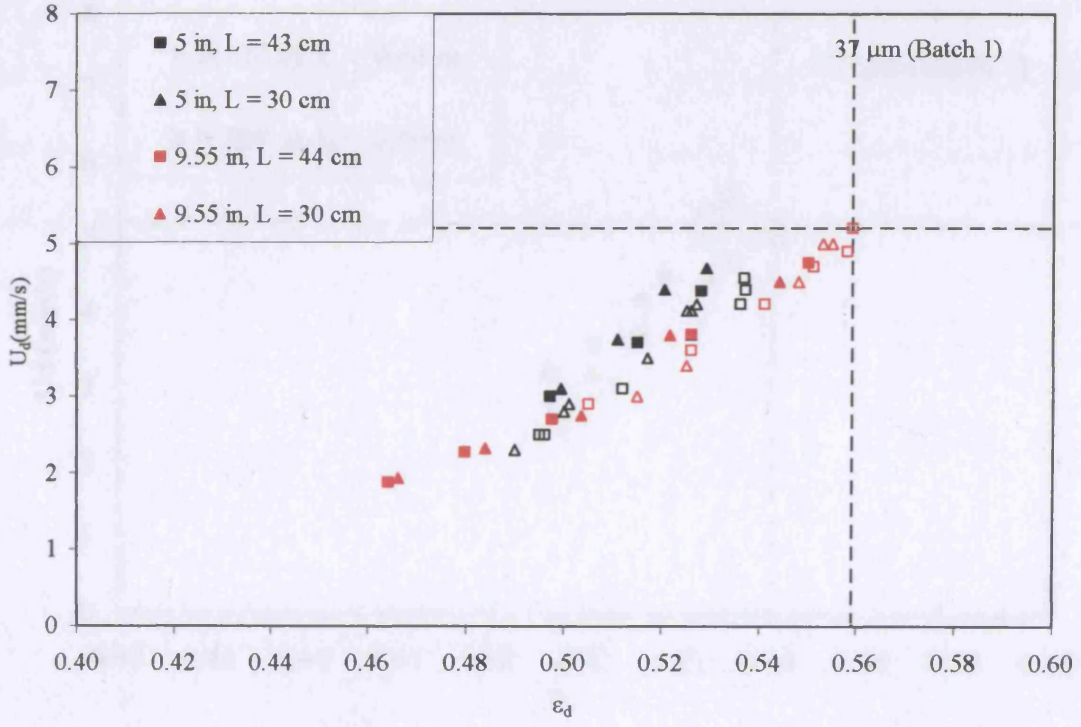

Figure 6.5 ε_d and U_d Characteristic curve for 37 μm Ballotini (Batch 1)

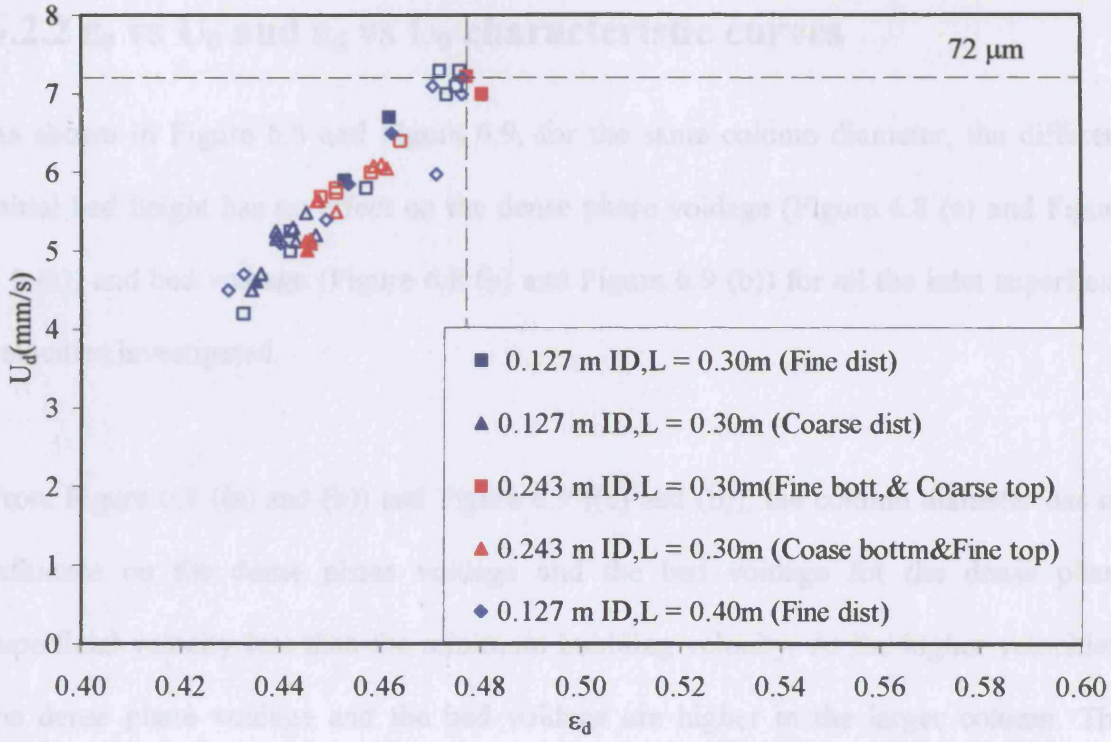

Figure 6.6 ε_d and U_d Characteristic curve for 72 µm Ballotini

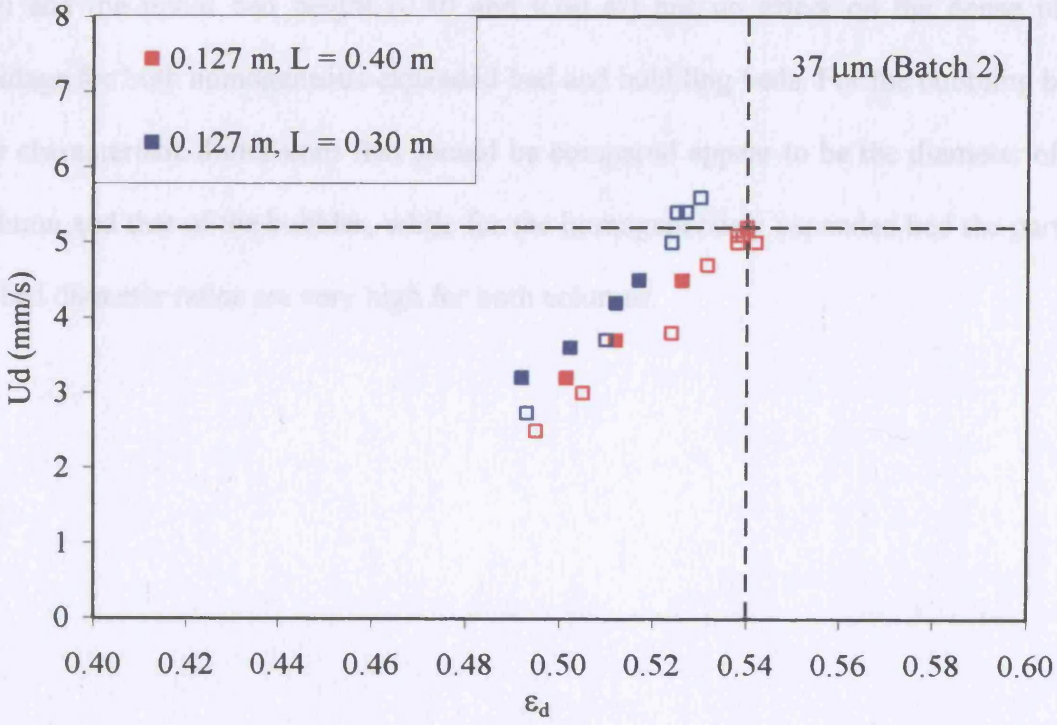

Figure 6.7 ε_d and U_d Characteristic curve for 37 µm Ballotini (Batch 2)

6.2.2 ε_0 vs U_0 and ε_d vs U_0 characteristic curves

As shown in Figure 6.8 and Figure 6.9, for the same column diameter, the different initial bed height has no effect on the dense phase voidage (Figure 6.8 (a) and Figure 6.9 (a)) and bed voidage (Figure 6.8 (b) and Figure 6.9 (b)) for all the inlet superficial velocities investigated.

From Figure 6.8 ((a) and (b)) and Figure 6.9 ((a) and (b)), the column diameter has no influence on the dense phase voidage and the bed voidage for the dense phase superficial velocity less than the minimum bubbling velocity. At the higher velocities, the dense phase voidage and the bed voidage are higher in the larger column. The results similar to those of Simone and Harriott (1980), who reported that the dense phase voidage in the bubbling region is larger for a larger column (0.05 and 0.124 m ID) and the initial bed height (0.40 and 0.60 m) has no effect on the dense phase voidage for both homogeneous expanded bed and bubbling beds. For the bubbling beds, the characteristic dimensions that should be compared appear to be the diameter of the column and that of the bubbles, while for the homogeneously expanded bed the particle to bed diameter ratios are very high for both columns.

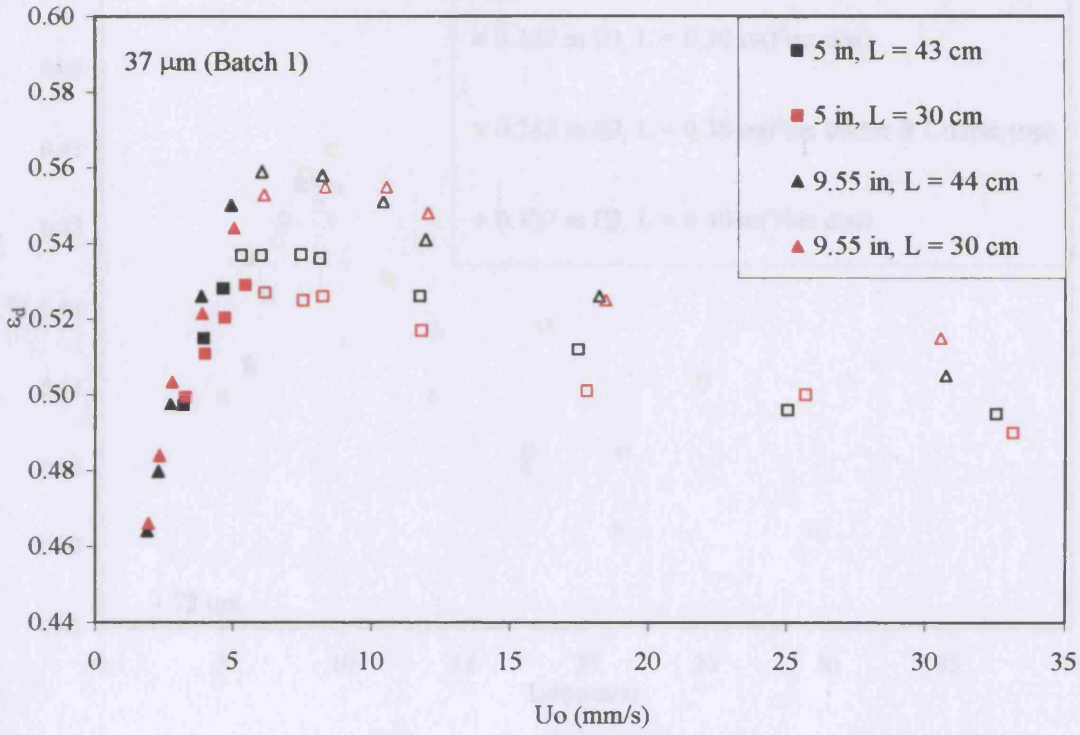

(a)

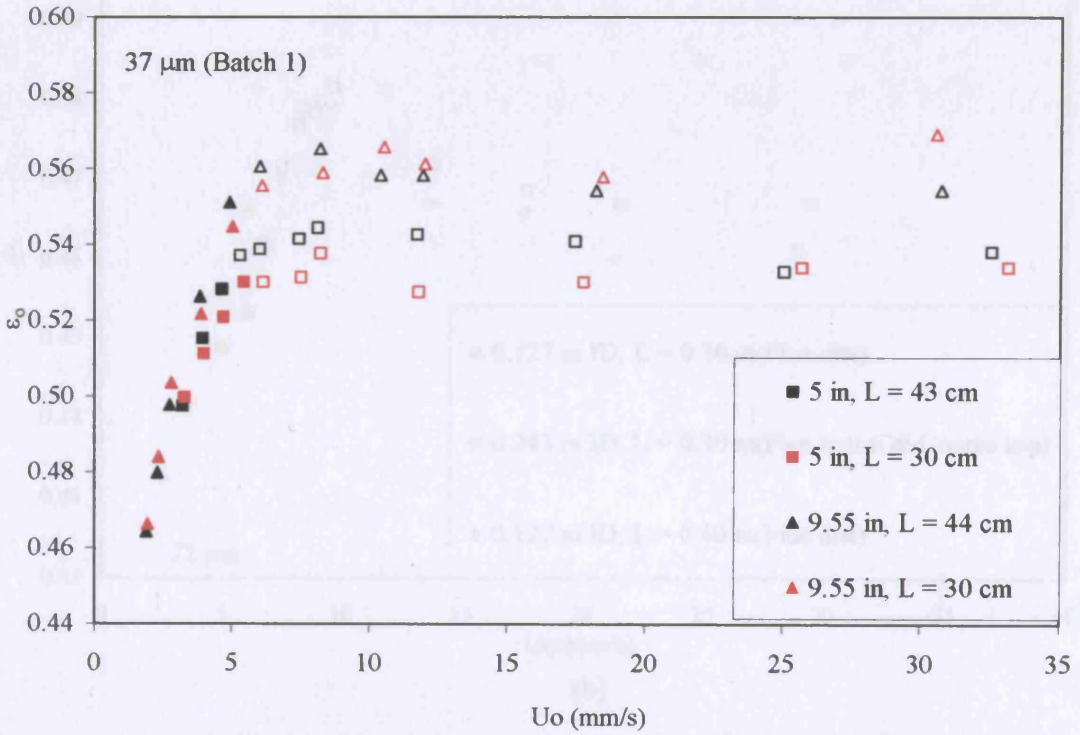

(b)

Figure 6.8 Bed expansion for 37 μm Ballotini (Batch1) (a) ε_d vs U_0 and (b) ε_0 vs U_0

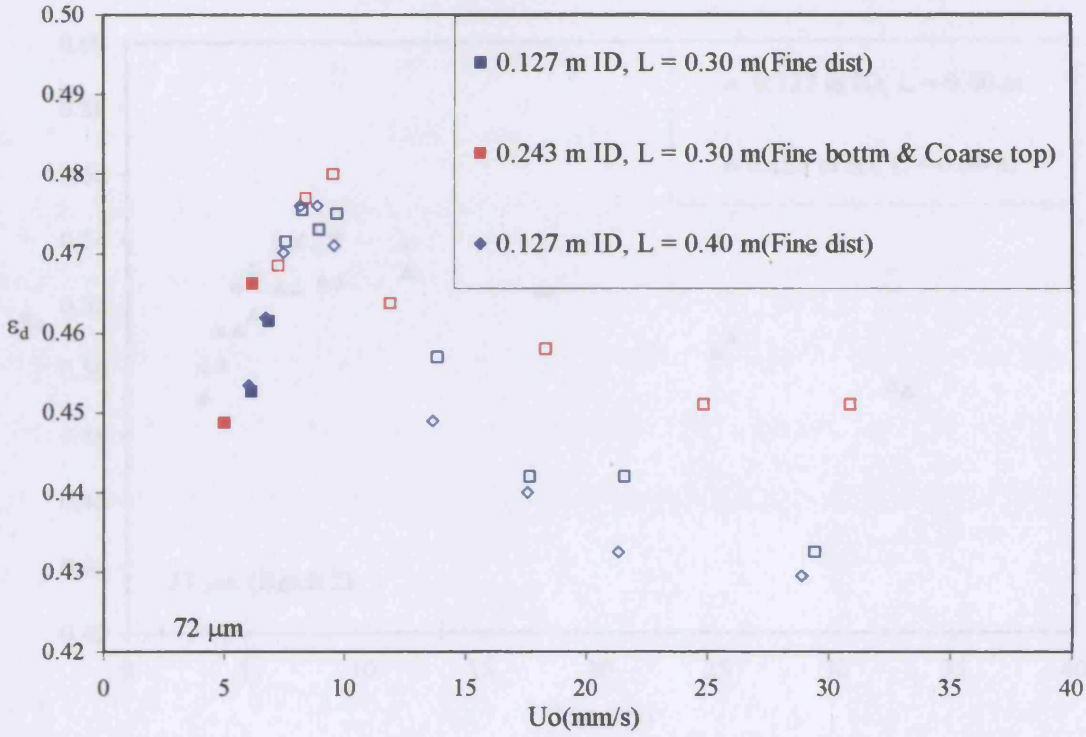

(a)

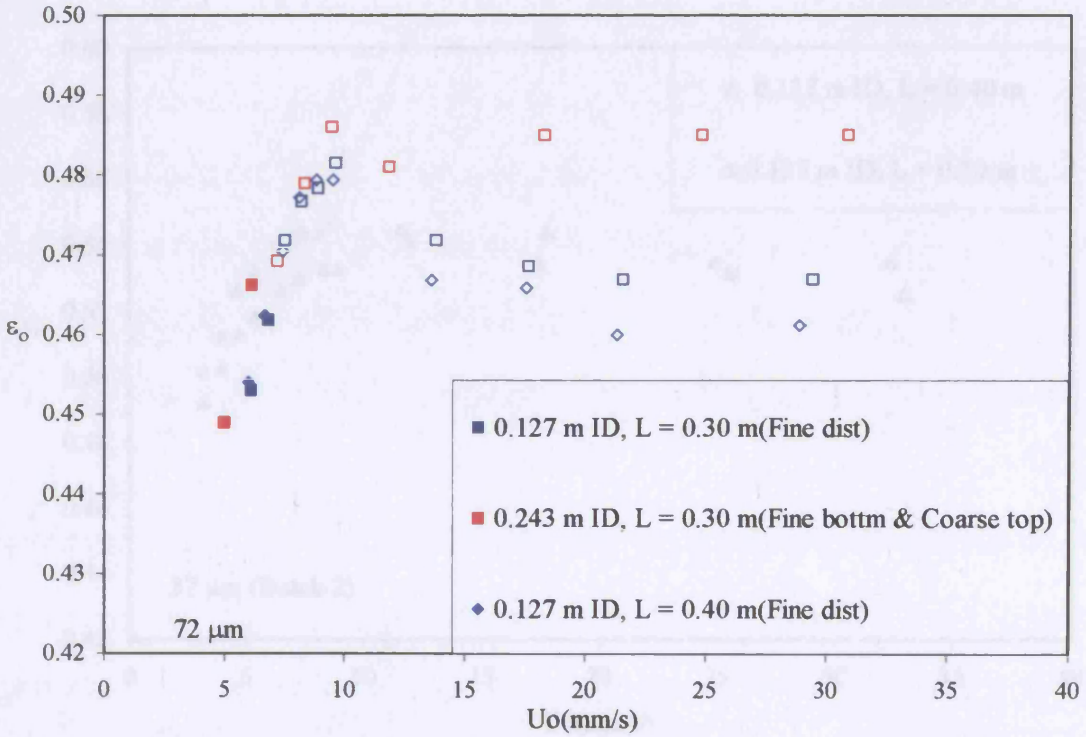

(b)

Figure 6.9 Bed expansion for 72 μm Ballotini (a) ε_d vs U_0 and (b) ε_0 vs U_0

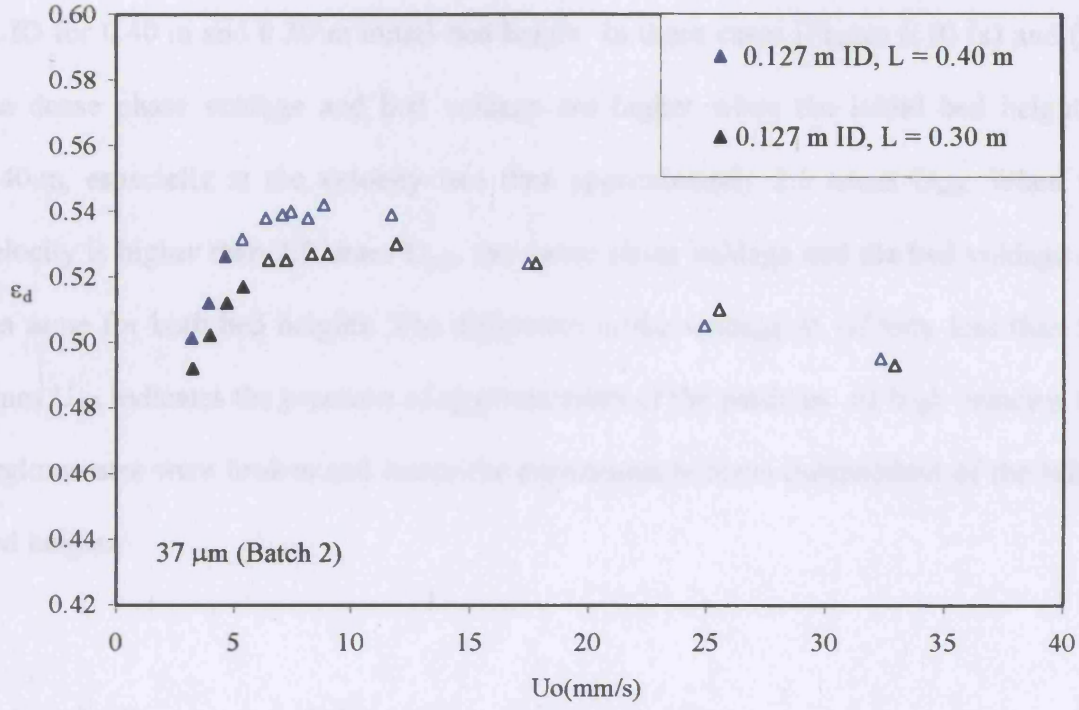

(a)

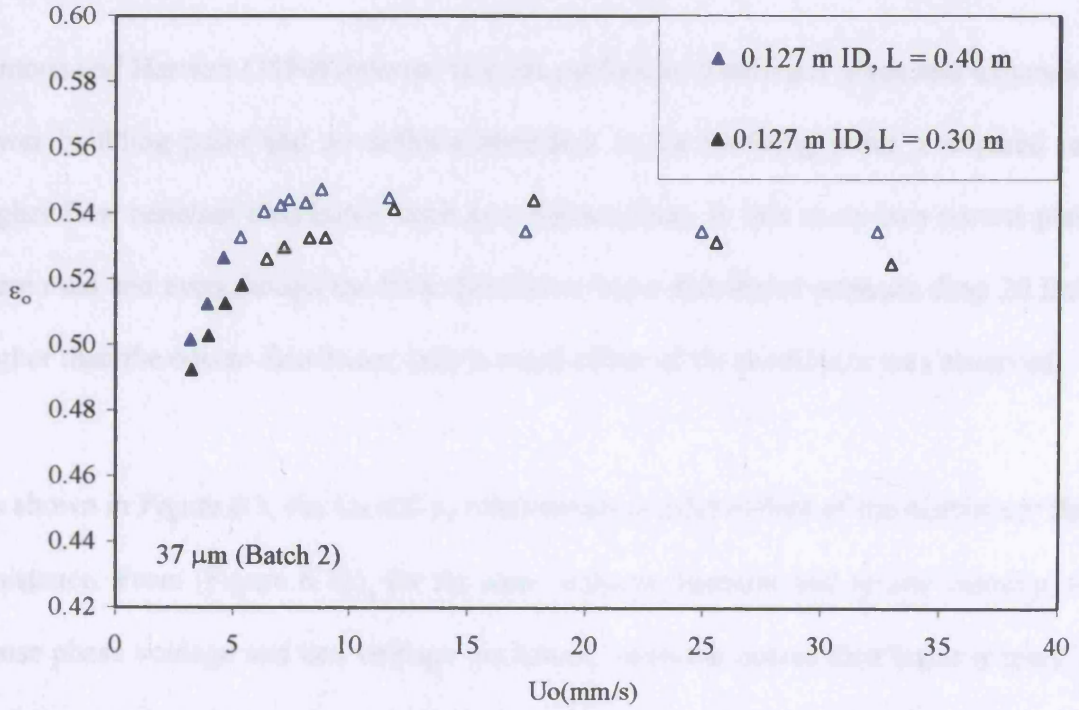

(b)

Figure 6.10 Bed expansion for 37 μm Ballotini (Batch 2) (a) ε_d vs U_0 and (b) ε_0 vs U_0

For the cohesive powder (37 mm (Batch 2)), the experiments were carried out in 0.127 m ID for 0.40 m and 0.30 m initial bed height. In these cases (Figure 6.10 (a) and (b)) the dense phase voidage and bed voidage are higher when the initial bed height is 0.40.m, especially at the velocity less than approximately 2.5 times U_{mb}. When the velocity is higher than 2.5 times U_{mb}, the dense phase voidage and the bed voidage are the same for both bed heights. The difference in the voidage at velocity less than 2.5 times U_{mb} indicates the presence of agglomeration of the particles. At high velocity, the agglomerates were broken and hence the expansions become independent of the initial bed heights.

6.3 Influence of distributor porosity

Simone and Harriott (1980) reported that the perforated distributor gives less expansion, lower bubbling point and no definite transition to the bubbling point, compared to a higher flow resistant distributor, such as a porous plate. In this study two porous plates were used and even though the finer distributor has a distributor pressure drop 20 times higher than the coarse distributor, only a small effect of the distributor was observed.

As shown in Figure 6.9, the U_d and ε_d relationship is independent of the distributor flow resistance. From (Figure 6.11), for the same column diameter and at low velocity, the dense phase voidage and bed voidage are lower; when the coarse distributor is used. In addition, there is not a clear transition indicating the minimum bubbling point. The bubbles start almost at the beginning of the fluidization stage. However, at very high velocity ($U_0 \approx 2.5U_{mb}$), the dense phase voidage and the bed voidage are the same as

those obtained using the fine distributor and the distributor flow resistance has no influence on the bed expansion.

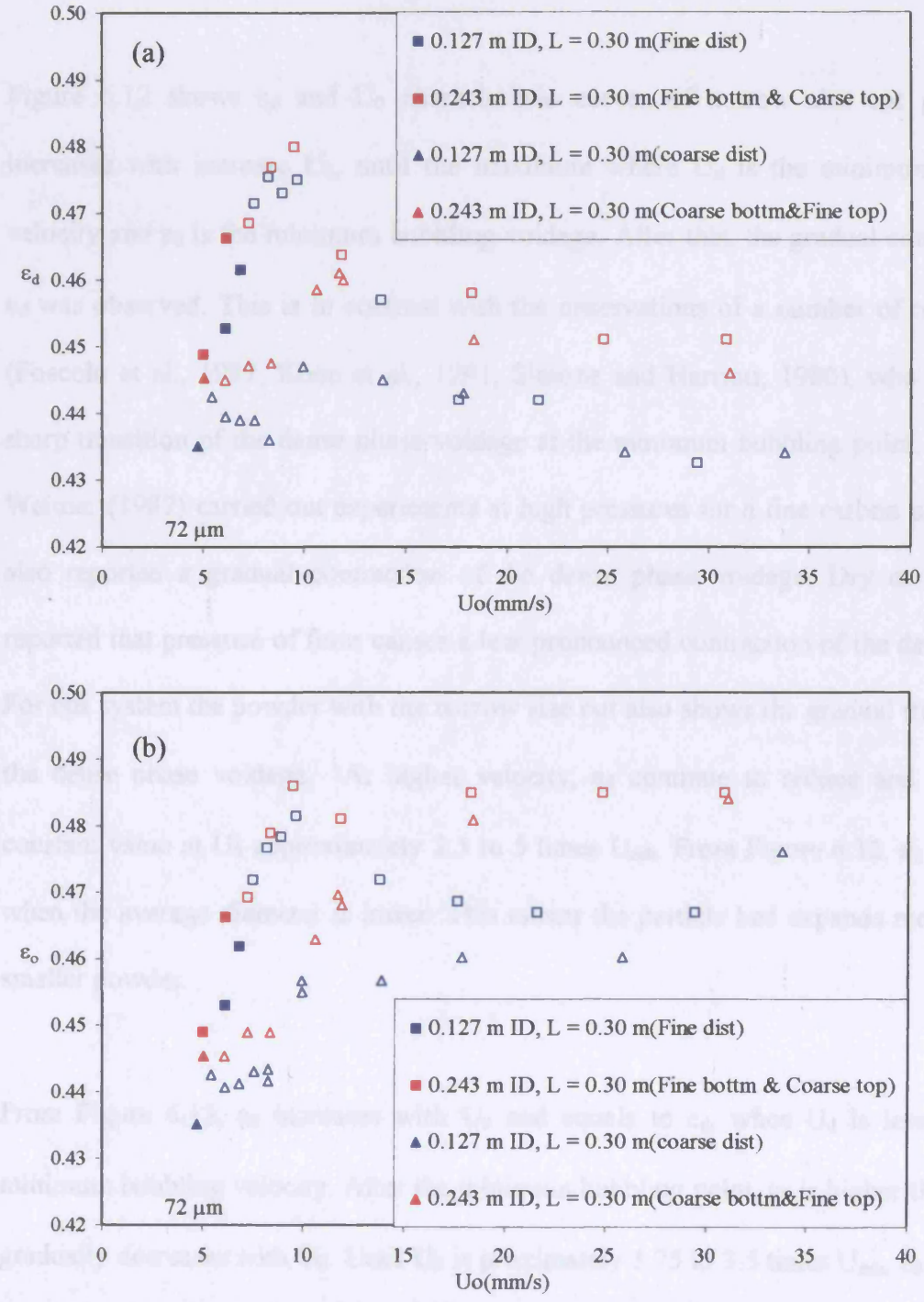

Figure 6.11 Bed expansion for 72 µm Ballotini at different column diameter and distributor flow resistance (a) ε_d vs U_0 and (b) ε_0 vs U_0.

[Full symbol = $U_0 < U_{mb}$ and empty symbol = $U_0 > U_{mb}$]

6.4 ε_0 vs U_0 and ε_d vs U_0 characteristic curves of narrow size and natural powders

Figure 6.12 shows ε_d and U_0 characteristic curves of narrow size cut powder. ε_d increases with increase U_0, until the maximum where U_d is the minimum bubbling velocity and ε_d is the minimum bubbling voidage. After this, the gradual contraction of ε_d was observed. This is in contrast with the observations of a number of researchers, (Foscolo et al., 1987; Khoe et al., 1991; Simone and Harriott, 1980), who reported a sharp transition of the dense phase voidage at the minimum bubbling point. Jacob and Weimer (1987) carried out experiments at high pressures for a fine carbon powder and also reported a gradual contraction of the dense phase voidage. Dry et al. (1983) reported that presence of fines causes a less pronounced contraction of the dense phase. For our system the powder with the narrow size cut also shows the gradual transition of the dense phase voidage. At higher velocity, ε_d continue to reduce and reaches a constant value at U_0 approximately 2.5 to 5 times U_{mb}. From Figure 6.12, ε_d is higher, when the average diameter is lower. This means the particle bed expands more for the smaller powder.

From Figure 6.13, ε_0 increases with U_0 and equals to ε_d, when U_d is less than the minimum bubbling velocity. After the minimum bubbling point, ε_0 is higher than ε_d and gradually decreases with U_0. Until U_0 is proximately 1.75 to 3.5 times U_{mb}, ε_0 increases slowly with U_0 or even is almost constant.

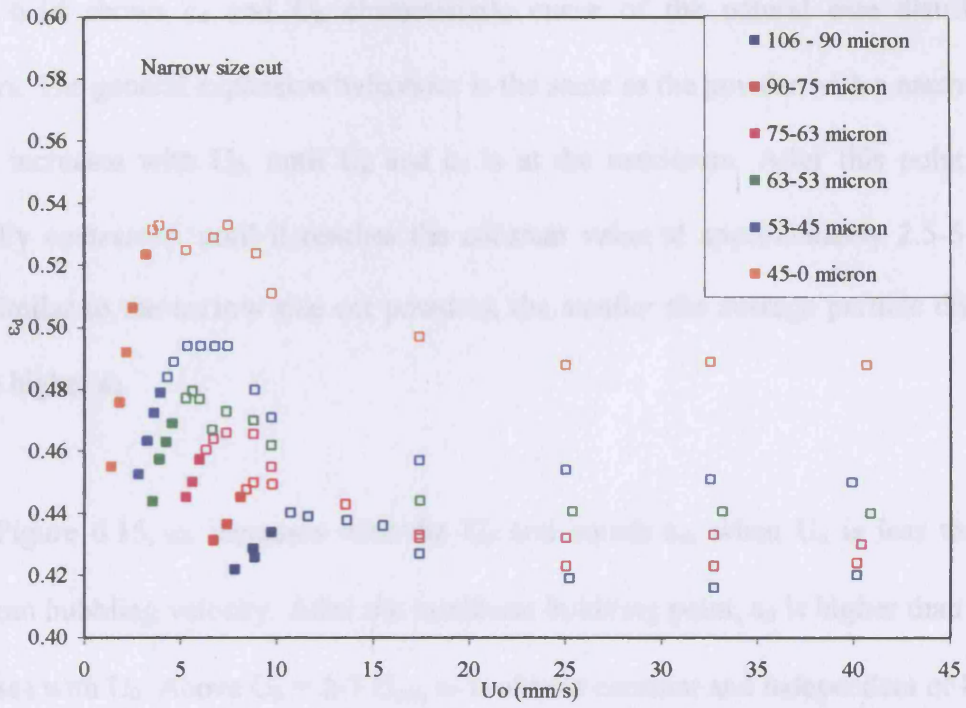

Figure 6.12 ε_d and U_0 characteristic curves for narrow size cut powders.

[Full symbol = $U_0 < U_{mb}$ and empty symbol = $U_0 > U_{mb}$]

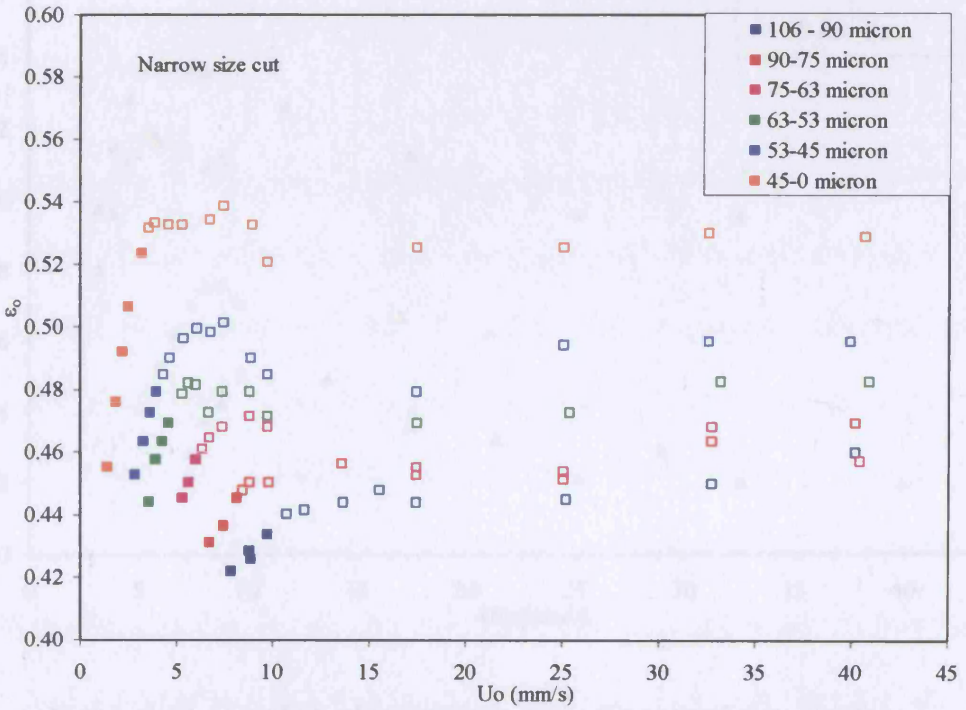

Figure 6.13 ε_0 and U_0 characteristic curve for narrow size cut powders.

[Full symbol = $U_0 < U_{mb}$ and empty symbol = $U_0 > U_{mb}$]

Figure 6.14 shows ε_d and U_0 characteristic curve of the natural size distribution powders. The general expansion behaviour is the same as the powder with a narrow size cut. ε_d increases with U_0, until U_d and ε_d is at the maximum. After this point, ε_d is gradually contracted, until it reaches the constant value at approximately 2.5-5 times U_{mb}. Similar to the narrow size cut powders, the smaller the average particle diameter has the higher ε_d.

From Figure 6.15, ε_0 increases with the U_0 and equals ε_d, when U_d is less than the minimum bubbling velocity. After the minimum bubbling point, ε_0 is higher than ε_d and decreases with U_0. Above U_0 = 2-3 U_{mb}, ε_0 is almost constant and independent of U_0.

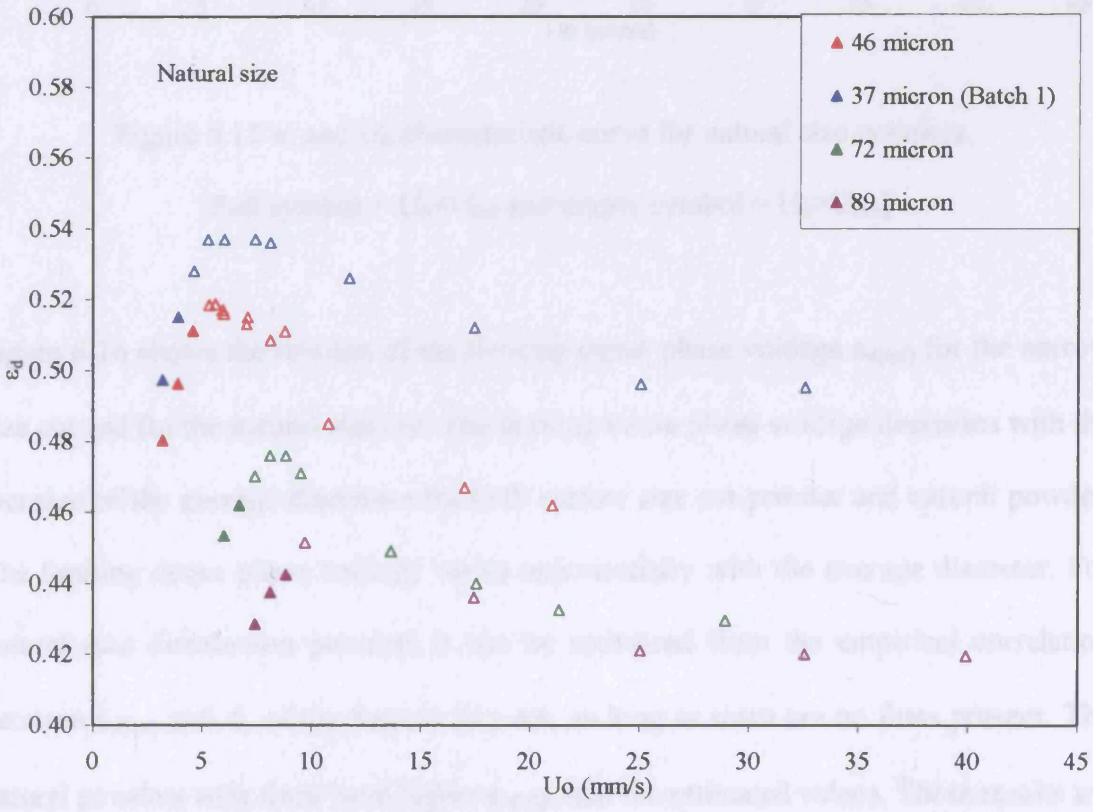

Figure 6.14 ε_d and U_0 characteristic curve for natural size powders.

[Full symbol = $U_0 < U_{mb}$ and empty symbol = $U_0 > U_{mb}$]

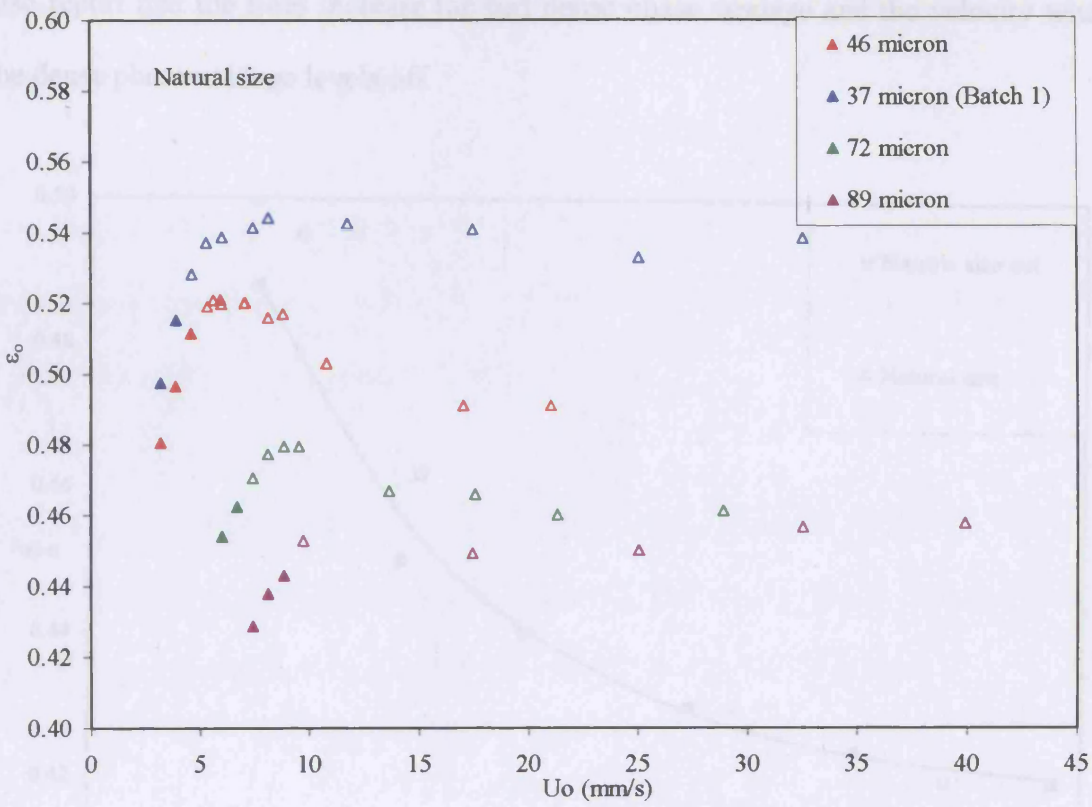

Figure 6.15 ε_0 and U_0 characteristic curve for natural size powders.

[Full symbol = $U_0 < U_{mb}$ and empty symbol = $U_0 > U_{mb}$]

Figure 6.16 shows the relation of the limiting dense phase voidage $\varepsilon_{d(inf)}$ for the narrow size cut and for the natural size cut. The limiting dense phase voidage decreases with the increase of the average diameters for both narrow size cut powder and natural powder. The limiting dense phase voidage varies exponentially with the average diameter. For natural size distribution powders it can be estimated from the empirical correlation between $\varepsilon_{d(inf)}$ and d_p of the narrow size cut, as long as there are no fines present. The natural powders with fines have higher $\varepsilon_{d(Inf)}$ than the estimated values. These results are similar to those reported by Geldart and Abrahamsen (1978) and Rowe et al. (1978). These authors report that increasing content of fines leads to an increase in dense phase superficial velocity and hence bed expansion. Dry et al. (1983) and Yadav et al. (1994)

also report that the fines increase the bed dense phase voidage and the velocity where the dense phase voidage levels off.

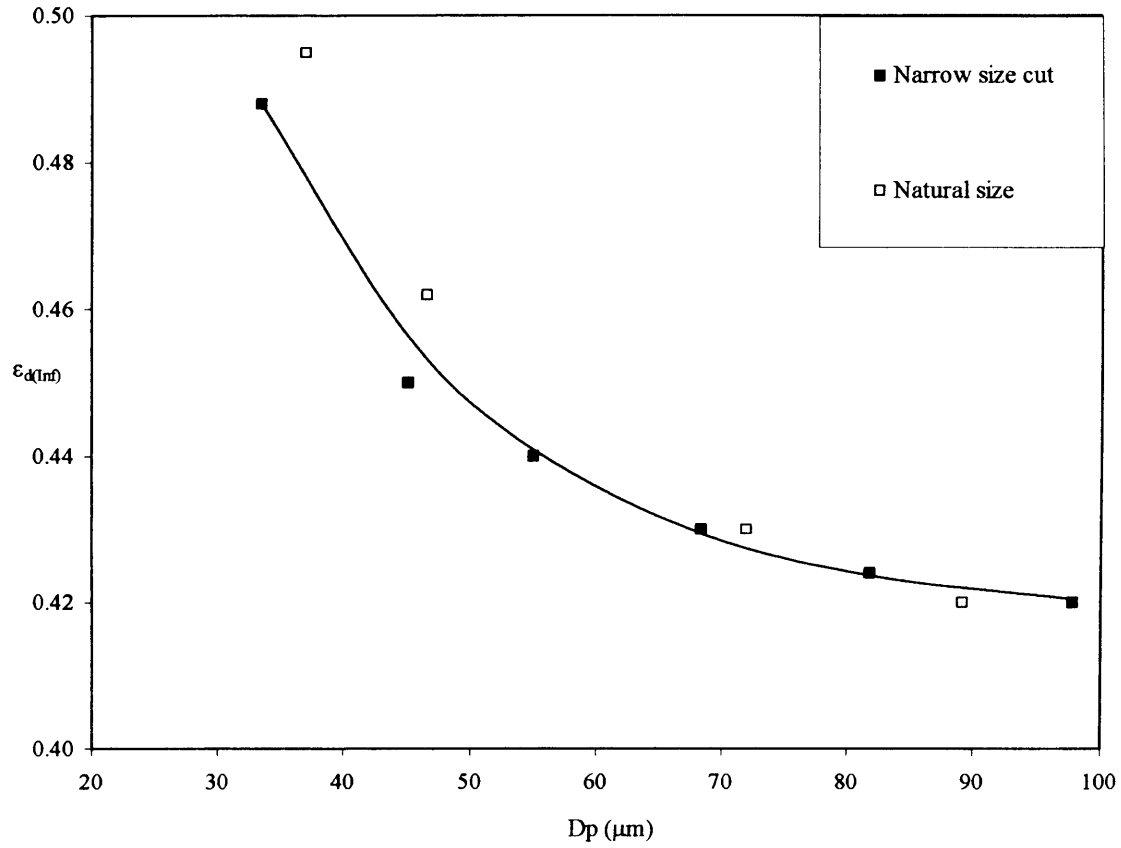

Figure 6.16 Infinite ε_d versus d_p relation for narrow size cut powders and natural size powder

6.5 ε_d and U_d characteristic curves of narrow size and natural size powders

Figure 6.17 shows the ε_d and U_d characteristic curve of the narrow size cut powders and natural size distribution powders. For all powders, the ε_d and U_d relationships before and after the minimum bubbling point show the same linear trend. This means that a

dense phase superficial velocity corresponds to the same dense phase voidage for both the expanded and bubbling beds.

From Figure 6.17, U_d increases with increased average diameter for narrow size cut powders and natural size powders. At the maximum expansion, $U_{d(max)}$ increases with particle size and $\varepsilon_{d(max)}$ decreases with the particle size.

The ε_d and U_d characteristic can be described using the empirical Richardson and Zaki correlation and drag force correlations. The following section shows the comparison between experimental values and those predicted from various correlations.

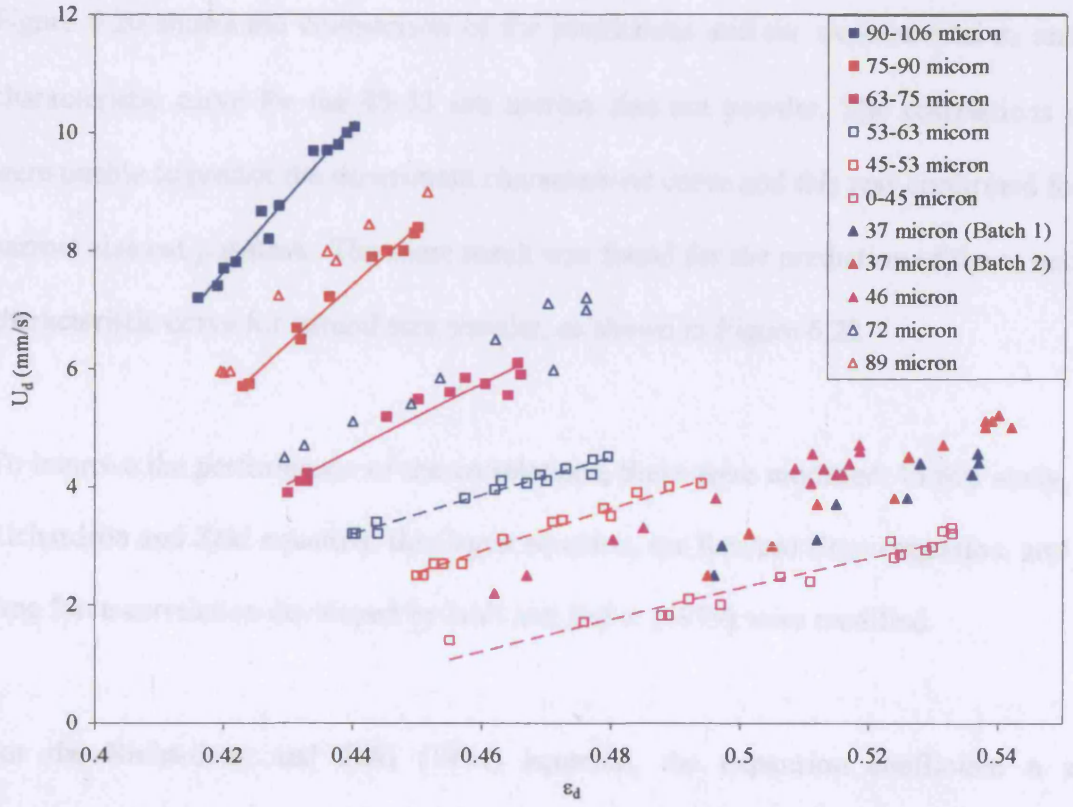

Figure 6.17 ε_d and U_d curves for narrow size cut and natural size distribution powders

6.6 Validation of fluidization drag force correlations and their modifications

In this work, the ε_d and U_d characteristic curves were described using the empirical Richardson and Zaki (1954) equation; the Ergun (1952) equation; the Revised Ergun equation (Foscolo et al., 1983); the drag force correlation developed by Ishii and Zuber (1979); the drag force correlation developed by Syamlal and O'Brien (1987) as used by Gelderbloom et al. (2003) in the CFD simulations of bubbling and collapsing fluidized beds. The details of the correlations mentioned above are summarised in Table 2.3, Chapter 2.

Figure 6.20 shows the comparison of the predictions and the experimental ε_d and U_d characteristic curve for the 45-53 μm narrow size cut powder. The correlations used were unable to predict the experiment characteristic curve and this was confirmed for all narrow size cut powders. The same result was found for the prediction of the ε_d and U_d characteristic curve for natural size powder, as shown in Figure 6.22.

To improve the performance of the correlations, these were modified. In this study, the Richardson and Zaki equation, the Ergun equation, the Revised Ergun equation, and the drag force correlation developed by Ishii and Zuber (1979) were modified.

For the Richardson and Zaki (1954) equation, the expansion coefficient n was determined from the experimental data. For the Ergun (1952) equation, the modification was made on the constant denoted 'X' as shown in eq. 6.1.

$$\frac{\partial P}{\partial z} = (X)\frac{\mu_f U(1-\varepsilon)^2}{d_p^2 \varepsilon^3} + 1.75\frac{(1-\varepsilon)}{\varepsilon^3}\frac{\rho_f U^2}{d_p} \qquad (6.1)$$

In the Revised Ergun equation, the exponent of the voidage ε was modified and the correlation was rewritten as:

$$\frac{\partial P}{\partial z} = \frac{\rho_F U^2(1-\varepsilon)}{d_p}\left(\frac{18}{Re_p} + 0.336\right)\varepsilon^{-m} \qquad (6.2)$$

In the drag force correlation of Ishii and Zuber (1979) the exponent (K) on the mixture viscosity was adjusted, and the maximum packing particle fraction was changed to 0.601:

$$\frac{\mu_M}{\mu_F} = \left(1 - \frac{1-\varepsilon}{\varepsilon_{dm}}\right)^{-K\varepsilon_{dm}} \qquad (6.3)$$

where, $\varepsilon_{dm} = 0.601$

Table 6.1 and Table 6.3 summarise the values of the modified factors on the correlations for the narrow size cut powders and the natural size powders, respectively. Table 6.2 and Table 6.4 summarise the adjusted value of the modified factors on the correlations for the narrow size cut powders and the natural size powders.

Figure 6.21 and Figure 6.23 show the comparison of the prediction and the experimental ε_d and U_d characteristic curves for the narrow size cut powder and the natural size powder. The modified Richardson and Zaki correlation and the Revised Ergun equations show the best fit. The same results were found for all powders investigated in this study.

Figure 6.18 shows the original Richardson and Zaki index and the modified index of the narrow size cut powders and natural size powders. n was found to be higher than the original value and ranges from 4.77 to 5.05 for the narrow size cut powders and from 4.82 to 5.43 for natural size distribution powders. In general n is varied randomly with average particle diameter and the average value of n was used. The modified n for the narrow size cut powders is approximately the same as that for the natural size distribution powders.

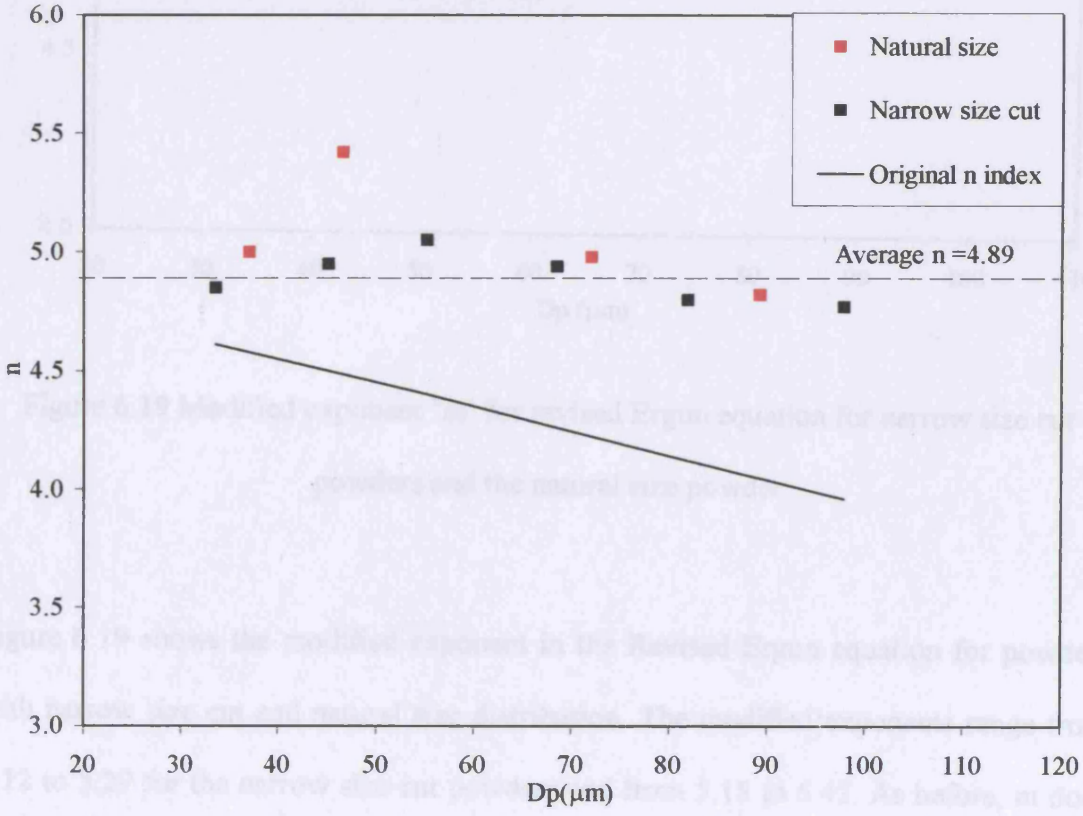

Figure 6.18 Modified Richardson and Zaki index and the Original index for narrow size cut powders and the natural size powder

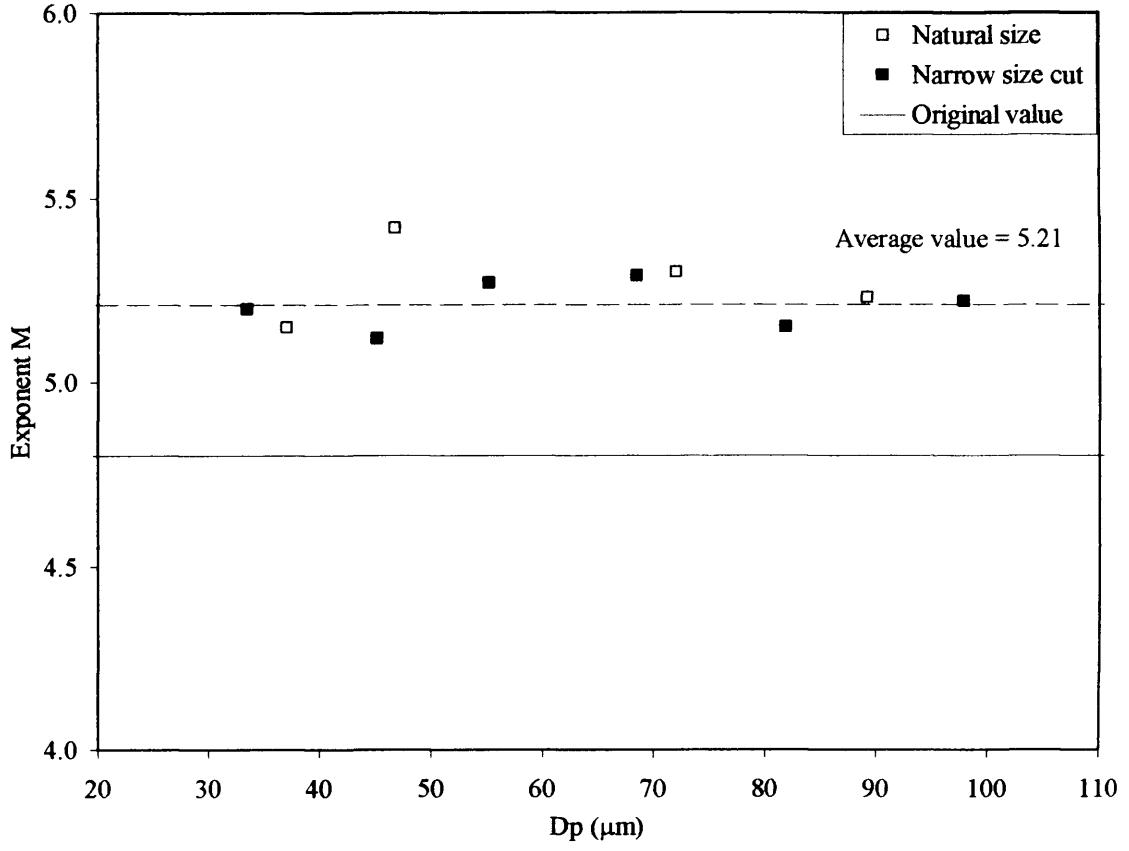

Figure 6.19 Modified exponent 'm' for revised Ergun equation for narrow size cut powders and the natural size powder

Figure 6.19 shows the modified exponent in the Revised Ergun equation for powders with narrow size cut and natural size distribution. The modified exponents range from 5.12 to 5.29 for the narrow size cut powders and from 5.15 to 5.42. As before, m does not seem to vary significantly with the average particle diameter and an average value of m can be used.

The average modified m from the narrow size cut was used as a standard, because the expansion characteristic of the narrow size cut powders are of uniform size and the uncertainty of the average size is negligible. In addition, the values of m of the natural

size distribution powders are also scattered around the average value m of narrow size. Thus, the average value m from the narrow size cut should be representative for both the system of uniform size and the natural size distribution. By using the average modified m from the narrow size cut powder, the modified revised Ergun equation can be written as:

$$\frac{\partial P}{\partial z} = \frac{\rho_f U^2 (1-\varepsilon)}{d_p}\left(\frac{18}{Re_p} + 0.336\right)\varepsilon^{-5.21} \qquad (6.4)$$

This can be related to the drag force correlation by

$$F_D = \varepsilon \Delta P \qquad (6.5)$$

and

$$F_D = \frac{\rho_F}{d_p}\left(\frac{18}{Re_p} + 0.336\right)U^2(1-\varepsilon)\varepsilon^{-4.21} \qquad (6.6)$$

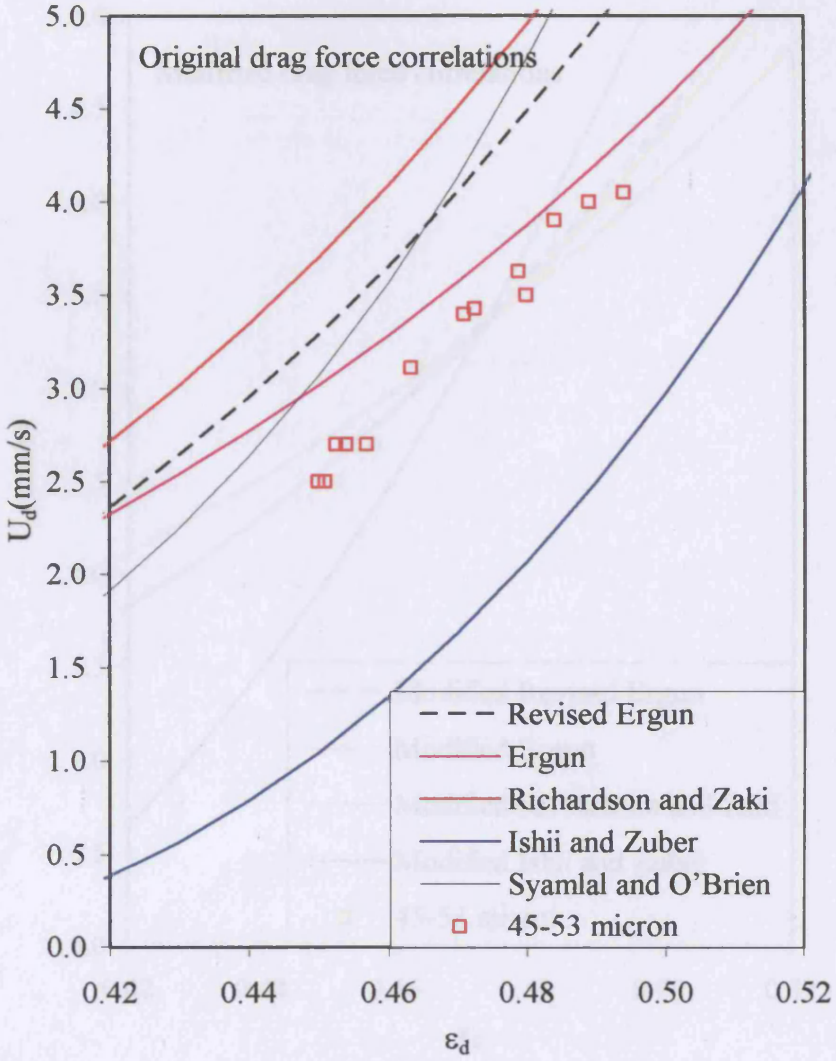

Figure 6.20 Prediction of ε_d and U_d characteristic curve using original pressure drop correlations for 45-53 μm narrow size cut powder

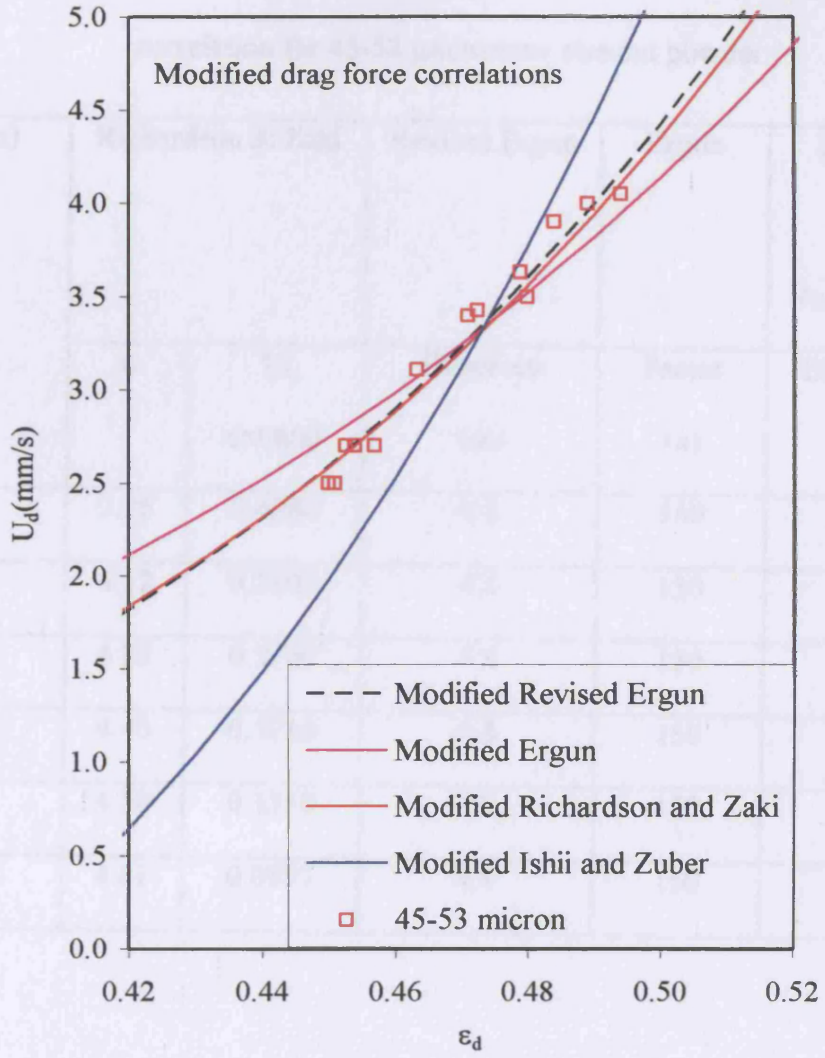

Figure 6.21 Prediction of ε_d and U_d characteristic curve, using a modified pressure drop correlations for 45-53 μm narrow size cut powder

Table 6.1 Summary of the original parameters for the modified pressure drop correlation for 45-53 μm narrow size cut powder

D_p(mm)	Richardson & Zaki		Revised Ergun	Ergun	Ishii & Zuber ($\varepsilon_{dm} = 0.62$)
	n	U_t (mm/s)	Exponent (m)	Factor (x)	Exponent (k)
98.82	3.96	0.4880	4.8	150	2.5
81.81	4.12	0.3690	4.8	150	2.5
68.41	4.26	0.2760	4.8	150	2.5
55.08	4.40	0.1910	4.8	150	2.5
45.1	4.50	0.1350	4.8	150	2.5
33.5	4.61	0.0597	4.8	150	2.5

Table 6.2 Summary of the modified parameters for the modified pressure drop correlation for 45-53 μm narrow size cut powder

D_p(mm)	Richardson & Zaki		Revised Ergun	Ergun	Ishii & Zuber (ε_{dm} = 0.60)
	n	U_t (mm/s)	Exponent (m)	Factor (x)	Exponent (k)
98.82	4.77	0.4880	5.22	210	1.50
81.81	4.80	0.3690	5.15	186	1.60
68.41	4.94	0.2760	5.29	202	1.80
55.08	5.05	0.1910	5.27	193	1.90
45.1	4.95	0.1350	5.12	165	1.85
33.5	4.85	0.0597	5.20	140	1.95

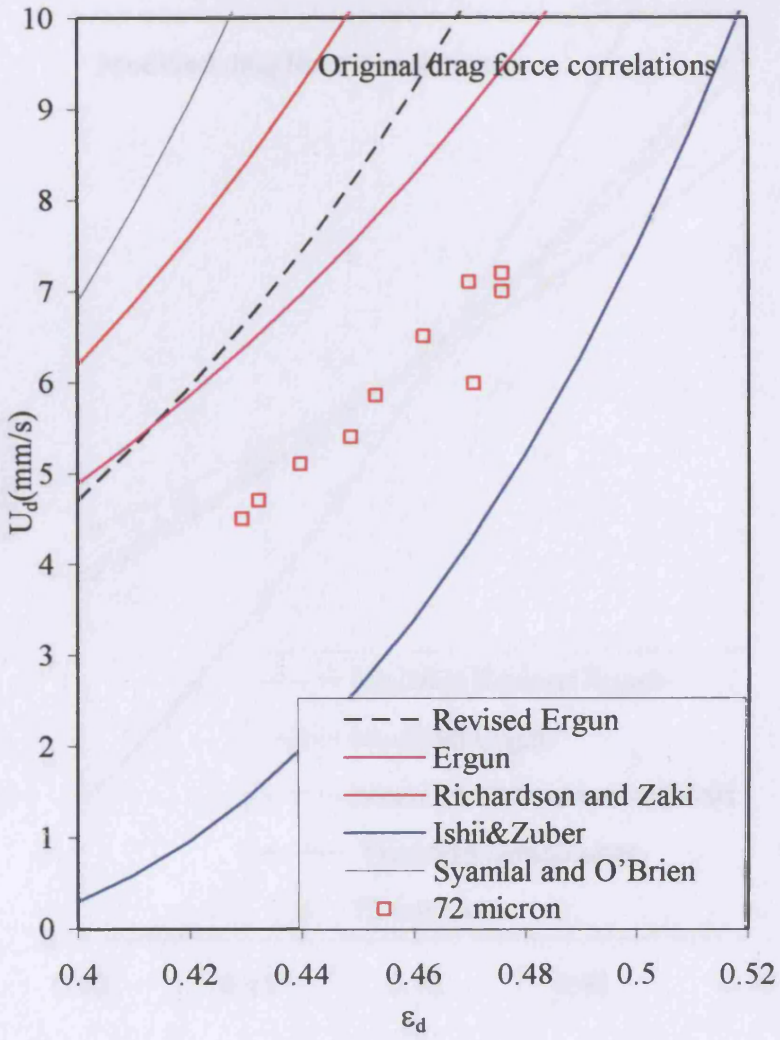

Figure 6.22 Prediction of ε_d and U_d characteristic curve using original pressure drop correlations for 72 μm natural size powder

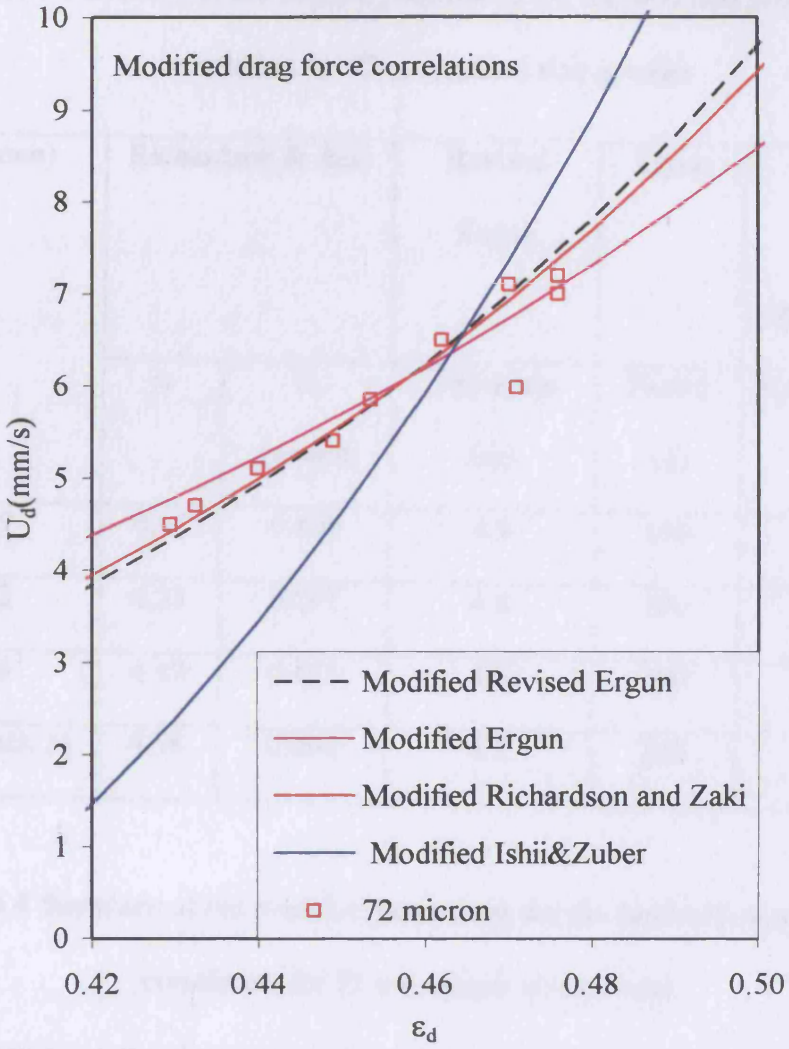

Figure 6.23 Prediction of ε_d and U_d characteristic curve using modified pressure drop correlations for 72 μm natural size powder

Table 6.3 Summary of the original parameters for the modified pressure drop correlation for 72 μm natural size powder

D_p(mm)	Richardson & Zaki		Revised Ergun	Ergun	Ishii & Zuber (ε_{dm} = 0.62)
	n	U_t (mm/s)	Exponent (m)	Factor (x)	Exponent (k)
89	4.05	0.420	4.8	150	2.5
72	4.23	0.297	4.8	150	2.5
46	4.49	0.143	4.8	150	2.5
37(Batch 1)	4.58	0.094	4.8	150	2.5

Table 6.4 Summary of the modified parameters for the modified pressure drop correlation for 72 μm natural size powder

D_p(mm)	Richardson & Zaki		Revised Ergun	Ergun	Ishii & Zuber (ε_{dm} = 0.60)
	n	U_t (mm/s)	Exponent (m)	Factor (x)	Exponent (k)
89	4.82	0.420	5.23	200	1.60
72	4.98	0.297	5.30	200	1.90
46	5.42	0.143	5.42	200	2.10
37(Batch 1)	5.05	0.094	5.15	150	2.10

6.7 ε_0 vs U_0 and ε_d vs U_0 characteristic curves of bimodal powders

Figure 6.24 and Figure 6.26 show ε_d and U_0 characteristic curves bimodal mixtures of 90-75/45-0 μm and 106-90/53-45 μm, respectively. As before, ε_d increases with increasing U_0, until a maximum value where U_d is the minimum bubbling velocity and ε_d is the minimum bubbling voidage. After this, the gradual contraction of ε_d was observed. At higher velocities, ε_d continues to reduce and reaches the constant value at U_0 around 3 to 5 times U_{mb}.

Figure 6.25 and Figure 6.27 show ε_0 and U_0 characteristic curves bimodal mixtures of 90-75/45-0 μm and 106-90/53-45 μm, respectively. ε_0 increases with U_0 and is equal to ε_d, when U_d is less than the minimum bubbling velocity. After the minimum bubbling point, ε_0 is higher than ε_d and gradually decreases with U_0. Until U_0 is proximately 2.5 times U_{mb}, ε_0 increases with U_0 or remains almost constant.

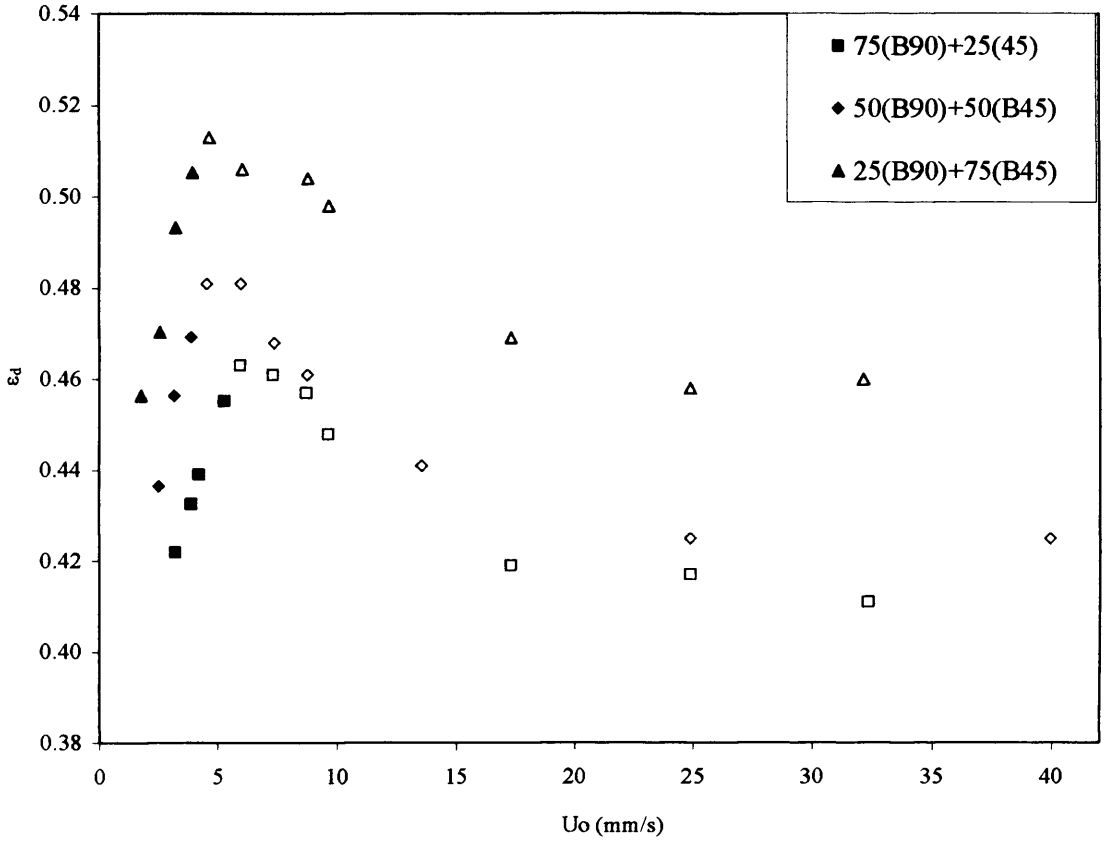

Figure 6.24 ε_d and U_0 characteristic curves for bimodal mixture of 90-75μm/45-0μm

[Full symbol = $U_0 < U_{mb}$ and empty symbol = $U_0 > U_{mb}$]

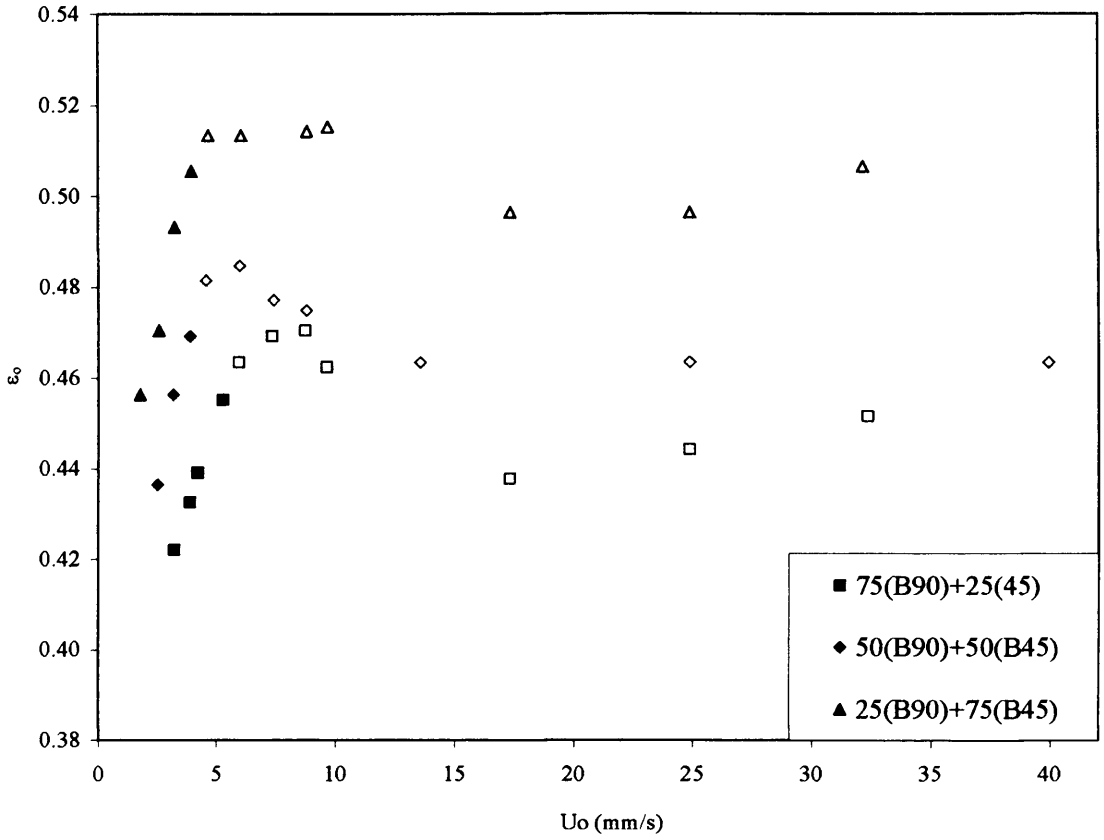

Figure 6.25 ε_0 and U_0 characteristic curves for bimodal mixture of 90-75μm/45-0μm

[Full symbol = $U_0 < U_{mb}$ and empty symbol = $U_0 > U_{mb}$]

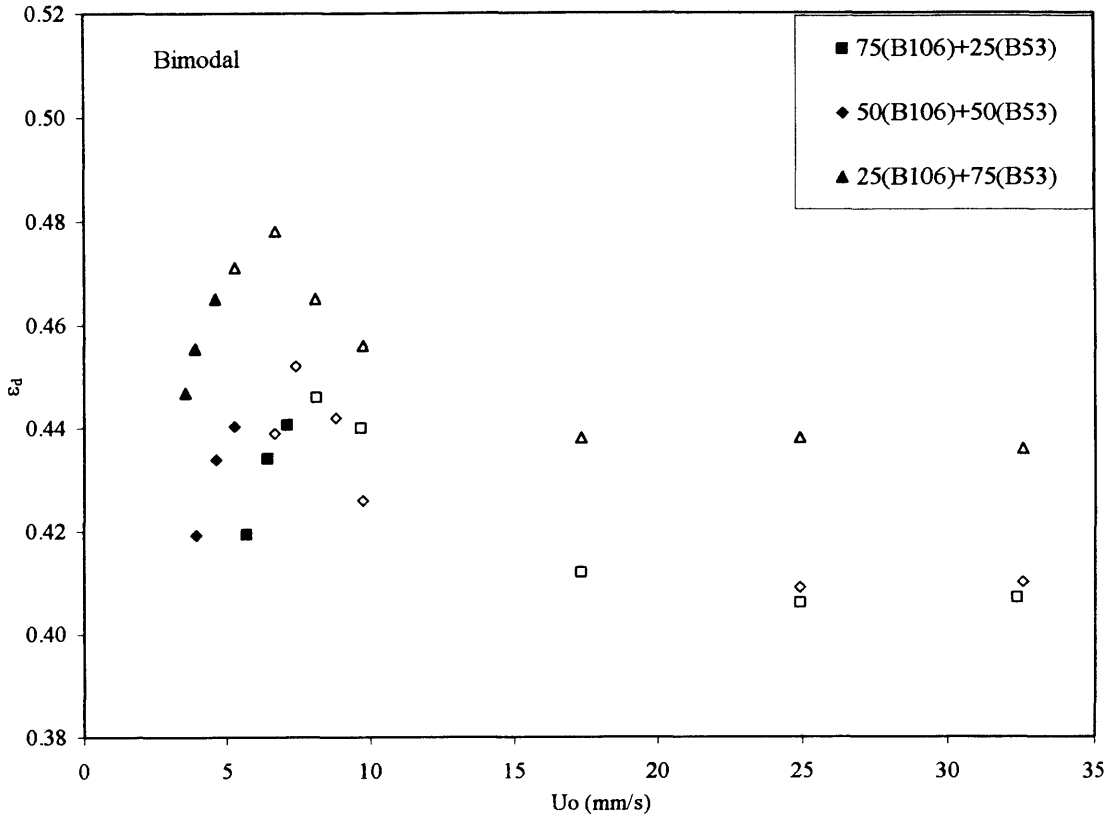

Figure 6.26 ε_d and U_0 characteristic curves for bimodal mixture of 106-90μm/53-45μm

[Full symbol = $U_0 < U_{mb}$ and empty symbol = $U_0 > U_{mb}$]

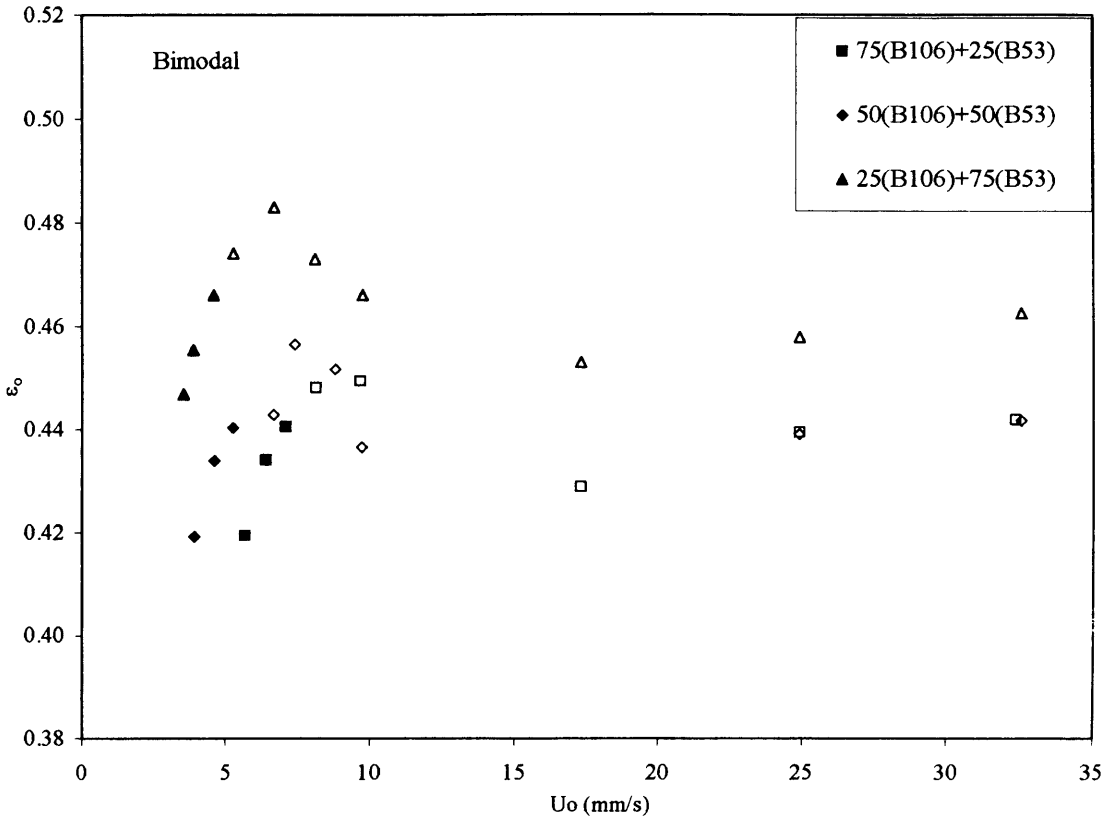

Figure 6.27 ε_0 and U_0 characteristic curves for bimodal mixture of 106-90μm/53-45μm

[Full symbol = $U_0 < U_{mb}$ and empty symbol = $U_0 > U_{mb}$]

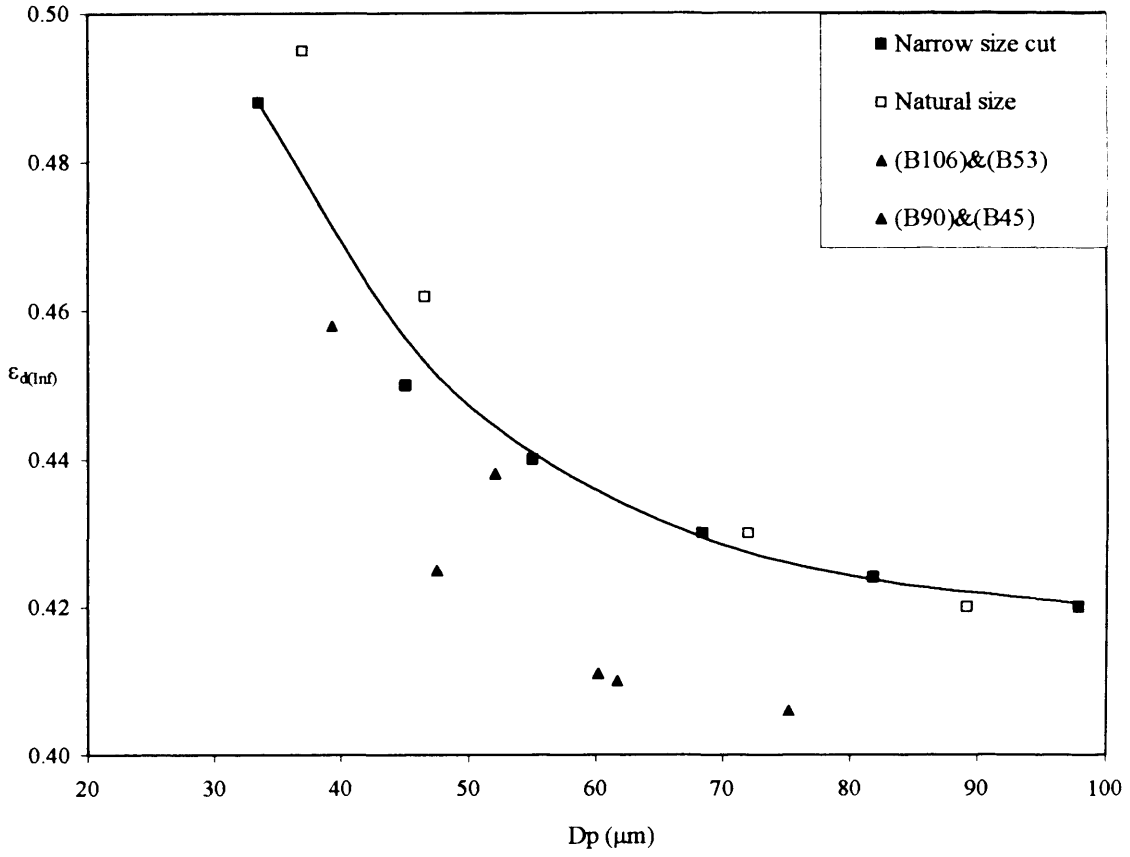

Figure 6.28Limiting ε_d versus d_p relation for narrow size cut powders, natural size and bimodal powders

The limiting dense phase voidage ($\varepsilon_{d(inf)}$) of the bimodal mixture of 90-75μm/45-0μm and 106-90μm/53-45μm were plotted in Figure 6.28 in comparison with the narrow size cut powders and the natural size distribution powders. The limiting dense phase voidage decreases with an increase of the average diameters for both bimodal mixtures. The limiting dense phase voidage of both bimodal mixtures are lower than those of the narrow size cut powder and the natural size distribution powder. $\varepsilon_{d(inf)}$ for the bimodal mixture can not be predicted using the empirical correlation obtained for the narrow size cut powders. In the case of the bimodal mixture, the fines do not seem to increase $\varepsilon_{d(Inf)}$

as reported by Geldart and Abrahamsen (1978), Rowe et al. (1978), Dry et al. (1983) and Yadav et al. (1994).

6.8 ε_d and U_d characteristic curves of bimodal powders

Figure 6.29 and Figure 6.30 show the ε_d and U_d characteristic curve of the bimodal mixture of 90-75μm/45-0μm and 106-90μm/53-45μm, respectively. For all powders, the ε_d and U_d relationships before and after the minimum bubbling point line on the same linear trend.

Figure 6.29 and Figure 6.30, U_d increases with increased average diameter. At the maximum expansion, $U_{d(max)}$ increases with particle size and $\varepsilon_{d(max)}$ decreases with the particle size.

The modified revised Ergun equation (eq. 6.4) was used to describe the expansion characteristic of the bimodal mixture as shown in Figure 6.31 and Figure 6.32. For the bimodal mixture of 90-75 μm/45-0 μm (Figure 6.31), the equation can describe fairly well the ε_d and U_d characteristic for all compositions. For the bimodal mixture of 106-90 μm/53-45μm (Figure 6.32), the modified revised Ergun equation gives slightly lower ε_d and U_d characteristic curve when the surface to volume average diameter is used. However, within the 5-10% experimental error of the average diameter, the equation can give a good prediction of the characteristic curves. It can be concluded that the modified revised Ergun equation is predictive for the system of bimodal mixture.

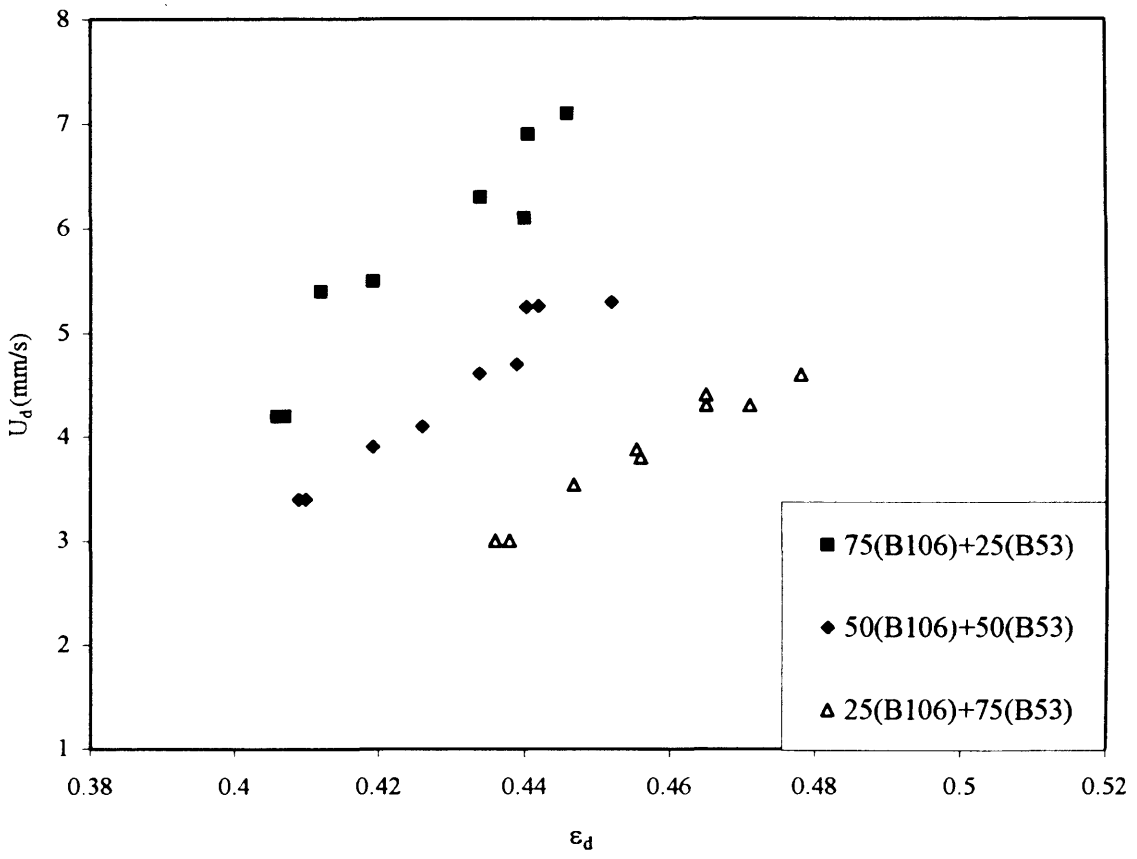

Figure 6.29 ε_d and U_d Characteristic curves for bimodal powder 106 –90 μm and 53-45 μm

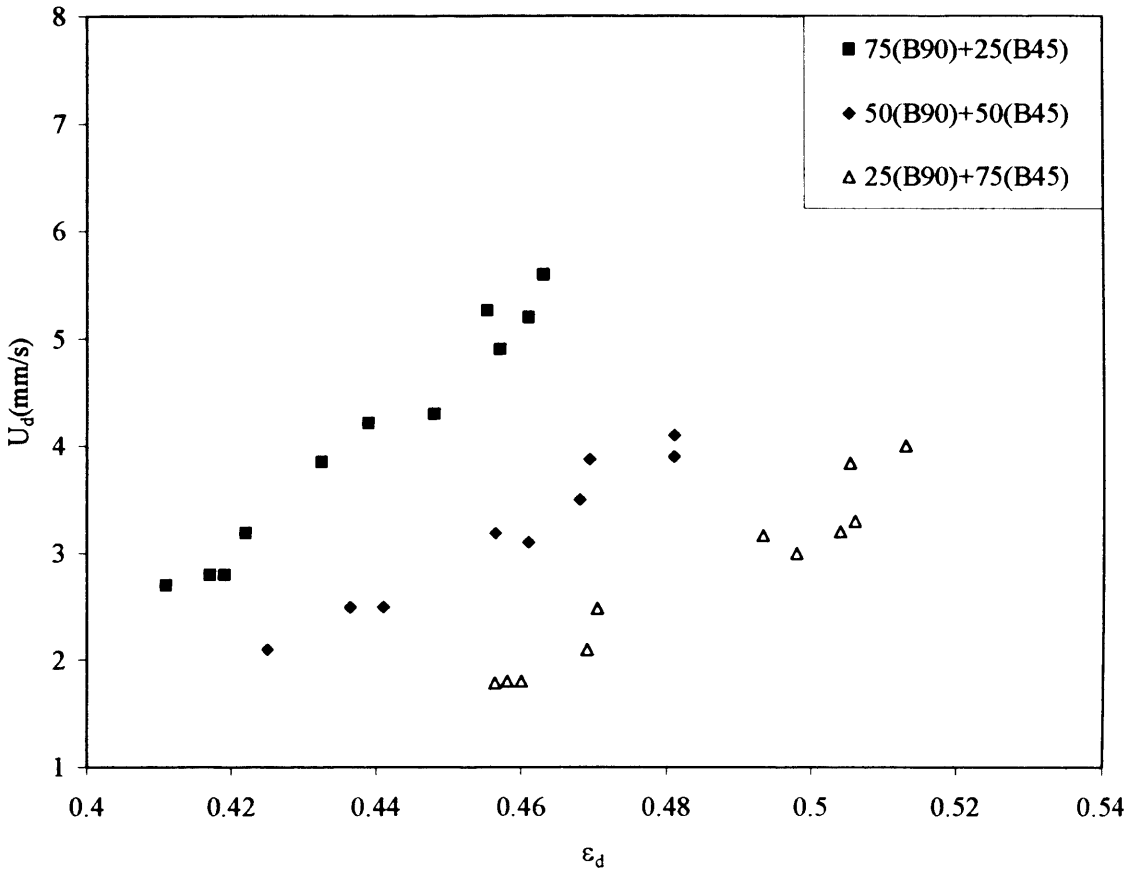

Figure 6.30 ε_d and U_d Characteristic curves for bimodal powder 90–75 μm and 45-0μm

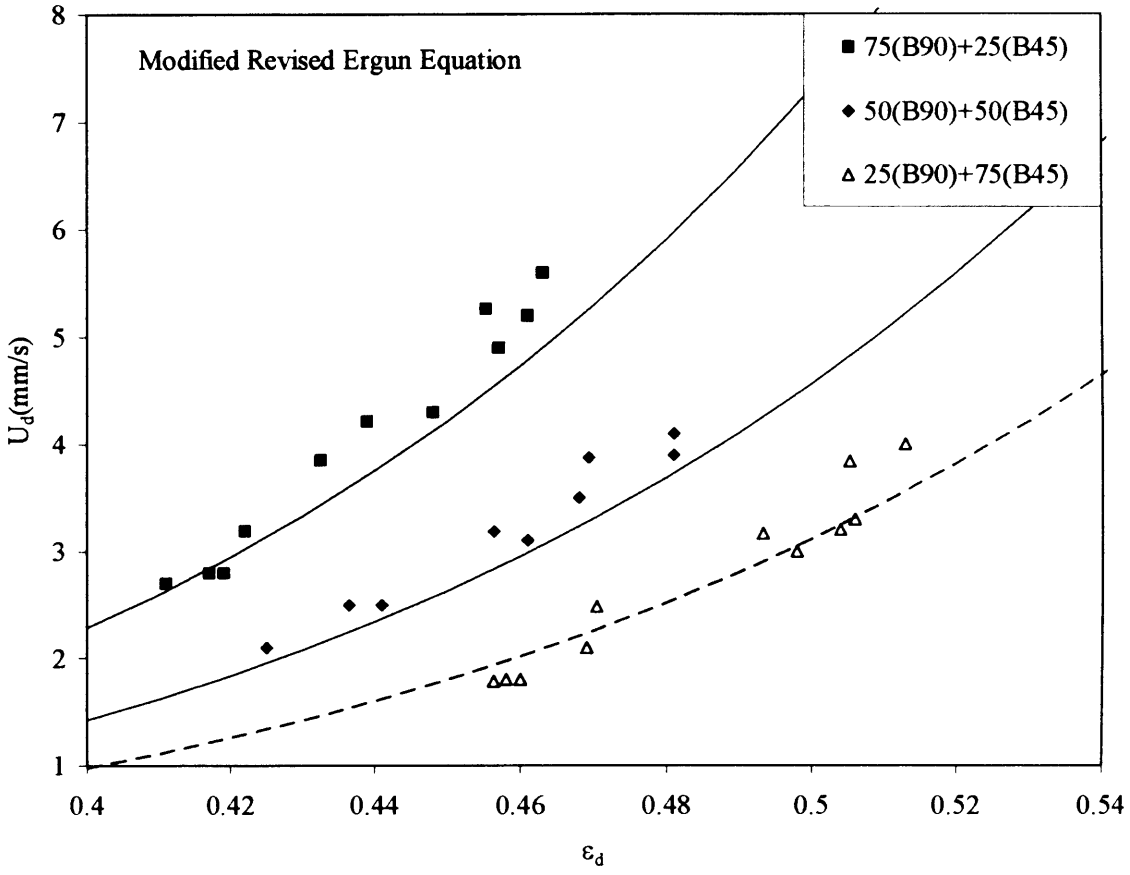

Figure 6.31 Modified Revised Ergun equation on describing ε_d and U_d characteristic curve of bimodal mixture of ballotini (90-75μm) and (45-0 μm)

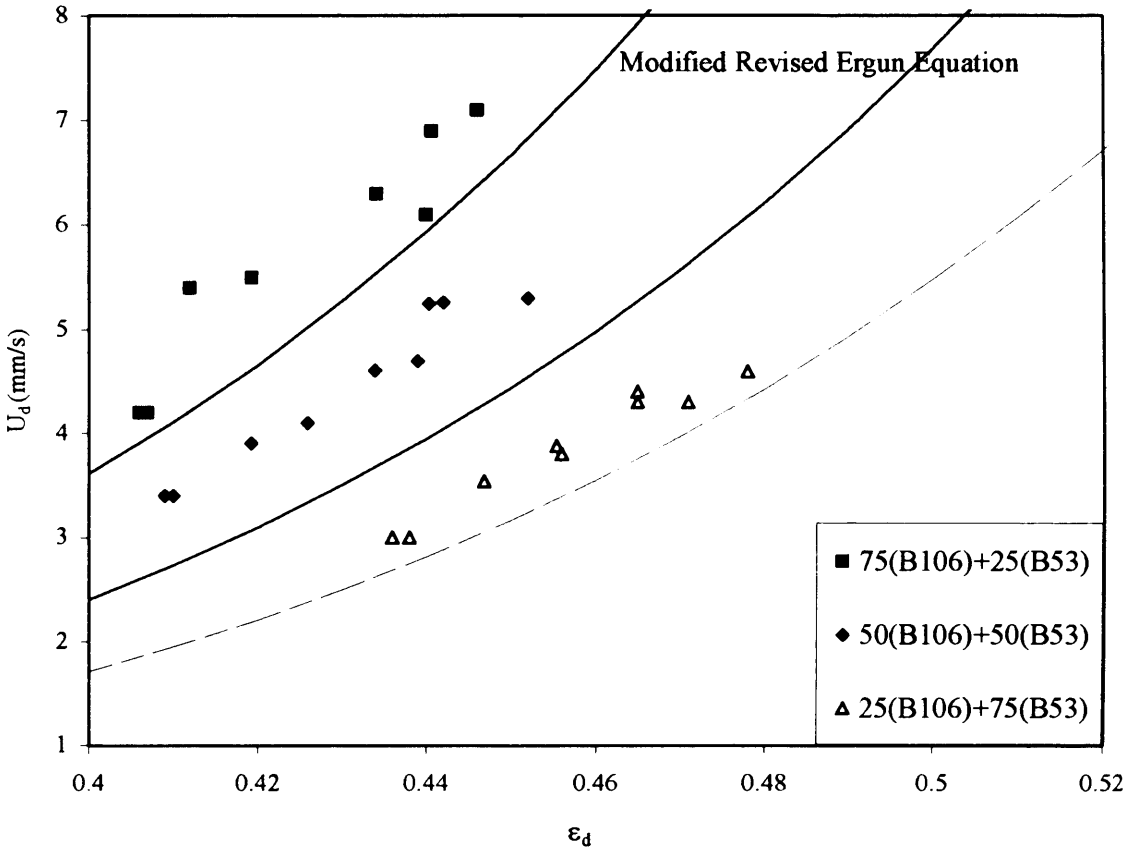

Figure 6.32 Modified Revised Ergun equation on describing ε_d and U_d characteristic curve of bimodal mixture of ballotini (106-90μm) and (53-45 μm)

6.9 Summary

The influences of the column diameter, the initial bed height and the distributor flow resistance on U_d and ε_d characteristics and ε_d and ε_0 versus U_0 characteristics were studied. It was found that the U_d and ε_d characteristic curve was independent of the column diameter, initial bed height and distributor flow resistance. For the relationship between ε_d and ε_0 with U_0, it was found that ε_d and ε_0 were independent with the initial bed height for all U_0. However, ε_d and ε_0 were independent of the column diameter for

the homogeneous expanded bed, but for bubbling beds at higher velocity ε_d and ε_0 are higher for the larger column. With regard to the distributor gas flow resistance; the coarse distributor caused a lower bed expansion at low U_0 and premature bubbling. However, at higher U_0 ($\approx$2.5 U_{mb}), ε_d and ε_0 are the same for both fine and coarse distributor.

The bed expansion characteristic of the natural size, narrow size and bimodal mixture were studied. For all powders, ε_d increases with U_0 until the maximum point where the bubble starts. After that, ε_d contracted gradually and reached a constant value at approximately 2.5-5 U_{mb}.

The bed voidage ε_0, coincides with ε_d for inlet velocities below the minimum bubbling point. After the minimum bubling point, ε_0 continued to increase slightly with U_0 and then gradually decreases. When U_0 is approximately 1.75 to 3.5 times U_{mb}, ε_0 increases slowly with U_0 or remains almost constant.

The limiting dense phase voidage, $\varepsilon_{d(Inf)}$, decreases with increase in particle size and varies as an exponential function with the particle size for the narrow size cut powders. The empirical correlation of $\varepsilon_{d(inf)}$ and d_p for the narrow size cut can be used to estimate $\varepsilon_{d(inf)}$ of the natural size distribution powder, when there are no fines in the mixture. For the natural size distribution powder with fines, $\varepsilon_{d(inf)}$ was higher compared to those of the narrow size powders. However, for the bimodal mixtures, $\varepsilon_{d(inf)}$ is lower than those of the narrow size cut powders and natural size distribution powders, whether or not the mixtures contain fines.

ε_d and U_d characteristic curves of the bubbling bed are the same as those of the homogeneous bed for all powders. This means that the dense phase behaviour can be determined from experiments on the homogeneous expanded beds.

The literature drag force correlations were not able to predict the ε_d and U_d characteristic curve for the narrow size cut and the natural size distribution powders. Suitable empirical modifications have been made to allow the correlation of the experimental results obtained in this study.

The modified Revised Ergun equation and the modified Richardson and Zaki expansion coefficient were found to describe well the ε_d and U_d characteristic curve. Based on the average m value of the narrow size, the modified revised Ergun equation for the viscous regime was used to describe the narrow size cut and the natural size distribution powders. This was then shown to describe the ε_d and U_d characteristic curve of the bimodal powders with sufficient accuracy. In the next Chapter these results will be used in the new stability criterion developed by Brandani and Zhang (2004) to describe the prediction of the minimum bubbling point of the powders investigated in this study.

Chapter 7: Minimum Bubbling Point

7.1 Introduction

The onset of the minimum bubbling point coincides with the point where the homogenous expanded bed becomes unstable and the first bubble is formed in the fluidised bed. The onset of bubbling can be measured in different ways: by visual observation of the bed surface, where inlet superficial velocity and the bed voidage, at which the first bubble appears, are noted; differential pressure drop profile along the column; the fluctuation of the pressure signal; the ε_d and U_d characteristic curve.

Visual observation of the first bubble has the disadvantage that it is not very accurate, since one is not able to distinguish premature bubbling from the actual minimum bubbling point.

The local minimum in the differential pressure drop profile indicates where the dense phase voidage is maximum. Once the bubbling commences the dense phase contracts. Figure 7.1 shows the differential pressure drop profile of the 37 μm (Batch 1) powder. The local minimum is reached at different velocities for pressure drops at different heights. The range of the velocities where the pressure reaches the minimum point gives

the possible range of the minimum bubbling point. To be able to pinpoint the exact value of the minimum bubbling point, the maximum dense phase voidage should be used and that should be the average value over the entire bed height.

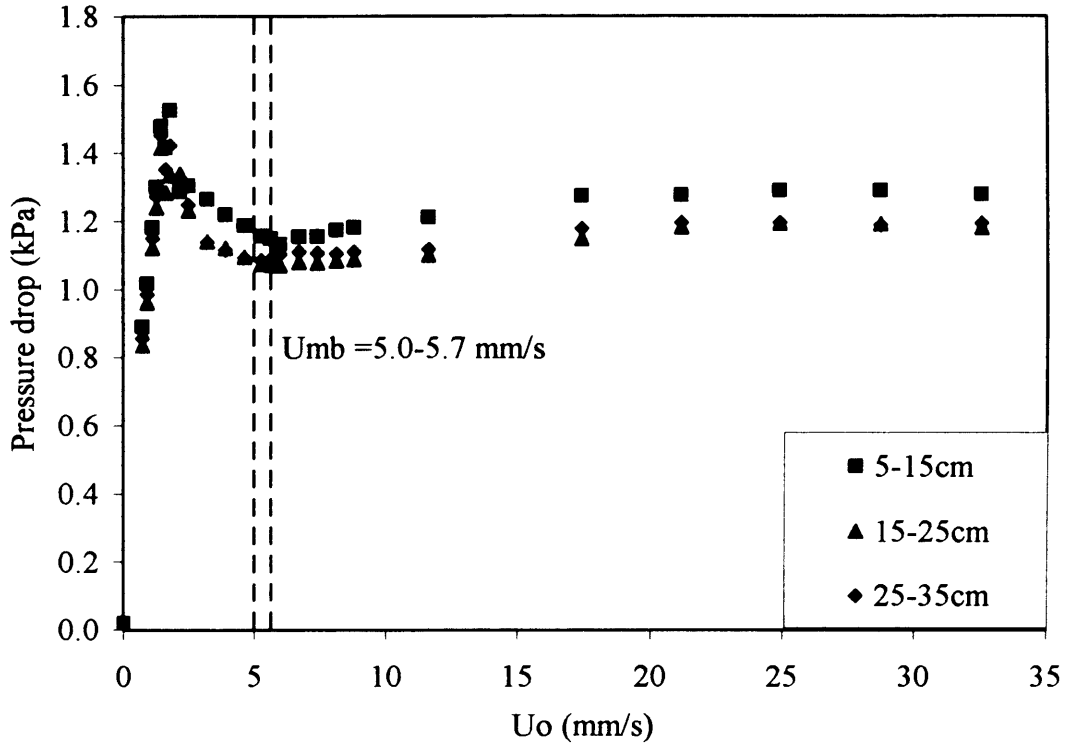

Figure 7.1 Differential pressure drop profile along column height (d_P = 37 μm (Batch1), ID = 0.127 m, L_I = 0.43 m)

The fluctuation of the pressure signal measured along the bed height will give an indication of bubbles moving through the bed. Figure 7.2 shows the signal of the differential pressure fluctuation. In this case, it is easy to detect large individual bubbles but it is more difficult to pinpoint the onset of bubbling, where small bubbles begin to form.

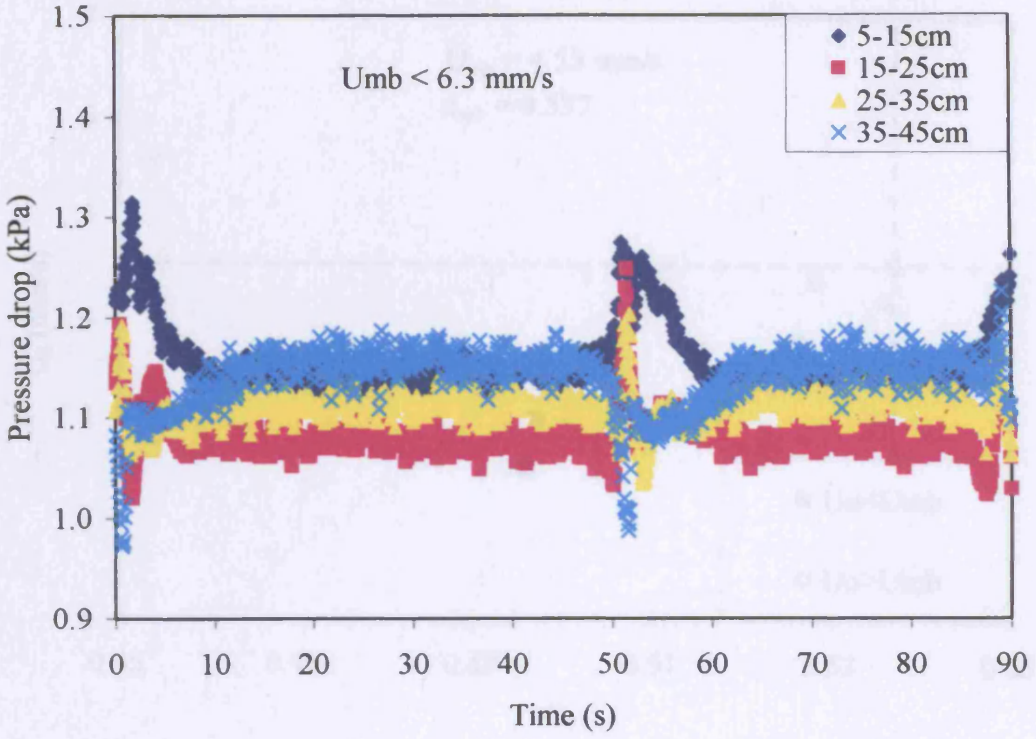

Figure 7.2 Differential pressure drop fluctuation along column height (d_P = 37 μm (Original powder, Batch 1), ID = 0.127 m, L_I = 0.43 m)

From the ε_d and U_d characteristic curve, the minimum bubbling point can be identified from the maximum point of ε_d and U_d, as shown in Figure 7.3. The values of ε_d and U_d are obtained using the bed collapse experiment, and the bed collapse model for the data interpretation. By this approach, the minimum bubbling point can be determined accurately. This method is used in this study to identify the onset of the minimum bubbling point.

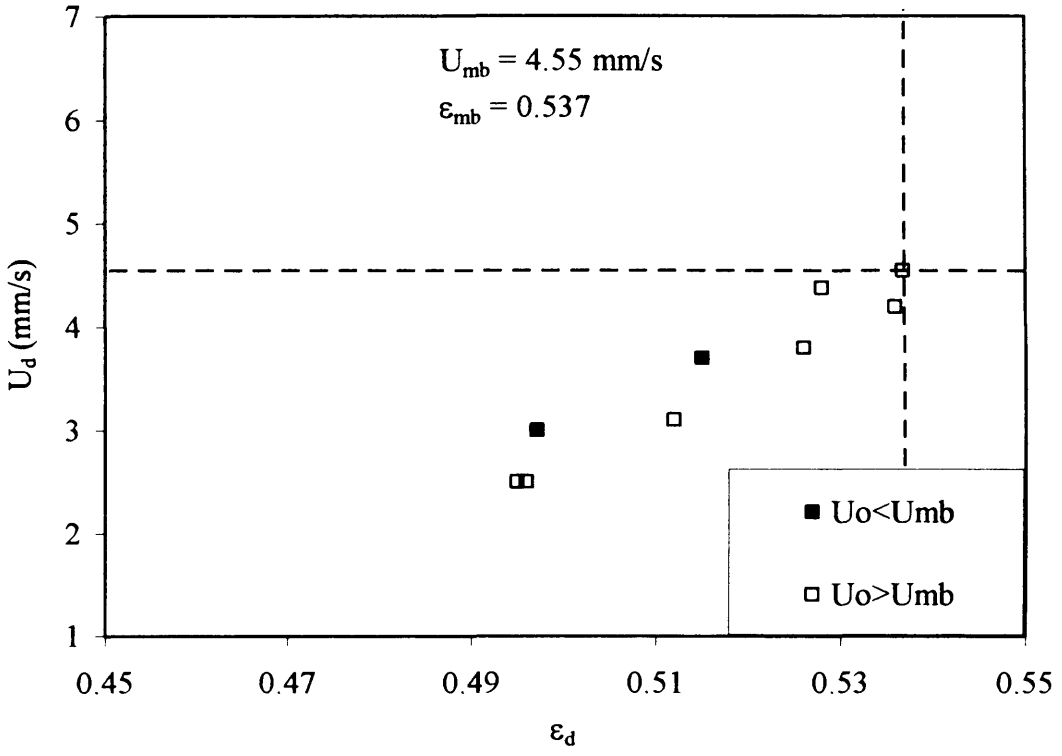

Figure 7.3 ε_d and U_d characteristic curve (d_P = 37 μm (Batch 1), ID = 0.127 m, L_I = 0.43 m)

It should be noted that by comparing U_d obtained from the bed collapse experiments starting from an initially homogeneous expanded bed with the inlet velocity U_0 the accuracy of the method can be checked. Figure 7.4 shows U_d in comparison with U_0 when the bed is a homogeneous expanded bed. There is approximately less than 3% error on the flow measurement.

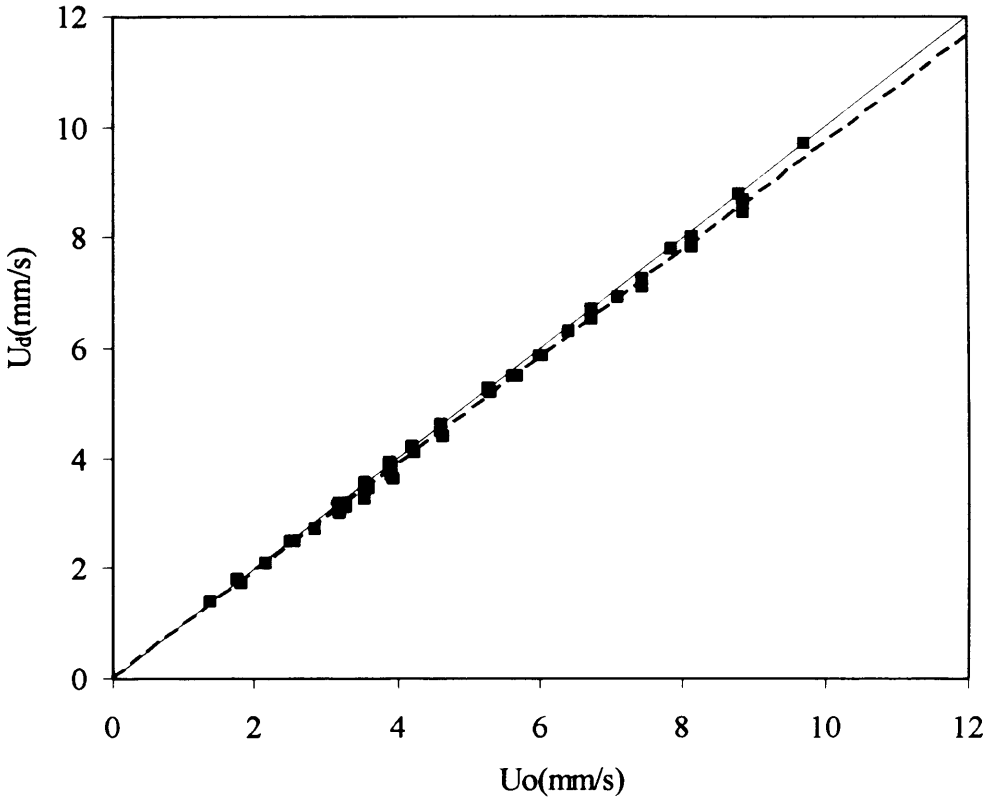

Figure 7.4 Comparison of U_d of homogenous expanded bed and U_0

Therefore the ε_d and U_d plot will yield values of ε_{mb} comparable to the other methods, but should yield improved accuracy for the determination of U_{mb}.

Since the minimum bubbling point is a point of instability to differential perturbation, it is easy to have premature bubbling. This can be seen from the differential pressure drop profile, where the local minimum of the pressure can be reached at different velocities the pressure readings at different heights. The error of U_0 together with premature bubbling can cause the difference between U_d and U_0 to reach approximately 7% as shown in Figure 7.5.

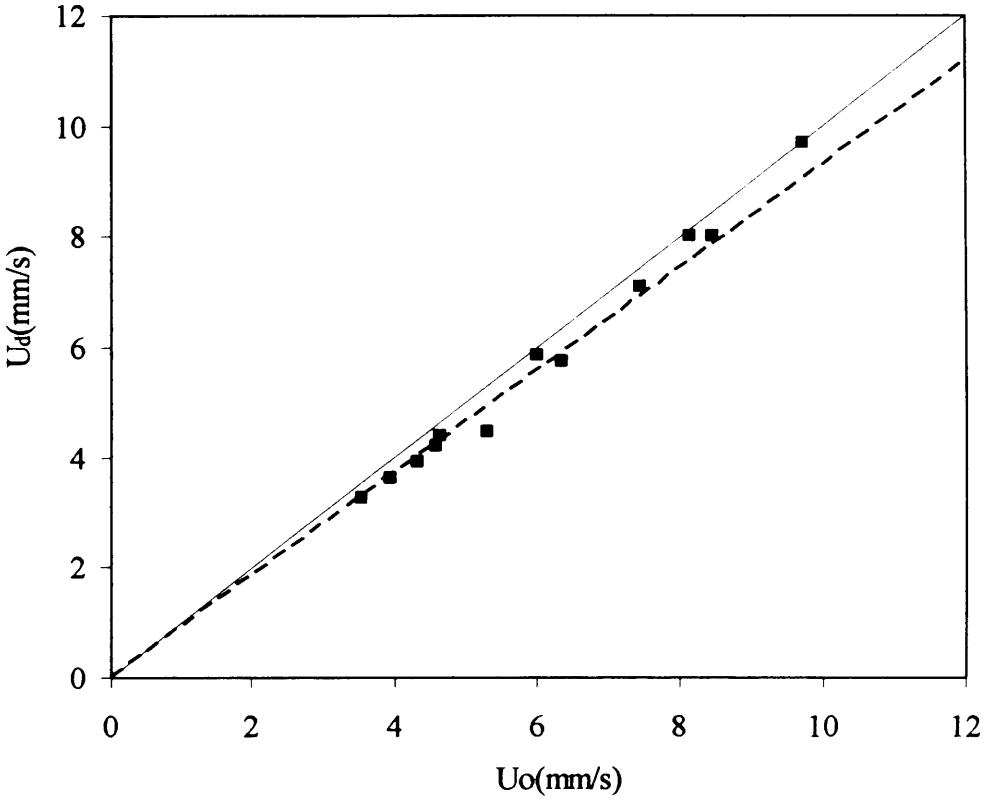

Figure 7.5 Comparison of U_d and U_0 if premature bubbling occurs.

7.2 Influence of column diameter and initial bed height on the onset of bubbling

For the 72 μm powder, the minimum bubbling voidage and the minimum bubbling velocity is approximately independent of the column diameter and the initial bed height. For the 37 μm (batch 1) powder, the range of minimum bubbling voidages is approximately 5% and that of the minimum bubbling velocity is approximately 12 %. This shows that the presence of fines can induce agglomeration and slightly cohesive behaviour which can lead to an increased uncertainty in the measurement of the minimum bubbling point.

Table 7.1 Summary of minimum bubbling points of powders

d_P (μm)	ID (m)	L_I (m)	W_P (kg)	ΔP_{Bed} (kPa)	H/D	ε_{mb}	U_{mb} (mm/s)
37(B1)	0.127	0.40	7.7971	5.93	3.37	0.537	4.55
		0.30	5.4022	4.11	2.38	0.529	4.68
	0.243	0.40	28.4350	6.00	1.79	0.559	5.20
		0.30	19.3876	4.09	1.24	0.555	5.00
72	0.127	0.40	7.7971	5.93	3.34	0.476	7.2
		0.30	5.4022	4.11	2.34	0.476	7.3
	0.243	0.30	19.3876	4.09	1.23	0.477	7.2
37(B2)	0.127	0.40	7.7971	5.93	3.38	0.539	5.1
		0.30	5.4022	4.11	2.40	0.530	5.60

7.3 Influence of distributor porosity on onset of bubbling.

As shown in Figure 6.11, the coarse distributor tends to cause premature bubbling in the fluidized bed and a smaller bed expansion. When the coarse distributor is used, there is no clear transition for the minimum bubbling. In this study, the fine distributor was used, because it leads to more accurate determination of the minimum bubbling point.

7.4 Onset of minimum bubbling stage of narrow size and natural size powders

From Figure 7.6, the minimum bubbling velocity increases with the average diameter for both narrow size cut and natural size distribution powders. This observation is in agreement with Simone and Harriott (1980) who carried out experiments on fine FCC catalysts of narrow size cut and natural size distribution powders. The minimum bubbling velocity (Figure 7.6) varies as a quadratic function with the average diameter. U_{mb} of the natural size distribution powder lines on the same trend as that for the narrow size cut, when the mixture has no fines. U_{mb} is higher when mixture contains fines. Similar results have been observed by Abrahamsen and Geldart (1978) and Simone and Harriott (1980). Abrahamsen and Geldart (1978) indicated that the presence of fines tends to increase the bed expansion and, hence, the minimum bubbling velocity. Simone and Harriott (1980) reported that the minimum bubbling point of the size distribution powder and the narrow size cut powder is the same for the powder of the same average size.

From Figure 7.7, ε_{mb} decreases with the increase of the average particle diameter and it varies as quadratic function of the average diameter for narrow size cut powder and natural size powder. ε_{mb} is higher for the natural size distribution powder whether or not the mixture contains fines. However, for the mixture containing no fines, ε_{mb} is closer to the trend line of the narrow size cut powder.

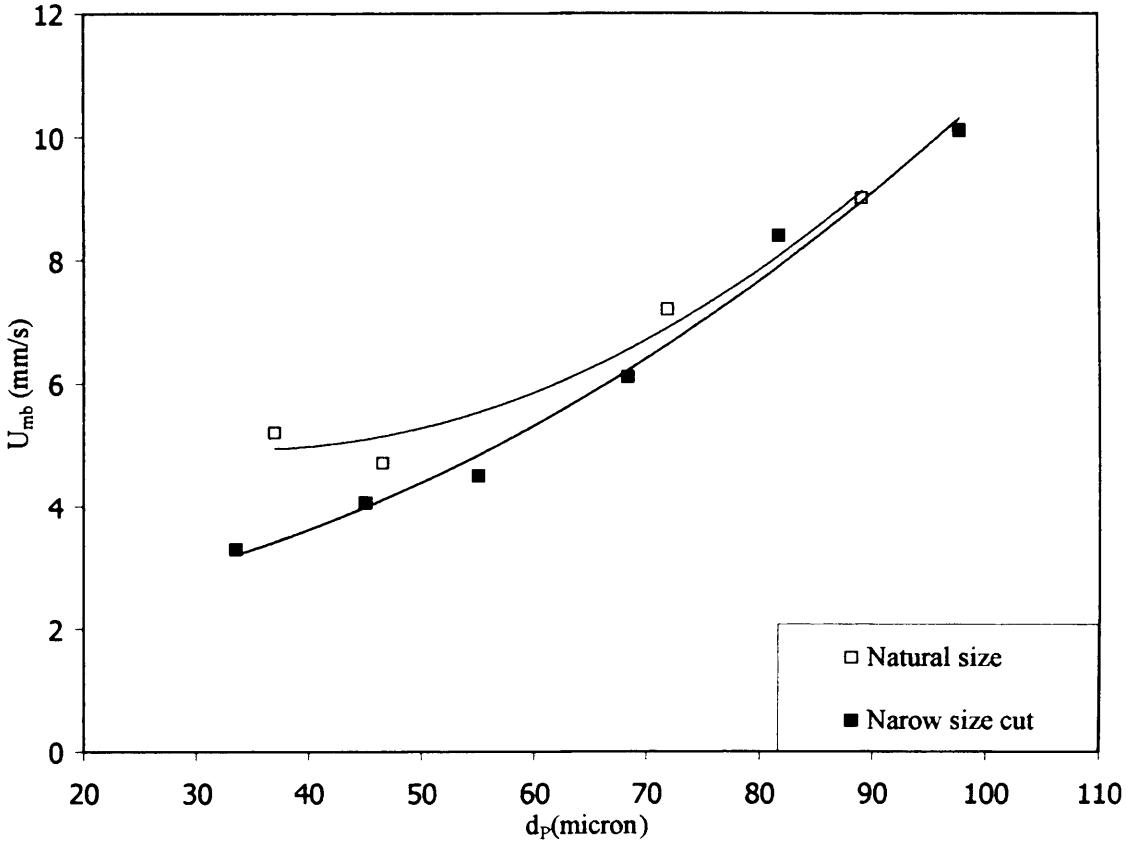

Figure 7.6 Minimum bubbling velocity for narrow size cut powders and natural size powders

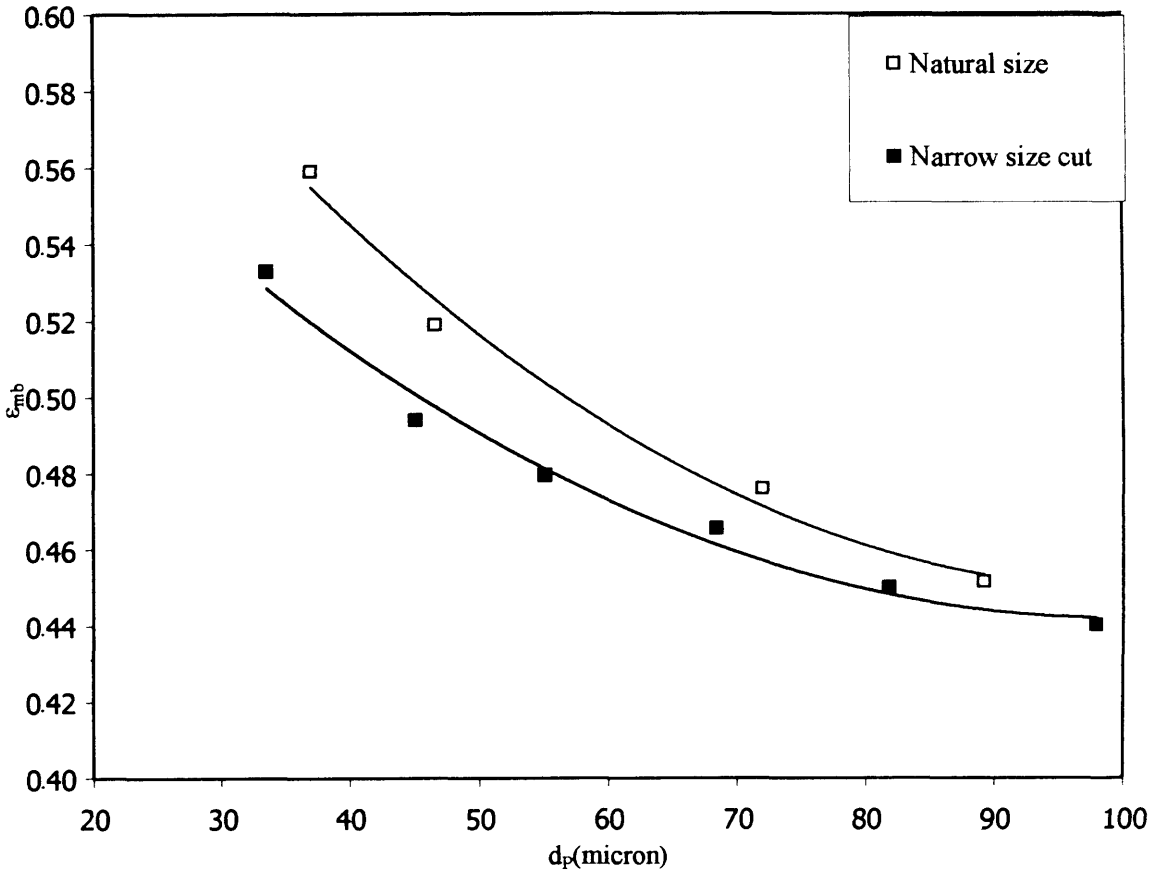

Figure 7.7 Minimum bubbling voidage narrow size cut powders and natural size powders.

7.5 Onset of bubbling for bimodal powders

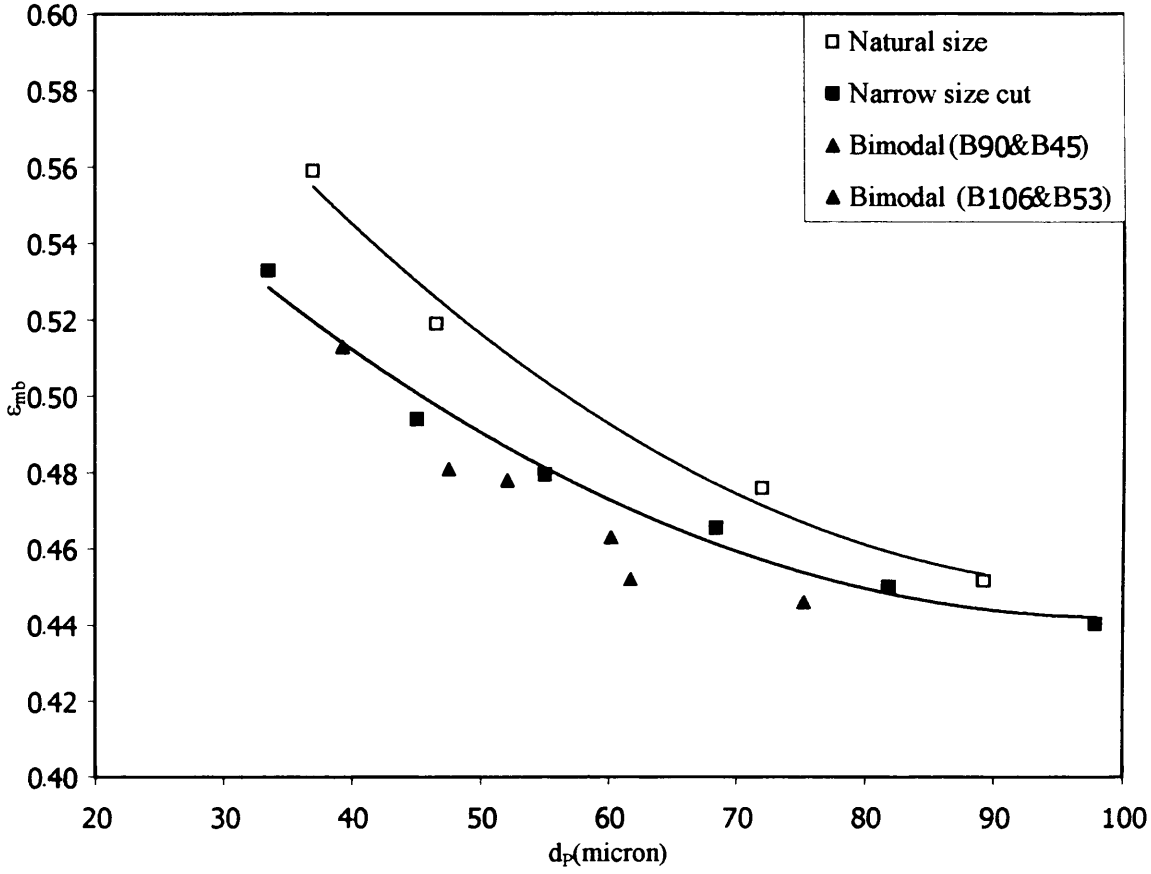

Figure 7.8 Minimum bubbling voidage narrow size cut powders, natural size and bimodal powders.

From Figure 7.8, ε_{mb} of both bimodal mixtures are slightly lower than those for the narrow size cut powder, but follow the same trend. In comparison with the natural size powders, ε_{mb} of the bimodal mixtures are lower than those of the natural size powders. This again shows that fines do not increase ε_{mb} for the bimodal mixture, as in the case of the natural size distribution powders.

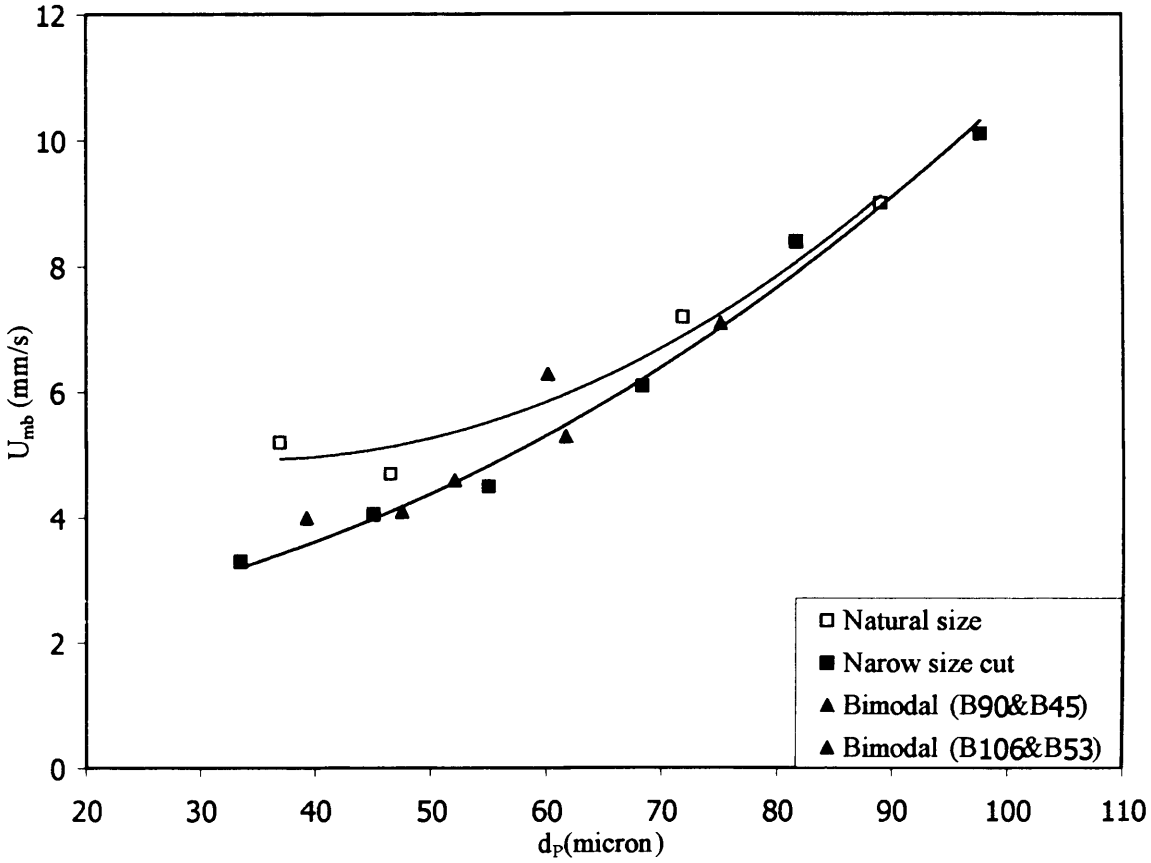

Figure 7.9 Minimum bubbling velocity for narrow size cut powders, natural size and bimodal powders

From Figure 7.9, U_{mb} of the bimodal powders are in good agreement with the trend of the narrow size cut powders, whether or not the mixture contains fines. For the bimodal mixture, the fines do not increase ε_{mb} and U_{mb} in comparison with the narrow size cut powders. The empirical correlation of the narrow size cut powder can be used to predict the onset of the minimum bubbling stage of the bimodal powders.

7.6 Prediction of the minimum bubbling point

The minimum bubbling point can be predicted theoretically using the stability criteria, mentioned in Chapter 2. In this work, the stability criterion developed by Brandani and Zhang, (2004) was used. The experimental minimum bubbling points of narrow size powders were used as a standard to investigate the predictive capability of the model.

The calculation procedures of the minimum bubbling point, when the stability criterion developed by Brandani and Zhang, (2004) is used, are as follows;

Step 1: The physical parameters are set: ρ_F; ρ_P; d_P; μ_F.

Step 2: Characteristic length (δ) is implemented in the dynamic wave velocity (U_D)

Step 3: The drag force correlation is used to calculate the continuity wave velocity (U_ε)

Step 4: An initial guess value for ε_{mb} is set.

Step 5: The appropriate drag force correlation and $U_D = U_\varepsilon$ are solved simultaneously for U_{mb} and ε_{mb}, by the iteration of ε_{mb} initial guessed value.

7.6.1 Stability criterion description

As discussed in Chapter 2, the model is based on the definition of a characteristic length δ, which should be of the order of the particle diameter (value used by Brandani and Zhang, 2004). In principle δ can be a function of the void fraction. Having established an accurate drag force correlation, for the powders used in this study. From the results obtained in the previous Chapter, δ can also be determined from the experimental minimum bubbling points. In this case the minimum bubbling criterion has to be modified to include the drag force correlation:

$$F_D = \frac{3}{4}\frac{\rho_F}{d_P} C_D U^2 (1-\varepsilon)\varepsilon^{-\beta} \qquad (7.1)$$

$$\beta = 4.21$$

Using the Dallavalle (1948) equation for the drag coefficient.

$$C_D = \left(0.63 + \frac{4.8}{\sqrt{Re_p}}\right)^2 \qquad (7.2)$$

The criterion of minimum bubbling becomes

$$U_\varepsilon = (1-\varepsilon)\left(\frac{\partial U}{\partial \varepsilon}\right)_{Equil} = \frac{1-\varepsilon}{\varepsilon}\cdot\frac{(\beta+1)U}{2+\frac{dC_D}{dRe}\frac{Re}{C_D}} \qquad (7.3)$$

and the dynamic wave velocity (Gibilaro, 2001)

$$U_D = \sqrt{V^2 - G} + V \qquad (7.4)$$

where, under the quasi-equilibrium approximation,

$$V = \frac{1-\varepsilon}{\varepsilon}\frac{\rho_F U}{\varepsilon\rho_P + (1-\varepsilon)\rho_F} \qquad (7.5)$$

$$G = \frac{\frac{1-\varepsilon}{\varepsilon^2}\rho_F U^2 - \delta[(1-\varepsilon)\rho_p + \varepsilon\rho_F]g}{\varepsilon\rho_p + (1-\varepsilon)\rho_F} \qquad (7.6)$$

7.6.2 Characteristic length (δ)

Brandani and Zhang (2004) used their model to predict over 110 literature minimum bubbling data points. The drag force correlation used was; (Gibibilaro, 2001)]

$$F_D = \frac{3}{4}\frac{\rho_F}{d_P} C_D U^2 (1-\varepsilon)\varepsilon^{-\beta} \qquad (7.7)$$

$$\beta = 3.8$$

and they assumed $\delta/d_P = 1$. With this choice of parameters, the predictions tend to deviate when the voidage is less than 0.45. For our experimental results, the model was applied to predict the minimum bubbling points of the narrow size cut powders. The characteristic length was chosen as $\delta/d_P = 1$ and the modified drag force correlation was used.

Figure 7.10 shows the predicted ε_{mb} in comparison with the experimental ε_{mb}. When $\delta/d_P = 1$, it was found that the model tends to underestimate ε_{mb} when the value of the voidage is less than approximately 0.5. This confirms the result found by Brandani and Zhang (2004), mentioned above.

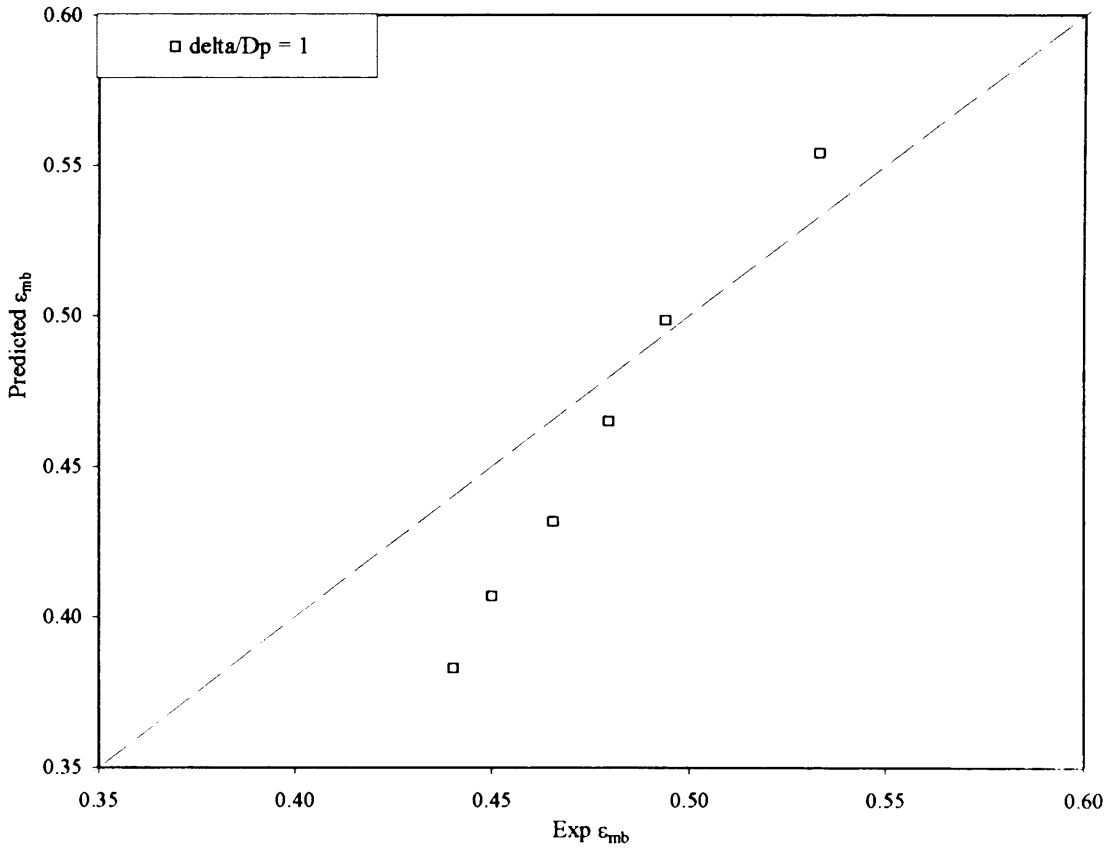

Figure 7.10 Comparison between predicted ε_{mb} and experimental ε_{mb}, when $\delta/d_P = 1$

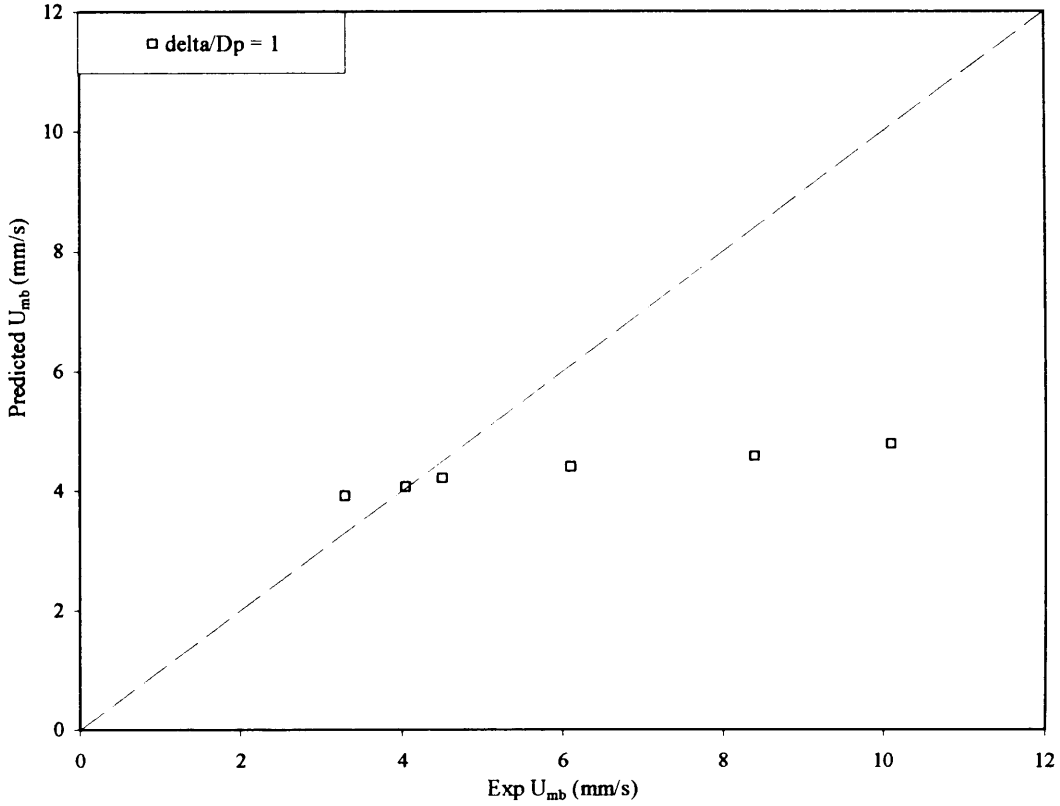

Figure 7.11 Comparison between predicted U_{mb} and experimental U_{mb}, when $\delta/d_P = 1$

Figure 7.11 shows the predicted U_{mb} in comparison with the experimental U_{mb}. When $\delta/d_P = 1$, the error in the predicted U_{mb} is due to the incorrect value of ε_{mb} clearly poor. From the comparison above, it is clear that the choice of a constant $\delta/d_P = 1$ is questionable. From the experimental results on the narrow size cut powders it is possible to establish the voidage dependency of δ. From the model derivation, the lower limit of δ/d_P should be approximately 0.5 since at high voidages the characteristic dimension should tend to the particle radius. For dense particle suspensions, the ratio should increase.

Figure 7.12 shows the values of δ/d_P as a function of bed voidage calculated using the original drag force correlation and modified drag force correlation. An exponential

dependency with $\varepsilon - \varepsilon_{mf}$ is observed. The empirical correlation given by eq. 7.8 is obtained when the modified drag force correlation was used, while eq. 7.9 is obtained when the original drag force correlation is used.

$$\frac{\delta}{d_p} = 0.65 + 3.82[e^{-37.7(\varepsilon-\varepsilon_{mf})}] \qquad (7.8)$$

$$\frac{\delta}{d_p} = 1.00 + 8.8[e^{-42(\varepsilon-\varepsilon_{mf})}] \qquad (7.9)$$

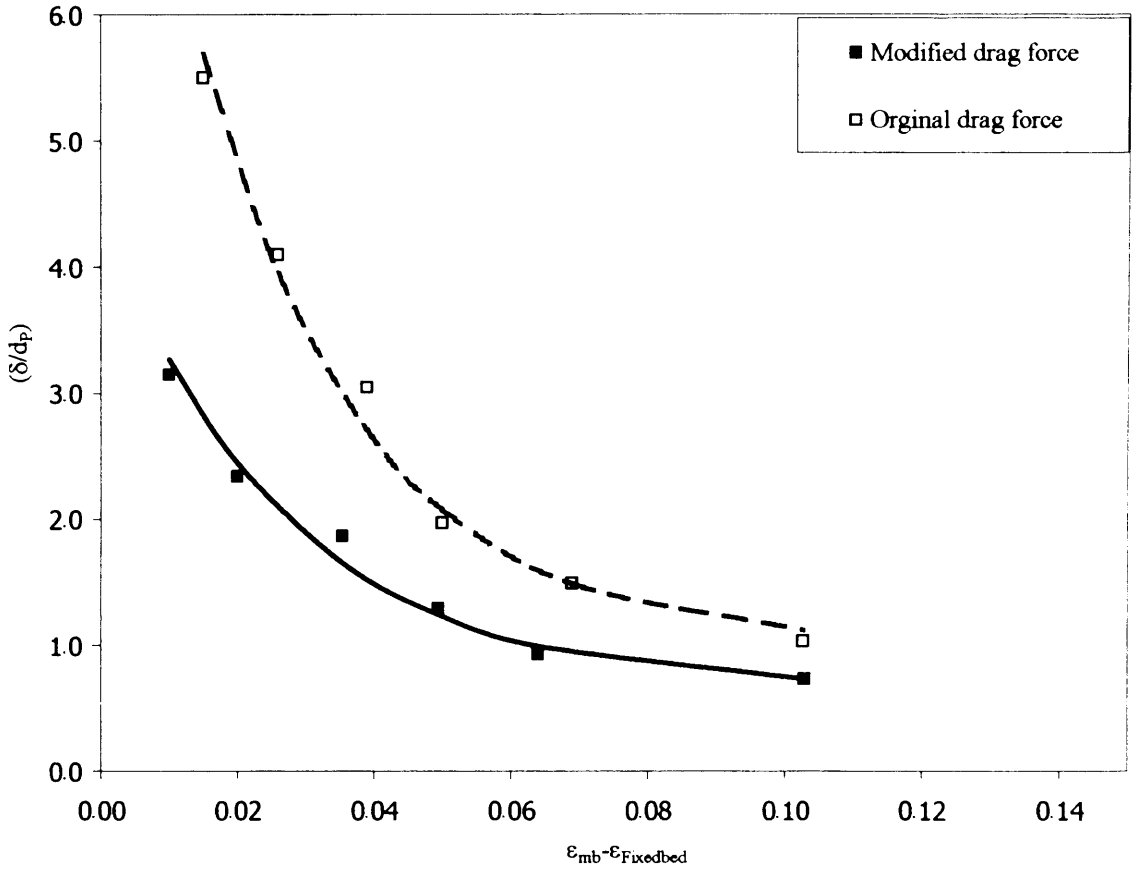

Figure 7.12 Experimental δ/d_P in relation with $\varepsilon_{mb} - \varepsilon_{Fixedbed}$ for narrow size cut powders

Figure 7.12 shows that for void fractions close to the fixed bed, the particles can be considered "continuous" only over lengths greater than 6 to 8 particle diameters.

Using the modified drag force correlation, the model accurately predicts the minimum bubbling velocities. When the original drag force correlation is used, the predicted minimum bubbling velocity is higher than the experimental values.

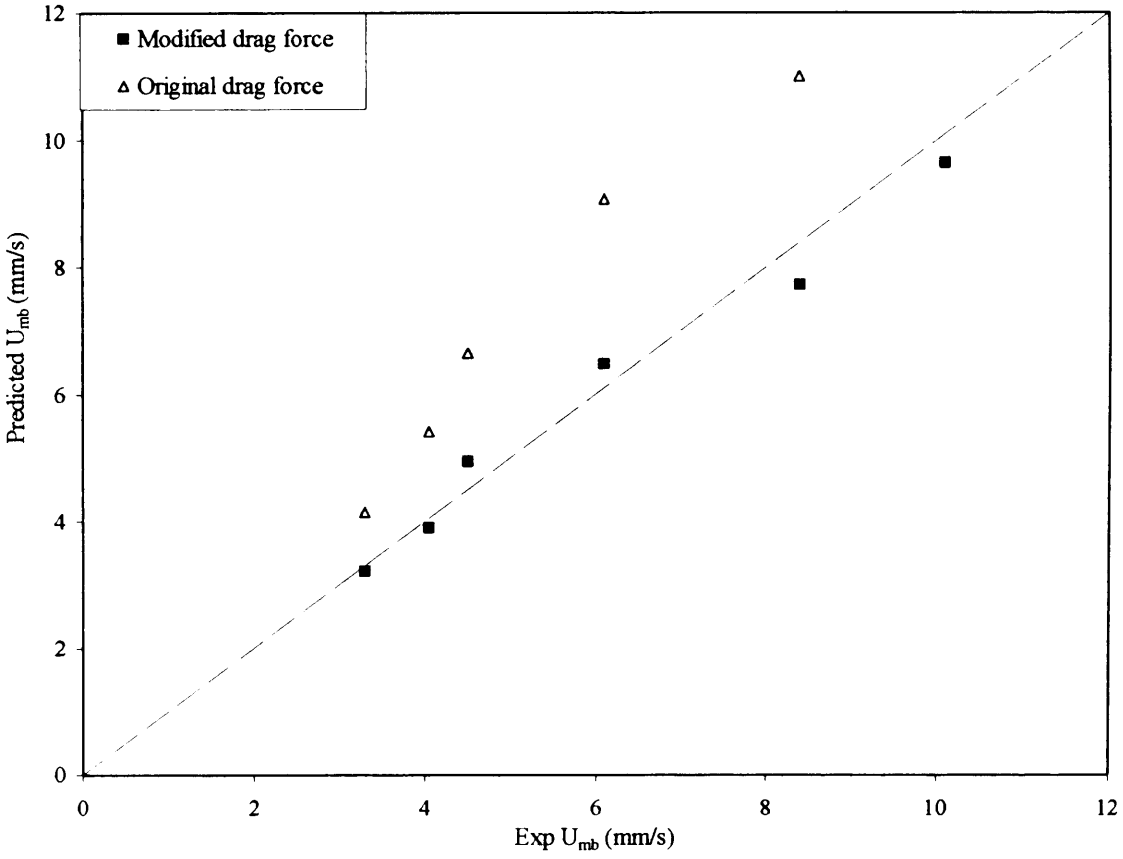

Figure 7.13 Comparison between predicted U_{mb} and experimental U_{mb}, when $\delta/d_P = f(\varepsilon)$ (using original and modified drag force correlations)

In conclusion, the stability criterion developed by Brandani and Zhang (2004) can be used to predict the minimum bubbling point of the narrow size cut powder, if the correct drag force correlation is used and if the ratio δ/d_P is expressed as a function of voidage. In this section a novel correlation for the minimum bubbling point of fluidized beds has been derived and it will be tested to predict the minimum bubbling point of the natural

size distribution powders and the bimodal powders, as well as experimental minimum bubbling data available in the literature.

7.6.3 Prediction of the minimum bubbling point for natural size powders and bimodal powders

The prediction of the minimum bubbling voidage using the modified stability criterion is shown in Figure 7.14. The prediction for the bimodal powder is in agreement with the experimental results. For the natural size powders, the prediction is approximately 4% less than the experimental results. This may be due to the fact that the characteristic length of the natural size powder is different from that of the narrow size cut where there is a uniform size in the assembly of particles. For the natural size distribution powder, the characteristic length may have to be higher to account for the variants of forces and voidage which is likely to be higher for the system with particle size dispersion. The prediction seems acceptable nevertheless taking into account the experimental uncertainty.

The prediction of the minimum bubbling velocity is shown in Figure 7.15. The prediction is approximately 7% lower than the experimental results. For the bimodal powders, where the prediction of the minimum bubbling voidage is in agreement with the experimental result, the predicted minimum bubbling velocity is lower than the experimental results. This is because the prediction of ε_d and U_d characteristic using the modified revised Ergun equation is in fact slightly less than the experimental results, as described in Chapter 6. For the natural size powders, the experimental minimum

bubbling velocity is less than the prediction. This follows the small error in the predicted minimum bubbling voidage.

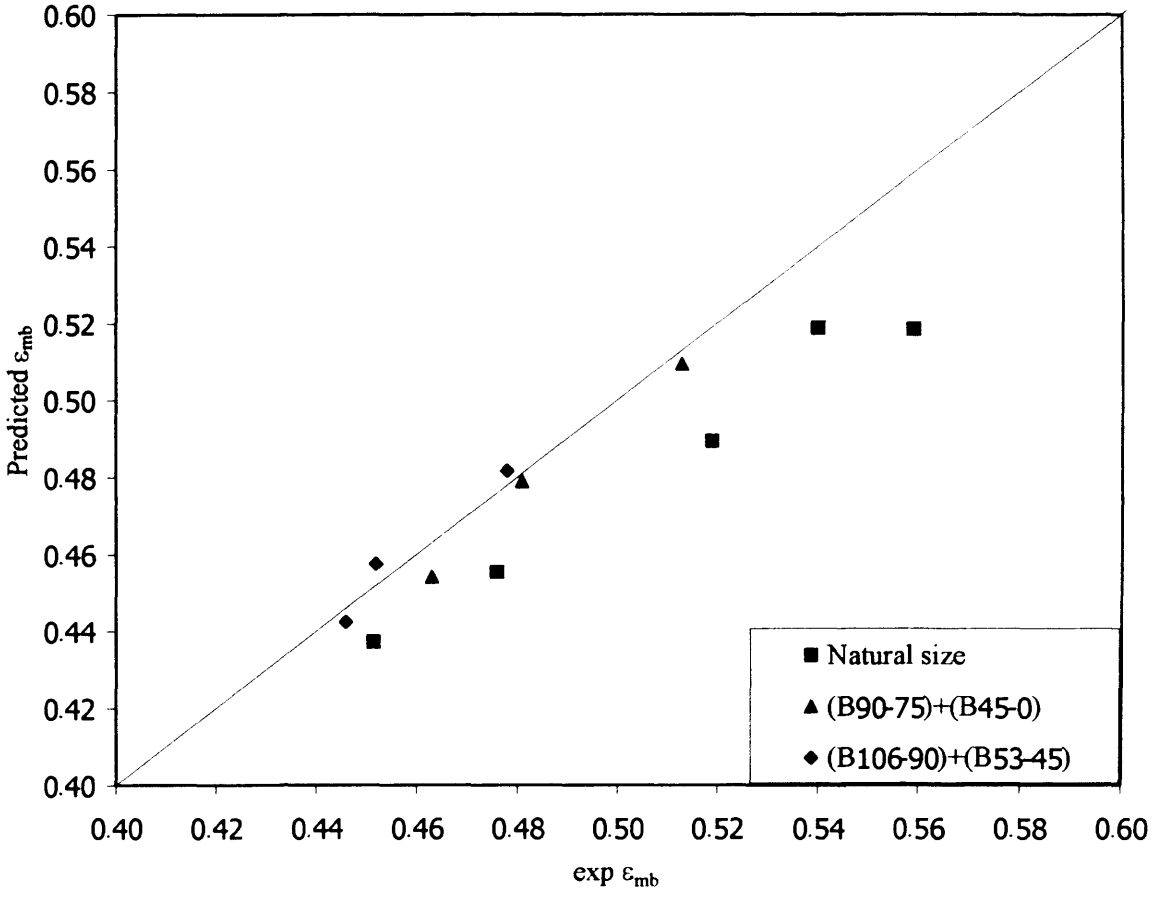

Figure 7.14 Prediction of the minimum bubbling voidage for the natural size powders and bimodal powder using the modified stability criterion

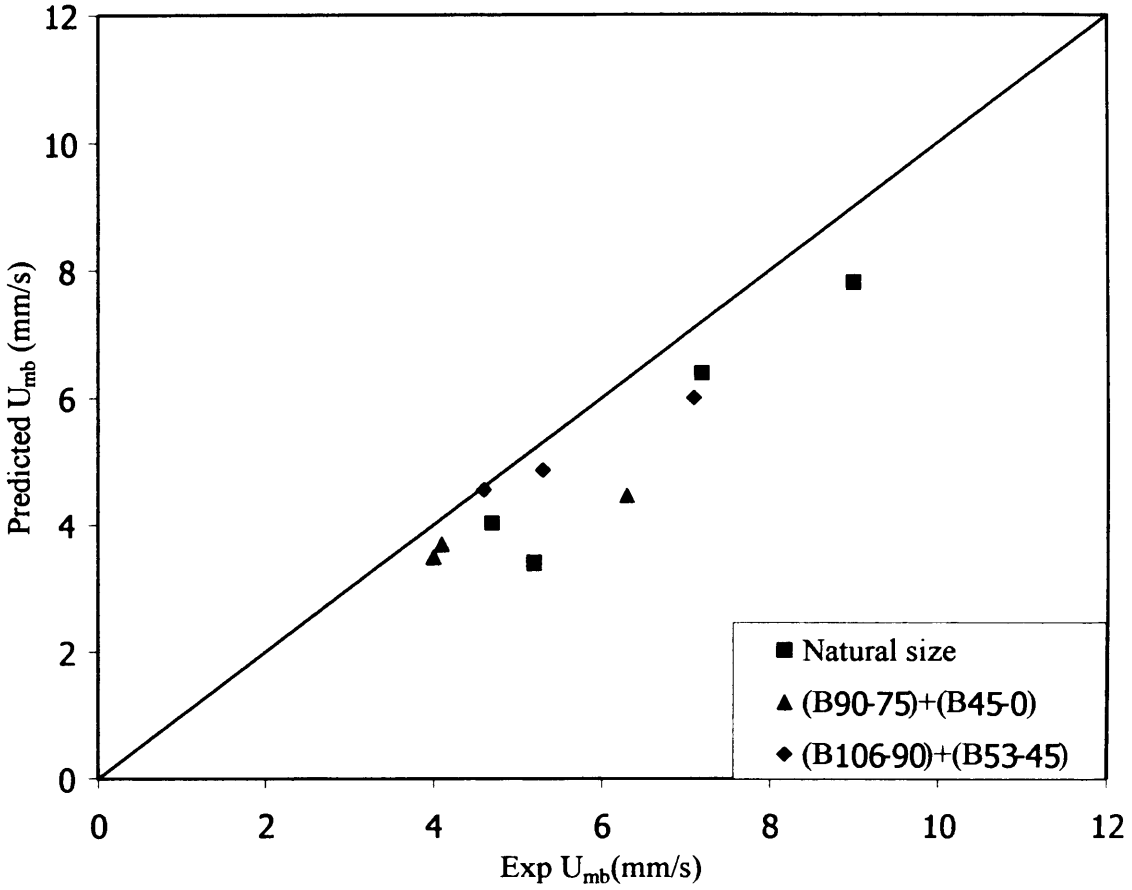

Figure 7.15 Prediction of the minimum bubbling velocity for the natural size powders and bimodal powder using the modified stability criterion

To ascertain the capability of the empirical correlation of δ/d_P and the modified pressure drop correlation, the stability criterion and the constitutive equations were validated using over 700 literature data points corresponding to various operating condition, type of powders, and type of gases. This comparison will be presented in the next section.

7.7 Validation of the modified stability criterion with literature data point

A detailed literature survey was used to establish a database of minimum bubbling points corresponding to various operating conditions, such as ambient condition (Godard and Richardson, 1968; Massimilla et al., 1972; Geldart, 1973; Musters and Reitema, 1977; Khoe et al., 1991; Kono et al., 1994; Rapagna et al., 1992; Foscolo et al., 1987; Kono et al., 1987; Rietema, 1973; Sobreiro and Monteiro, 1982; Foscolo et al., 1989; Reitema and Piepers, 1990; Marzocchella and Salatino, 2000; Donsi and Massilmilla, 1973), elevated temperatures (Lettieri et al., 2001; Xie and Geldart, 1995; Rietema, 1973), elevated pressures (Godard et al., 1968; Rapagna et al., 1992; Guedes De Carvalho, 1981; Peipers et al., 1984; Reitema and Piepers, 1990; Jacob and Weimer, 1987; Sobreiro and Monteiro, 1982; Foscolo et al., 1989; Marzocchella and Salatino, 2000; King and Harrison, 1982; and, Poletto et al., 1993), supercritical conditions (Vogt et.al., 2001), and high gravitational strength conditions (Reitema and Muster, 1978). The solid materials used in the studies reported in the literatures can be divided into two groups; rigid materials and non-rigid materials. The rigid materials can be divided further into porous and non-porous materials. The non-rigid materials are the polymeric materials. The gases are air, nitrogen, hydrogen, carbon dioxide, Argon, and Neon. These distinctions will be used to gain an insight in the predictions obtained from the model.

All the data points considered are for gas fluidization. In order to map the fluidization type based on the physical properties of particle and gas, the density ratio (ρ_f/ρ_p) versus Archimedes number of the data points was super-imposed on the generalized powder

classification for fluidization by any fluid, developed by Foscolo et al. (1991) as shown in Figure 7.16.

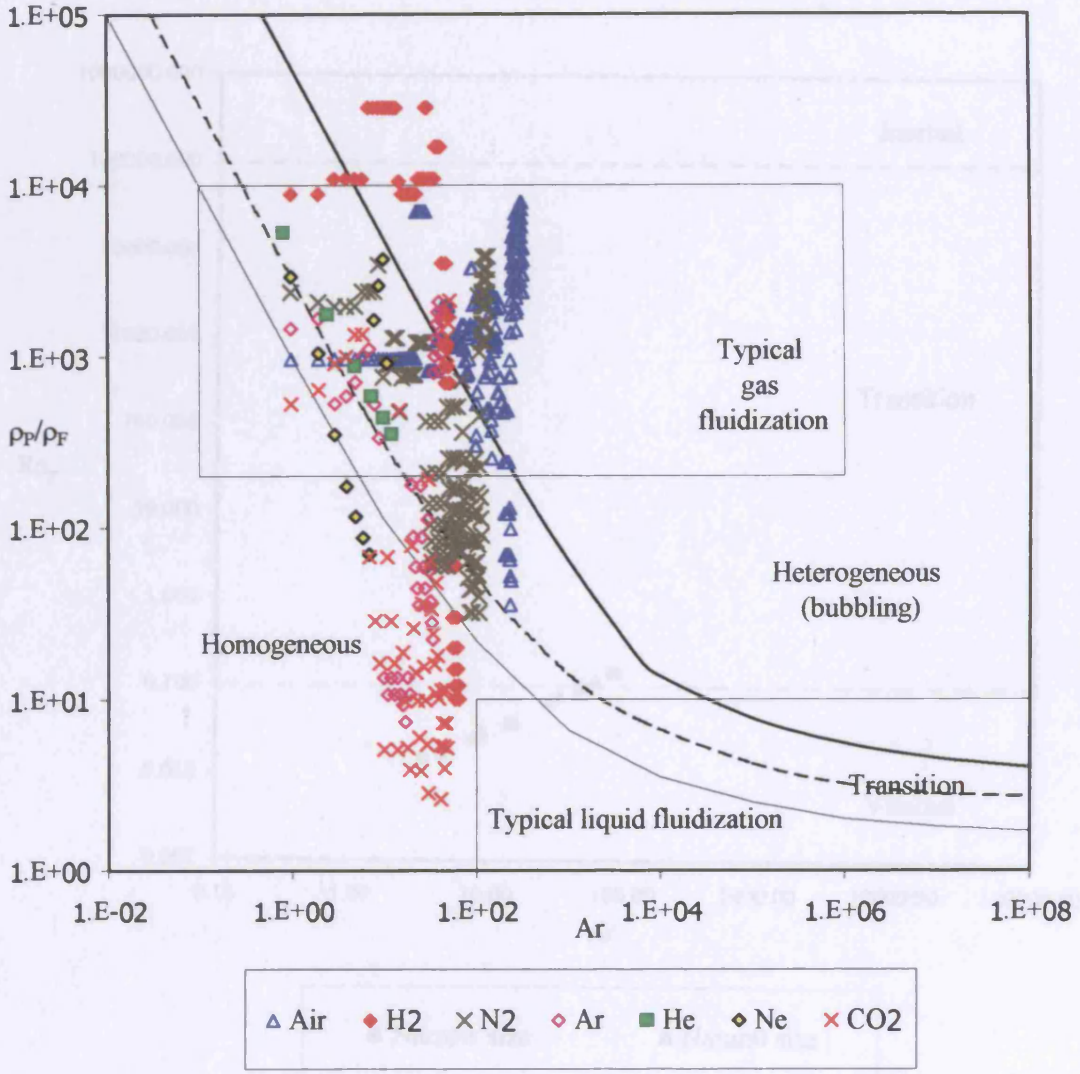

Figure 7.16 The generalized powder classification for fluidization by any fluid.

Most of the data points fall in the region of typical gas fluidization. However, some of data points, fluidized by carbon dioxide at high pressures, fall in the liquid fluidization region. The operating conditions of these experiments are at supercritical condition, where fluid properties are similar to liquid at high temperature and pressure. Fluidization types for the majority of the powders are within the transition region and

bubbling region. For the transition region, the fluidized bed will expand homogeneously first up to the transition to the bubbling fluidization. The minimum bubbling voidage is higher than the minimum fluidization voidage in this case

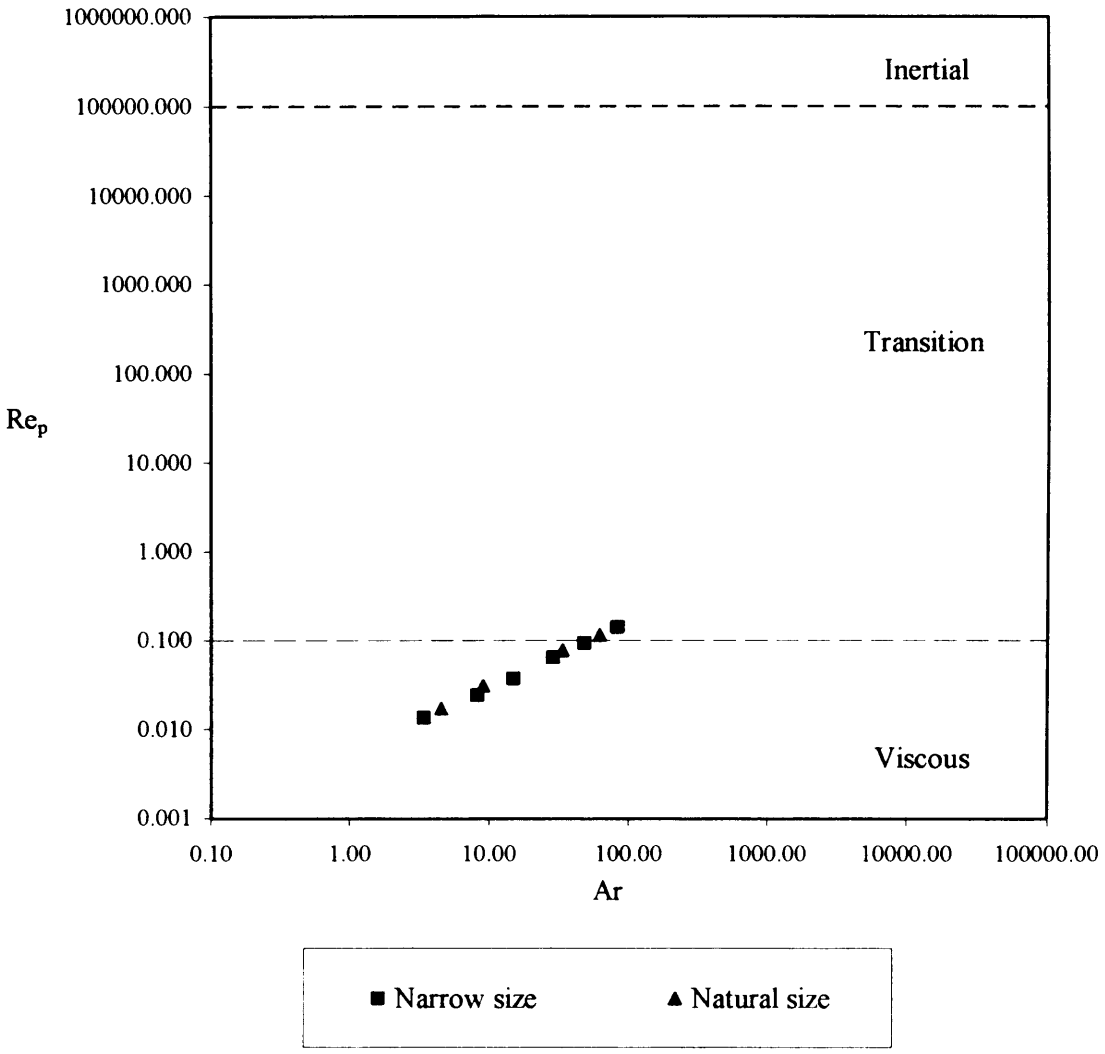

Figure 7.17 Reynolds numbers as function of Archimedes numbers for narrow size cut powders and natural size powders.

Figure 7.17 shows the Reynolds number versus Archimedes number of the narrow size cut and the natural size distribution powders. The systems investigated in the present study fall within the creeping flow range. Hence, the modified drag force correlation

and empirical correlation of δ/d_P should be applied within this limit. The use of these correlations outside the creeping flow region should be checked carefully.

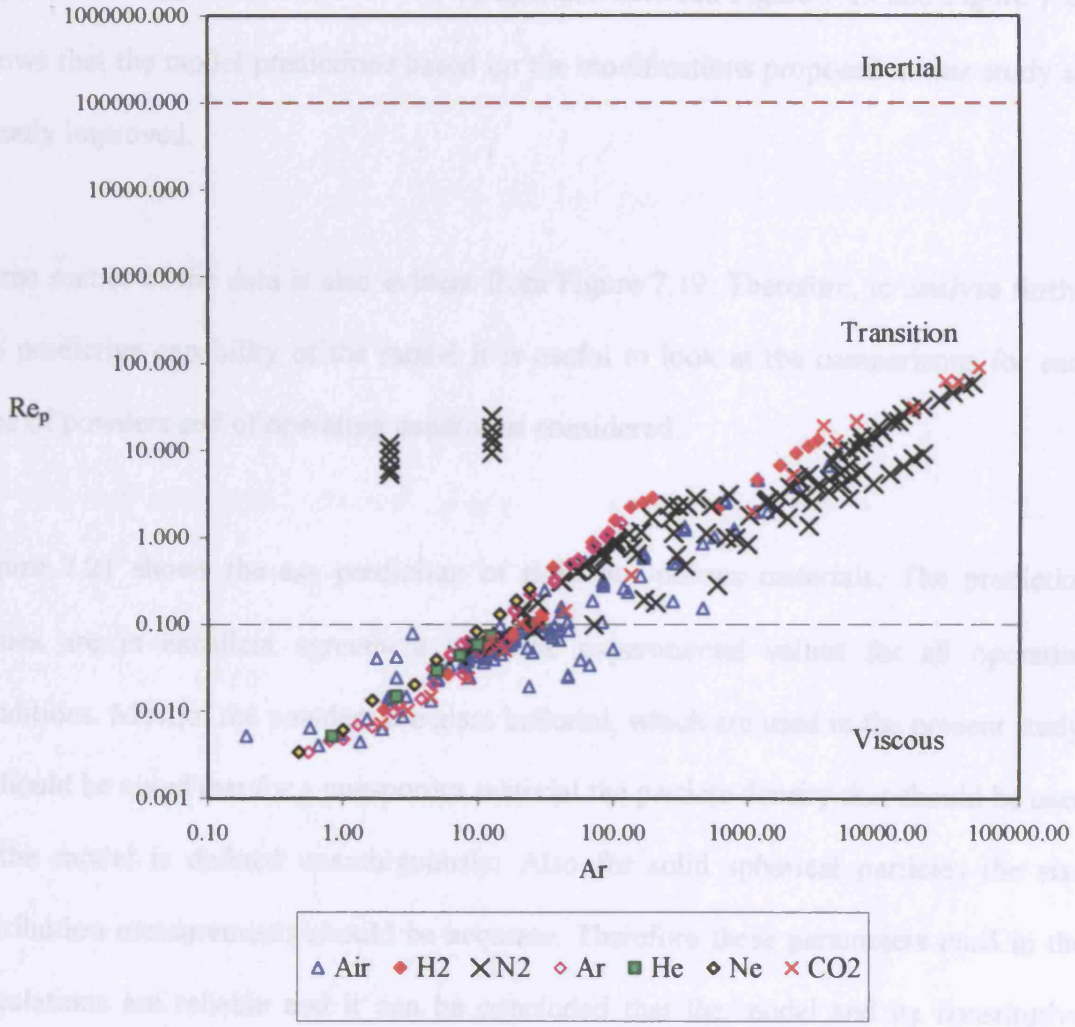

Figure 7.18 Reynolds numbers as function of Archimedes numbers for the literature data points.

The Reynolds numbers versus Archimedes numbers of the literature data points are shown in Figure 7.18. Most of the data points fall in the creeping flow region and some of them continue well within the transition region.

Figure 7.19 shows the comparison of the predicted ε_{mb} and the experimental ε_{mb}, when $\delta/d_P = f(\varepsilon,\varepsilon_{mf})$. Figure 7.20 shows the comparison of the predicted ε_{mb} and the experimental ε_{mb} when $\delta/d_P = 1$. The comparison between Figure 7.19 and Figure 7.20, shows that the model predictions based on the modifications proposed in this study are greatly improved.

Some scatter of the data is also evident from Figure 7.19. Therefore, to analyse further the predictive capability of the model it is useful to look at the comparisons for each type of powders and of operating conditions considered.

Figure 7.21 shows the ε_{mb} prediction of rigid non-porous materials. The prediction values are in excellent agreement with the experimental values for all operating conditions. Most of the powders are glass ballotini, which are used in the present study. It should be noted that for a non-porous material the particle density that should be used in the model is defined unambiguously. Also for solid spherical particles the size distribution measurements should be accurate. Therefore these parameters used in the calculations are reliable and it can be concluded that the model and its constitutive equations can be applied to non-porous materials, even though some experiments are in the transition region.

Figure 7.22 shows prediction of ε_{mb} for rigid porous materials. The model can predict within +/-7% uncertainty many experimental data points. Some data are outside this range and the prediction capability is less satisfactory.

The explanation for the poor prediction of some data points for porous materials may be from the error in the values of the particle density. For porous materials, one should use the density over the particle volume, i.e. including the pores, and this should not be measured using a density bottle, since this will yield a "skeletal" density.

Another possible explanation is due to the fact that porous materials tend to adsorb humidity and other components, and the density can be affected significantly by the relative humidity of the fluidizing air.

For non rigid polymeric materials (Figure 7.23), the model does not yield accurate predictions. As these are non-rigid and most of solids belonging to this category are resins, these powders can be deformed during fluidization, or could undergo swelling in the presence of water. If the particle adsorbs gases or vapours, the particle density will be affected as in the case of porous solid particles. If the density measurement is carried out in a density bottle and the material interacts with water, again the reported density could be affected and in the presence of swelling the larger particle size would lead to higher experimental ε_{mb} values in comparison to the predicted values. From Figure 7.23, the experimental ε_{mb} is higher than the predicted values for most cases in this category.

Figure 7.28 to Figure 7.30 show the predictive capability of U_{mb} for rigid non-porous, rigid porous and non-rigid polymeric powders. The model predicts reasonably well the non-porous materials. For rigid porous materials, the data points that predicted ε_{mb} correctly tend to have a reasonable agreement between the experiment and the predicted U_{mb}. Where a poor prediction of ε_{mb} was obtained, the predicted U_{mb} tend yield poor results as well. In general, in the determination of the minimum bubbling point, the

uncertainty on the velocity measurement is greater than that of the voidage measurement. This is because near the minimum bubbling point the change in bed height is gradual. Also, since the drag correlations are strongly dependent on the void fraction, any error in the voidage at minimum bubbling will result in a much larger error in the predicted velocity.

Figure 7.24, Figure 7.25, Figure 7.26 and Figure 7.27, show the prediction of ε_{mb} for different operating conditions, which are high pressure, high temperature, high gravitational strength, and supercritical condition respectively. The prediction for high-pressure conditions (Figure 7.24) is good except for porous materials. In this case the weight of the fluidizing gas in the pores may be non-negligible. For high temperature operation (Figure 7.25), the prediction is worse as the content of fines is increased. This may be due to agglomeration. For the high gravitational field strength (Figure 7.26), the prediction is good. Finally, for the supercritical systems, there is an excellent agreement between the prediction and the experiment.

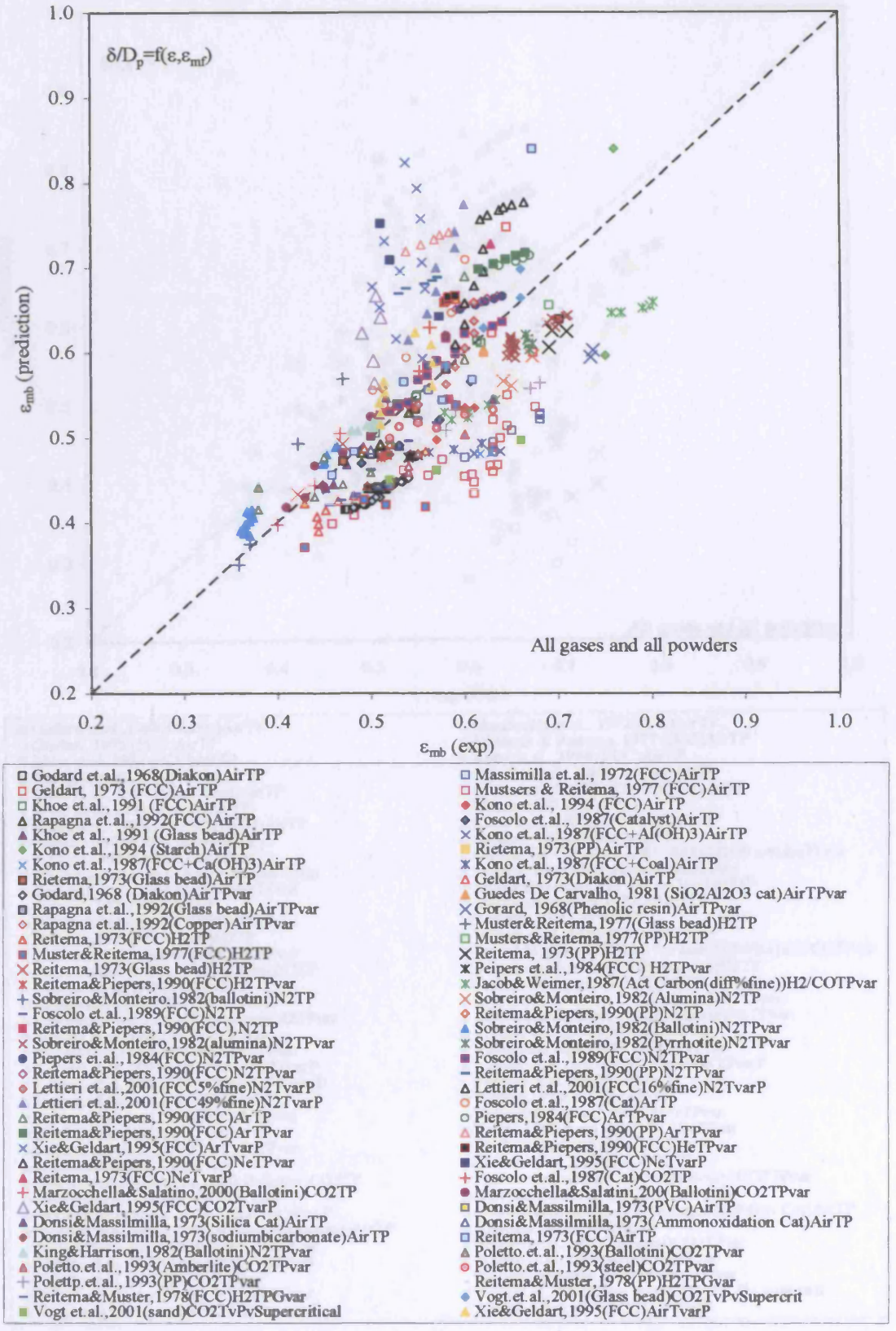

Figure 7.19 Prediction of literature ε_{mb} for all gases and all powders when $\delta/d_P = f(\varepsilon)$

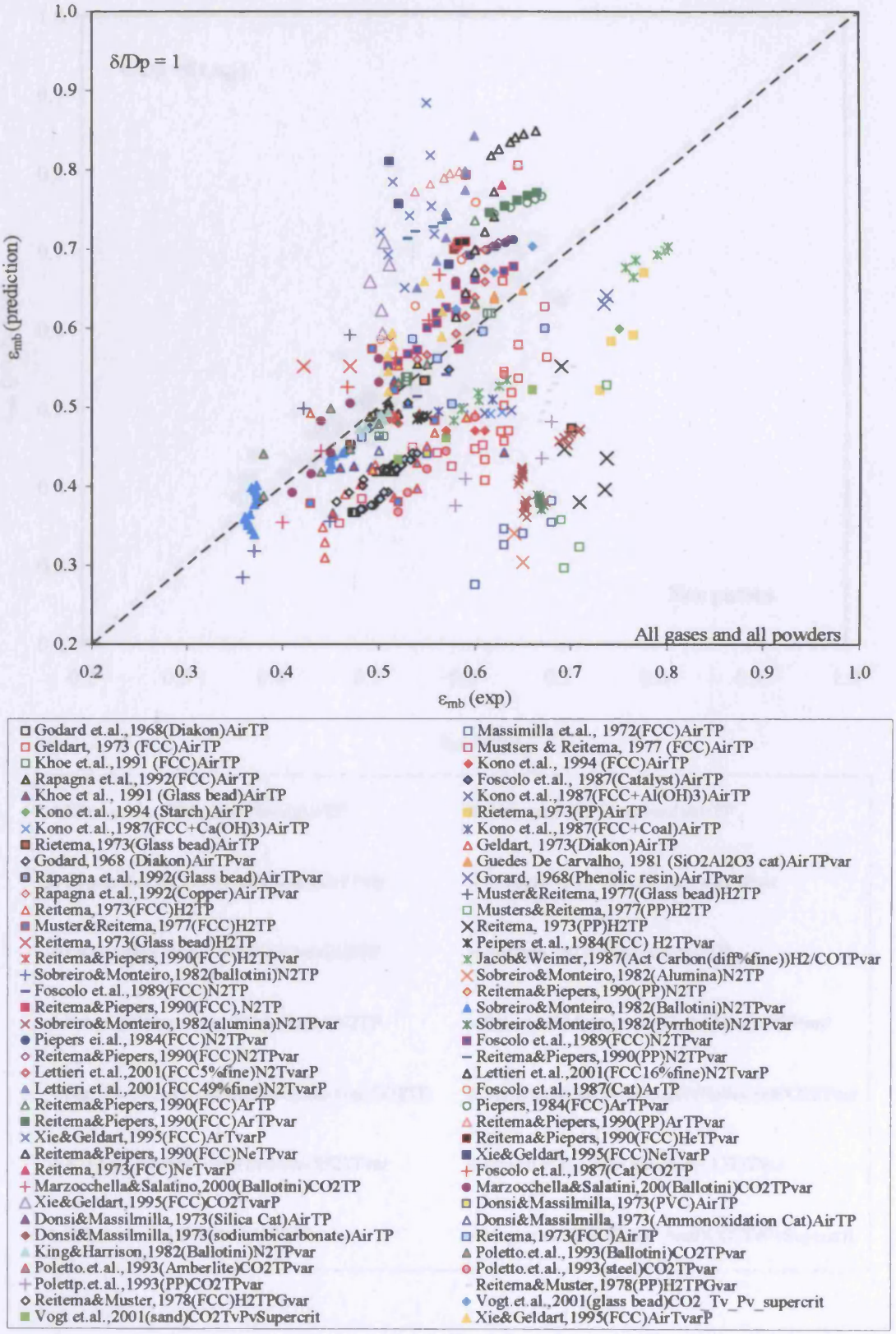

Figure 7.20 Prediction of literature ε_{mb} for all gases and all powders when $\delta/d_P = 1$

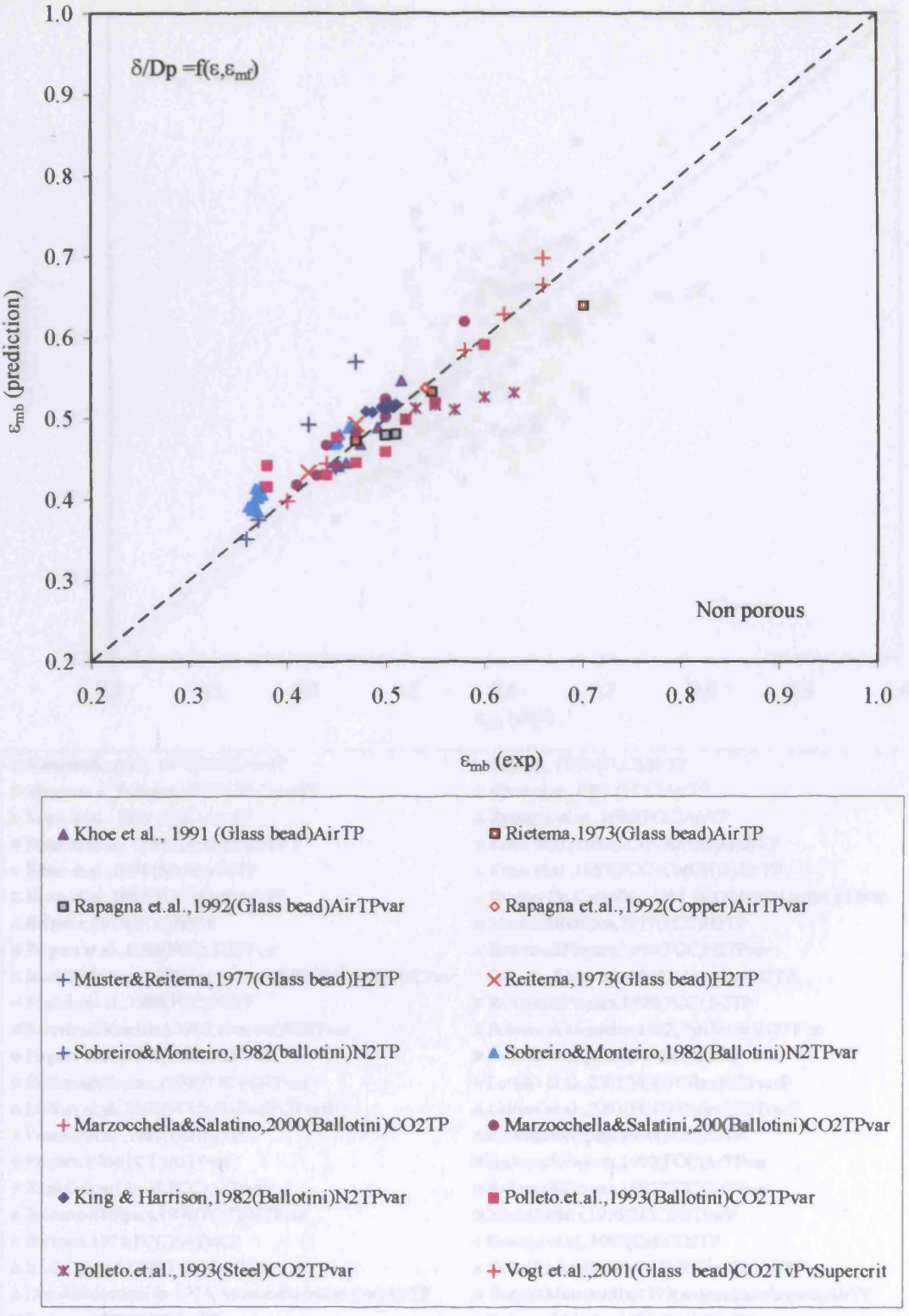

Figure 7.21 Prediction of literature ε_{mb} for non-porous powders when $\delta/d_P = f(\varepsilon)$

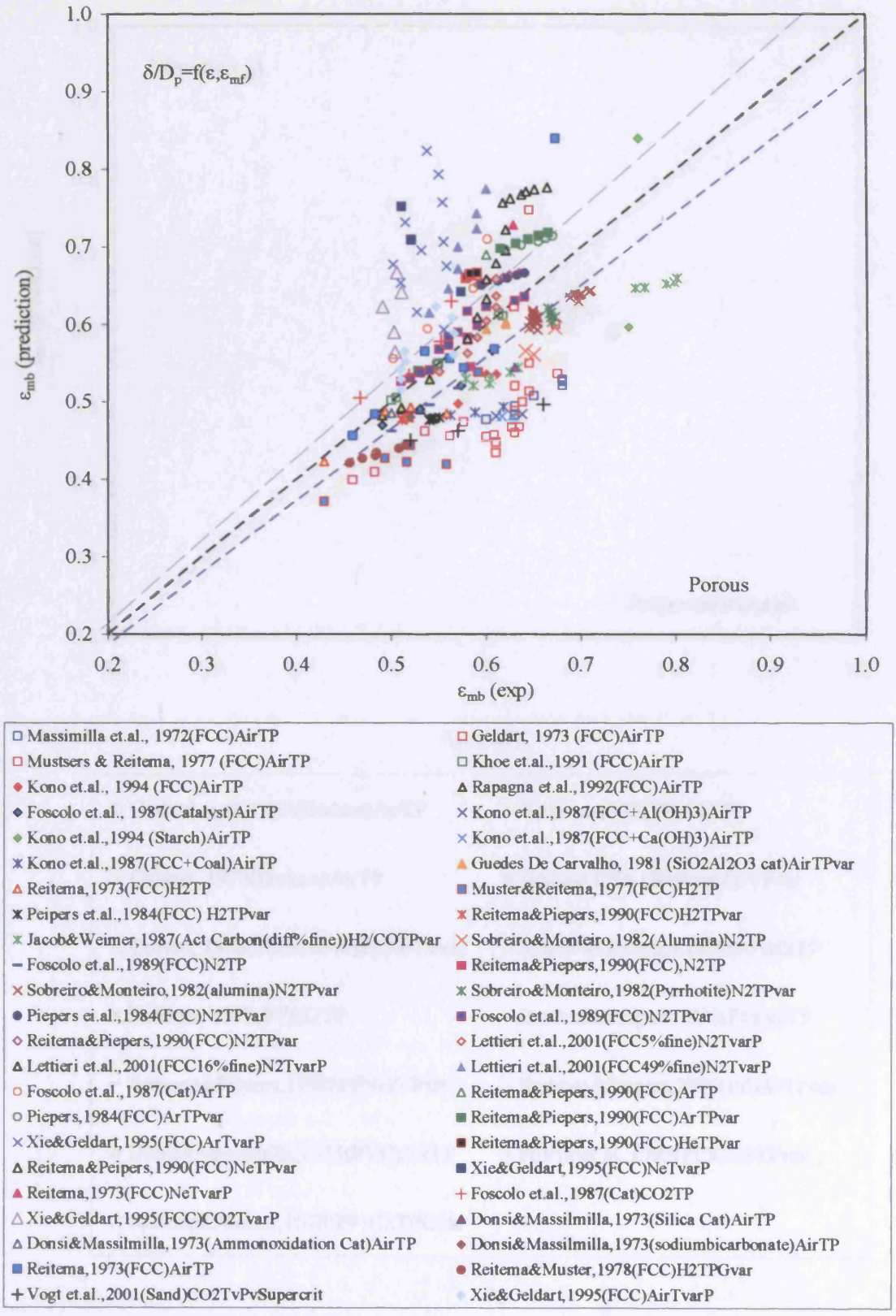

Figure 7.22 Prediction of literature ε_{mb} for porous materials, when $\delta/d_P = f(\varepsilon)$

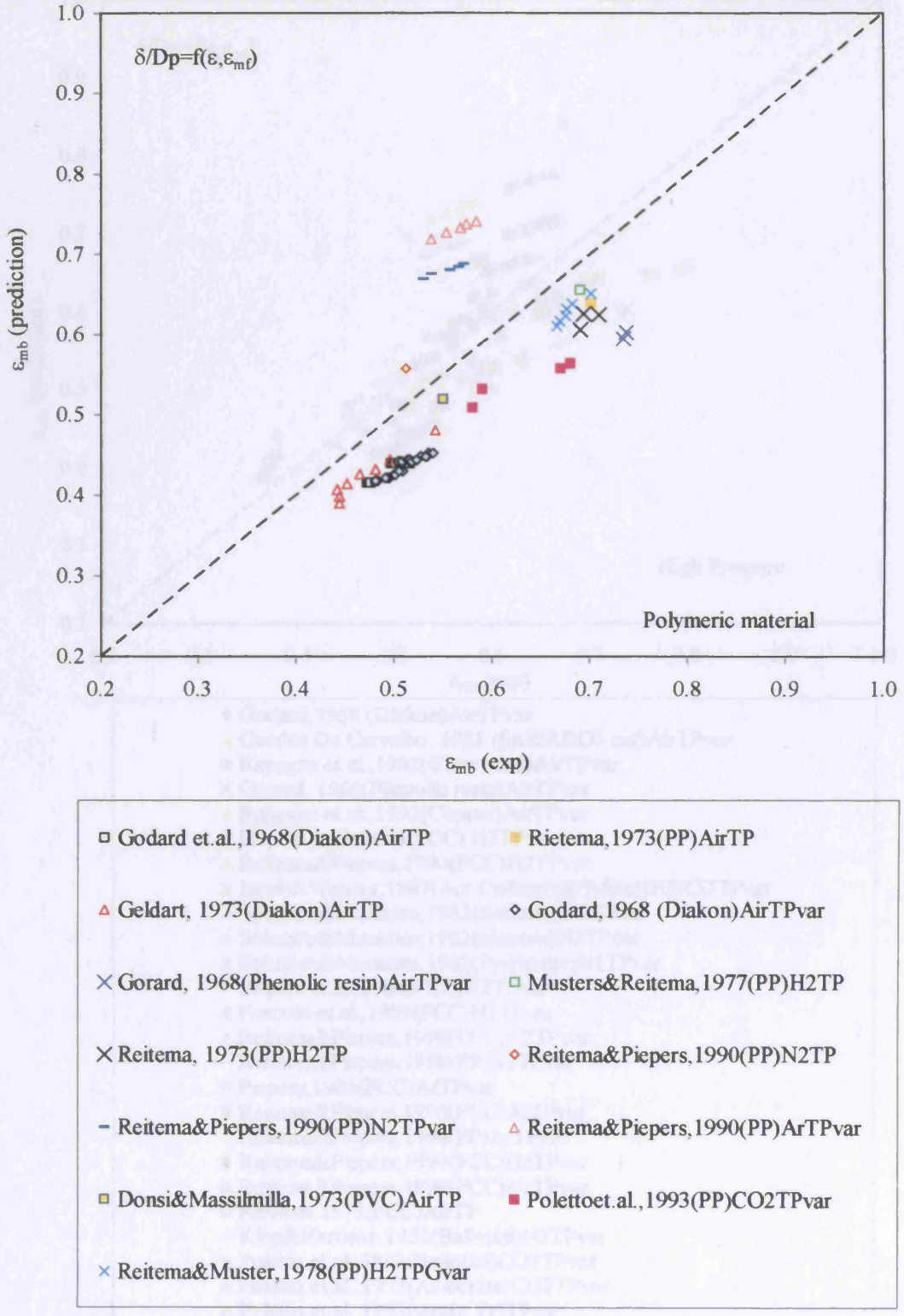

Figure 7.23 Prediction of literature ε_{mb} for polymeric materials when $\delta/d_P = f(\varepsilon)$

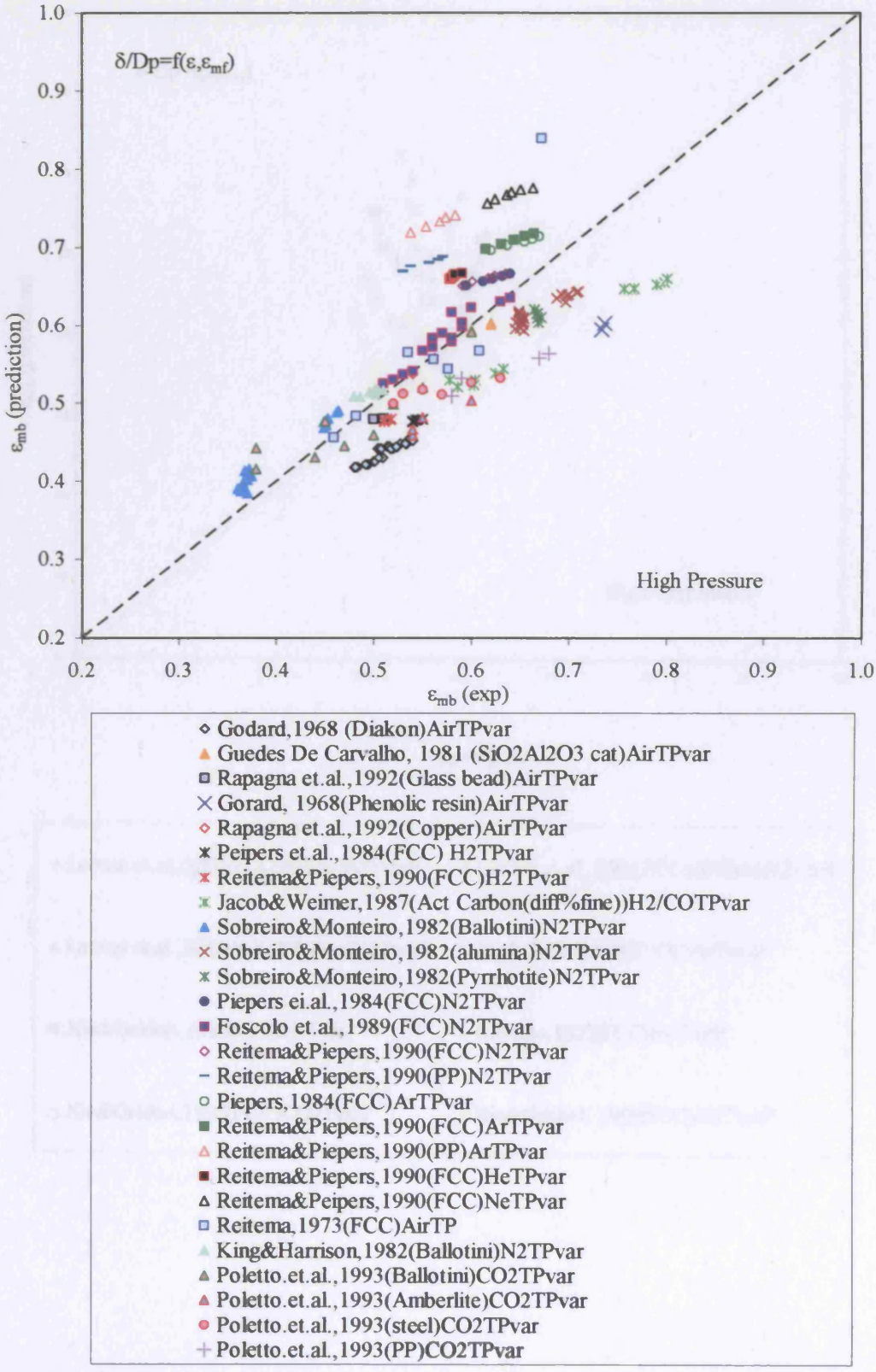

Figure 7.24 Prediction of literature ε_{mb} for high pressure when $\delta/d_P = f(\varepsilon)$

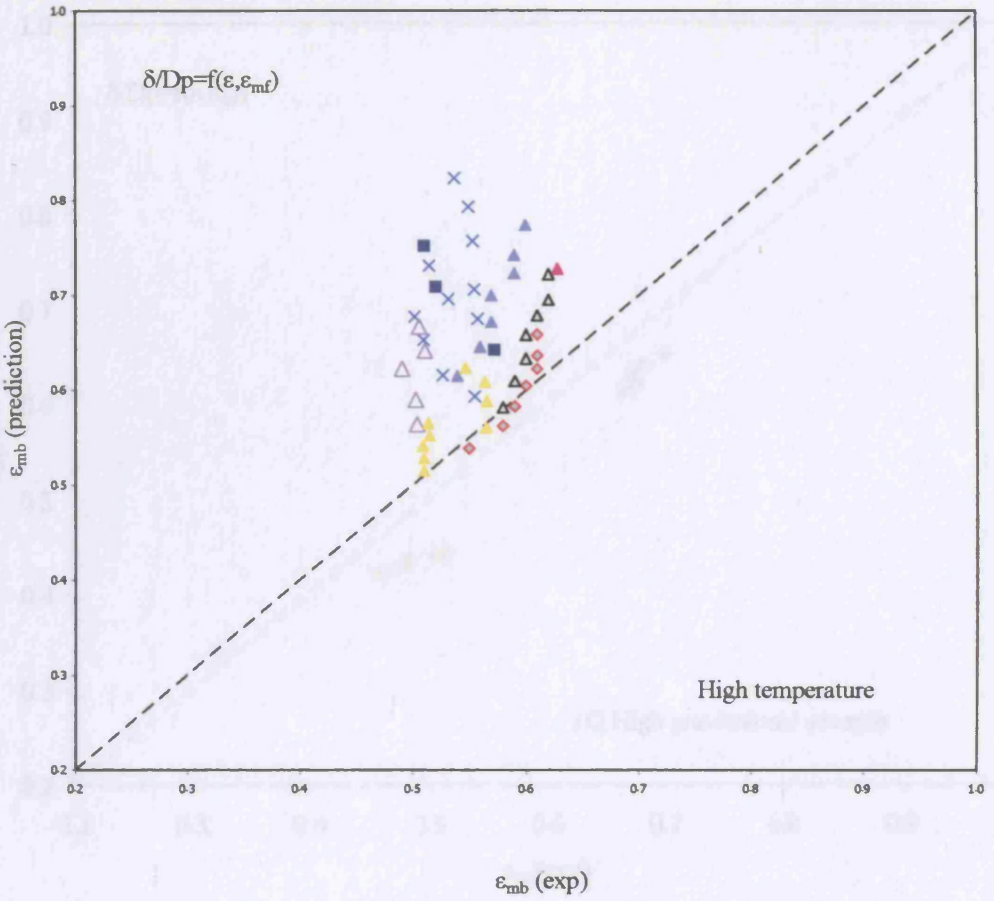

◇ Lettieri et.al.,2001(FCC5%fine)N2TvarP
△ Lettieri et.al.,2001(FCC16%fine)N2TvarP
▲ Lettieri et.al.,2001(FCC49%fine)N2TvarP
× Xie&Geldart,1995(FCC)ArTvarP
■ Xie&Geldart,1995(FCC)NeTvarP
▲ Rietema,1973(FCC)NeTvarP
△ Xie&Geldart,1995(FCC)CO2TvarP
▲ Xie&Geldart, 1995(FCC)AirTvarP

Figure 7.25 Prediction of literature ε_{mb} for high temperature when $\delta/d_P = f(\varepsilon)$

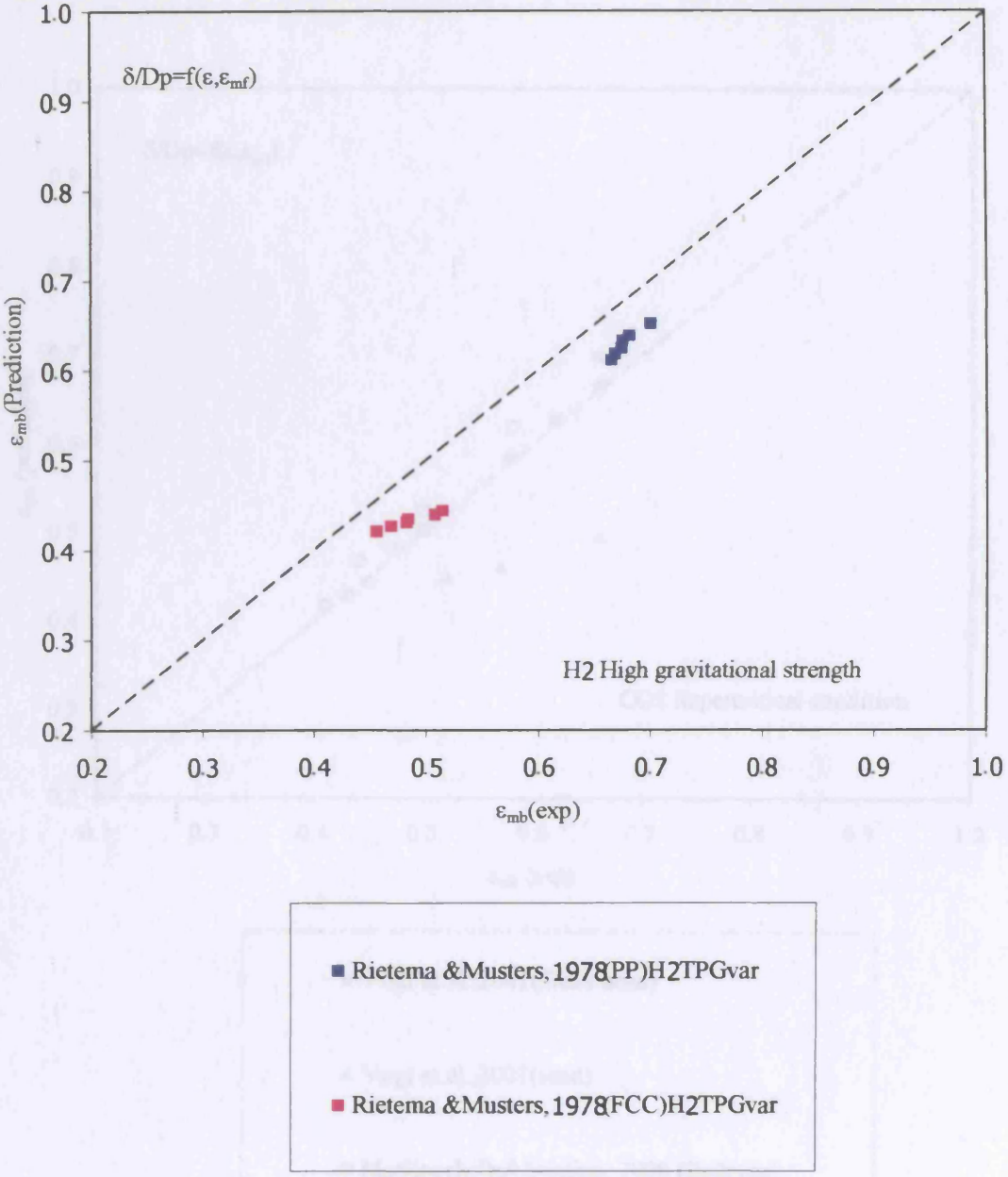

Figure 7.26 Prediction of literature ε_{mb} for high gravitational strength when $\delta/d_P = f(\varepsilon)$

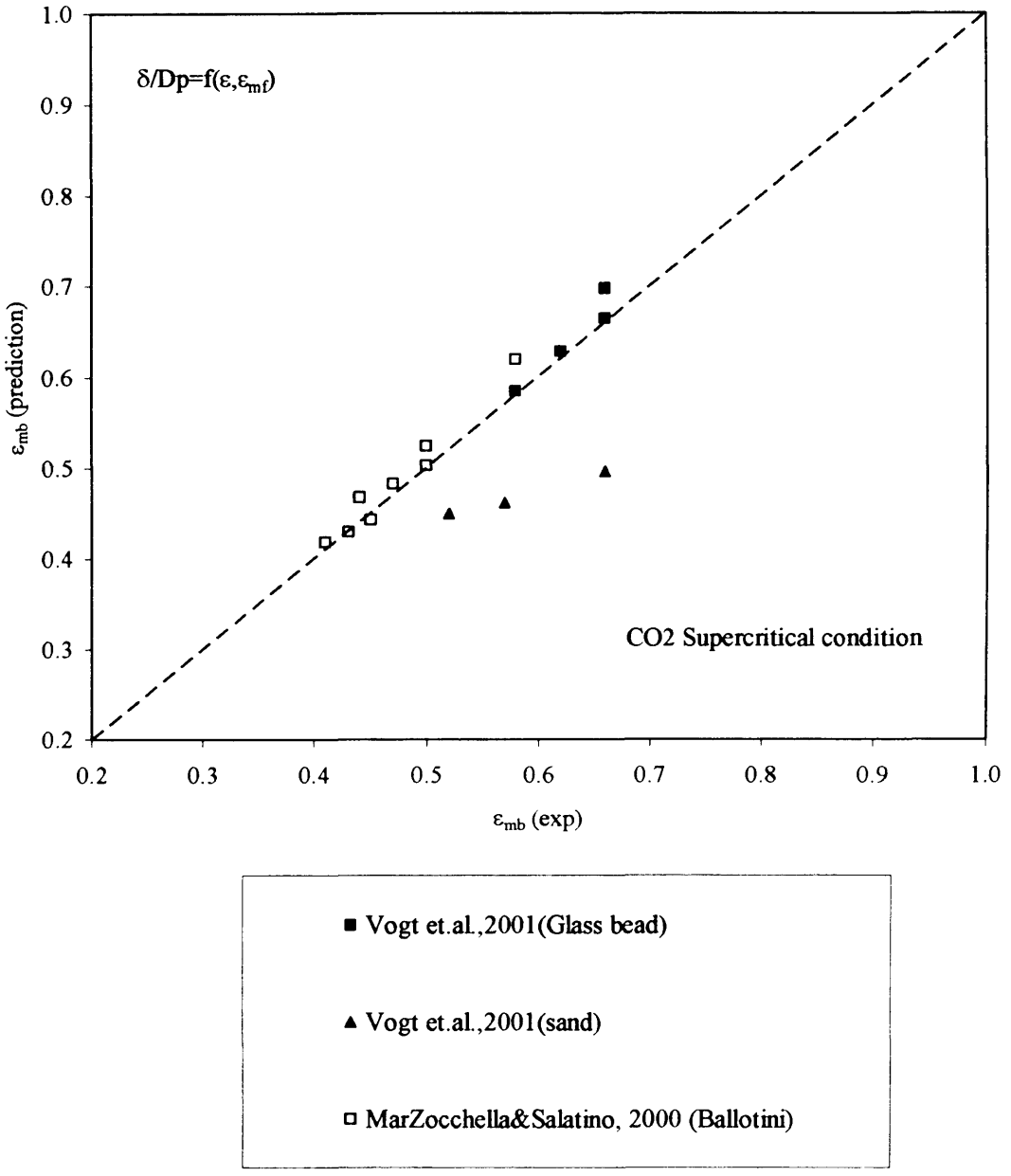

Figure 7.27 Prediction of literature ε_{mb} for supercritical condition when $\delta/d_P = f(\varepsilon)$

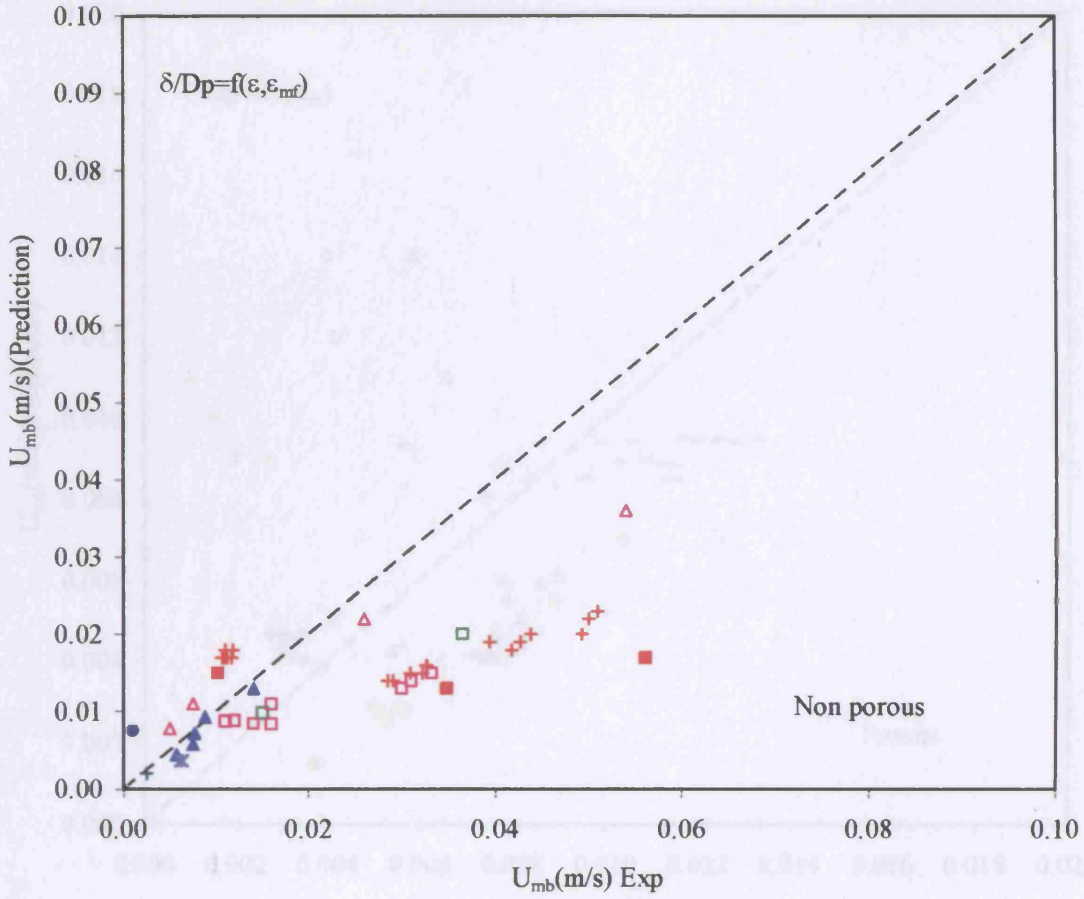

Figure 7.28 Prediction of literature U_{mb} for non-porous powders when $\delta/d_P = f(\varepsilon)$

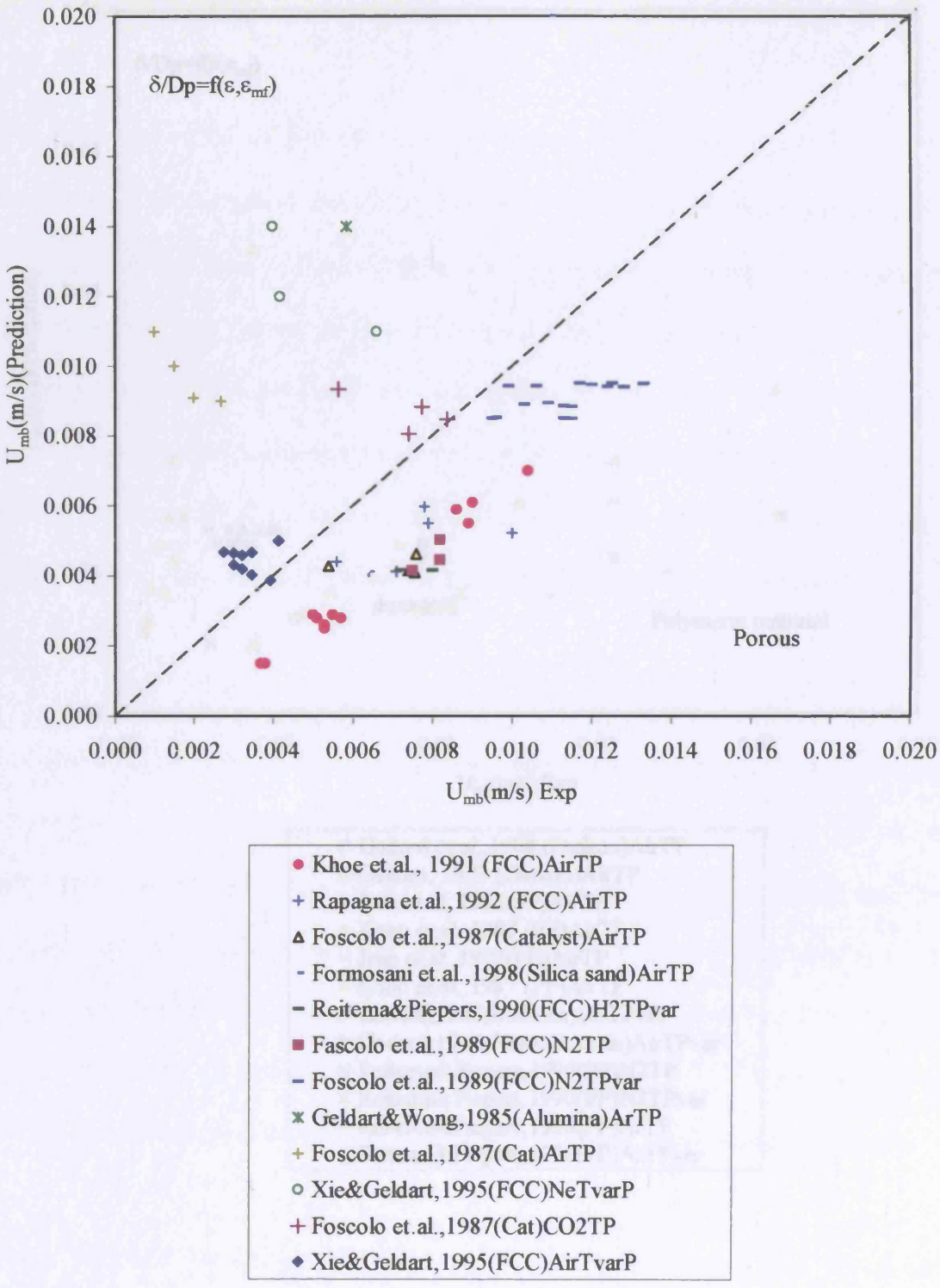

Figure 7.29 Prediction of literature U_{mb} for porous powders when $\delta/d_P = f(\varepsilon)$

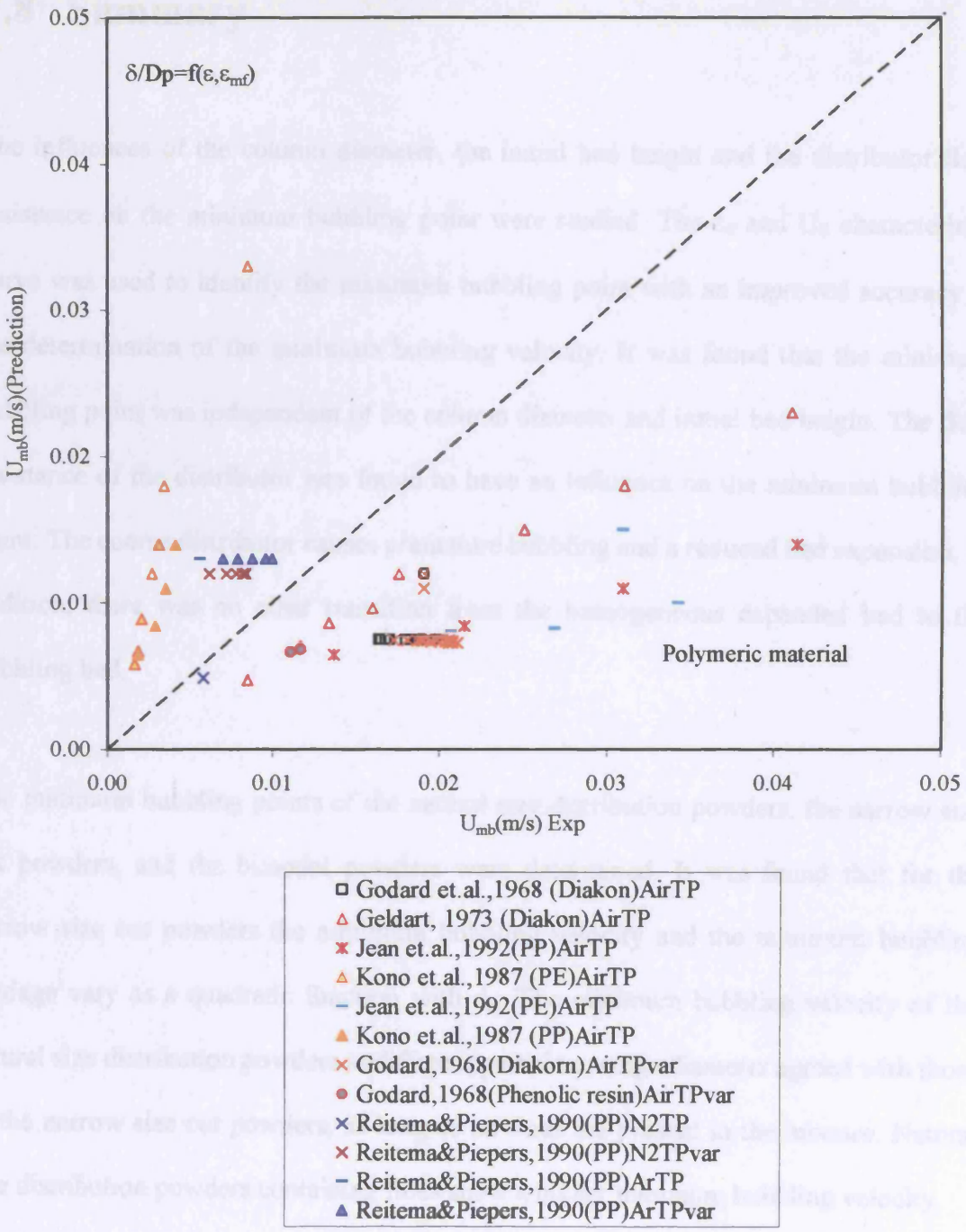

Figure 7.30 Prediction of literature U_{mb} for polymeric material when $\delta/d_P = f(\varepsilon)$

7.8 Summary

The influences of the column diameter, the initial bed height and the distributor flow resistance on the minimum bubbling point were studied. The ε_d and U_d characteristic curve was used to identify the minimum bubbling point with an improved accuracy in the determination of the minimum bubbling velocity. It was found that the minimum bubbling point was independent of the column diameter and initial bed height. The flow resistance of the distributor was found to have an influence on the minimum bubbling point. The coarse distributor causes premature bubbling and a reduced bed expansion. In addition, there was no clear transition from the homogeneous expanded bed to the bubbling bed.

The minimum bubbling points of the natural size distribution powders, the narrow size cut powders, and the bimodal powders were determined. It was found that for the narrow size cut powders the minimum bubbling velocity and the minimum bubbling voidage vary as a quadratic function with d_P. The minimum bubbling velocity of the natural size distribution powders at different particle average diameter agreed with those of the narrow size cut powders, as long as no fines are present in the mixture. Natural size distribution powders containing fines show a higher minimum bubbling velocity.

Higher minimum bubbling voidages were found for the natural size distribution powders at different average particle diameters, compared to the narrow size cut powders. The minimum bubbling voidage is even higher, when the powder contains fines. For the bimodal powder, the minimum bubbling voidages were lower than the natural size cut powder, but followed approximately the same trend.

The minimum bubbling velocities for the natural size distribution powders were on the same trend of the narrow size cut powder, when there are no fines in the mixture. With fines, the minimum bubbling velocities were higher. For the bimodal powder, the minimum bubbling velocities were on the same trend of the narrow size cut powder whether or not the mixture contained fines.

The recently developed stability criterion of Brandani and Zhang (2004) has been extended using the experimental results obtained in this study. Combining a modified drag force correlation and introducing a voidage dependency for the ratio δ/d_P a new correlation was proposed. This new correlation was further tested against more than 700 data points taken from the literature. A careful analysis of the results indicates that for non-porous rigid particles the model results in accurate predictions of the minimum bubbling point.

Chapter 8: Conclusions and Future Work

8.1 Introduction

Fluidization characteristics of fine powders, belonging to group A of Geldart's powder classification, were studied in detail using pressure drop measurements from fluidization and de-fluidization experiments and the bed collapse technique. To obtain the correct properties of the powders from the bed collapse experiment, a model has been developed, which takes into account the system configuration for both one- and two-valve experiments.

The effect of particle size has been investigated on four different sizes of natural size distribution powders. In order to understand the effect of each individual size cut on the behaviour of the original powder, the original powders were sieved into 6 different size cuts; according to $2^{1/4}$ sieve size aperture series and fluidization characteristics of each size cut were studied. Bimodal powders were prepared mixing narrow size cut powders to compare these with the natural size distribution powders. In addition, the effects of column diameter, initial bed height and distributor porosity on the fluidization characteristics were also studied.

The experimental ε_d and U_d characteristic curves were used to test drag force correlations reported in the literature. It was found that all the correlations commonly used in CFD simulations do not describe accurately the experimental results. Modifying the literature equations it was possible to correlate the experimental ε_d and U_d curves and using this information to predict the minimum bubbling point using a CFD model recently developed at UCL. A correlation for the dependence with voidage of the characteristic parameter of the model was obtained from the experimental results. The predictions from the new minimum bubbling criterion were compared to an extensive database of literature values.

8.2 Bed collapse model

A model was developed in order to describe the bed collapse curves taking into account the effect of the experimental system configuration. A procedure to estimate the model parameters: the windbox volume, the distributor pressure drop, the discharge valve flow characteristics and the pressure drop in the fixed bed was applied to the experimental apparatus available in our laboratory. The model was applied to the two variants of the bed collapse experiment, the 1- and 2 –valve configurations. The intrinsic particle properties of the dense phase voidage, dense phase superficial velocity and the bed voidage can be obtained from the use of the model applied to the analysis of the experimental results. In addition, the model can be used to predict under which conditions the 1-valve or 2-valve configuration will yield the correct extrapolation to obtain the dense phase voidage from the experimental curve. Finally, the model can also

predict the bed collapse curve, the location of the fixed bed interface, the transient pressure drop profile, the bubble escape time and the bed collapse times.

Based on this study we can conclude that both 1-valve and 2-valve experiments have advantages and limitations, and for this reason both should be performed to unambiguously determine the intrinsic properties of Geldart type A powders. Accurate U_d and ε_d correlation can be found when applying our model to both the 1-valve/2-valve bed collapse experiments.

8.3 Influence of column diameter, initial bed height and the distributor flow resistance on the fluidization characteristics

The influences of the aspect ratio, column diameter, initial bed height and distributor flow resistance on the minimum fluidization point, the fixed bed pressure drop, U_d and ε_d characteristic, ε_d and ε_0 versus U_0 characteristic and the minimum bubbling point were studied.

The minimum fluidization voidage and, hence, the fixed bed pressure drop was slightly affected by the aspect ratio and the column diameter, due to the influence of these on ε_{mf}. The minimum fluidization velocity was independent of the aspect ratio, column diameter, initial bed height, and distributor flow resistance.

The U_d and ε_d characteristic curve was independent of the column diameter, initial bed height and distributor flow resistance. The relationship between ε_d and ε_0 with U_0, it was found that ε_d and ε_0 were independent of the initial bed height for all U_0. However, ε_d and ε_0 were independent of the column diameter for the homogeneous expanded bed, but at higher velocities ε_d and ε_0 are higher for a larger column. The distributor gas flow resistance influences the onset of bubbling with the coarse distributor leading to a lower bed expansion at low U_0 and to premature bubbling. At velocities higher than U_0 ($\approx$2.5 U_{mb}), ε_d and ε_0 are the same for both fine and coarse distributor.

The ε_d and U_d characteristic was used to identify the minimum bubbling point. It was found that the minimum bubbling point was independent of the column diameter and the initial bed height, but was influenced by the flow resistance of the distributor.

8.4 Fluidization characteristics of narrow size cut, natural size distribution and bimodal powders with average particle size

The pressure drop characteristics of natural size distribution powders, narrow size cut powders and bimodal powders were investigated. It can be generally concluded that minimum fluidization velocity is increased as a quadratic function with the increase of the average diameter. With the increase of the average diameter, the minimum fluidization voidage is decreased, and the fixed bed gas flow resistance is decreased. In addition, the relation of U_{mf} and $\Delta P_{fixed\ bed}$ with d_p of the narrow size cut can be used to estimate of U_{mf} and $\Delta P_{fixed\ bed}$ natural size distribution powder and bimodal mixtures as

long as there is no fines in the mixture. However, when the mixture contains fines, U_{mf}, and $\Delta P_{fixed\ bed}$ cannot be predicted using the relation from narrow size cut powders. U_{mf}, and $\Delta P_{fixed\ bed}$ of the natural size cut and bimodal with fine were approximately on the same trend. Furthermore, the minimum fluidization voidage of the natural powders with fines and the bimodal mixtures, with and without fines is smaller than that estimated from the narrow size cut relation.

From the pressure drop profile of all powder mixtures, there is no evidence of particle segregation in the fluidized bed and the gradual contraction of ε_0 is observed from the pressure drop profile. It was suggested that in order to define the accurate minimum bubbling point, the highest dense phase expansion from the ε_d and U_d characteristic curve should be used.

The bed expansion characteristic of the natural size, narrow size and bimodal mixtures were studied. For all powders investigated, ε_d increases with U_0 until the minimum bubbling point. After that, ε_d gradually contracts. ε_d continued to decrease after the minimum bubbling point and reached a constant value at approximately 2.5-5 U_{mb}.

The bed voidage ε_0, coincides with ε_d for $U_0 < U_{mb}$ and above the minimum bubbling point, ε_0 continues to increase slightly with U_o and gradually decreases and levels off at very high velocities.

The limiting dense phase voidage, $\varepsilon_{d(Inf)}$ decreases with increase particle size and varies as an exponential function with the particle size for the narrow size cut powders. The empirical correlation of $\varepsilon_{d(inf)}$ and d_p for the narrow size cut can be used to estimate $\varepsilon_{d(inf)}$

of the natural size powder, when there is no fine content in the mixture. For the natural size distribution powder with fines, $\varepsilon_{d(inf)}$ was higher compared to that of the narrow size cut powders. However, for the bimodal mixtures, $\varepsilon_{d(inf)}$ is lower than that of the narrow size cut powders and natural size distribution powders, whether or not the mixtures contain fines.

ε_d and U_d characteristic curve of the bubbling bed is the same as that of the homogeneous bed for all powders. This means that the dense phase behaviour can be obtained from the behaviour of the homogeneous expanded bed.

The minimum bubbling points of the natural size distribution powders, the narrow size cut powders, and the bimodal powders were measured. It was found that the minimum bubbling velocity varies as a quadratic function with d_p, as well as the minimum bubbling voidage for the narrow size cut powders. In comparison with the narrow size cut powders, the minimum bubbling velocity of the natural size distribution powder at different average particle diameter were on the same trend as those of the narrow size cut powders, as long as there was no fine in the mixture. However, natural size powders with fine content give higher minimum bubbling velocity.

Higher minimum bubbling voidages were found for the natural size distribution powder at different average particle diameters, compared to the narrow size powder. The minimum bubbling voidage is even higher, when the powder contains fines. For the bimodal powder, the minimum bubbling voidages were lower than the natural size distribution powder, but they followed the trend of the narrow size cut powders.

The minimum bubbling velocities for the natural size distribution powder were on the same trend of the narrow size cut powder, when there is no fine content in the mixture. With fines in the mixture, the minimum bubbling velocities were higher. For the bimodal powder, the minimum bubbling velocities followed the trend of the narrow size cut powder whether or not the mixture contained fines.

8.5 Drag force correlations and their modification

Drag force is a key parameter in models that describe fluidized beds. With the knowledge of the drag force correlation, the expansion of the dense phase of the homogeneous expanded bed and the bubbling bed can bed described. The drag force correlation is also used to calculate the kinematic wave velocity for the prediction of the minimum bubbling point. The drag force correlations commonly used in CFD simulations were validated in this work with the fixed bed pressure drop, dense phase expansion characteristic and the minimum bubbling point.

The revised Ergun equation (Foscolo et al., 1983) was used to predict the fixed bed pressure drops of all the powders carried out in this work and it was found that the correlation underestimated the fixed bed pressure drop of all powders. Therefore, the revised Ergun equation together with the drag force correlation used in CFD simulation were further validated using the experimental ε_d and U_d characteristic curves.

The literature drag force correlations: the Ergun equation; the Revised Ergun equation; the drag force correlation of Ishii and Zuber, 1979; the drag force correlation developed by Syamlal and O'Brien (1987); and the Richardson and Zaki (1954) correlation, were

used to describe the measured ε_d and U_d characteristic curve of the narrow size powder and the natural size power. It was found that in the case of the particles in suspension, none of the above correlations could describe correctly the ε_d and U_d characteristic curve, unless the modifications were made on the correlations.

The modified Revised Ergun equation and the Richardson and Zaki equation with expansion coefficient obtained from the experimental data were found to describe well the ε_d and U_d characteristic curve. Based on the average value of the exponent m of the narrow size, the following revised Ergun equation was proposed to describe the system of narrow size cut powder and natural size cut powder.

$$\frac{\partial P}{\partial z} = \frac{\rho_f U^2 (1-\varepsilon)}{d_p}\left(\frac{18}{Re_p} + 0.336\right)\varepsilon^{-5.21}$$

In the form of drag force, the correlation can be re-written as;

$$F_D = \frac{3}{4}\frac{\rho_f}{d_p} C_D U^2 (1-\varepsilon)\varepsilon^{-4.21}$$

These equations allow reasonable prediction of the behaviour of all powders investigated, with some deviation for the cases where large fractions of fines are present.

8.6 Prediction of the minimum bubbling point

The recently developed stability criterion of Brandani and Zhang (2004) and the modified drag force correlation were used to predict the minimum bubbling point of the narrow size cut powders. The stability criterion of Brandani and Zang, (2004) using the modified drag force correlation is given by:

$$U_\varepsilon = U_D$$

$$U_\varepsilon = (1-\varepsilon)\left(\frac{\partial U}{\partial \varepsilon}\right)_{Equil} = \frac{1-\varepsilon}{\varepsilon}\cdot\frac{(\beta+1)U}{2+\frac{dC_D}{dRe}\frac{Re}{C_D}}$$

$$U_D = \sqrt{V^2 - G} + V$$

Where $\beta = 4.21$ and Dallavalle (1948) equation is used for the drag coefficient.

$$C_D = \left(0.63 + \frac{4.8}{\sqrt{Re_p}}\right)^2$$

$$V = \frac{1-\varepsilon}{\varepsilon}\frac{\rho_f U}{\varepsilon\rho_p + (1-\varepsilon)\rho_f}$$

$$G = \frac{\frac{1-\varepsilon}{\varepsilon^2}\rho_f U^2 - \delta[(1-\varepsilon)\rho_p + \varepsilon\rho_f]g}{\varepsilon\rho_p + (1-\varepsilon)\rho_f}$$

δ/d_p was found to be an exponential function with the voidage and the empirical correlation was proposed.

$$\frac{\delta}{d_p} = 0.65 + 3.82\,e^{-37.7(\varepsilon-\varepsilon_{mf})}$$

The criterion was then used to predict the minimum bubbling point of the natural size powders and the bimodal powders and good agreement was found with the experimental results for the bimodal mixture.

The new stability criterion was tested with a detailed comparison with 700 minimum bubbling points taken from literature. The criterion can predict very well the minimum bubbling voidage for various operating conditions of rigid non-porous materials. The model prediction of the minimum bubbling velocity is good. It was noted that the

minimum bubbling velocity is more subject to uncertainty than the bed voidage at minimum bubbling.

8.7 Future work

- More experimental investigations should be carried out to extend the understanding of the influence of type of particle size distribution on the fluidization characteristic, as well as the effect of fines.
- Experimental investigations on the effect of size, size distribution and fines should also be extended to cover various types of powders, especially porous materials, which have many industrial applications.
- The modified drag force correlation proposed in this work should be validated with more ε_d and U_d characteristic curves of more types of size distributions and more type of powders from the experiments mentioned. This is to ascertain that drag forces can generally describe with various types of powders. In particular the drag force correlation should be extended to cover the transition and inertial flow regimes.
- The drag force correlation and the voidage dependency of the characteristic dimension δ should be implemented in CFD simulations to compare the full model predictions in 2- and 3-D with experimental results.

References

Abrahamsen A.R. & Geldart D., *Behaviour of gas-fluidized beds of fine powders part I. Homogeneous expansion,* Powder Technology, vol. 26, no. 1, pp. 35-46, 1980a.

Abrahamsen A.R. & Geldart D., *Behaviour of gas-fluidized beds of fine powders part II. Voidage of the dense phase in bubbling beds*, Powder Technology, vol. 26, no. 1, pp. 47-55, 1980b.

Allen T., *Particle size measurement*, 4th ed., Chapman and Hall, 1990

Andersson K.E.B., *Pressure drop in ideal fluidization*, Chemical Engineering Science, vol. 15, pp. 276-297, 1961.

Anderson T.B. & Jackson R., *A fluid mechanic description of fluidized beds*, Industrial & Engineering Chemistry Fundamentals, vol. 47, no. 5, p. 527, 1967.

Barreto G.F., Yates J.G. & Rowe P.N., *The measurement of emulsion phase voidage in gas fluidized beds of fine powders*, Chemical Engineering Science, vol. 38, no. 3, pp. 345-350, 1983.

Barreto G.F., *Behaviour of beds of fine powders fluidized by gases at pressures up to 20 bar*, PhD Thesis, University of London, London, 1984.

Barreto G.F., Mazza G.D., & Yates J.G., *The significance of bed collapse experiments in the characterization of fluidized beds of fine powders*, Chemical Engineering Science, vol. 43, no. 11, pp. 3037-3047, 1988.

Bridgwater J., *Spouted bed*, in Fluidization, 2 edn, J.F.Davidson, R.Clift, & D.Harrison, eds., Academic Press, London, pp. 201-224, 1985.

Brandani S. & Foscolo P.U., *Analysis of discontinuities arising from the one-dimensional equations of change for fluidization*, Chemical Engineering Science, vol. 49, no. 5, pp. 611-619, 1994.

Brandani S. & Astarita G., *Analysis of the discontinuities in magnetized bubbling fluidized beds*, Chemical Engineering Science, vol. 51, no. 20, pp. 4631-4637, 1996.

Brandani S. and Zhang K., *A model for the prediction of the behaviour of fluidized Beds*. AIChE Annual Meeting, Austin, TX, USA, Nov. 7-12, 2004. (Powder Technology, in press, 2006)

Brandani S. *The kinematic theory of fluidized bed expansion and contraction.* AIChE Annual Meeting, Cincinnati, OH, USA, Oct. 30- Nov. 4, 2005.

Carman P.C. *Fluid flow through granular beds.*Trans. Inst. Chem. Eng., vol. 15, 150, 1937.

Cheremisinoff N.P., *Review of experimental methods for studying the hydrodynamics of gas-solid fluidized beds*, Industrial & Engineering Chemistry: Process Design and Development, vol. 25, no. 2, pp. 329-351, 1986.

Crowther M.E. & Whitehead J.C., *Fluidisation of fine particles at elevated pressure*, in Fluidization: Proceedings of Engineering Foundation Conference, England, 2 edn, J.F.Davidson & D.L.Keairns, eds., Cambridge University Press, Cambridge, pp. 65-70, 1978.

Dallavalle J.M., *Micromeritics*, Pitman, 1948.

De Jong J.A.H. & Nomden J.F., *Homogeneous gas-solid fluidization*, Powder Technology, vol. 9, pp. 91-97, 1974.

Delebarre A., Morales J. & Ramos L., *Influence of the bed mass on its fluidization characteristics*, Chemical Engineering Science, vol. 98, pp. 81-88, 2004.

Di Felice R., *The void function for fluid-particle interaction systems*, International Journal of Multiphase Flow, vol. 20, pp. 153-159, 1994.

Donsi G. & Massimilla L., *Bubble-free expansion of gas fluidized beds of fine particles*, AIChE Journal, vol. 19, no. 6, pp. 1104-1110, 1973.

Dry R.J., Judd M.R. & Shingles T., *Two-phase theory and fine powders*, Powder Technology, vol. 34, no. 2, pp. 213-223, 1983.

Epstein N., *Comments on a unified model for particulate expansion of fluidized beds and flow in fixed porous media*, Chemical Engineering Science, vol. 39, no. 10, pp. 1533-1534, 1984.

Ergun S., *Fluid flow through packed columns*, Chemical Engineering Progress, vol. 48, no. 2, pp. 89-94, 1952.

Foscolo P.U., Gibilaro L.G. & Waldram S.P., *A unified model for particulate expansion for fluidised beds and flow in fixed porous media*, Chemical Engineering Science, vol. 38, no. 8, pp. 1251-1263, 1983.

Foscolo P.U., Gibilaro L.G., Waldram S.P. & Di Felice R., *The effect of interparticle forces on the stability of fluidized beds*, Chemical Engineering Science, vol. 40, no. 12, pp. 2379-2381, 1985.

Foscolo P.U. & Gibilaro L.G., *Fluid dynamic stability of fluidised suspensions: the particle bed model*, Chemical Engineering Science, vol. 42, no. 6, pp. 1489-1500, 1987.

Foscolo P.U., Di Felice R. & Gibilaro L.G., *An experimental study of the expansion characteristics of gas fluidized beds of fine catalysts*, Chemical Engineering Progress, vol. 22, pp. 69-78, 1987.

Foscolo P.U., Di Felice R. & Gibilaro L.G., *The pressure field in an unsteady-stage fluidized bed*, AIChE Journal, vol. 35, no. 12, pp. 1921-1926, 1989.

Foscolo P.U., Gibilaro L.G. & Di Felice R., *Hydrodynamic scaling relationships for fluidisation*, Applied Science Research, vol. 56, pp. 21-29, 1991.

Garside J. & Al-Dlbouni M.R., *Velocity-voidage relationships for fluidization and sedimentation in solid-liquid systems*, Industrial & Engineering Chemistry: Process Design and Development, vol. 16, no. 2, pp. 206-214, 1977.

Geldart D., *The effect of particle size and size distribution on the behaviour of gas-fluidised beds*, Powder Technology, vol. 6, pp. 201-215, 1972.

Geldart D., *Type of gas fluidization*, Powder Technology, vol. 7, pp. 285-292, 1973.

Geldart D. & Abrahamsen A.R., *Homogeneous fluidization of fines powders using various gases and pressures*, Powder Technology, vol. 19, pp. 133-136, 1978.

Geldart D. & Wong A.C.Y., *Fluidization of powders showing degrees of cohesiveness- I Bed expansion*, Chemical Engineering Science, vol. 39, no. 10, pp. 1481-1488, 1984.

Geldart D., *Gas fluidization technology*, Wiley, Chester, 1986.

Geldart D. & Buczek B., *The effect of the size of the fines on the fluidization behaviour of equilibrium cracking catalyst*, in Fluidization VI: Proceedings of the International

Conference on Fluidization, *Canada*, J.R.Grace, L.W.Shemilt, & M.A.Bergougnou, eds., Engineering Foundation, New York, pp. 179-186, 1989.

Gelderbloom S.J., Gidaspow D. & Lyczkowski R.W., *CFD Simulations of bubbling/collapsing fluidized beds for three Geldart groups*, AIChE Journal, vol. 49, no. 4, pp. 844-858, 2003.

Gibilaro L.G., Waldram S.P. & Foscolo P.U., *A simple mechanistic description of the unsteady state expansion of liquid fluidised beds*, Chemical Engineering Science, vol. 39, no. 3, pp. 607-610, 1984.

Gibilaro L.G., Di Felice R., Waldram S.P. & Foscolo P.U., *Generalized friction factor and drag coefficient correlations for fluid-particle interactions*, Chemical Engineering Science, vol. 40, no. 10, pp. 1817-1823, 1985.

Gibilaro L.G., *Fluidization-Dynamics*, Butterworth, Oxford, 2001.

Godard K. & Richardson J.F., *The behaviour of bubble-free fluidised bed*, Institute of Chemical Engineering Symposium Series, vol. 30, pp. 126-135, 1968.

Guedes de Carvalho J.R.F., *Dense phase expansion in fluidized beds of fine particles*, Chemical Engineering Science, vol. 36, pp. 413-416, 1981.

Harrison D., Davidson J.F. & de Kock J.W., *On the nature of aggregative and particulate fluidization*, Transaction Institute of Chemical Engineers, vol. 39, pp. 202-211, 1961.

Ishii M. & Zuber N., *Drag coefficient and relative velocity in bubbly, droplet or particulate flows*, AIChE Journal, vol. 25, no. 5, pp. 843-855, 1979.

Jackson R., *The mechanics of fluidized beds: Part 1. The stability of the state of uniform fluidization*, Transaction Institute of Chemical Engineers, vol. 41, pp. 13-21, 1963.

Jackson R., *The nature and role of effective stress in fluidized systems*, in Fluidization IX, Proceedings of the ninth engineering foundation conference on fluidization, Colorado, USA, L.Fan & T.Knowlton, eds., Engineering foundation, New York, pp. 1-13, 1998.

Jacob K.V. & Weimer A.W., *High-pressure particulate expansion and minimum bubbling of fine carbon powders*, AIChE Journal, vol. 33, no. 10, pp. 1698-1706, 1987.

Jean R. & Fan L., *On the model equations of Gibilaro and Foscolo with corrected buoyancy force*, Powder Technology, vol. 72, pp. 201-205, 1992.

Kai T., Wakiri A. & Takahashi T., *Emulsion phase expansion and sedimentation velocity in fluidized beds of fine particles*, Journal of Chemical Engineering of Japan, vol. 20, no. 3, pp. 282-286, 1987.

Kai T. & Takahashi T., *A model for predicting the relationship between maximum voidage in homogeneous fluidization and emulsion phase voidage in bubbling fluidization*, Journal of Chemical Engineering of Japan, vol. 22, no. 4, pp. 334-340, 1989.

Khan A.R. & Richardson J.F., *Fluid-particle interactions and flow characteristics of fluidized beds and settling suspensions of spherical particles*, Chemical Engineering Communications, vol. 78, pp. 111-130, 1989.

Khoe G.K., Ip T.L. & Grace J.R., *Rheological and fluidization behaviour of powders of different particle size distribution*, Powder Technology, vol. 66, no. 2, pp. 127-141, 1991.

King D.F. & Harrison D., *The dense phase of a fluidized bed at elevated pressures*, Transaction Institute of Chemical Engineers, vol. 60, pp. 26-30, 1982.

Kono H.O., Chiba S., Ells T., Daniell P. & Suzuki M., *Aerated fine particle system: homogeneous and bubbling fluidization and segregation*, in Fluidization: World Congress III of Chemical Engineering, Tokyo, pp. 453-456, 1986.

Kono H.O., Ells T.S., Chiba S., Suzuki M. & Morimoto E., *Quantitative criteria for emulsion phase characterization and for the transition between particulate and bubbling fluidization*, Powder Technology, vol. 52, no. 1, pp. 69-76, 1987.

Kono H.O., Aksoy E. & Itani Y., *Measurement and application of the theological parameters of aerated fine powders- a novel characterization approach to powder flow properties*, Powder Technology, vol. 81, pp. 177-187, 1994.

Kunii D. & Levenspiel O., *Fluidization Engineering*, Wiley, New York, 1969.

Lettieri P., Yates J.G. & Newton D., *The influence of interparticle forces on the fluidization behaviour of some industrial materials at high temperature*, Powder Technology, vol. 110, no. 1-2, pp. 117-127, 2000.

Lettieri P., Brandani S., Yates J.G. & Newton D., *A generalization of the Foscolo and Gibilaro particle-bed model to predict the fluid bed stability of some fresh FCC catalysts at elevated temperatures*, Chemical Engineering Science, vol. 56, no. 18, pp. 5401-5412, 2001.

Lettieri P., Newton D. & Yates J.G., *Homogeneous bed expansion of FCC catalysts, influence of temperature on the parameters of the Richardson and Zaki equation*, Powder Technology, vol. 123, pp. 221-231, 2002.

Lim K.S., Zhu J.X. & Grace J.R., *Hydrodynamics of gas-solid fluidization*, International Journal of Multiphase Flow, vol. 21, pp. 141-193, 1995.

Makkawi Y.T. & Wright P.C., *The voidage function and effective drag force for fluidized beds*, Chemical Engineering Science, vol. 58, pp. 2035-2051, 2003.

Massimilla L., Donsi G. & Zucchini C., *The structure of bubble-free gas fluidized beds of fine fluid cracking catalyst particles*, Chemical Engineering Science, vol. 27, pp. 2005-2015, 1972.

Marzocchella A. & Salatino P., *Fluidization of solids with CO2 at pressures from ambient to supercritical*, AIChE Journal, vol. 46, no. 5, pp. 901-910, 2000.

Mazumadar P. & Ganguly U.P., *Effect of aspect ratio on bed expansion in particulate fluidization*, The Canadian Journal of Chemical Engineering, vol. 63, pp. 850-852, 1985.

Mostoufi N. & Chaouki J., *Prediction of effective drag coefficient in fluidized beds*, Chemical Engineering Science, vol. 54, pp. 851-858, 1999.

Murray J.D., *On the mathematics of fluidization: Part 1. Fundamental equations and wave propagation*, Journal of Fluid Mechanics, vol. 20, no. 3, pp. 465-493, 1965.

Mutsers S.M.P. & Rietema K., *The effect of interparticle forces on the expansion of a homogeneous gas-fluidized bed*, Powder Technology, vol. 18, no. 2, pp. 239-248, 1977a.

Mutsers S.M.P. & Rietema K., *Gas–solids fluidization in a centrifugal field. The effect of gravity upon bed expansion*, Powder Technology, vol. 18, no. 2, pp. 249-256, 1977b.

Nie Y. & Liu D., *Dynamics of collapsing fluidized beds and its application in the simulation of pulsed fluidized beds*, Powder Technology, vol. 99, no. 2, pp. 132-139, 1998.

Park J.J., Park J.H., Chang I.S., Kim S.D. & Choi C.S., *A new bed-collapsing technique for measuring the dense phase properties of gas-fluidized beds*, Powder Technology, vol. 66, no. 3, pp. 249-257, 1991.

Piepers H.W., Cottaar E.J.E., Verkooijen A.H.M. & Rietema K., *Effects of pressure and type of gas on particle-particle interaction and the consequences for gas-solid fluidization behaviour*, Powder Technology, vol. 37, no. 1, pp. 55-70, 1984.

Pigford R.L. & Baron T., *Hydrodynamic Stability of a Fluidized Bed*, Industrial & Engineering Chemistry Fundamentals, vol. 4, no. 1, pp. 81-87, 1965.

Poletto M., Salatino P. & Massimilla L., *Fluidization of solids with CO2 at pressures and temperatures ranging from ambient to nearly critical conditions*, Chemical Engineering Science, vol. 48, no. 3, pp. 617-621, 1993.

Rapagna S., Di Felice R., Foscolo P.U. & Gibilaro L.G., *Experimental verification of the scaling rules for fine powder fluidization*, in Fluidization VII, Brisbane, O.E.Potter & D.J.Nicklin, eds., United Engineering Foundation, New York, pp. 579-589, 1992.

Richardson J.F. & Zaki W.N., *The sedimentation of a suspension of uniform spheres under conditions of viscous flow*, Chemical Engineering Science, vol. 3, pp. 65-73, 1954.

Rietema K., *Application of mechanical stress theory to fluidization*, in Proceedings of the International Symposium on Fluidization, Eindhoven, Netherlands, University Press, Amsterdam, pp. 154-175, 1967.

Rietema K., *The effect of interparticle forces on the expansion of a homogeneous gas-fluidised bed*, Chemical Engineering Science, vol. 28, no. 7, pp. 1493-1497, 1973.

Rietema K. & Mutsers S.M.P., *The effect of gravity upon the stability of a homogeneously fluidized bed, investigated in a centrifugal field*, in Fluidization: Proceedings of Engineering Foundation Conference, England, J.F.Davidson & D.L.Keairns, eds., Cambridge University Press, Cambridge, pp. 81-86, 1978.

Rietema K. & Piepers H.W., *The effect of interparticle forces on the stability of gas-fluidized beds–I. Experimental evidence*, Chemical Engineering Science, vol. 45, no. 6, pp. 1627-1639, 1990.

Rowe P.N., *Drag forces in a hydraulic model of a fluidized bed: I*, Transaction Institute of Chemical Engineers, vol. 39, pp. 175-180, 1961.

Rowe P.N., Santoro L. & Yates J.G., *The division of gas between bubble and interstitial phases in fluidised beds of fine powders*, Chemical Engineering Science, vol. 33, pp. 133-140, 1978.

Simone S. & Harriott P., *Fluidization of fine powders with air in the particulate and the bubbling regions*, Powder Technology, vol. 26, pp. 161-167, 1980.

Slis P.L., Willemse T.H.W. & Kramers H., *The response of the level of a liquid fluidized bed to a sudden change in the fluidizing velocity*, Applied Science Research, no. 8, pp. 209-218, 1959.

Smolders K. & Baeyens J., *Gas fluidized beds operating at high velocities: a critical review of occurring regimes*, Powder Technology, vol. 119, no. 2-3, pp. 269-291, 2001.

Sobreiro L.E.L. & Monteiro J.L.F., *The effect of pressure on fluidized bed behaviour*, Powder Technology, vol. 33, pp. 95-100, 1982.

Srivastava A. & Sundaresan S., *Role of wall friction in fluidization and stand pipe flow*, Powder Technology, vol. 124, pp. 45-54, 2002.

Toomy R.D. & Johnstone H.F., *Gaseous fluidization of solid particles*, Chemical Engineering Progress, vol. 48, no. 5, pp. 220-226, 1952.

Tung Y. & Kwauk M., *Dynamic of collapsing fluidized beds*, in Fluidization Science and Technology, M.Kwauk & D.Kunii, eds., Gordon and Breach, New York, pp. 155-166, 1982.

Van Wachem B.G.M., Schouten J.C., Van den Bleek C.M., Krishna R. & Sinclair J.L., *Comparative analysis of CFD models of dense gas-solid systems*, AIChE Journal, vol. 47, no. 5, pp. 1035-1051, 2001.

Verloop J. & Heertjes P.M., *Shock waves as a criterion for the transition from homogeneous to heterogeneous fluidization*, Chemical Engineering Science, vol. 25, no. 5, pp. 825-832, 1970.

Vogt C., Schreiber R., Werther J. & Brunner G., *Fluidization at supercritical fluid conditions, in Fluidization X Proceeding of the Tenth Engineering Foundation Conference of Fluidization, China*, M.Kwauk, J.Li, & W.Yang, eds., United Engineering Foundation, New York, pp. 117-124, 2001.

Wallis G.B., *One-dimensional waves*, Mcgraw-Hill, New York; Maidenhead, 1969.

Wen C.Y. & Yu Y.H., *Mechanics of fluidization*, Chemical Engineering Progress Symposium Series, vol. 62, no. 62, pp. 100-110, 1966.

Xie H.Y. & Geldart D., *Fluidization of FCC powders in the bubble-free regime: effect of types of gases and temperature*, Powder Technology, vol. 82, no. 3, pp. 269-277, 1995.

Yadav N.K., Kulkarni B.D. & Doraiswamy L.K., *Experimental evaluation and modelling of agglomerating fine powders fluidized beds*, Industrial & Engineering Chemistry Research, vol. 33, pp. 2412-2420, 1994.

Appendix A: Particle size and density analysis

1. Particle size measurements and size analysis

The particle size measurements were carried out using sieve analysis and laser light scattering methods.

Sieve analysis; sieve series are arranged so that the aperture size is on consecutive $2^{1/4}$ U.K. British standard (B.S.) screens. The powder is divided into narrow size fractions with mass fraction x_i of size d_{Pi}. The surface to volume average diameter can be defined as:

$$d_P = \frac{1}{\sum x_i / d_{Pi}}$$

d_{Pi} = (Lower sieve aperture size + Upper sieve aperture size)/2

For spherical particles, the surface to volume diameter of the individual size cute is equal to d_{Pi} (Abrahamsen and Geldart, 1980a).

Generally, it is difficult to obtain accurate results through sieving for particle sizes below 40 μm because of the very fine particles become cohesive and tend also to adhere

to the wires of the mesh. For these particles the laser light scattering technique is often preferred since it can give a more accurate size analysis.

Laser light scattering method; the particles are suspended in de-ionized water. The suspension is held across the path of a laser light beam and the scattered light is collected by an array of photo-detectors, positioned perpendicular to the optical axis. The scattered light distribution is sampled and processed using appropriate scatter analysis software which can yield particle size information over the range 0.1-600 μm. (Allen, 1990)

2. Particle size distribution and particle size

2.1 Particle size distributions of natural size ballotini powders (Figure A1 – A5)

The particle size distribution from the sieve analysis for the natural size powders are shown in Figure A1 to Figure A5

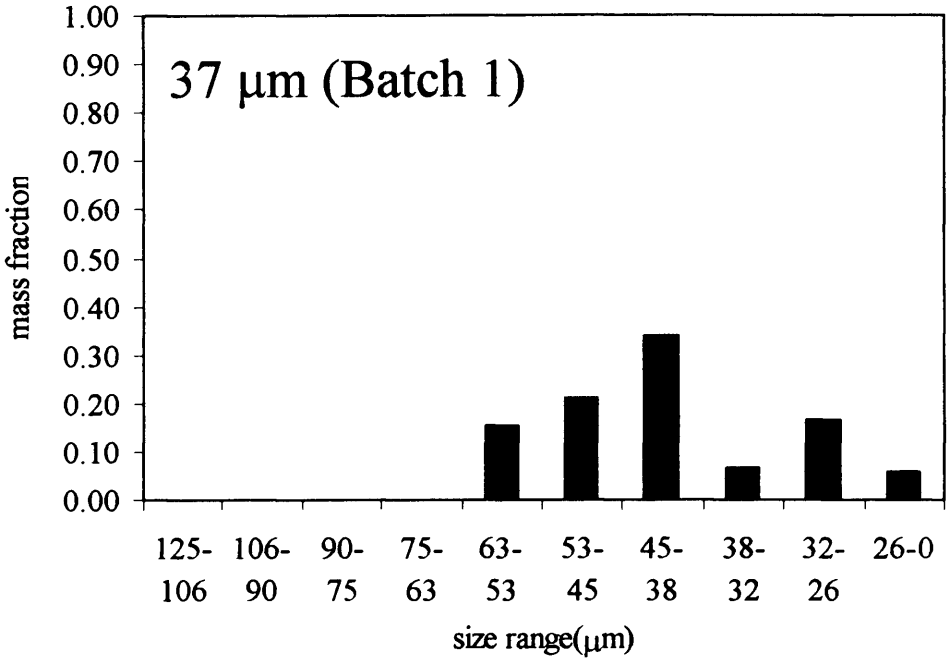

Figure A1 Particle size distribution of mixed size ballotini 37 μm (Batch 1)

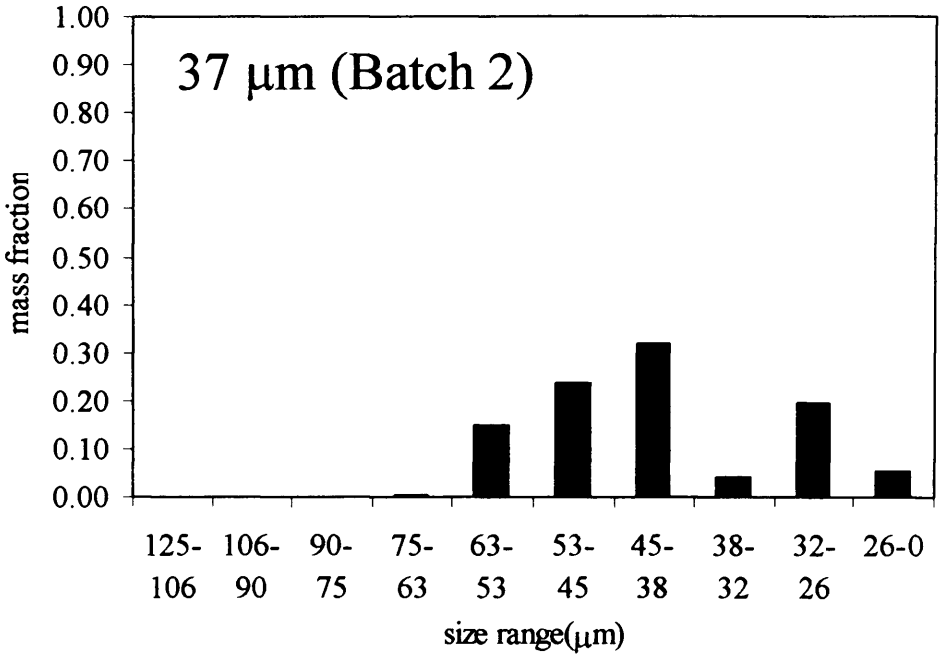

Figure A2 Particle size distribution of mixed size ballotini 37 μm (Batch 2)

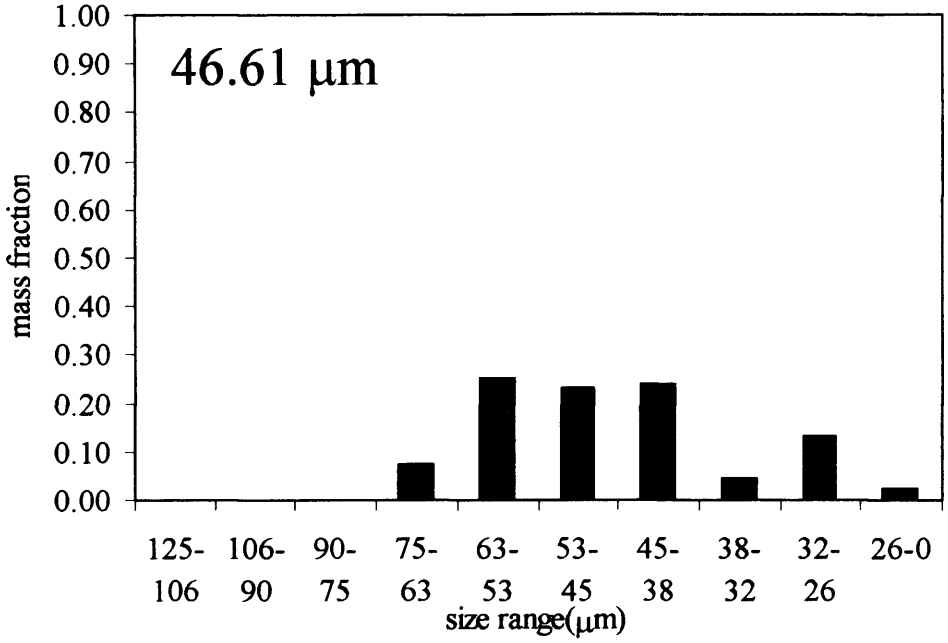

Figure A3 Particle size distribution of mixed size ballotini 46.61 μm

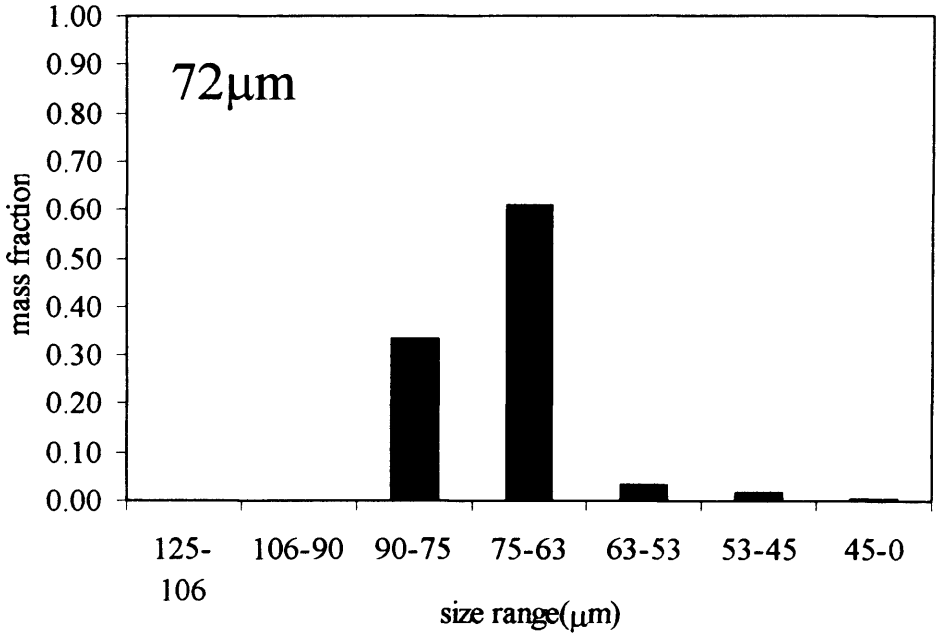

Figure A4 Particle size distribution of mixed size ballotini 72 μm

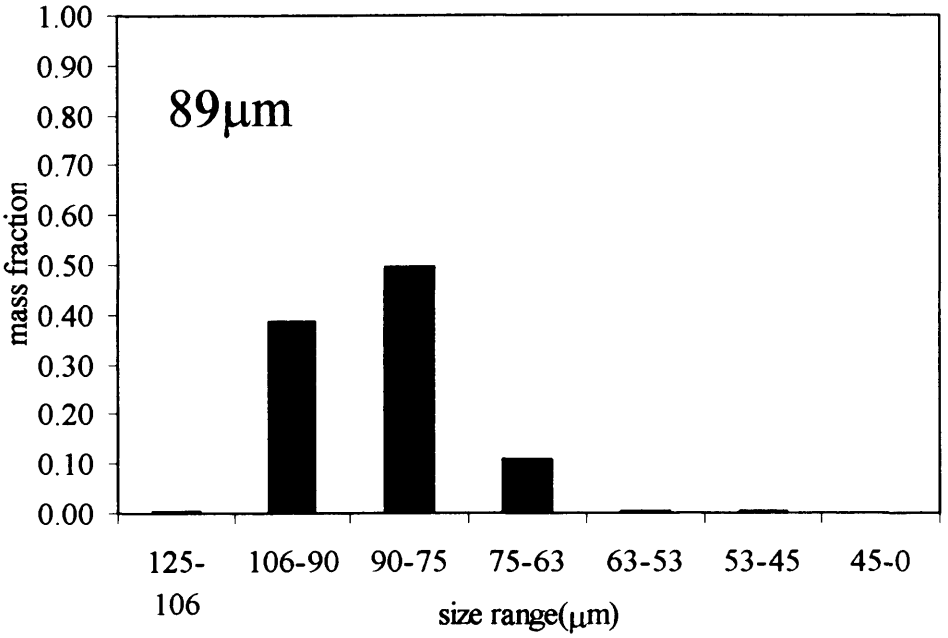

Figure A5 Particle size distribution of mixed size ballotini 89 μm

2.2 Particle size distribution of narrow cut ballotini powders (Figure A6 – A11)

The particle size distribution from the sieve analysis for the narrow cut powders are shown in Figure A6 to Figure A11

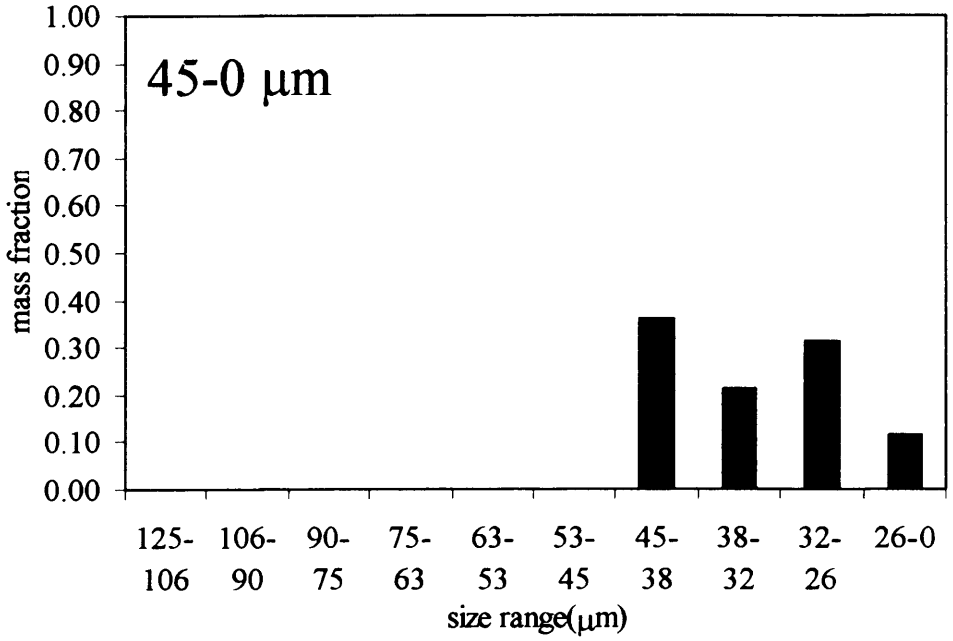

Figure A6 Particle size distribution of narrow size ballotini 45-0 μm

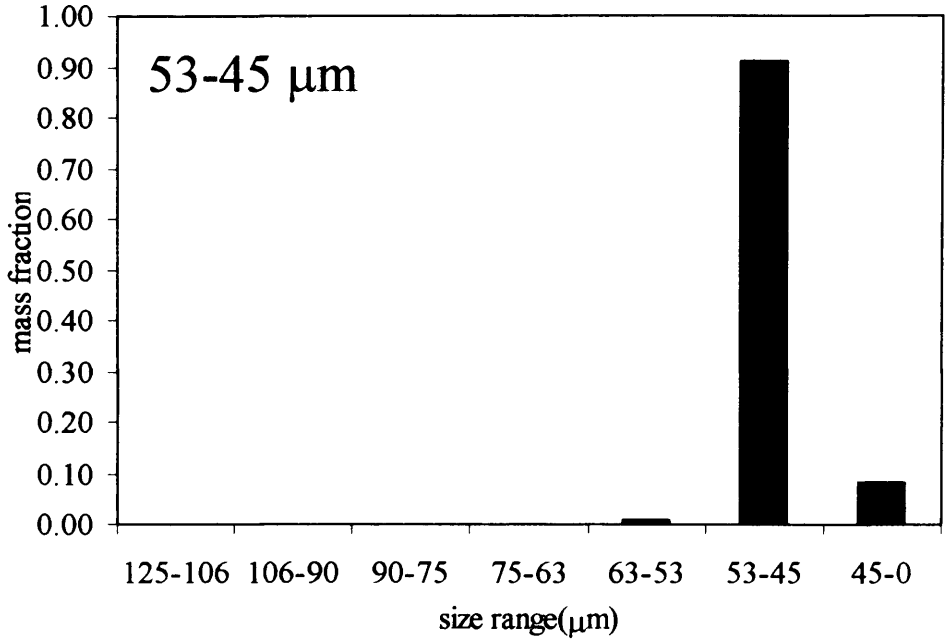

Figure A7 Particle size distribution of narrow size ballotini 53-45 μm

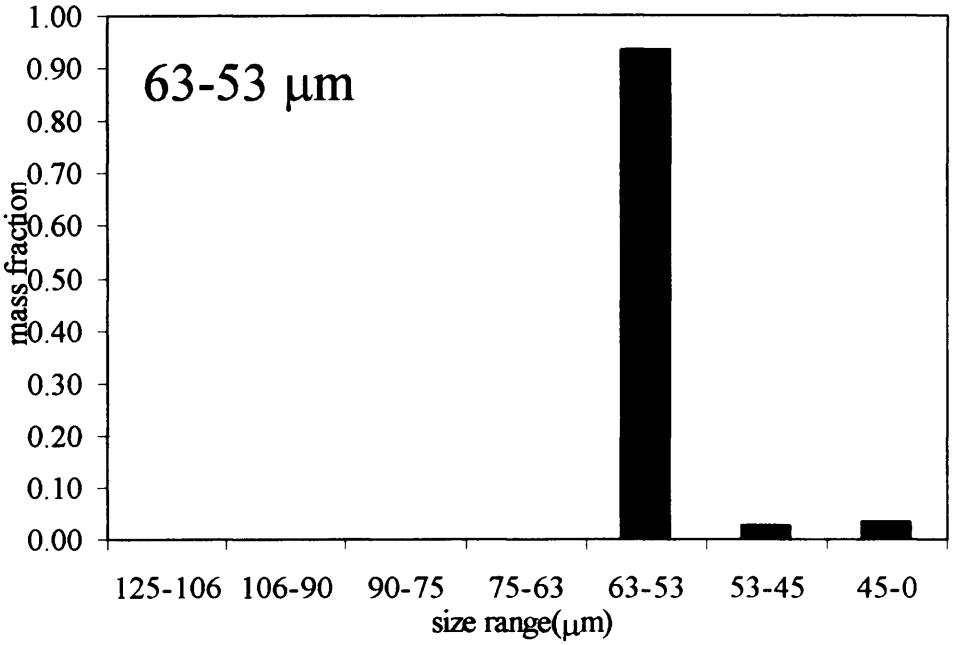

Figure A8 Particle size distribution of narrow size ballotini 63-53 μm

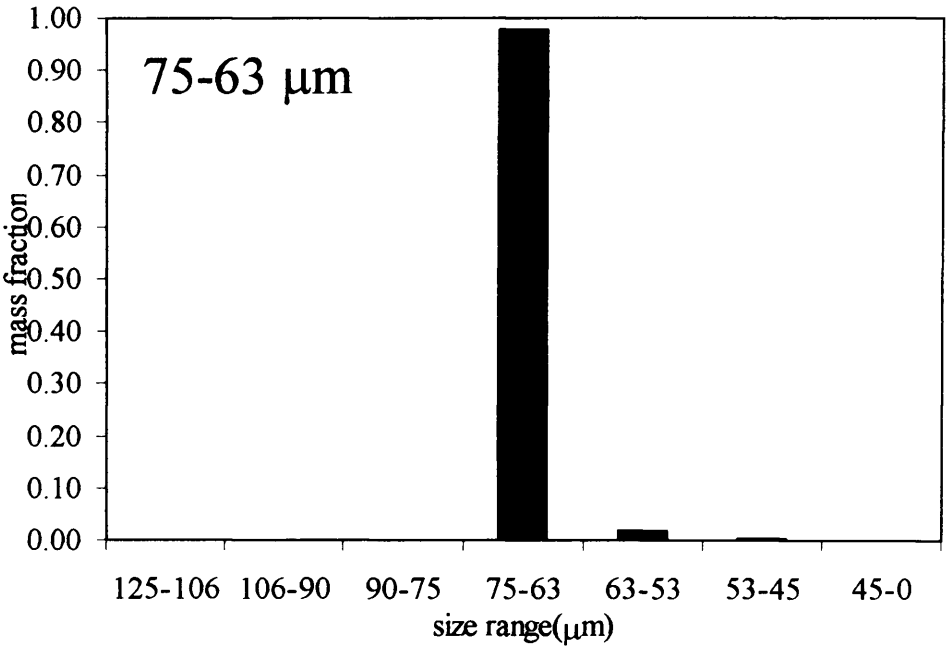

Figure A9 Particle size distribution of narrow size ballotini 75-63 μm

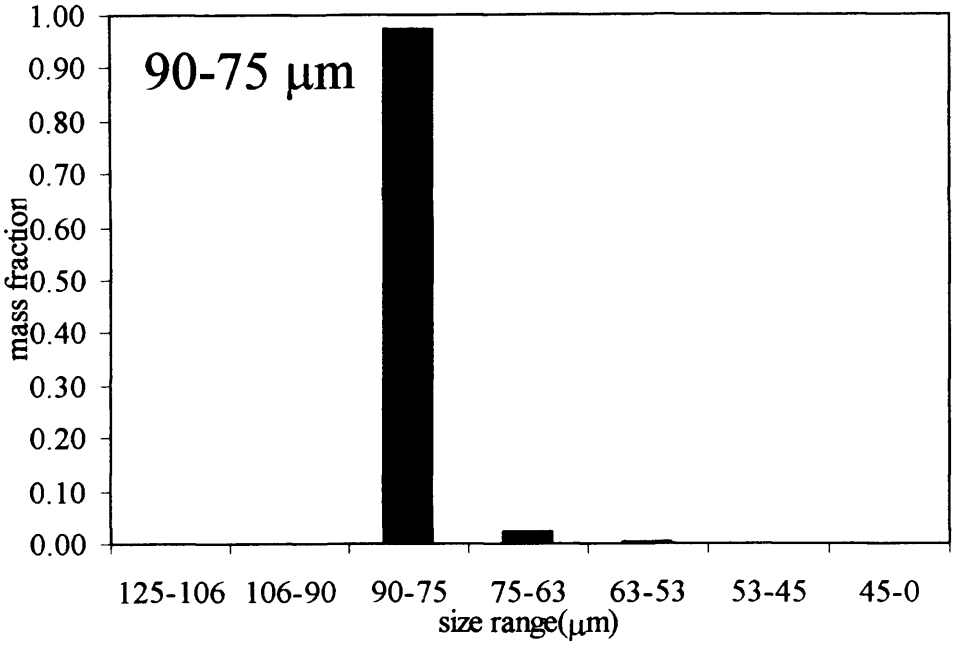

Figure A10 Particle size distribution of narrow size ballotini 90-75 μm

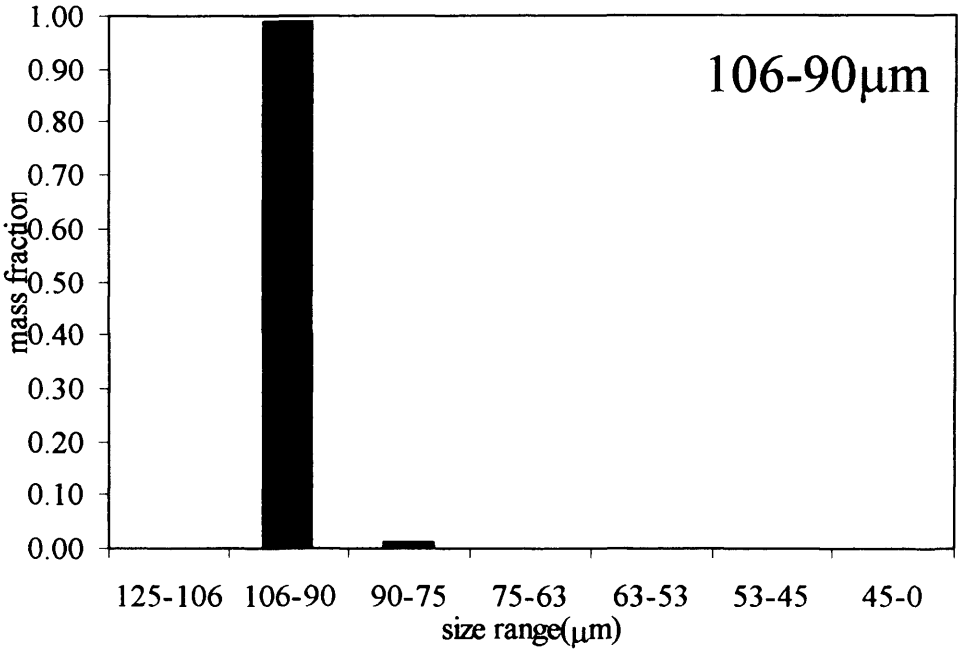

Figure A11 Particle size distribution of narrow size ballotini 106-90 μm

Table A1and Table A2 shows the average particle size (d_P) of the natural size distribution ballotini and narrow size cut ballotini powders from the sieve analysis and the laser light scattering method. It was found that average particles, analysed from the two methods gave similar results. The particle size difference from these two methods is within 3 μm and becomes slightly larger, 5 μm, for the smaller particle size range of 0-45 μm. As a result, the average particle sizes were calculated based on the size analysis obtained from sieving method, except for the fine particles in the 0-45 μm range where the light scattering results were used.

Table A1 Average size (d_P) of the natural size ballotini

Powder	d_P (μm) In use	d_P (μm) from Sieve analysis	d_P (μm) from laser light scattering method
37 μm (Batch 1)	37	36.54	38.82
37 μm (Batch 2)	37	37.98	38.00
46.61 μm	46.61	43.96	46.61
72 μm	72	71.93	69.27
89 μm	89	89.16	88.92

Table A2 Average size (d_P) of the narrow size cut ballotini

Powder	d_P (μm) In use	d_P (μm) from Sieve analysis	d_P (μm) from laser light scattering method
45-0 μm	33.50	28.96	33.83
53-45 μm	45.10	45.10	47.53
63-53 μm	55.08	55.08	55.32
75-63 μm	68.41	68.41	66.02
90-75 μm	81.81	81.81	79.57
106-75 μm	97.82	97.82	94.47

3. Particle density measurement

A 50 ml density bottle was used to measure particle density. Distilled water was used as a medium and from a series of measurements the particle density was found to be 2480 kg/m^3.

The procedures of the density measurement are as follows;

- Weigh the empty and dry bottle (W_B)
- Weigh the powder (W_P)
- Load the powder in the bottle
- Weigh the powder and bottle (W_{B+P})

- Fill the bottle with the distilled water until it is full. Make sure that there is no bubble inside the bottle
- Close the cap and dry the external part
- Weigh the bottle again (W_{B+P+W})
- Empty the content and rinse it thoroughly
- Fill empty bottle with distilled water, dry the external part and weigh it (W_{B+W}).
- Powder density calculation

Weight of 50 ml water = $W_{B+W} - W_B$

Volume of 50 ml water = $W_{B+W} - W_B$ / water density

Weight of the water in the bottle with powder = $W_{B+P+W} - W_{B+P}$

Volume of water in the bottle with powder = $(W_{B+P+W} - W_{B+P})$/water density

Volume of powder = $[W_{B+W} - W_B$ / water density$]$- $[(W_{B+P+W} - W_{B+P})$/water density$]$

Density of powder = W_P/volume of powder

Appendix B: Pressure Transducer Calibration

1. Pressure transducer A (0-13.79 kPa)

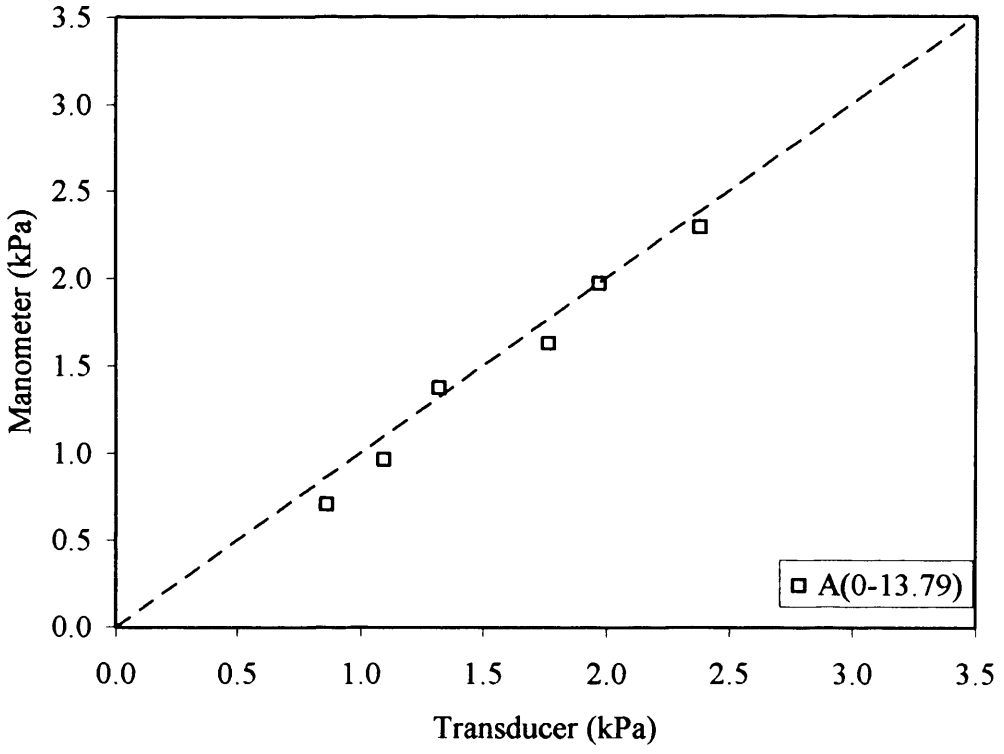

Figure B.1 Pressure transducer A calibration

2. Pressure transducer B (+/-0.50 kPa)

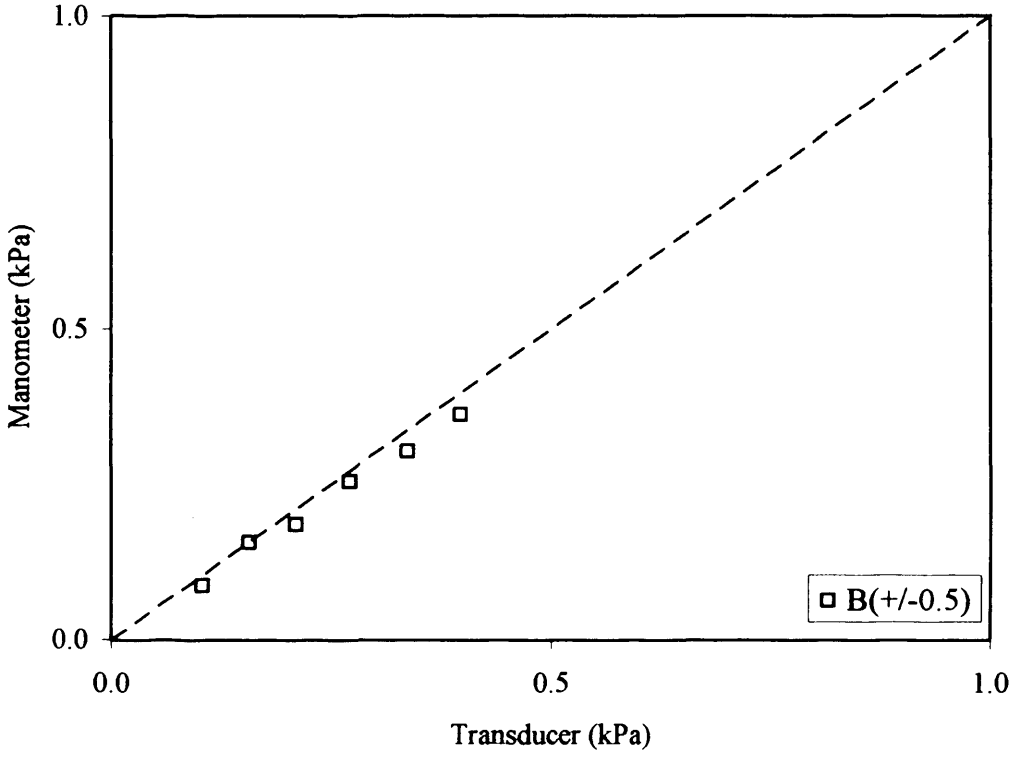

Figure B.2 Pressure transducer B calibration

3. Pressure transducer C (0-1 kPa)

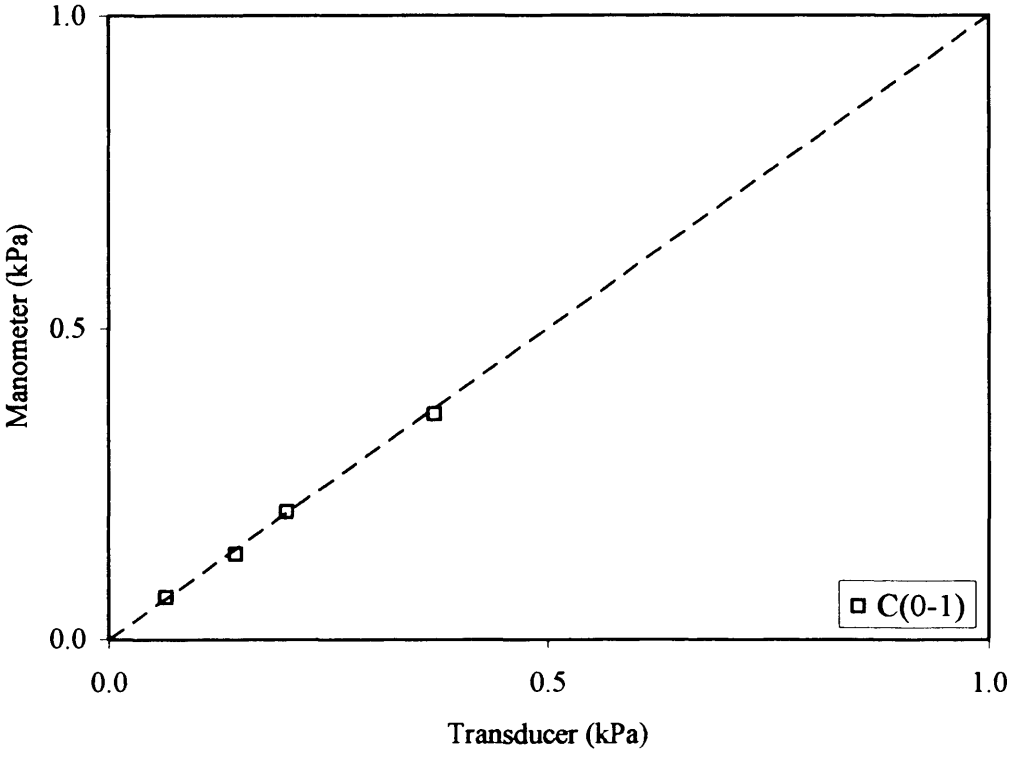

Figure B.3 Pressure transducer C calibration

4. Pressure transducer D (0-1 kPa)

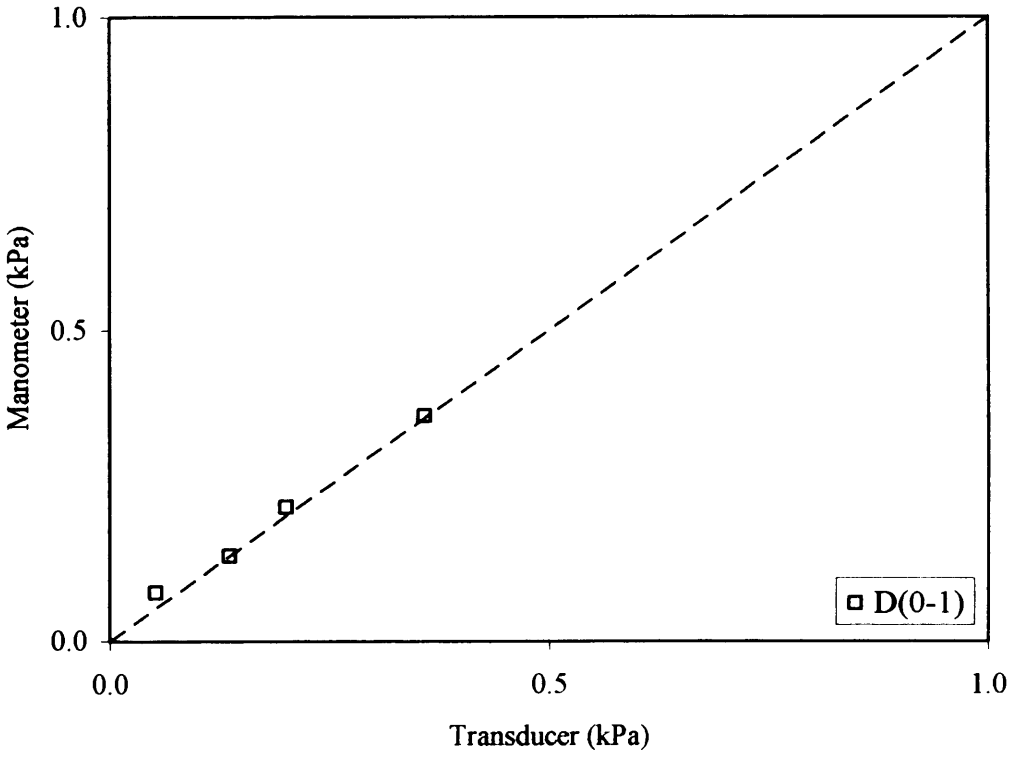

Figure B.4 Pressure transducer D calibration

5. Pressure transducer E (+/-1.49 kPa)

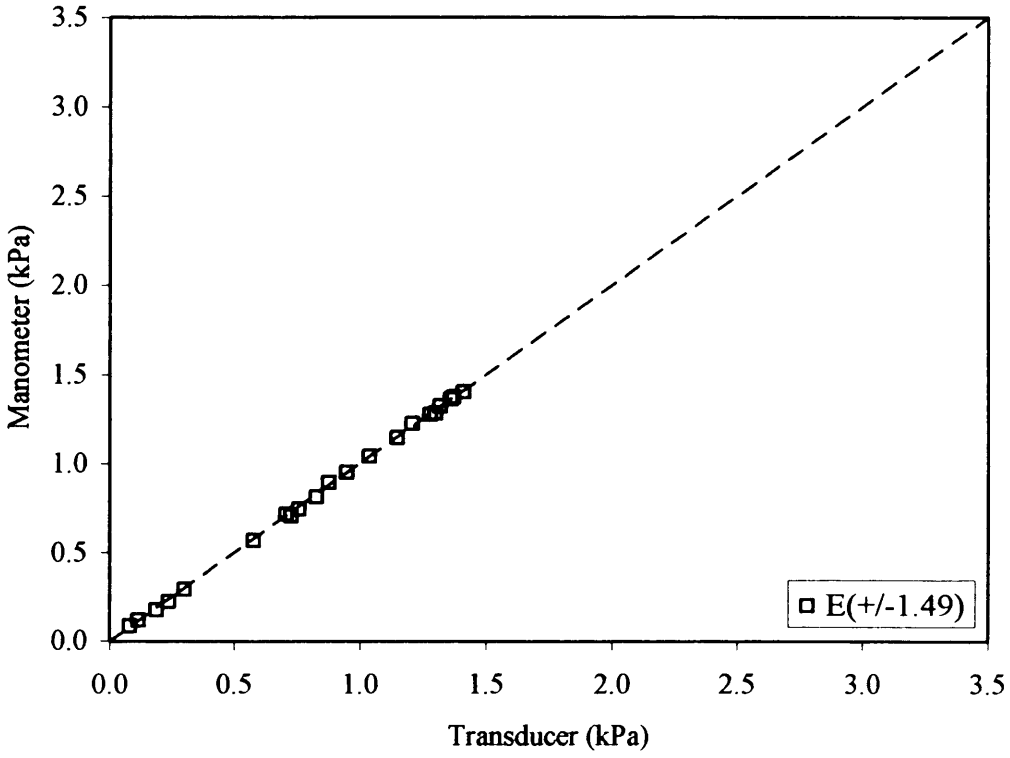

Figure B.5 Pressure transducer E calibration

6. Pressure transducer F (+/-1.49 kPa)

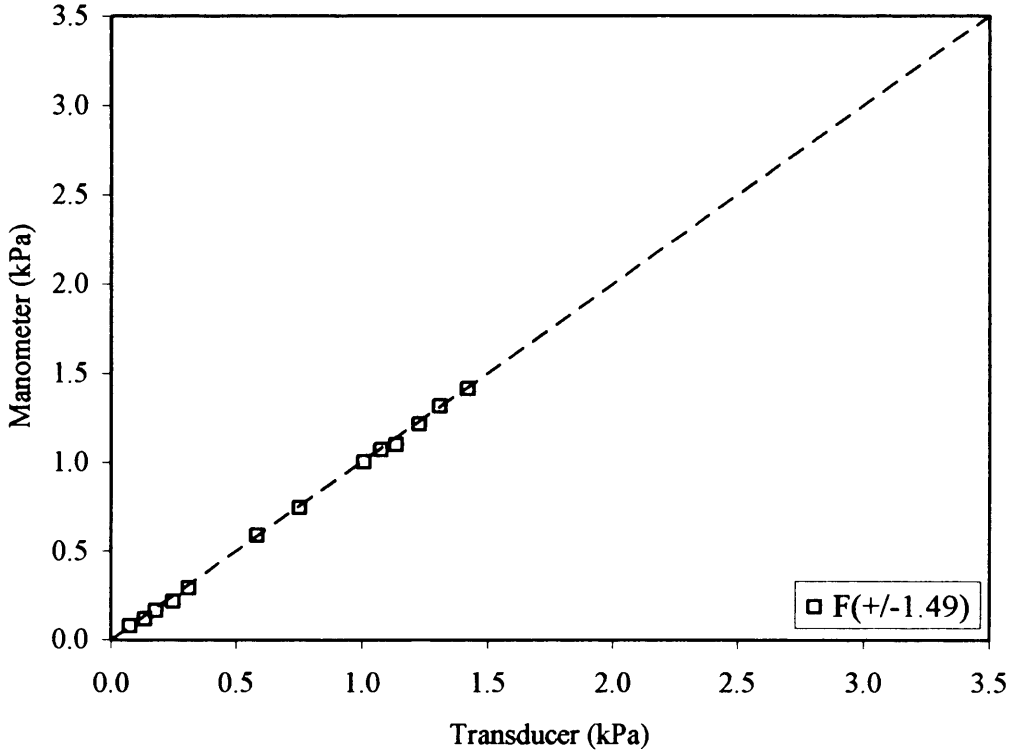

Figure B.6 Pressure transducer F calibration

7. Pressure transducer G (+/-1.49 kPa)

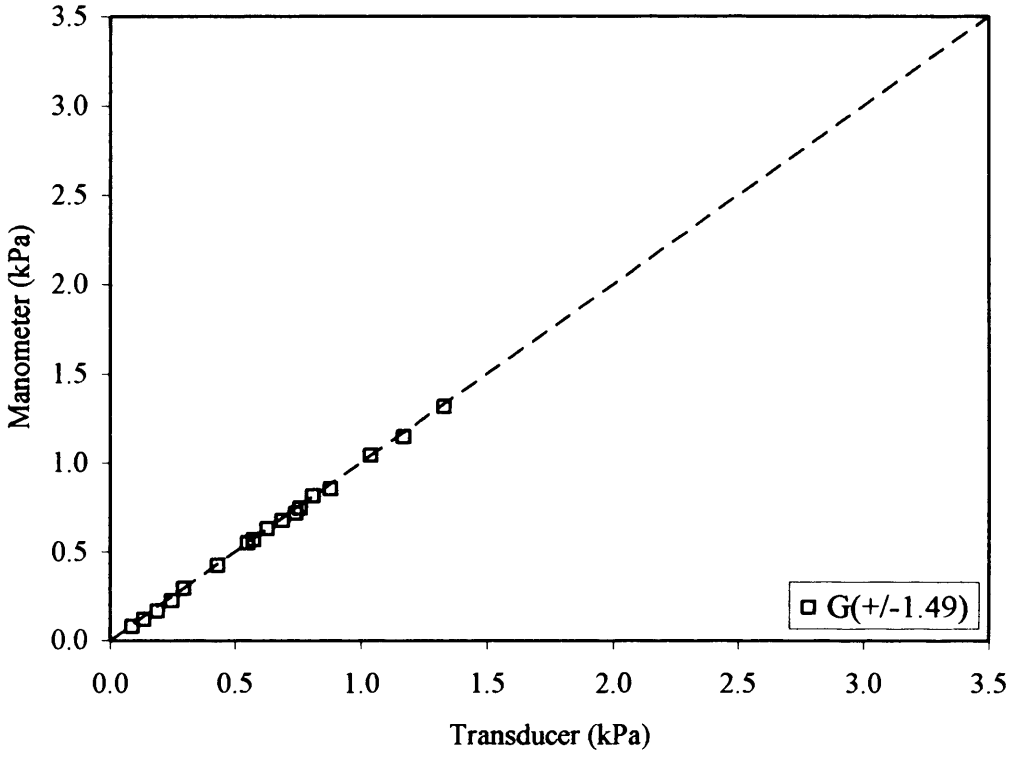

Figure B.7 Pressure transducer G calibration

8. Pressure transducer H (+/-3.45 kPa)

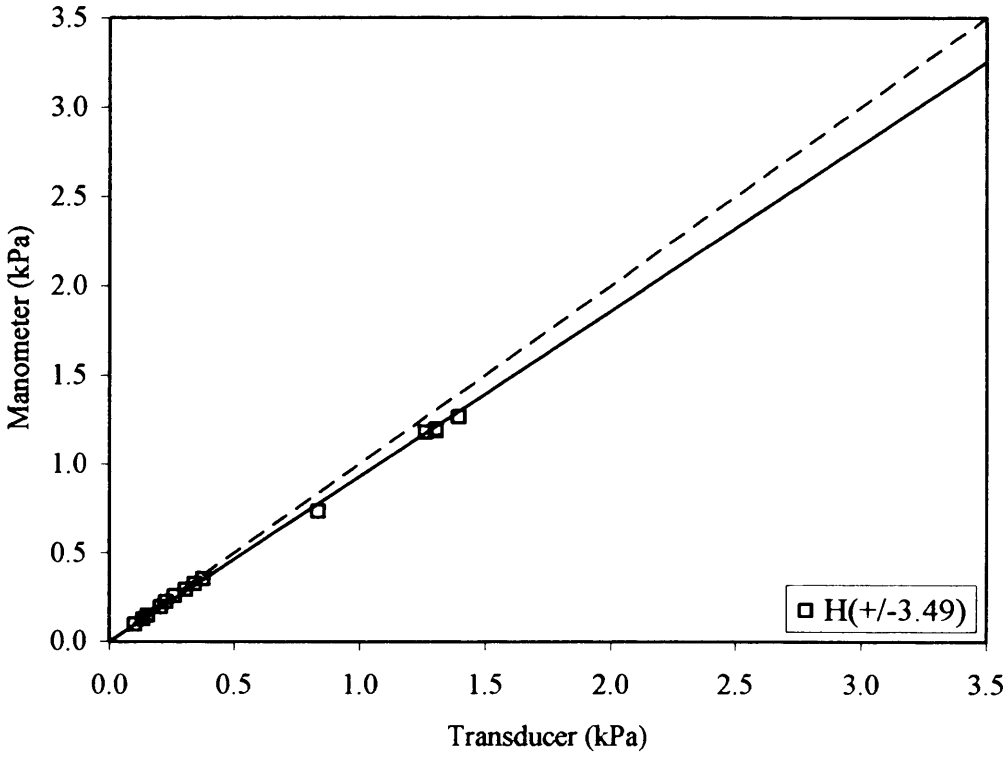

Figure B.8 Pressure transducer H calibration

Appendix C: Rotameter, Distributor and Discharge Valve Characteristic Curves

1. Rotameter characteristic curve

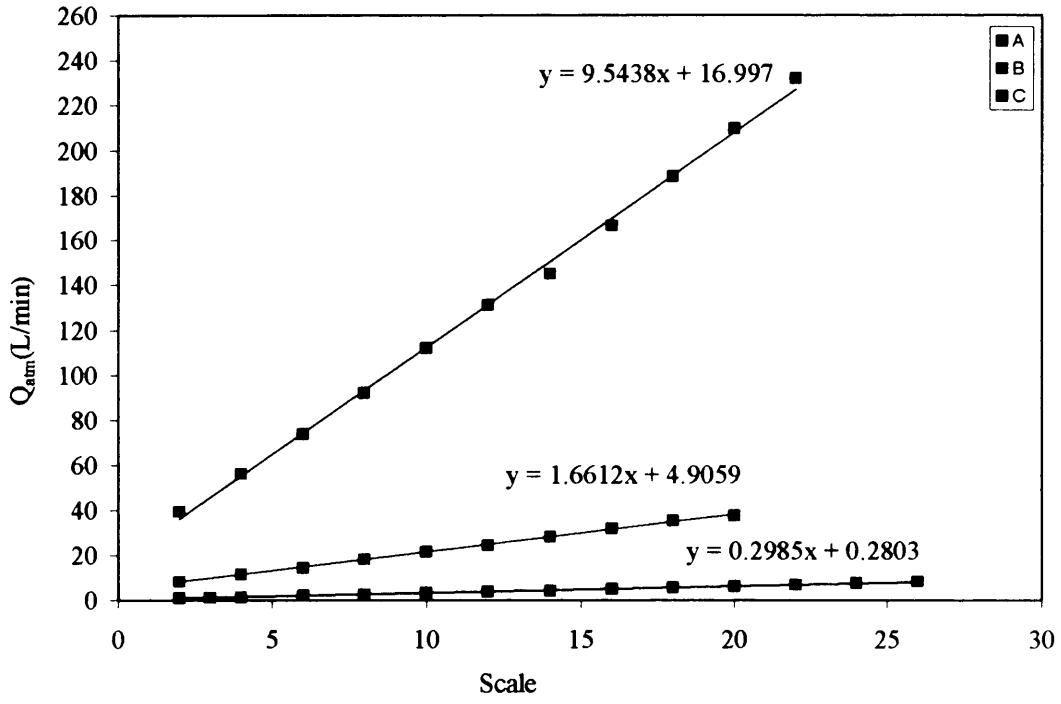

Figure C.1 Rotameter characteristic curve

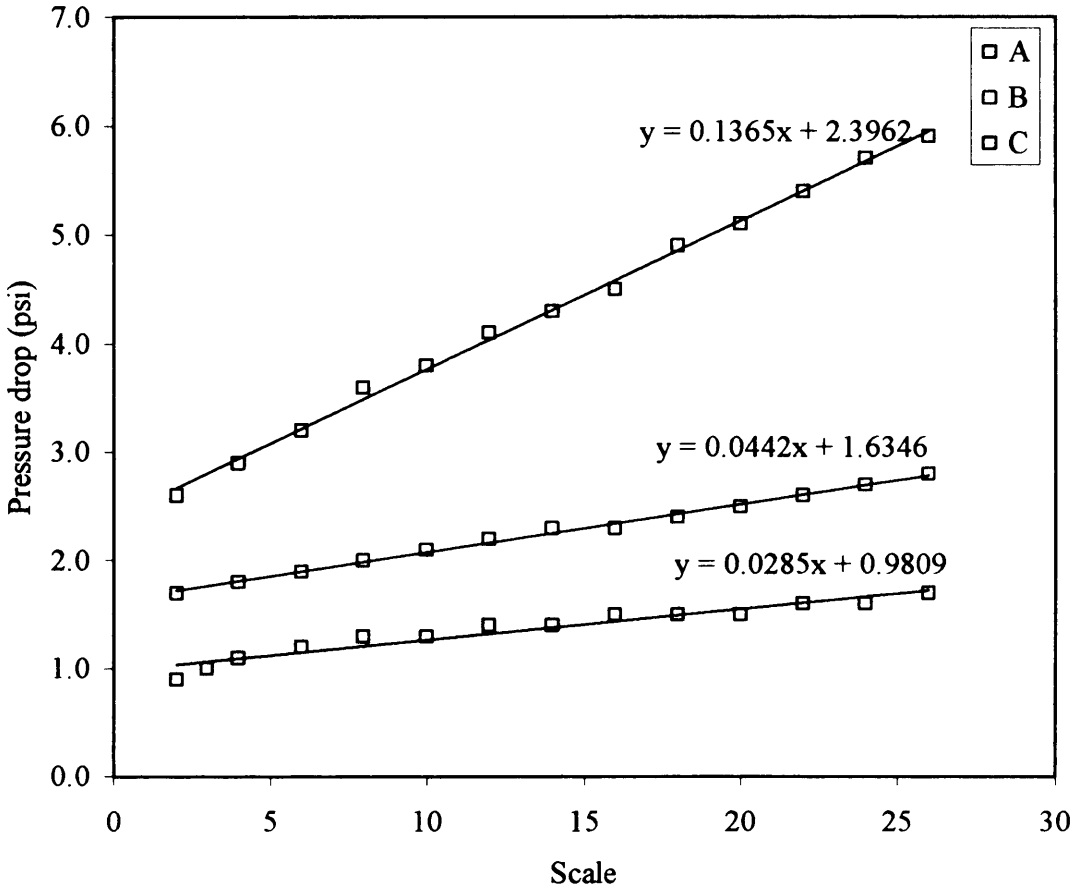

Figure C.2 Pressure drop inside the rotameter

2. Distributor characteristic curve

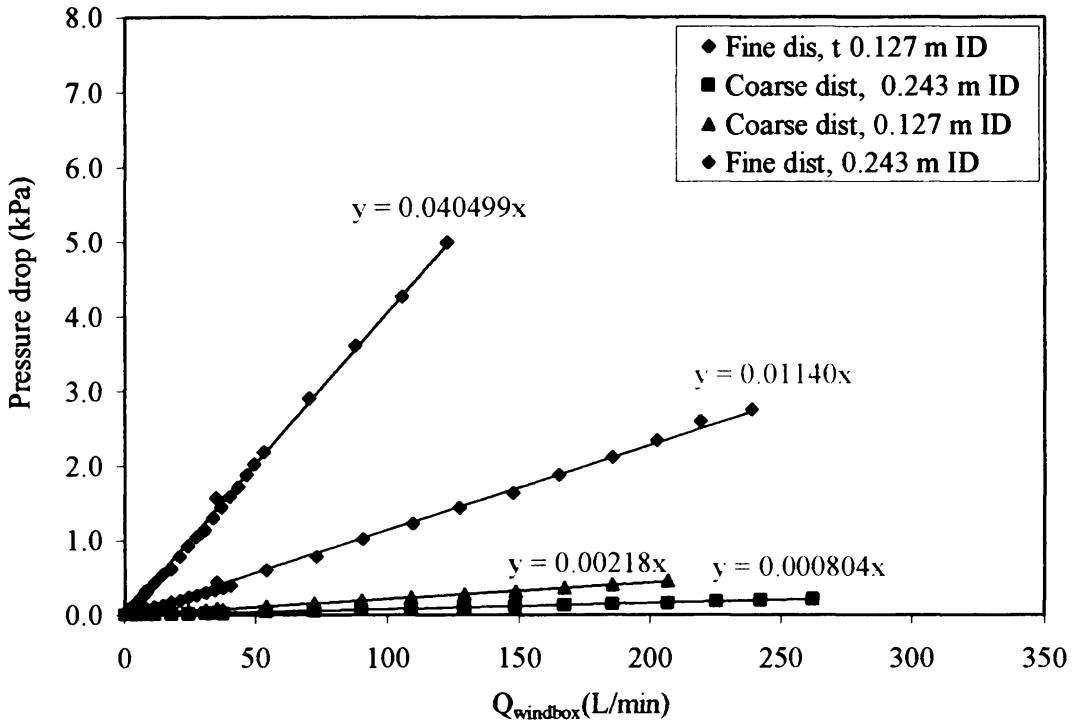

Figure C.3 Distributor characteristic curve

3. Discharge valve pressure drop

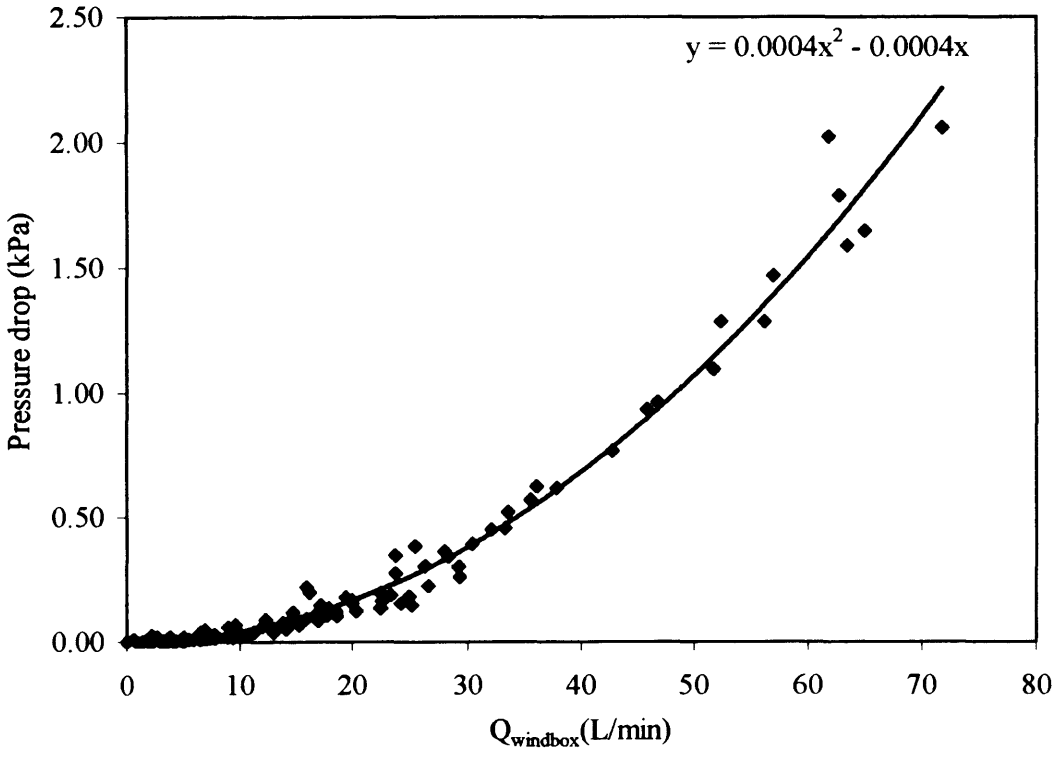

Figure C. 4 Discharge valve pressure drop

Appendix D: Publications

1. Publication

- Parimanan Cherntongchai and Stefano Brandani, *A model for the interpretation of the bed collapse experiment*, Powder Technology, Vol. 151, pp 37-43, 2005

2. Conference Proceeding

- Parimanan Cherngtongchai and Stefano Brandani, "*A Model for the Interpretation of the Bed Collapse Experiment*", Proceeding in AIChE Annual Meeting, San Francisco, USA, 2003